MEAN-FLOW MEASUREMENTS OF A TURBULENT MIXING LAYER FROM HELIUM SLOT INJECTION INTO A SUPERSONIC AIRSTREAM

by

Fei Thomas Kwok

Thesis submitted to the Faculty of the

Virginia Polytechnic Institute and State University

in partial fulfillment of the requirements for the degree of

MASTER OF SCIENCE

in

AEROSPACE ENGINEERING

APPROVED:

Dr. Wing Fai Ng, Cochairman

Dr. Dana A. Walker, Cochairman

Dr. Joseph A. Schetz

November, 1989

Blacksburg, Virginia

MEAN-FLOW MEASUREMENTS OF A TURBULENT MIXING LAYER FROM HELIUM SLOT INJECTION INTO A SUPERSONIC AIRSTREAM

by

Fei Thomas Kwok

Dr. Wing Fai Ng, Cochairman

Dr. Dana A. Walker, Cochairman

AEROSPACE ENGINEERING

(ABSTRACT)

This investigation studies the mixing in a shear layer developed from helium slot injection into a parallel supersonic airstream and compares the results to those of previous slot-injection tests. The objectives of this study include documenting the helium slot-injection flowfield; providing a baseline for use as a reference for future work; contributing representative and consistent data to the general database; and increasing understanding of shear layer dynamics, especially as a result of foreign-gas injection. The helium injectant exits the slot at $\gamma = 1.67$, $M_j = 1.78$, $P_{t_j} = 0.892$ atm, and $T_{t_j} = 287°$ K tangentially to an airstream at $\gamma = 1.4$, $M_\infty = 3$, $P_{t_\infty} = 6.5$ atm, and $T_{t_\infty} = 282°$ K. The freestream has Re/cm $= 5.4 \times 10^5$ and a boundary-layer thickness of $\frac{\delta_{air}}{H} = 0.58$. The pertinent ratios are $\frac{P_j}{P_\infty} = 0.838$, $\frac{U_j}{U_\infty} = 2$, and $\frac{\rho_j}{\rho_\infty} = 0.1$. The slot height H is 1.21 cm. Along with short-duration Schlieren and Shadowgraph photography, concentration, Pitot, cone-static, and stagnation-temperature measurements are taken at each of four streamwise stations (x/H = 0.3, 4.2, 10.5, 21.1) to document the devel-

opment of the mixing layer. In light of the binary-gas mixture, local concentration information is required to reduce the data to pertinent mean-flow variables (M, ρ, U, ρU, P, and T). As expected, slot injection in general shows poor initial penetration of the injectant into the freestream, and, thus, poor initial mixing. Nevertheless, the helium case shows better mixing than a similar air-injection case of a previous experiment, as the mixing shear layer grows 25 percent larger than that in the air case by the last station. Also, about 30 percent more freestream air is entrained into the shear layer in the helium case and is confined mainly to the top third of the mixing layer. The higher mixing rate stems from larger gradients in velocity and density and lower ρU values which result in more active transport mechanisms in the helium injection test.

Acknowledgements

As is usually the case, the invaluable assistance of many was involved in the completion of this work. First, I wish to thank affectionately my parents and my entire family for their love and support not only throughout my college years but as always.

Next, I must acknowledge the efforts of my committee members: Dr. Dana A. Walker for his advice, confidence, and patience; Dr. Wing F. Ng for his ideas, guidance, and energy; and Dr. Joseph A. Schetz for his supervision, motivational support, and extensive experience. Most students normally have only one main advisor with whom they share their work. I was fortunate to have three, and I thank them equally.

I need to recognize and for the time they spent helping to develop and do this project. I also must mention Dr. Russ Thomas, who gave me some useful information and hints, and and

who assisted in running some of the early tests. Their assistance and friendship are greatly appreciated.

I thank

and many others who provided help at opportune moments. Final gratitudes are given to

in the AE shop and the people in the ME shop for all their help in making and finding parts.

This work was supported by the Applied Physics Laboratory of Johns Hopkins University, with as technical monitor.

Table of Contents

INTRODUCTION 1

EXPERIMENTAL APPARATUS 7

2.1 The Wind Tunnel 7

2.2 The Helium Supply System 10

2.3 The Injector and Model 12

2.4 The Optical Equipment 17

WIND TUNNEL INSTRUMENTATION 20

3.1 The Wind Tunnel Data Acquisition System 20

3.2 The Traverse Mechanism and LVDT 21

3.3 Other Support Instrumentation 23

PROBES AND RELATED INSTRUMENTATION 24

4.1 The Gas Concentration Measurement 26

4.1.1 Principle of Operation 26

4.1.2 Probe Configuration 28

4.2 The Pressure Measurement 32
4.2.1 The Traversed Pressure Probes 33
4.2.2 The Settling Chamber Pressure Probes 34
4.3 The Temperature Measurement 36
4.3.1 The Traversed Temperature Probe 36
4.3.2 The Settling Chamber Temperature Probes 38

PROCEDURES AND DATA PROCESSING 39
5.1 Calibration 40
5.1.1 The Aspirated, Concentration Probe 40
5.1.2 The Pitot Probe 42
5.1.3 The Cone-Static Probe 43
5.1.4 The Thermocouple Probe 44
5.1.5 The Settling Chamber Probes 45
5.1.6 The Probe Position 45
5.2 A Tunnel Run 47
5.3 Data Reduction 50
5.3.1 The Concentration Reduction 51
5.3.2 The Mean-Flow Reduction 52
5.3.3 Entrainment 57
5.3.4 The Nondimensionalization Scheme 58

RESULTS 61
6.1 Flow Visualization 61
6.2 Profile Data 67
6.2.1 Concentration Results 67
6.2.2 Other Mean-Flow Results 77

COMPARISON WITH AIR INJECTION AND DISCUSSION **102**

7.1 Flow Visualization 103

7.2 Mean-Flow Data and Modeling 106

CONCLUDING REMARKS **126**

8.1 Conclusions 126

8.2 Future Work 127

APPENDICES **129**

Error Analysis **130**

Static-Pressure Ratio Derivation **134**

Other Effects on Concentration-Probe Response **136**

Dimensional Helium Profiles **139**

Tables of Data **154**

E.1 Nondimensional Data 154

E.2 Dimensional Data 164

Computer Programs **173**

REFERENCES **193**

VITA 199

List of Illustrations

Figure 1. General Flow Structure of Slot Injection 3

Figure 2. The Virginia Tech Supersonic Wind Tunnel 9

Figure 3. The Helium Supply System 11

Figure 4. The Test Section Configuration 13

Figure 5. The Injector Block 14

Figure 6. The Floorplate Layout 16

Figure 7. Schematic of the Optical System 19

Figure 8. The Computer-Controlled Data Acquisition System 22

Figure 9. Common Aspects of the Traversed Probes 25

Figure 10. Schematic of the Concentration Probe 27

Figure 11. The Probe Tip and Diffuser Cap 30

Figure 12. The Cone-Static Probe Tip 35

Figure 13. Stagnation-Temperature Probe Tip 37

Figure 14. The Concentration-Probe Calibration Setup 41

Figure 15. The Cathetometer Reference Points 48

Figure 16. Spark-Schlieren of the Helium/Air Flowfield 63

Figure 17. Nanosecond Shadowgraph of the Helium/Air Flowfield 65

Figure 18. Hot-Film Voltage Profiles 69
Figure 19. P1 Profiles 70
Figure 20. P2 Profiles 71
Figure 21. P2/P1 Profiles 72
Figure 22. Concentration Profiles in Mole Fraction 75
Figure 23. Concentration Profiles in Mass Fraction 76
Figure 24. Downstream Injectant Core Decay 78
Figure 25. Downstream Penetration 79
Figure 26. Mixing Layer Development 80
Figure 27. Reaction Layer Thickness 81
Figure 28. Pitot Pressure Profiles 83
Figure 29. Cone-Static Pressure Profiles 84
Figure 30. Total Temperature Profiles 85
Figure 31. Mach Number Profiles 86
Figure 32. Speed of Sound Profiles 87
Figure 33. Velocity Profiles 88
Figure 34. Density Profiles 89
Figure 35. Mass Flux Profiles 90
Figure 36. Static Temperature Profiles 91
Figure 37. Static Pressure Profiles 93
Figure 38. Total Pressure Profiles 94
Figure 39. Static Pressure Adjustment 95
Figure 40. Effect on Mach Number 96

Figure 41. Effect on Density 97
Figure 42. Effect on Speed of Sound 98
Figure 43. Effect on Velocity 99
Figure 44. Effect on Total Pressure 100
Figure 45. Effect on Static Temperature 101
Figure 46. Spark-Schlieren of the Air/Air Flowfield 104
Figure 47. Nanosecond Shadowgraph of the Air/Air Flowfield 105
Figure 48. Pitot Pressure Comparison 107
Figure 49. Cone-Static Pressure Comparison 108
Figure 50. Total Temperature Comparison 109
Figure 51. Mach Number Comparison 111
Figure 52. Density Comparison 112
Figure 53. Velocity Comparison 113
Figure 54. Mass Flux Comparison 114
Figure 55. Static Pressure Comparison 116
Figure 56. Characteristic Layers of the Flowfield 123
Figure 57. Downstream Decay of the Maximum Concentration 125

List of Tables

Table 1. Table of Pc/Pt2 Reference Values 55

Table 2. Nondimensionalization Parameters 59

List of Symbols

a	speed of sound
A	area
$A1$	fin area to stabilize in yaw
$A2$	fin area to support extension
b	constant in hot-film voltage equation
c	constant in hot-film voltage equation
d	hot-film diameter
f	function
H	slot height = 1.21 cm (0.475 inch)
k	thermal conductivity
l	hot-film length
m	constant in hot-film voltage equation
m	mass flow rate
M	Mach number
MW	molecular weight
n	constant in $\frac{dm}{dx}$ equations
P	penetration in y of helium into airstream

P	pressure
$P1$	stagnation pressure before sonic orifice
$P2$	pressure after sonic orifice (back pressure)
q	dynamic pressure
r	ratio of "slow"-stream velocity to "fast"-stream velocity
R	resistance
R	gas constant
s	ratio of "slow"-stream density to "fast"-stream density
t	time
T	temperature
u, U	axial/streamwise velocity
v	normal velocity in y-direction
V	voltage
x	streamwise direction, measured from splitter-plate lip
y	vertical direction, measured from tunnel floor
z	slotwise (spanwise) direction
α	mass fraction
γ	specific heat ratio
δ	thickness
δ'	$\frac{d\delta}{dx}$
Δ	height measured from floor to top of the mixing layer
μ	fluid viscosity

ν	volume fraction
ρ	density
χ	mole fraction

Subscripts

air	air or air-side
c	cone-static
ch	sensor-plane channel
conv	convective
crit	critical
Case 1	helium slot injection
Case 2	unheated-air slot injection
e	slot exit plane
ENT	entrained
exp	experimental
He	helium or helium-side
H_2	hydrogen
i	constituent
in	incompressible
j	injectant/wall jet
m	mixture
max	maximum

rl	reaction layer
s	series
s4	Station 4
t	total/stagnation
vis	visual
w	wire/film property at operating temperature
*	choked
∞	freestream
1	before normal shock
2	after normal shock

Chapter 1

INTRODUCTION

With increased interest in supersonic and hypersonic atmospheric flight, considerable research is needed to investigate all aspects of developing vehicles which operate in this flow regime[1]. One main concern is the combustion dynamics involved in the supersonic combustion ramjets (SCRAMjets) that propel these vehicles. Inherently, mixing at high Mach numbers is relatively low. Moreover, at hypersonic flight Mach numbers of 8 to 20, the combustor Mach number remains supersonic. With such high velocities and low residence times, fuel must mix with air and burn quickly to prevent the need for excessively long combustors[2] . Therefore, a strong need to investigate turbulent mixing qualities in this speed regime and various ways to augment mixing is present.

Many fuel injection schemes are possible, each having its own advantages and disadvantages[2-6]. This study investigates the turbulent mixing layer resulting from supersonic, tangential injection through a two-dimensional slot into a

supersonic airstream. Figure 1 shows the flow structure. When the two parallel streams interact, a shear layer forms, trailing off the splitter-plate lip. This slot-injection flowfield is also characterized by expansions and shocks which propagate from the lip. The freestream boundary layer "rides" along the top of the shear layer until the shear layer spreads and engulfs both the external boundary layer and the injectant core.

Slot injection has several advantages. First, since the fuel injects parallel to the main flow, the momentum of the fuel adds to the total thrust produced by the engine. Secondly, tangential injection creates minimum disturbances within the combustor. With fewer shocks and perturbations, total pressure losses decrease, thus increasing engine efficiency. Another possible advantage is film cooling, where the injected fuel acts as a protective layer between the high stagnation-temperature freestream and the combustor wall[7-11]. Other benefits include skin-friction reduction[12,13] and boundary-layer energization which helps prevent the boundary layer from separating. Finally, because 2-D slot injection is a relatively simple case in terms of overall features, it acts as an appropriate baseline whereby the effectiveness of other configurations can be measured. The main disadvantage of slot flow is the lack of transverse penetration of the injectant which promotes initial mixing, so that mixing rates become relatively low and spreading angles are small.

Another important motivation for experimental measurements is the inadequacies of most computational methods in modeling high-speed, turbulent, compressible flow. Even in the relatively simple case of slot injection, this

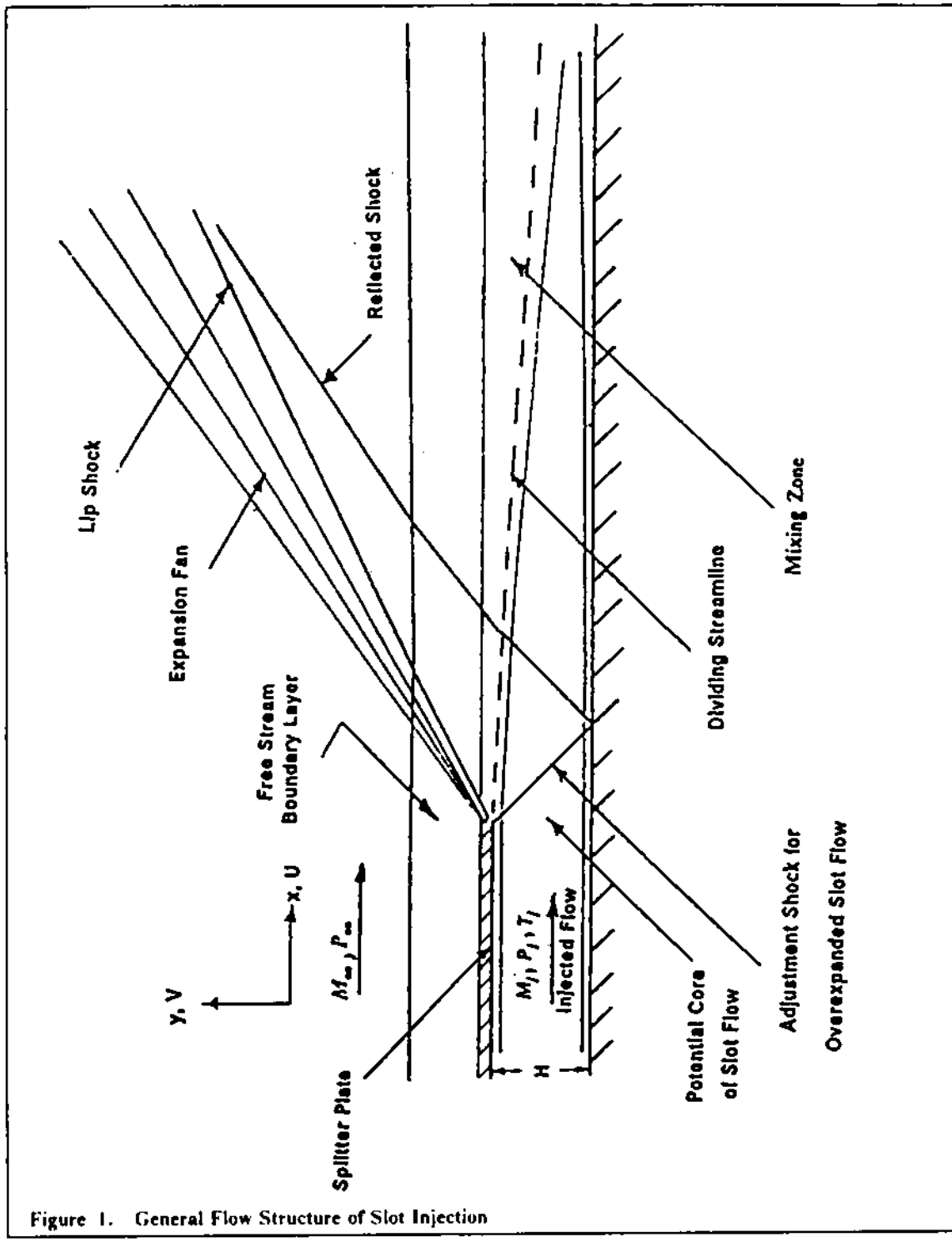

Figure 1. General Flow Structure of Slot Injection

problem holds true. Models based exclusively on free shear layer aspects or boundary layer qualities cannot fully represent the slot flowfield since merging of a shear layer and a wall boundary layer region exists. Turbulence modeling is complex with merging viscous layers and the resulting presence of large gradients, especially in foreign gas injection. Although more current models attempt to address these deficiences[14,15], experimental measurements remain indispensable.

The literature contains numerous earlier studies of slot injection into a supersonic stream. These tests use various initial conditions, configurations, and techniques and investigate different aspects of slot injection[7,10-13,16-18]. The vast majority of these past experiments, however, do not provide great detail in measuring the complete flowfield character. Some recent air injection tests with the same slot configuration and external flow as in this investigation[19-24] present a more thorough examination of the flowfield. This study results from a logical progression along the same test matrix. The new parameter here is the use of helium instead of air as the injectant.

The test configuration has $M_\infty = 3$, $P_{t\infty} = 6.5$ atm (95 psia), and $T_{t\infty} = 282°$ Kelvin. The combustor model consists of a 1.21 cm (0.475 in) rearward-facing slot step for tangential injection of helium. The floorplate is 30.5 cm (12 in) in the direction of the flow and 22.9 cm (9 in) in the spanwise direction. These dimensions roughly model those of a typical combustor. Helium enters the test section at $M_j = 1.78$, $P_{tj} = 0.892$ atm (13.1 psia), and $T_{tj} = 287°$ Kelvin. These conditions give $\frac{P_j}{P_\infty} = 0.838$, $\frac{U_j}{U_\infty} = 2.0$, and $\frac{\rho_j}{\rho_\infty} = 0.1$. The static pressure ratio matches the previous air slot-injection tests. The higher injectant velocity

than the external stream velocity matches the SCRAMjet case up to about a flight Mach number of 15.

To measure gas species in the turbulent mixing layer, an aspirated, concentration probe is developed based on a similar configuration by Ng and Epstein[25,26]. This probe is custom designed and built and is a practical improvement over past designs. The probe chokes at an internal orifice and swallows the stand-off shock, two qualities essential for proper operation. In the past, some concentration probes have been used; in most cases, they were operated in subsonic flows and often were of the sampling-probe variety, where remote gas-chromatography analysis of a captured mixture sample was required[17,27-35] . This new probe provides quick, on-site measurements in a supersonic flow with an accuracy within 2 percent mole fraction of helium.

The gas composition indicates mixing zones. It also is required to reduce Pitot, cone-static, and stagnation temperature profiles obtained from three other probes to such flow variables as Mach number, density, velocity, pressure, and mass flux. The gas concentration enters into these calculations through the specific-heat ratio and gas constant. Once the data is reduced, trends can be compared to the previous air injection cases in the same physical configuration.

In general, helium mixes better than air as indicated by the more rapid growth of the mixing layer and higher entrainment rates. Also, the flowfield can be categorized into three characteristic regions: a reaction layer which gives limits on combustion (if helium is assumed to directly model hydrogen-gas fuel), a turbulence layer which defines the region with relatively high turbulence, and a

mixing layer that contains the other two regions. By monitoring the development of these layers, the effectiveness of mixing in the slot-injection field can be determined. Comparisons of the influence of different injectant gases also shed more light on gradient effects on the shear layer.

Measurements are taken at four streamwise stations, and at each station the four mean-flow probes are traversed from the floor to just beyond the mixing layer height Δ. To supplement this data, Spark-Schlieren and Nanoshadowgraph photographs provide useful visual information on the flowfield. This thesis first describes the main experimental apparatus used, including wind tunnel equipment and support instrumentation. A description of the mean-flow probes and their calibration procedure are mentioned. This report also outlines the data-reduction procedure and examines both qualitative and quantitative results from the tests. Finally, comparisons with previous studies are made, and some analytical models are used to provide a theoretical basis of comparison for the data.

The data documented here can be used as a reference for future computational and analytical work, as a basis for comparison with other injection schemes and experimental data, and as input into turbulence data reduction (e. g., data from hot wires).

Chapter 2

EXPERIMENTAL APPARATUS

2.1 The Wind Tunnel

The Virginia Tech Supersonic Wind Tunnel is a blowdown-type facility with computer control to insure accurate and repeatable runs. The four water-cooled Ingersoll-Rand Model 90 reciprocating compressors pump air through a dehydrating prefilter which absorbs most of the oil from the flow. The air then passes through two dryers that absorb the remaining oil and moisture in the system. Finally, an after-filter consisting of fine screens and fabric socks removes any dust and particles from the airflow before the air is stored in holding tanks. There are sixteen storage tanks with a total volume of 79 m^3 (2800 ft^3).

A hydraulic, regulating valve coupled with a computer-controlled feedback circuit maintains the desired settling chamber pressure. Downstream of the

control valve, a pneumatic butterfly valve governs the on/off operation of the tunnel. Once the tunnel is started, air streams into the settling chamber where a transition cone and a series of screens straighten the flow and improve flow uniformity. Temperature and pressure probes measure the settling chamber quantities.

Accelerating through a two-dimensional nozzle, the airstream enters the 23 X 23 cm (9 X 9 in) test section and discharges through a step diffuser with a 10° wedge on the upper side of the tunnel to augment pressure recovery[20] . The exhaust is blown out a shrouded exit duct into a muffler and then into the atmosphere. Figure 2 shows the wind tunnel layout.

In the test configuration, the tunnel operates at Mach 3. The control valve maintains the total pressure at 6.5 ± 0.05 atm (95 ± 1 psia) for approximately 8 seconds of usable run time. During this time, the total pressure fluctuates no more than 1 percent from its steady-state value, and the total temperature decreases less than 4 percent due to adiabatic expansion in the storage tanks from a mean of about 282 deg Kelvin. Six seconds is required to allow transients and oscillations to damp out before acquiring data. This high-speed flow has Reynolds number per cm of 5.4×10^5 (Re/foot = 1.6×10^7).

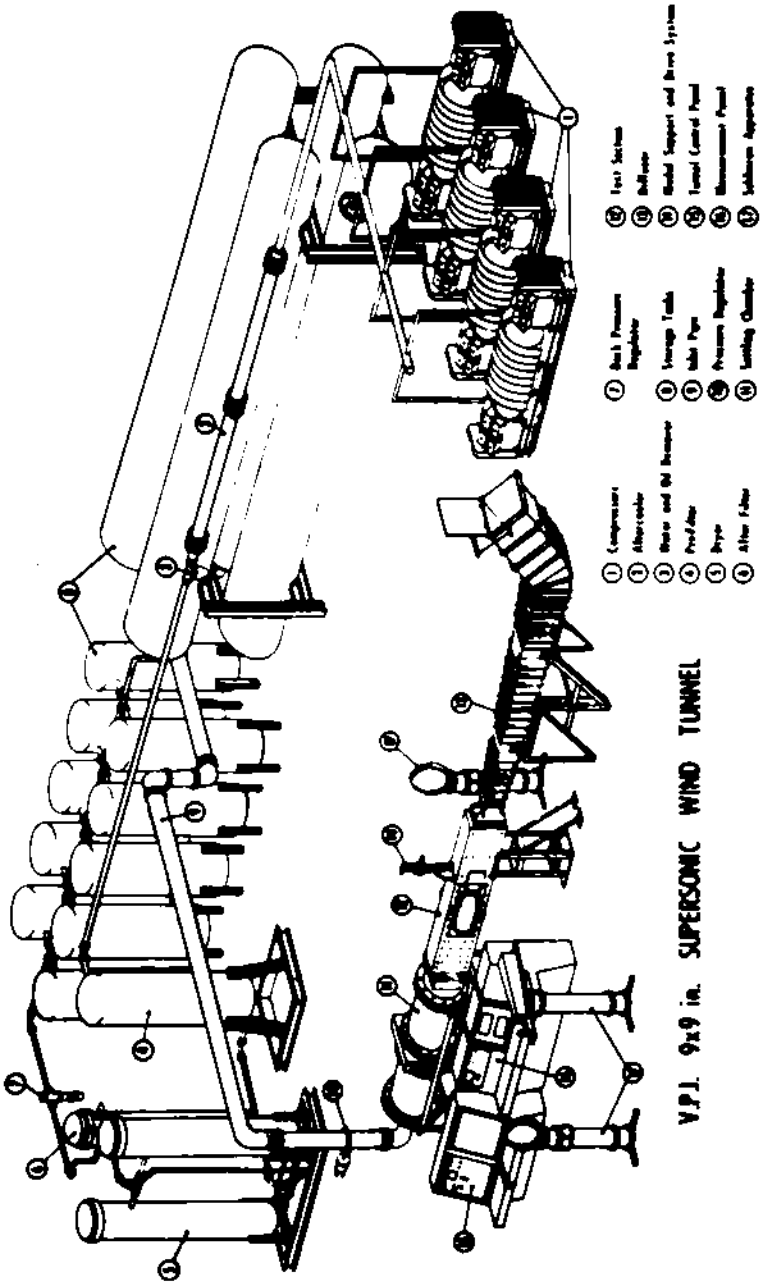

Figure 2. The Virginia Tech Supersonic Wind Tunnel

2.2 *The Helium Supply System*

An array of twelve commercial gas bottles linked to a common manifold supplies helium for injection into the wind tunnel. The maximum pressure in the manifold is 153 atm (2250 psia). Two Grove Controls, Inc., Powreactor Dome Controller pressure regulators (Model RBX204-015) control the discharge of helium into two lines of 1.27 cm (1/2 inch) copper tubing equipped with pressure gauges and on/off valves to monitor the helium flow. Supplied by a single air cylinder, the reference pressure for the regulators is maintained at 25.5 atm (375 psia). The two separate supply lines connect to a high-pressure union under the injector block in the tunnel test section and merge into one stream. Figure 3 represents the supply system.

During the experiment, a run time of 10 seconds (the actual time for data acquisition is 8 seconds, but the helium is turned on 2 seconds before data-taking to allow for the decay of transients) drains the total pressure in the supply manifold by 17 atm (250 psia). Moreover, with a manifold pressure of 68 atm (1000 psia) or less, the resulting mass flow is not adequate to hold the desired pressure in the plenum chamber of the injector. Thus, for twelve full helium tanks, only five to six runs can be made before reloading the helium rack. The mean injectant temperature is about 5 deg Kelvin higher than the freestream total temperature.

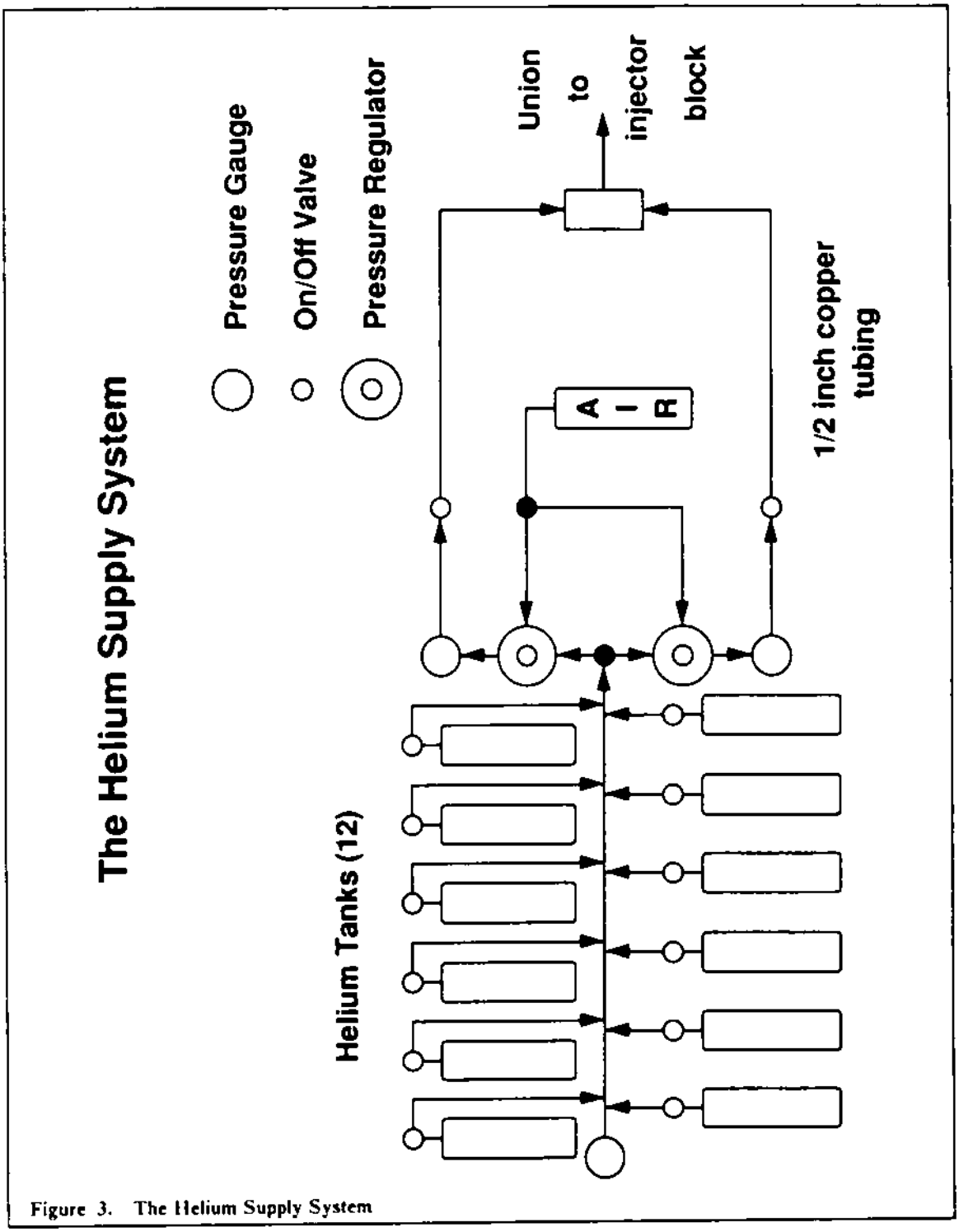

Figure 3. The Helium Supply System

2.3 *The Injector and Model*

Entering through a high-pressure, 3-way union connected to the injector block under the test section, the helium flow is controlled by a manually operated 3.2-cm (1.25-inch) gate valve, preset by trial and error to adjust the plenum chamber pressure. After the valve, the flow passes through two manifolds which distribute the gas evenly in the plenum chamber of the injector block. Probes monitor pressure and temperature within this settling chamber. Next, a flow straightener made of 0.48-cm (3/16-inch) OD stainless steel tubes encased in wire mesh improves the flow quality. The gas then expands through a converging-diverging nozzle configured to turn the stream 90° and is exhausted tangentially to the freestream through a two-dimensional, rearward-facing slot. The slot height H is 1.21 cm (0.475 inch) with a splitter-plate thickness of 0.038 cm (0.015 inch). The slot height is on the order of the thickness of the freestream boundary layer at this location along the tunnel. The top of the slot coincides with the centerline of the test section so that effectively only half of the nozzle is used. The exhaust area is 27.6 cm² (4.27 in²) , and the effective area ratio $\frac{A_e}{A^*}$ is 1.34. Figure 4 and Figure 5 show the layout of both the test section and injector block.

The floorplate model is screwed onto the side of the injector block. The top surface of this plate lines up with the bottom of the slot exit area, and so the floorplate is offset downward 1.21 cm from the test-section centerline. As seen in Figure 6, the floorplate is a 22.9 X 30.5 cm (9 X 12 inch) block with a pair of

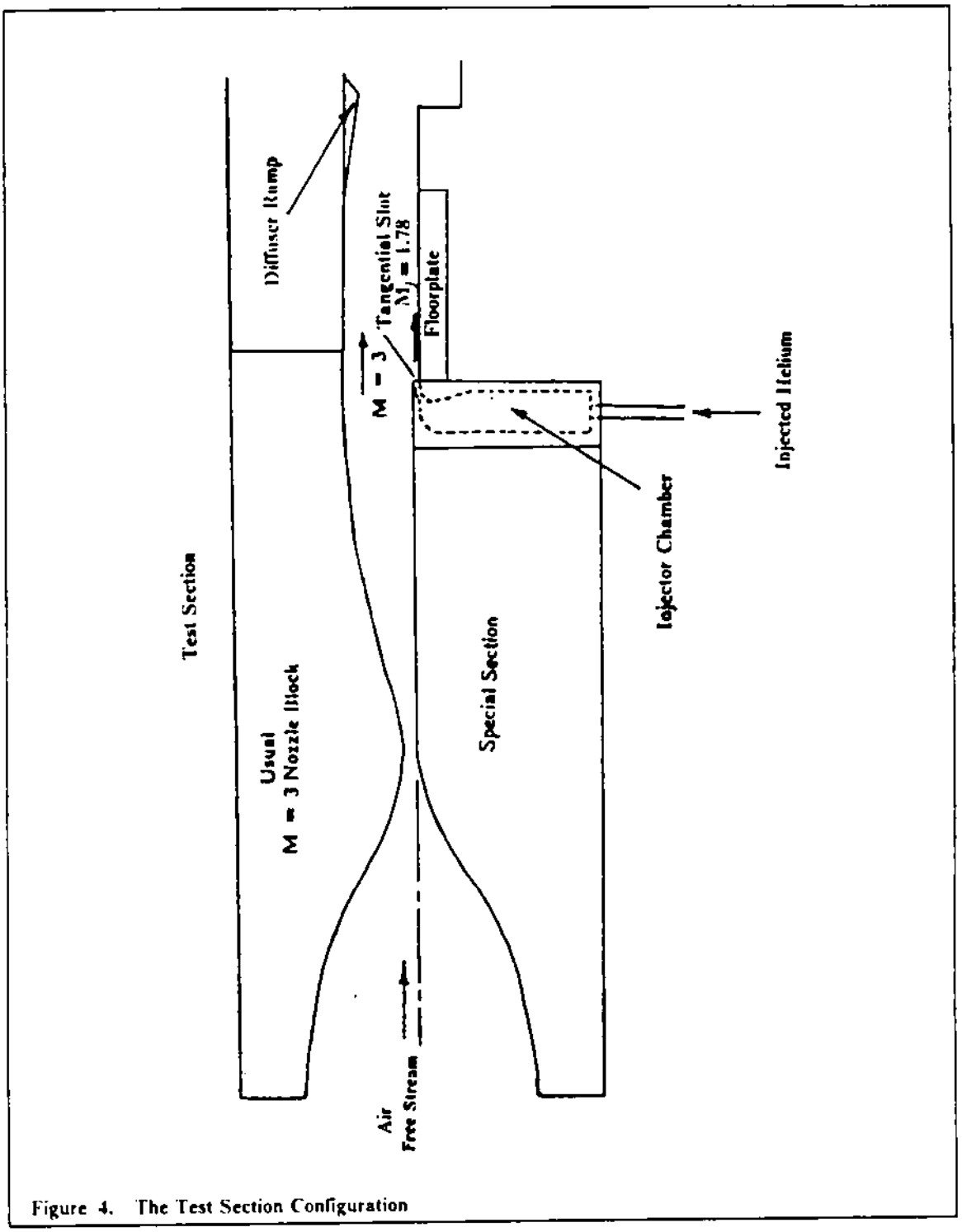

Figure 4. The Test Section Configuration

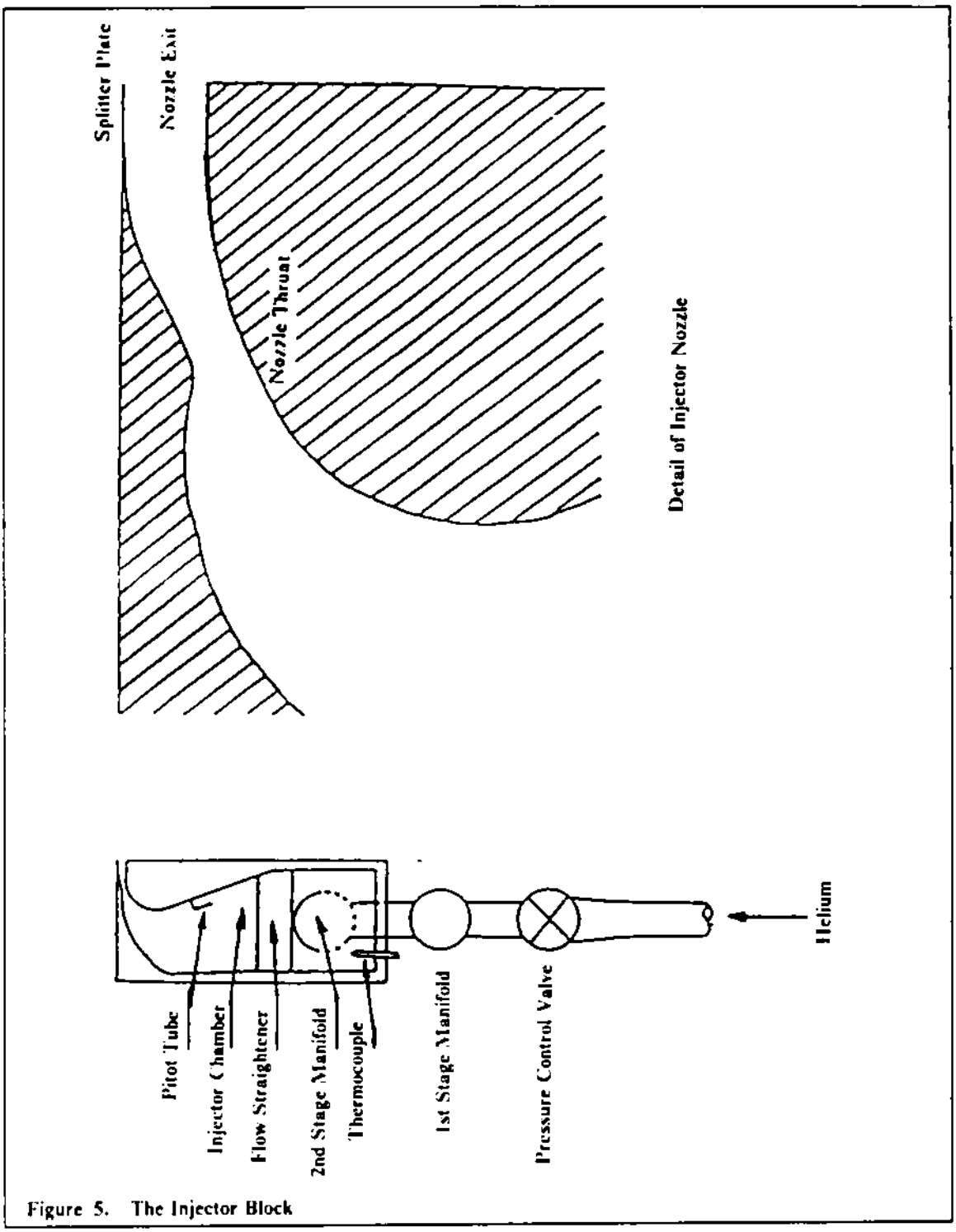

Figure 5. The Injector Block

0.635-cm (1/4-inch) holes drilled at each of three positions along the plate for probe insertion. At each point, the two holes are offset 2.54 cm (1 inch) on either side of the plate centerline. This alignment of holes allows for experimental verification of the two-dimensionality of the flowfield. At a fourth position where the diffuser connects to the floorplate, instead of a hole, a slot is cut crosswise on the model to facilitate setup for this and other experiments which use the same diffuser. The probe at this fourth position is shifted 1.78 cm (0.7 inch) transversely toward the plate centerline from the probe location at the other three holes because of an extra plate required to fasten a probe inserted through this slot. These positions are located nominally 7.62 cm (3 in) downstream of the four axial measurement stations. With a slot height H of 1.21 cm, Stations 1, 2, 3, and 4 are defined as $x/H = 0.3$ (1 8 inch from the slot exit), $x/H = 4.2$ (2 inches), $x/H = 10.5$ (5 inches), and $x/H = 21.1$ (10 inches), respectively.

In the test configuration, the plenum chamber pressure is maintained at 0.892 atm (13.1 psia). The helium flow accelerates to Mach 1.78 with a resulting exit static pressure P_j of 0.148 atm (2.17 psia) and $P_j/P_\infty = 0.838$. This static pressure ratio matches that of previous tests involving air slot injection, so that the helium-air flowfield can be compared with the earlier air-air results. In those experiments[19-24], the mild overexpansion of the injectant produces minimal adjustment shocks in the near-slot region and causes the freestream air to turn down into the injectant, inducing entrainment and mixing. **App. B** summarizes the derivation of the helium slot-flow conditions.

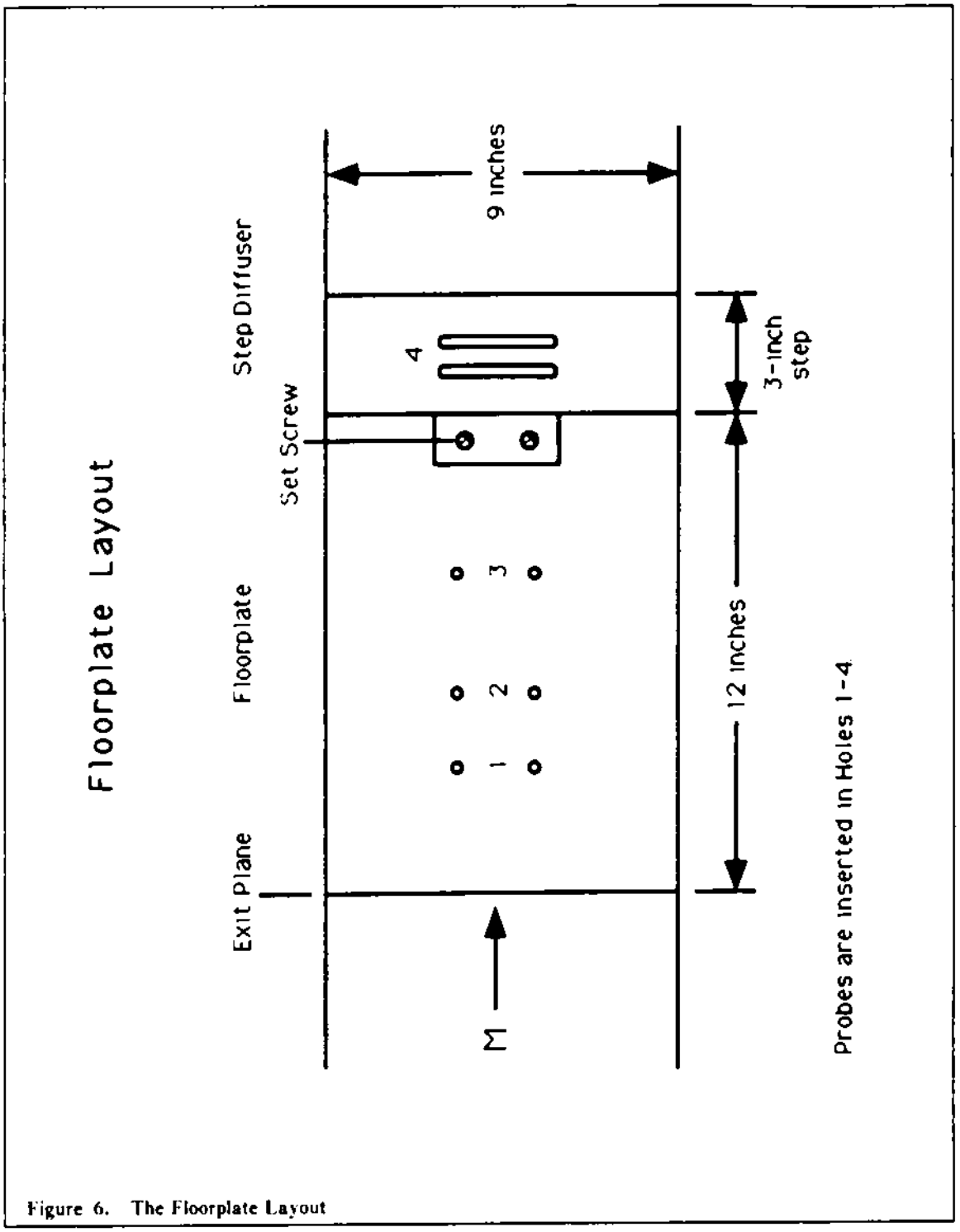

Figure 6. The Floorplate Layout

2.4 *The Optical Equipment*

Two optical setups provide good visual records of the flowfield. First, a Spark-Schlieren system highlights the various flow regions and the boundaries between them by emphasizing density gradients. A General Radio Company Type 1531-AB Strobotac with a 1.2-microsecond flash transmits a light beam that reflects off a collimating mirror and then passes through the two Schlieren-quality windows on the test section. Another collimating mirror sends the light onto a horizontal knife-edge which blocks part of the beam to emphasize vertical gradients in the flow, and the adjusted light beam hits a final mirror that reflects the beam into a camera. The camera is prefocused on a lighted filament in a lamp bulb placed in the middle of the test section.

In a simpler configuration, the Nanosecond Shadowgraph employs a Xenon Corporation Novatron 289B Nanopulse Lamp powered by a Model 437A Nanopulser which sends light to the collimating mirror that reflects the beam into the test section. The camera in this case is positioned so that the photographic plate sits 33 cm (13 in) from the window. The 20-nanosecond flash freezes the flowfield more effectively, so that eddy features within the shear layer become more visible.

Figure 7 summarizes the optical system. In both photographic setups, a manual remote triggers the flash at the desired time. Also, in both cases, four separate photographs--with the mirrors, knife-edge, and camera adjusted slightly

to sequence the photos--comprise the final composite picture. The film is Polaroid Type 57 (ASA 3000).

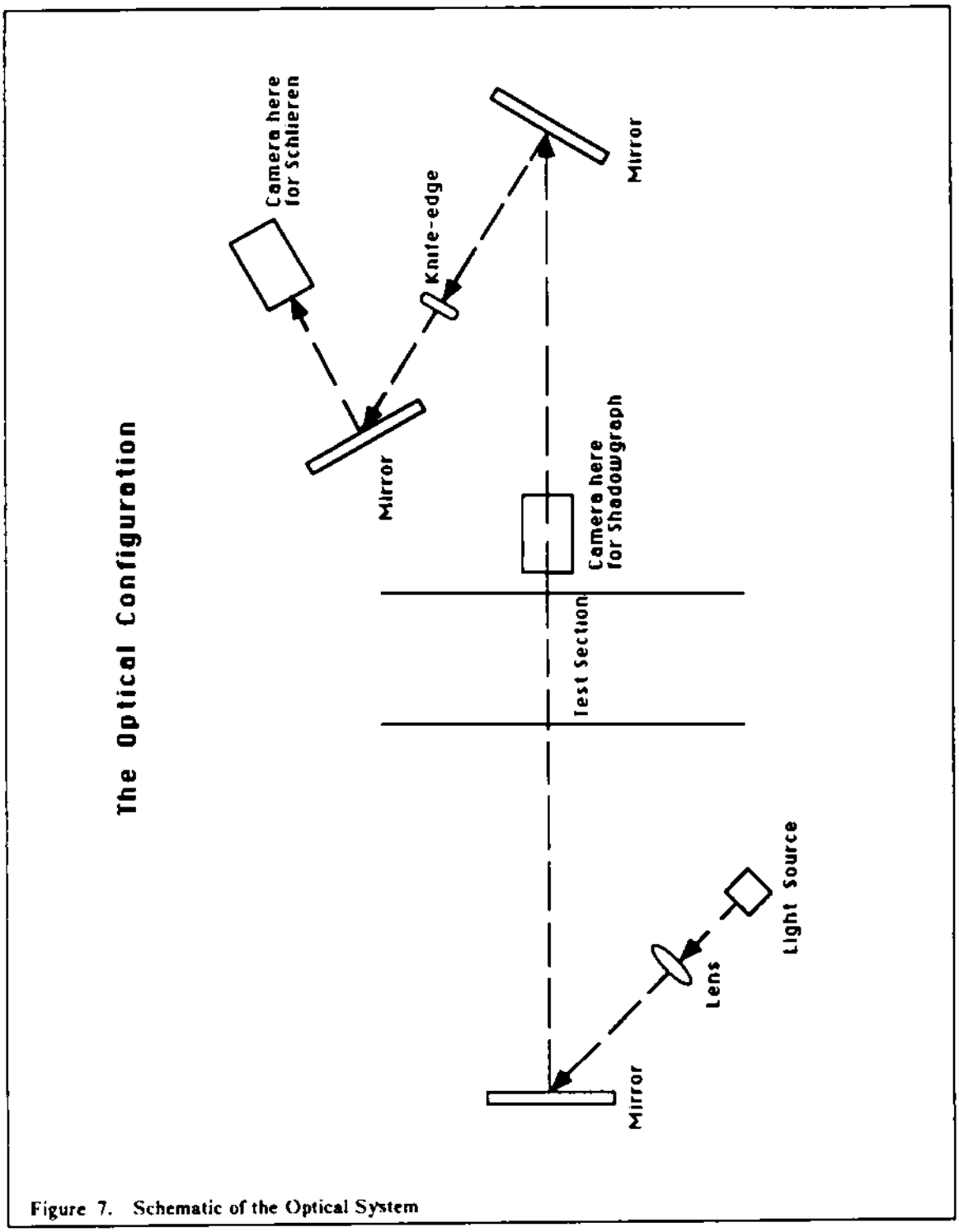

Figure 7. Schematic of the Optical System

Chapter 3

WIND TUNNEL INSTRUMENTATION

3.1 The Wind Tunnel Data Acquisition System

An IBM-PC equipped with a Metrabyte DASH-16F multifunction, high-speed, analog/digital I/O board is the basis of the data acquisition system. This expansion card inserts into a standard slot in the IBM computer. A/D ports are operated in single-ended mode, which permits simultaneous sampling of 16 channels, and in unipolar configuration, which assigns digital values 0-4095 to 0-10 volts. With a 12-bit limit and 8-microsecond conversion time, the board can sample at a 100 kHz maximium rate. In addition, the board provides two D/A output ports and several digital I/O terminals for relay switching in operations such as turning on valves. One D/A output controls the tunnel settling chamber

pressure. The computer executes a FORTRAN program (Program 1 in **App. F**) which controls all operations and stores the data on floppy disks.

The DASH-16F board is interfaced to a converter box by way of a 37-pin connector. With enough ports to accomodate all functions of the Metrabyte board, the box acts as a junction for BNC cables receiving and transmitting signals. Figure 8 maps out the complete data acquisition system.

3.2 The Traverse Mechanism and LVDT

A Computer Devices Corporation Model 34D-9209A stepper motor powers the traverse assembly equipped with a Trans-Tek Series 240 Linear Voltage Displacement Transducer (LVDT) to indicate its position. The motor rotates a gear which moves a slotted rod up and down. Attached to the rod frame by linkages, a mounting bracket with a 0.635-cm (1/4-in) through hole clamps down on the probe stem inserted through one of the holes in the tunnel floorplate. Moving concurrently with the slotted rod, the LVDT rod produces a linear voltage output in response to a change in traversing distance. Thus, by calibrating the LVDT for each probe setup, probe displacements can be determined with accuracy. The voltage output of the LVDT is adjustable and filtered to reduce noise. With a relay board inserted in an expansion slot, the IBM-PC computer communicates with the traverse control circuit and fully controls the motion of the assembly.

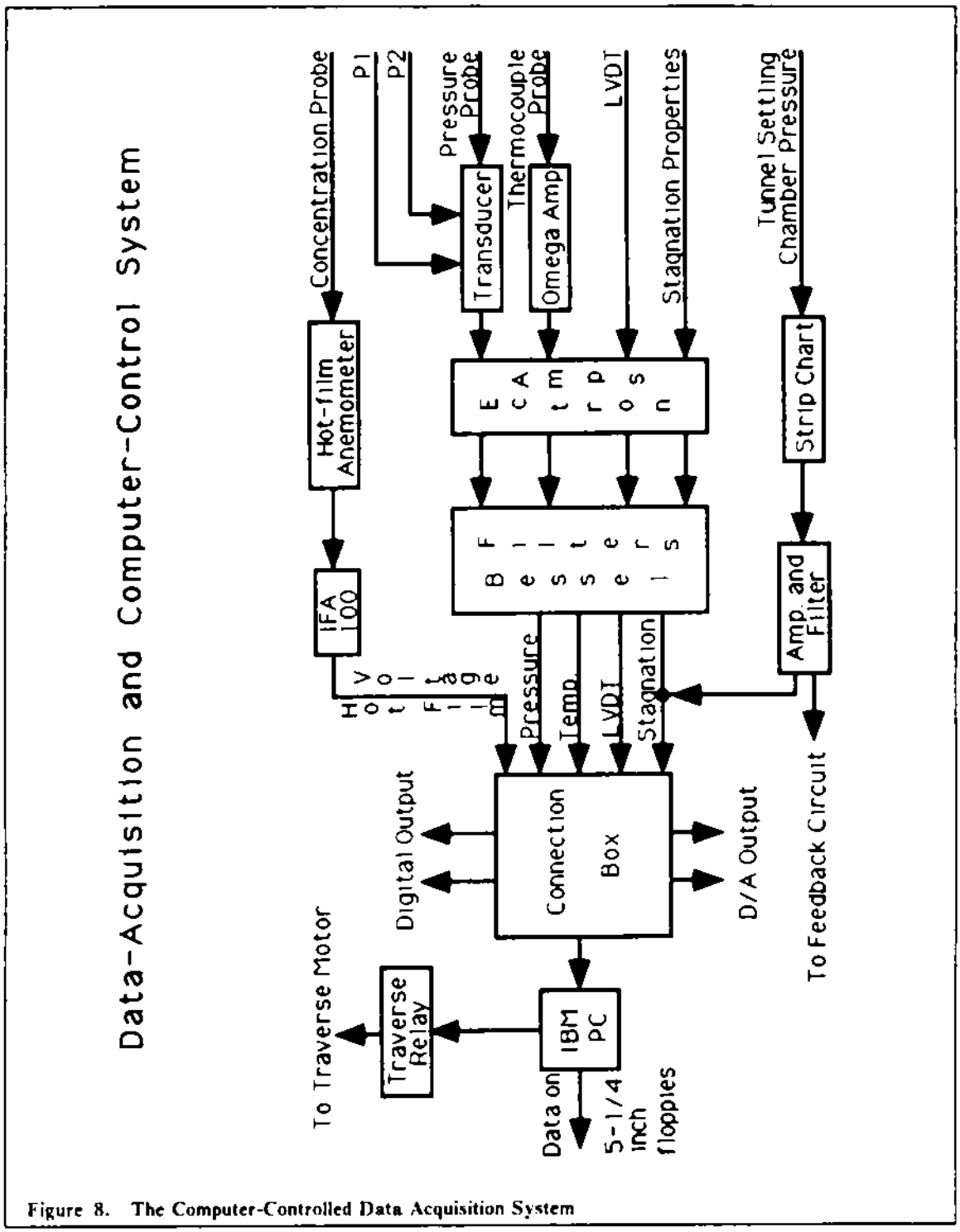

Figure 8. The Computer-Controlled Data Acquisition System

3.3 Other Support Instrumentation

All signals are conditioned for optimum voltage range and signal-to-noise ratio. An Ectron Model 562 DC amplifier driven by a Model 516-5SG Excitation Supply unit amplifies millivolt signals from the transducers by a maximum gain of 1000. With an array of six Ectron amplifiers, all signals are processed simultaneously. The amplifiers have standard gain and voltage-offset switches. In conjunction with the Ectrons, a custom-built array of six 4-pole Bessel low-pass filters removes any high-frequency noise from each signal. These filters cut-off at 340 Hz and have a range of $\pm$ 15 v .

The wind tunnel settling-chamber pressure transducer provides real-time monitoring of the tunnel operation. Consequently, if a problem arises, the anomaly can be quickly diagnosed and corrected. To facilitate this, a Hewlett-Packard 17501A strip chart recorder directly transfers the input pressure signal in millivolts to an output line graph. This procedure gives a constant, permanent visual history of the tunnel pressure.

Finally, the wind tunnel requires other support control circuits and equipment. These circuits operate valves not controlled by the computer and also switch tunnel operation between the main wind tunnel and a secondary tunnel. In addition, a tunnel control panel turns on a solenoid valve which provides water to the system, starts the compressors, and switches valves to begin loading the system with compressed air.

Chapter 4

PROBES AND RELATED INSTRUMENTATION

Four traversed probes and four stationary settling chamber probes detail the mean-flow quantities of the flow. All the traversed probes have a nominal vertical stem length of 13.3 cm (5.25 in) and a nominal streamwise extension (from probe tip to center of the vertical stem) of 7.62 cm (3 in). Also, fins soldered onto the body of the probes, another mutual aspect, limit yawing and tip deflection during runs. These probes are inserted through the 0.635-cm (1/4-in) holes in the model floorplate and fastened to the traverse assembly. The stationary probes are fixed at convenient locations in the tunnel and injector. Figure 9 depicts common features of the traversed probes.

The following sections detail individual aspects of each probe.

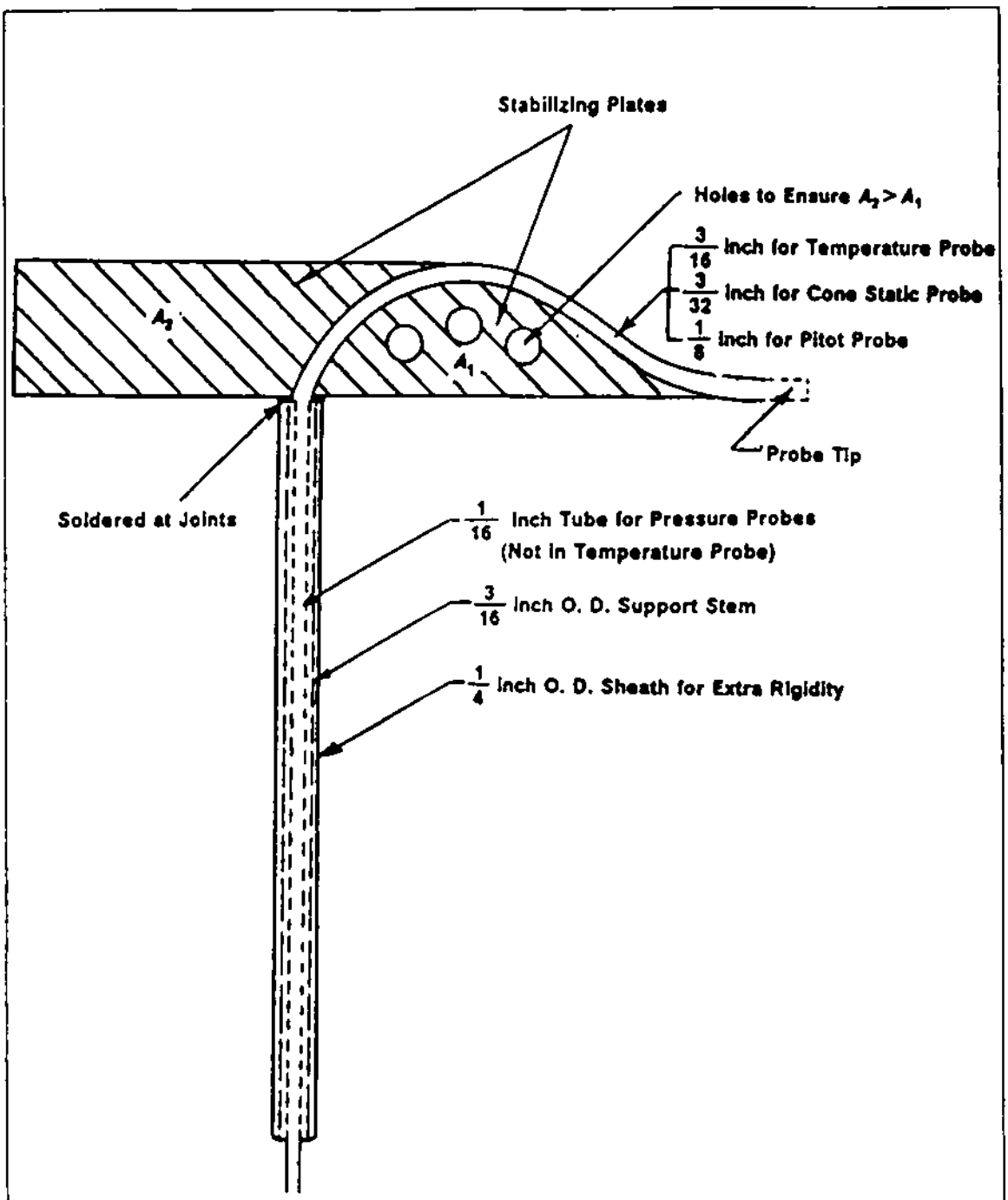

Figure 9. Common Aspects of the Traversed Probes

4.1 The Gas Concentration Measurement

A newly designed, custom-built aspirating probe measures the local steady-state gas concentration in the flowfield. The developmental procedure originates from one developed by Ng and Epstein[25] . In this design, a sample of the flow enters the probe but does not need to be stored for later analysis. On-site analysis is performed on the sample, which is easier and much faster. As shown in Figure 10, the probe design is fairly simple which helps when repairing the probe, and the final product proves very rugged and sturdy. In fact, the most delicate part of the probe, the hot film, usually lasts for many runs.

4.1.1 Principle of Operation

Inside the probe, suction through a hose attached to a nylon insert at the base of the probe pulls the gases to a vacuum. Suction serves two purposes: it causes the probe to swallow the standoff shock, so no flow spillage occurs and the entire sample is captured, and suction chokes the probe flow at an orifice inside the probe channel, thus "aspirating" the probe.

Derived from classical hot-wire theory and one-dimensional gas dynamics, the heat-transfer equation which describes the response of a constant-temperature hot film operating in a choked-exit flow is

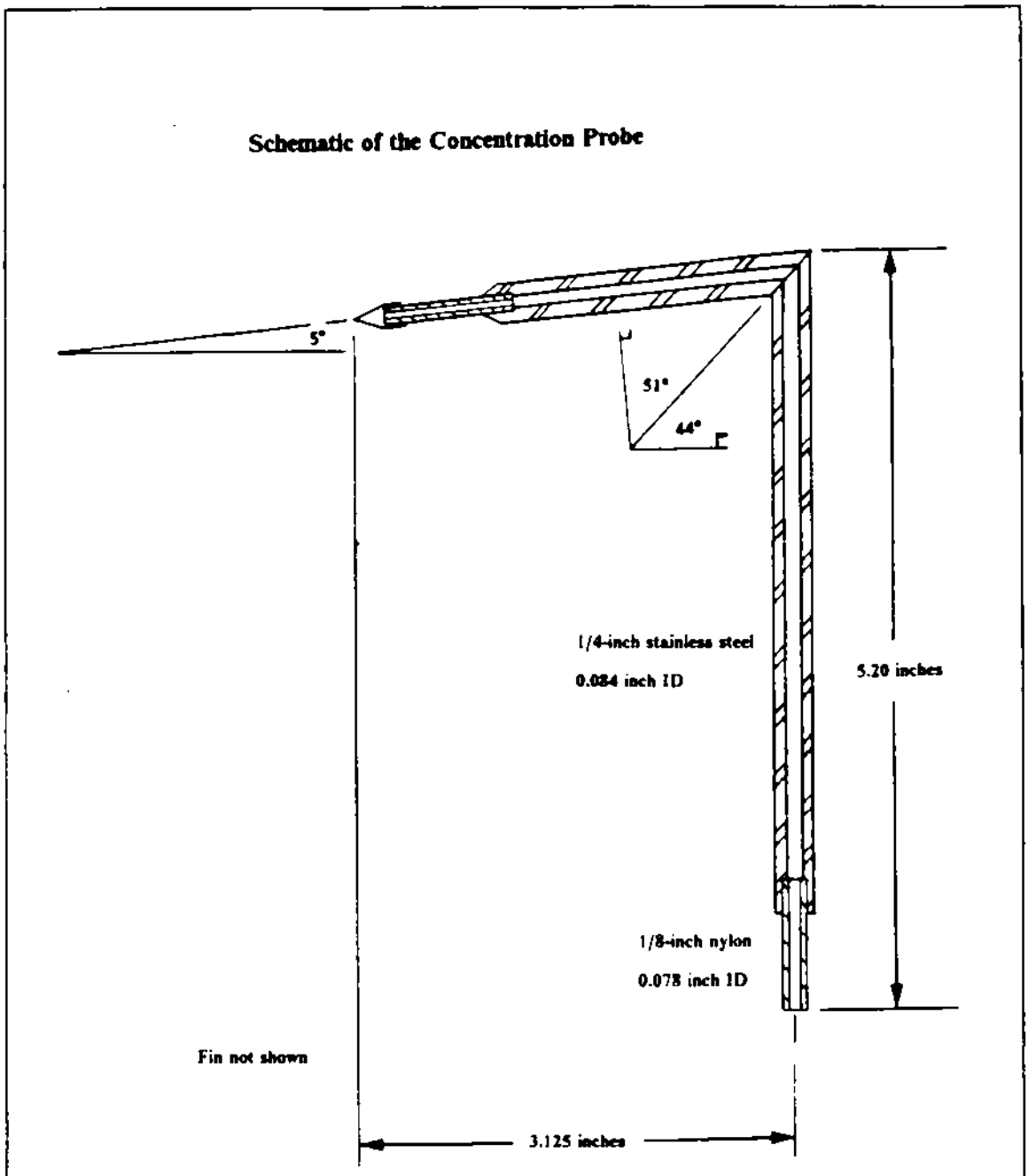

Figure 10. Schematic of the Concentration Probe

$$V^2 = \frac{(R_s + R_w)^2}{R_w} \pi l k \left\{ c \left[\frac{d}{\mu} \frac{P_t}{\sqrt{T_t}} \frac{A^*}{A_{ch}} \sqrt{\frac{\gamma}{R}} \left(\frac{2}{\gamma + 1} \right)^{\frac{\gamma+1}{2(\gamma-1)}} \right]^m + b \right\} (T_w - T_t) \quad [4.1]$$

With k, μ, γ, and R functions of gas composition, the above equation can be represented as

$$V^2 = f(\text{gas composition}, P_t, T_t) \quad [4.2]$$

Therefore, with P_t and T_t known, the formula empirically retrieves gas composition.

4.1.2 Probe Configuration

The body of the probe consists of two, spot-welded 0.635-cm (1/4-in) stainless steel tubes. The probe streamwise extension inclines at a 5° angle to provide better access for measurements near the floor.

A 2.29-cm (0.9-in) stainless-steel extension with a 0.952-cm (0.375-in) aluminum diffuser cap houses most of the critical components of the probe. As seen in Figure 11, the cap has a 0.028-cm (0.011-in) inlet diameter, limiting the spacial resolution of the probe to 6.13×10^{-4} cm^2 (9.50×10^{-5} in^2). Inside the cap, a diverging channel merges with a 0.121-cm (0.0475-in) diameter constant-area channel beginning at the hot-film plane within the extension. Subsequently, the

flow accelerates through a 0.056-cm (0.022-in) orifice, the sonic throat. By one-dimensional gas dynamics, the area ratios are chosen to allow for this choking and also to swallow the stand-off shock and insure that the supersonic flow shocks down between the inlet and the hot-film plane inside the probe. The hot film is a TSI 101212-20 sensor with a diameter of 0.0051 cm (0.002 in) and a sensor length of 0.102 cm (0.040 in), which gives an l/d of 20.

A pressure tap 0.127 cm (0.05 in) in diameter drilled in the probe-extension wall ahead of the sonic orifice measures the total pressure in the 0.121-cm channel. In reality, this measurement is the wall static pressure; however, the Mach number of the flow decreases to about 0.05 in the constant-area channel resulting in a P/P_t of 0.998. Therefore, in the 0.121-cm duct, the static pressure is essentially the total pressure. This pressure is called *P1* and functions as P_t in Eqn. [4.2]. A second hole is placed far enough beyond the sonic orifice to allow a back pressure measurement; this is *P2*. Moreover, the ratio *P2/P1* indicates whether the suction chokes the orifice; of course, the *P2/P1* criterion depends on gas composition, but it is around 0.5. Hypodermic tubing leads the pressures to receiving transducers. The *P1* measurement goes into a Statham PA285TC-50-350 0-50 psia transducer (better than ± 0.034 atm accuracy, infinite resolution); *P2* is sent to a MB Electronics Model 151-EBAP-236 0-10 psia transducer (± 0.007 atm, infinite resolution). Ectron amplifiers and Bessel filters condition the final signals so that the input to the A/D converter falls within the appropriate 0 to 10-volt range. The time response of the *P1* and *P2*

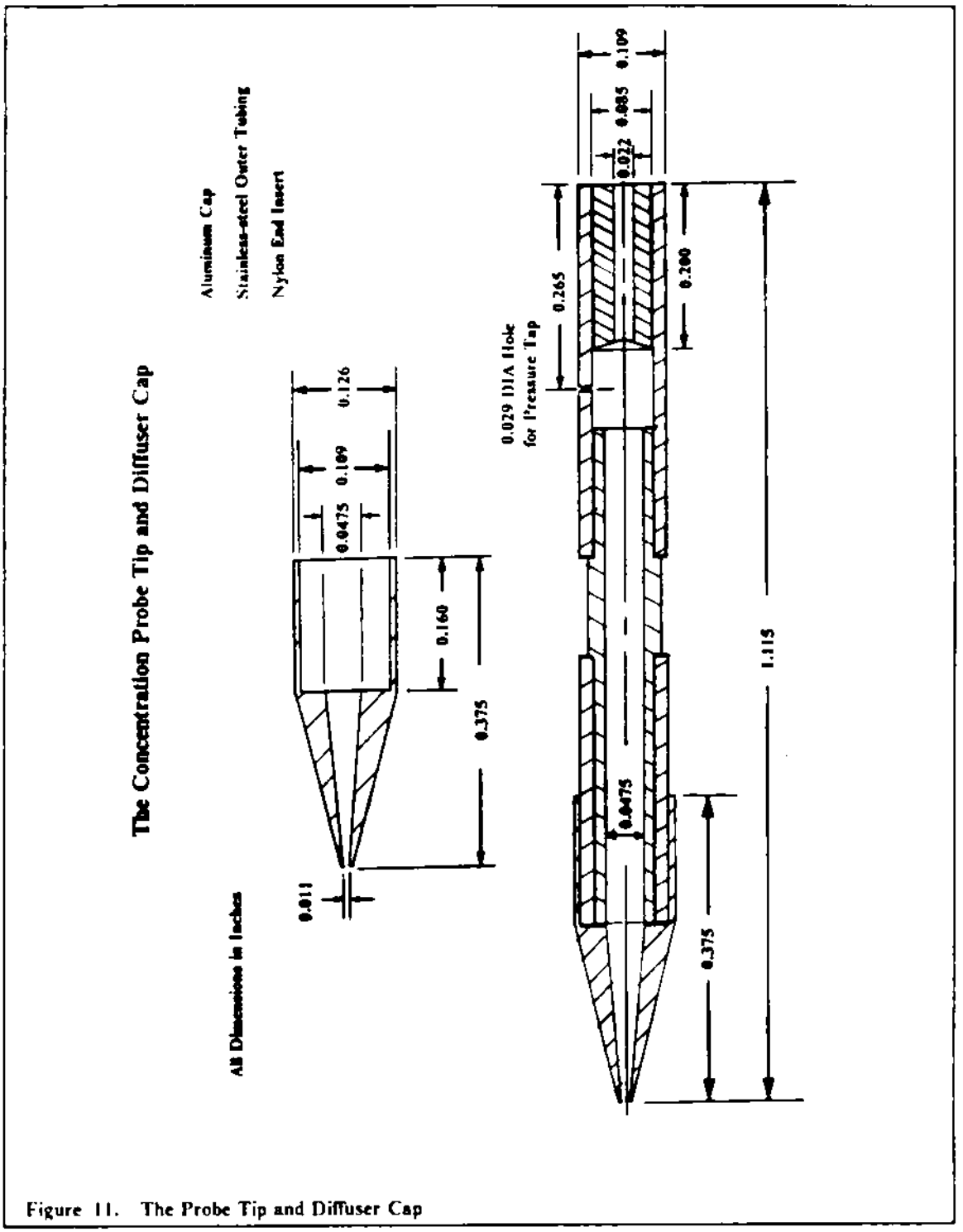

Figure 11. The Probe Tip and Diffuser Cap

measurements is on the order of 0.05 to 0.1 sec (similar to the cone-static probe response).

In contrast, because of the small size of the probe extension, a separate traverse using a diffuser thermocouple probe is required for the stagnation temperature profile. Though a shock of less strength occurs in front of the temperature probe as compared to the shock in the concentration probe, the after-shock total temperature in both cases is just the total temperature ahead of the shock, since stagnation temperature remains constant across a shock. Therefore, the total temperature as read by the thermocouple probe is the same as that seen by the hot film. Of course, some discrepancies can occur due to the temperature being taken in a separate run than the hot film and total pressure, which are sampled together. The differences are small, however. For example, the tunnel freestream differs no more than 5 percent from run to run, and the injectant temperature changes by only 1 percent from run to run. Moreover, during a run, the freestream temperature drops by about 2.5 percent maximum while the injectant temperature decreases by less than 1 percent. So, with these small variations coupled with the observed property that temperature changes of 10° K not alter the resulting concentration level significantly (see **App. C**), these effects can be neglected. Nonetheless, the nondimensionalization scheme accounts for most of these variations.

The two lead wires from the probe extension connect to a BNC junction that joins to a coaxial cable fastened to a Dantec anemometer, a 55M01 Main Unit coupled with a 55M10 CTA Standard Bridge. The output from the Dantec goes

into a TSI Intelligent Flow Analyzer Model 100 (IFA-100) which filters the input at 300 Hz and offsets the signal to within the required 0-10 volt range. On the high end, the hot-film voltage usually exceeds 10 volts, so that this DC adjustment prevents clipping of the signal. The 300-Hz limit cuts off the high-frequency background noise coupled with the signal. At the maximum level, this noise fluctuates at 0.2 v peak-to peak. This level is very high compared to noise from an identical bare hot film in quiescent air, about 2 mv peak-to-peak. A reason for the noise may be due to oscillation of the swallowed shock within the diffuser cap[36].

In its present configuration, the concentration probe has an accuracy slightly better than about 2 percent mole fraction of helium. A numerical error analysis combines the maximum errors incurred in the *PI* measurement ($\pm$ 1 percent), the total temperature measurement ($\pm$ 2 percent), and the day-to-day drift of the hot-film dc voltage (1 percent) to retrieve this error band. The voltage variation arises from sensor aging, instrument drift, and usage[36]. Reference [37] gives more information on the concentration probe.

4.2 The Pressure Measurement

For a complete set of data, four pressure probes measure four different pressure quantities in the flow. Two separate pressure probes are traversed vertically through the flowfield. A Pitot probe reads the total pressure behind a

normal shock, and a cone-static probe records the surface cone pressure behind an oblique shock emanating from the cone tip. In addition, two stationary instruments record the total pressures in the tunnel and the injector.

4.2.1 The Traversed Pressure Probes

The Pitot probe has a rectangular inlet 0.042 X 0.310 cm (0.0165 X 0.122 in), and a lip thickness of 0.00254 cm (0.001 in), resulting in a capture area of 1.3 mm^2 (0.002 in^2) . The inlet is shaped from 0.317-cm (1/8-in) stainless steel tubing which connects to 0.159-cm (1/16-in) tubing that runs down the vertical stem of the probe. A 0.476-cm (3/16-in) inner sleeve and a 0.635-cm (1/4-in) outer sheath stiffen and protect the stem. Also, soldered to the probe body, two fins add stability: one fin prevents excessive flexing of the streamwise extension of the probe and the second stabilizes in yaw ($A1$ and $A2$, respectively). Tygon tubing attaches to a 0.159-cm OD extension at the base of the stem and leads to a Statham PA285TC-50-350 pressure transducer.

For the cone-static probe, a brass cone with a 10-degree ($\pm$ 2 arc minutes) semivertex angle is fixed onto the tip of the probe body. The cone base diameter is 0.157 cm (0.062 in). The cone has four 0.033-cm (0.013-in) diameter pressure ports drilled 0.27 cm (0.106 in) from the cone tip and 90° angles from one another. Joined by a common chamber, the four separate pressure measurements coalesce into one averaged value. This design corrects any small misalignment of the probe and mitigates adverse influences from small fluctuations within a

flow region, as long as gradients are not too great within this region, such as across a shock. The probe has a capture area of 1.0 mm^2 (0.002 in^2) and a 0.08-second time response, the slower of the two probes[23] . Other external details are similar to the Pitot probe (Figure 9 on page 26). Figure 12 details the brass cone tip.

From the probe, the pressure information goes on to a MB Electronics 0-0.681 atm (0-10 psia) pressure transducer. Each pressure signal passes through an Ectron amplifier and a 4-pole Bessel filter for final signal conditioning.

4.2.2 The Settling Chamber Pressure Probes

A Pitot probe connected to a 0-6.8 atm (0-100 psia) Setra Systems 50 mv/1 psia pressure transducer measures P_{t_∞}, total pressure in the wind tunnel settling chamber. This signal feeds into the strip chart recorder. The transmission is subsequently amplified, filtered, and sent to the A/D converter. The same signal also runs through the controller feedback circuit to adjust the free-stream pressure to the desired level.

Inserted through a hole drilled into the injector housing, another small Pitot tube monitors the total pressure in the injector plenum chamber. The 0.159-cm (1/16-in) plastic tubing carries the pressure to a Heise C-53332 $\pm$ 0.0034atm ($\pm$ 0.05 psia) pressure dial for visual, real-time verification of the pressure and also to a Statham PA285TC-50-350 transducer. Again, the final signal is amplified and filtered.

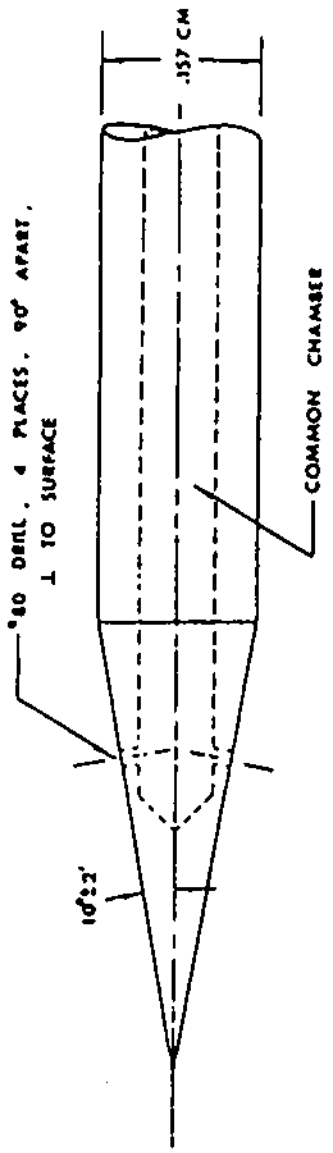

Figure 12. The Cone-Static Probe Tip

4.3 The Temperature Measurement

Stagnation temperature measurements characterize the temperature distribution in the flowfield. A single thermocouple probe details the temperature profile in the tunnel flow, and two separate stationary probes track the wind tunnel and injector settling chamber temperatures.

4.3.1 The Traversed Temperature Probe

A ceramic-tipped, vented thermocouple probe profiles the after-shock stagnation temperature T_{t2} at the four stations. The ceramic cap and vent holes provide radiation protection and sufficient outflow to produce a 0.98 recovery factor[23] (Figure 13). Located 0.953 cm (0.375 in) from the tip on opposite sides of the cap, the discharge holes are 0.038 cm (0.015 in) in diameter. The probe has an inlet diameter of 0.19 cm (0.075 in). The outer sheath is 0.635-cm (1/4-in) tubing, and a fin stabilizes the probe in yaw.

The working end of the probe consists of an Omega Engineering Type-K (Chromel-Alumel) butt-welded thermocouple wire housed in a 0.476-cm (3/16-in) stainless-steel extension. The wire has a 0.0127-cm (0.005-in) diameter with a thermal time response of 0.1 second. The lead wires run to an adaptor that plugs into an Omega Engineering Thermocouple DC Millivolt OMNI IIB amplifier

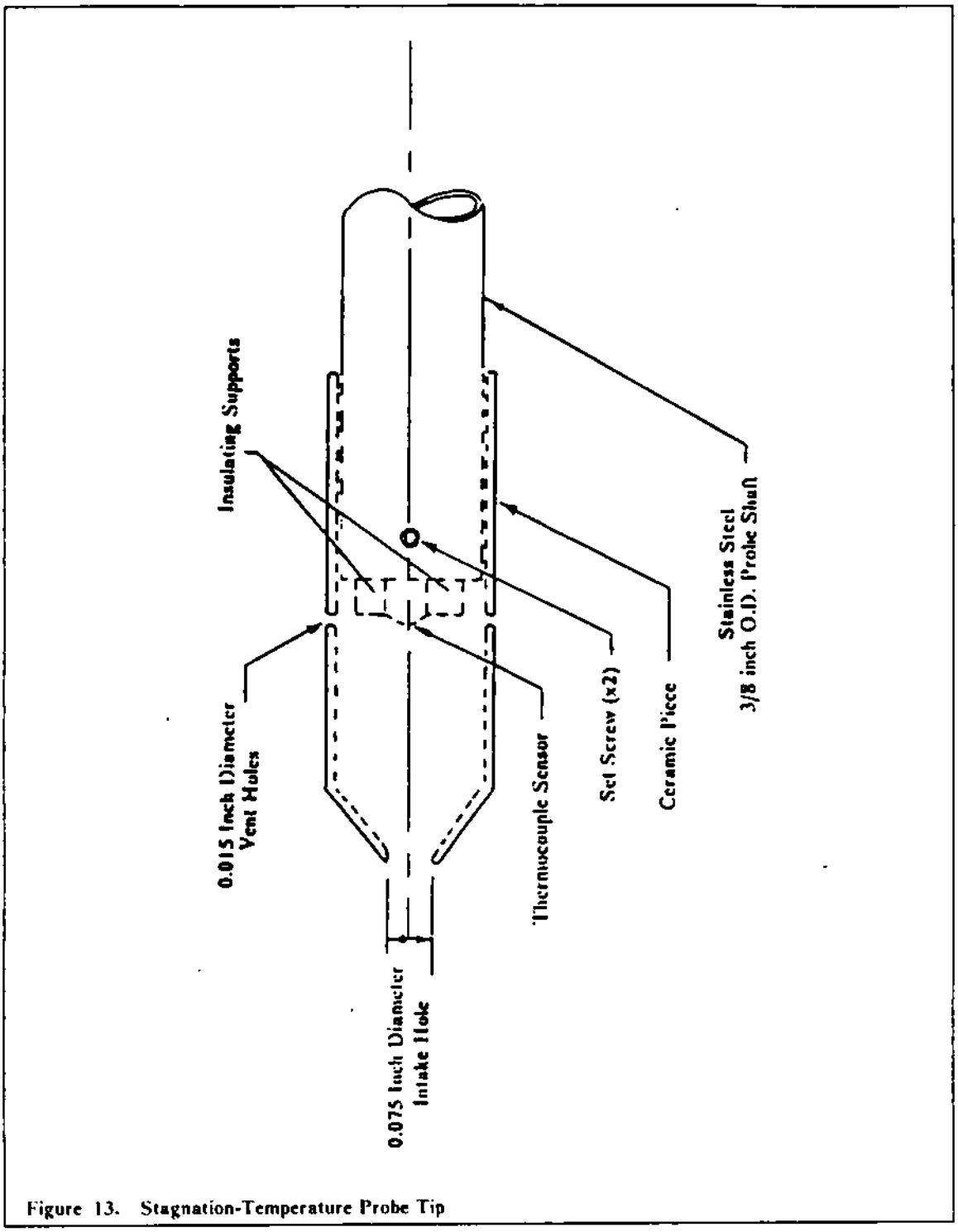

Figure 13. Stagnation-Temperature Probe Tip

that has an electronic ice-point reference junction. An Ectron amplifier supplements the signal.

4.3.2 The Settling Chamber Temperature Probes

In both the tunnel settling chamber and the injector plenum chamber, Omega Type-K thermocouples in conjunction with Omega amplifiers track the temperature. A probe similar to the settling chamber pressure probe is inserted into the tunnel chamber. For the injector measurement, epoxy attaches the thermocouple to a brass pipe fitting; the fitting screws into a tapped hole underneath the injector block. Once again, the millivolt output from the Omega system is amplified and filtered so the final signal falls between 0 and 10 volts.

Chapter 5

PROCEDURES AND DATA PROCESSING

This chapter includes a description of the calibration procedure for each of the probes and related equipment, a typical tunnel run, and the data-reduction process. With the four unprocessed profiles--hot-film voltage, thermocouple, and Pitot and cone-static pressures--and accompanying measurements, calibration constants are applied to the digital data to obtain files in engineering units. A FORTRAN program then reduces the hot-film data to a concentration profile, and another FORTRAN program subsequently takes this profile and applies it to the processing of the other profiles to retrieve Mach number, density, velocity, and mass-flux distributions across the shear layer at the four stations.

5.1 Calibration

All probes and equipment are calibrated so that digital data sampled by the Metrabyte board can be converted to engineering units. This procedure involves subjecting a probe to the controlled variation of pertinent variables which affect the response of the probe. A least-squares fit produces a calibration curve.

5.1.1 The Aspirated, Concentration Probe

The calibration of the concentration probe is the longest and most difficult to make. The calibration takes 3 to 4 hours and requires careful, incremental monitoring of the flow variables.

After the hot-film sensor is tuned for stable response, the probe is calibrated in the special setup shown in Figure 14. An air cylinder and a helium cylinder supply gases to a 11500 cm^3 (700 in^3) pressure vessel. The vessel has openings for a thermocouple, a pressure tube, and the concentration probe. Suction is provided by a Welch Scientific Company Model-1402 Duo-seal vacuum pump powered by a General Electric Model 5KC42JG14E 1/2-hp AC motor.

The calibration procedure involves pressurizing the vessel with a known mixture of helium and air and systematically varying the tank pressure with suction. The anemometer voltage output, *P1* (pressure before the throat), *P2* (pressure after the throat), and T_t are then recorded. This procedure is repeated

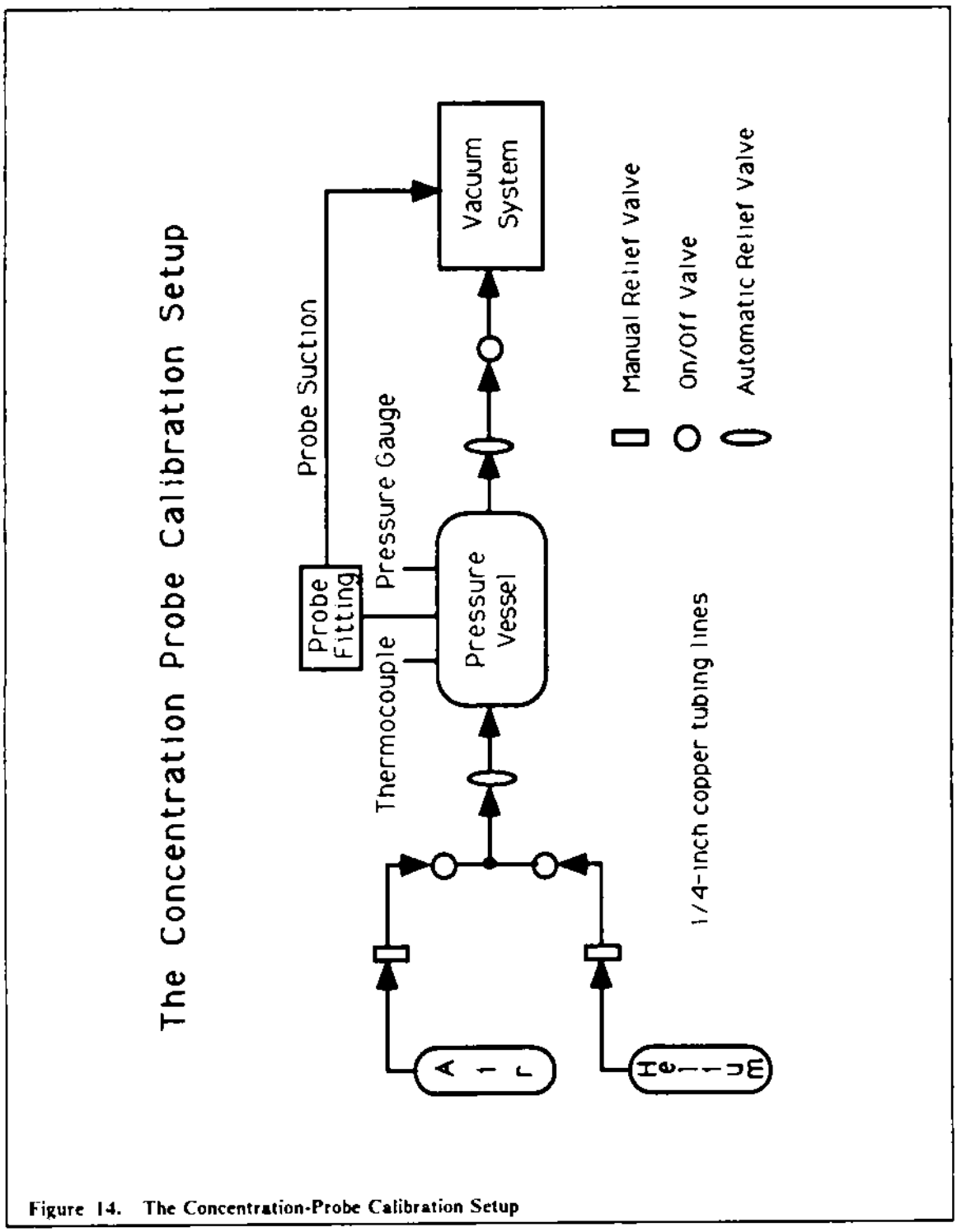

Figure 14. The Concentration-Probe Calibration Setup

at several gas compositions. Partial pressures exactly determine the mole fraction of a gas mixture, i. e.,

$$\chi_i = \frac{\text{Moles of } i}{\text{Moles of } m} = \frac{P_i}{P_m} \qquad [5.1]$$

where i is the gas constituent and m refers to the mixture properties. Also, the mole fraction equals identically the volume fraction v_i, i. e.,

$$v_i = \frac{\text{Volume of } i}{\text{Volume of } m} \equiv \chi_i \qquad [5.2]$$

and the mass fraction α_i is determined from the mole fraction by

$$\alpha_i = \frac{\text{Mass of } i}{\text{Mass of } m} = \chi_i \times \frac{MW_i}{MW_m} \qquad [5.3]$$

A FORTRAN program fits a least-squares curve to the points, thus obtaining a functional relationship with a set of constants c, b, and m (see Eqn. [4.1]) for each concentration. The maximum error from the curve fit is 2 percent. Further details are provided in Reference [37].

5.1.2 The Pitot Probe

The Pitot-probe calibration requires application of a known pressure to the transducer. The equipment is arranged exactly as in the test setup to eliminate any inconsistencies due solely to differences in preparation. To calibrate the

transducer, a compressed-air cylinder forces air to the input port of an AMETEK Pneumatic Pressure Tester (Type-K, Model-MK100, accurate to $\pm$ 0.05 percent). The output port of this "dead-weight" tester connects to the pressure transducer. Known weights are added to a column on the tester, and air is supplied until the force of the compressed air lifts the stack of weights. The voltage at the A/D converter is correlated to this pressure so that for several calibration points a curve-fit program can superimpose a line over the points. The maximum error in the line fit is 0.1 percent.

This procedure remains the same for the *PI* measurement in the concentration probe since both the Pitot and *PI* pressures use the same type of transducer.

5.1.3 The Cone-Static Probe

The pressure on the cone surface for the investigated flow regime stays below atmospheric pressure; therefore, the dead weight tester cannot be used since it does not function below atmospheric pressure. This probe also requires a transducer with greater sensitivity than the one used for the Pitot measurement. So, for this probe, a Pressure Systems, Inc., (PSi) Digital Pressure Measurement System calibrates the output from the MB Electronics 0-10 psia transducer against known reference pressures. It contains a 32-port transducer array ($\pm$ 15 psig range) , a pressure calibration unit (PCU), and a data acquisition and control unit (DACU). A port on the transducer array and the transducer are

connected to a small pressure cylinder at atmospheric pressure; another end of the cylinder leads to a small vacuum pump which provides suction to decrease the pressure in the cylinder. At each pressure, the PSi system self-calibrates from the supplied reference pressures, samples the pressure at its transducer array, and converts the data to engineering units. At the same time, the IBM-PC scans the signal from the 0-0.681 atm (0-10 psia) transducer. A line fits a functional relation to the data with an error of 0.2 percent. *P2* calibration is the same.

5.1.4 The Thermocouple Probe

The thermocouple is calibrated by placing the probe in a beaker of distilled water and varying the water temperature over a range of 0°C to 100°C. With the instrumentation configured as in the experiment, the tip of a self-calibrating Omega Engineering HH-80K thermocouple (accurate to 0.1°C) measures the flow temperature near the entrance to the traversed probe. Ice first lowers the water temperature to near-freezing. Then an electrical heater increases the water temperature gradually from the cold point to near-boiling. Several points are taken in this range. The line fit gives a typical maximum error of 0.2 percent.

5.1.5 The Settling Chamber Probes

The settling chamber probes are calibrated exactly like the traversed probes. Specifically, the P_{t_∞} measurement requires the pneumatic pressure tester to calibrate up to 7 atm, since in this study the tunnel works steadily at 6.5 atm. Since the pressure levels are lower (0.4 to 1.4 atm), the PSi systems is used to calibrate P_{t_j}. The two settling chamber thermocouples use the exact same calibration method as the traversed thermocouple; in fact, since these temperature probes all have Type-K thermocouple wires, each probe can be plugged into another probe's setup without needing to recalibrate the system. The functional relations give an error of about 0.2 percent in all cases.

5.1.6 The Probe Position

For convenience, this investigation defines x as the streamwise direction positive downstream and y as the vertical direction with the origin at the bottom of the slot exit plane on the floorplate. Therefore, the axial stations are arranged along the x-axis with the probe at each x location traversing up in the positive y-direction. The z-axis runs along the width of the slot. Since the flow is essentially two-dimensional, this dimension is not important.

The vertical position is indicated by the LVDT. The LVDT is calibrated against the vertical height so that the exact location of the probe at any given instant in time will be known. A PTI cathetometer (Cat. No. 2210) indicates

relative distances to ± 0.001 cm (see **App. A** for uncertainty). Initially, because the cathetometer rests on a separate platform, three adjustment screws on the base of the instrument align the scope with both the x and y-planes of the test section model, which is not inclined the same as the cathetometer platform. Two pairs of points act as reference locations during this adjustment: one pair along the width of the slot area provides the x-plane alignment, and the second lies along the length of the floorplate, thus giving the y-plane orientation. For example, the scope focuses on a point on the floorplate near the slot, and the platform screws adjust the instrument until the scope crosshairs intersect exactly at that point. Then, the scope focuses on a second point at the back end of the floorplate. If the crosshairs intersect at this second reference point without altering the screw settings, then no adjustment is necessary, and the scope lines up with this plane. If not, a change is made. Of course, this procedure results in an iterative method in that the adjustment for one point slightly shifts the relative position of the others, so that a number of slight readjustments are necessary to home in on the final orientation. Next, a 1.27 cm (0.5 in)-high machined block with one corner situated near the tip of a probe fixes the probe offset from the floorplate. The cathetometer measures the corner, and then 1.27 cm is subtracted from this reading to give the relative floor position. Now, with the offset known, the traverse moves the probe to several y-positions to map out the entire traversed height. The LVDT-signal adjustment rod assures the final output falls within the prescribed 0 to 10-volt range. A line relates these calibration points with about 1 percent error. This calibration is done at every

station for each probe before a tunnel run, except that the orientation of the cathetometer with the test section needs to be done only once. Figure 15 summarizes the reference points used in the cathetometer alignment and LVDT calibration procedures.

5.2 A Tunnel Run

Before every tunnel-run sequence, all equipment, instrumentation, and connections and the helium supply are checked for proper operation. Then the tunnel control panel switches on the compressors, which pump the storage tanks from atmospheric pressure to a holding level of 9.5 atm (140 psia). Next, the FORTRAN program which controls the tunnel and takes data is initialized; this includes entering governing parameters into the program such as a sample rate of 150 Hz (sufficient to encode all the low-frequency signals), a tunnel pressure of 6.5 atm, traverse commands, time delays to allow proper sequencing, and channel numbers (usually 6 channels per run).

When the air in the storage tanks reaches the correct pressure, the IBM-PC initiates the run. After a 2-sec lapse from the time the program is triggered, the on/off butterfly valve opens, releasing the compressed air into the wind tunnel. This moment is denoted time $t = 0$ sec for reference and convenience. The helium supply switches on at $t = 4$ sec, and at 6 sec the traverse starts moving the probe up and data acquisition begins. These delays allow all flow transients

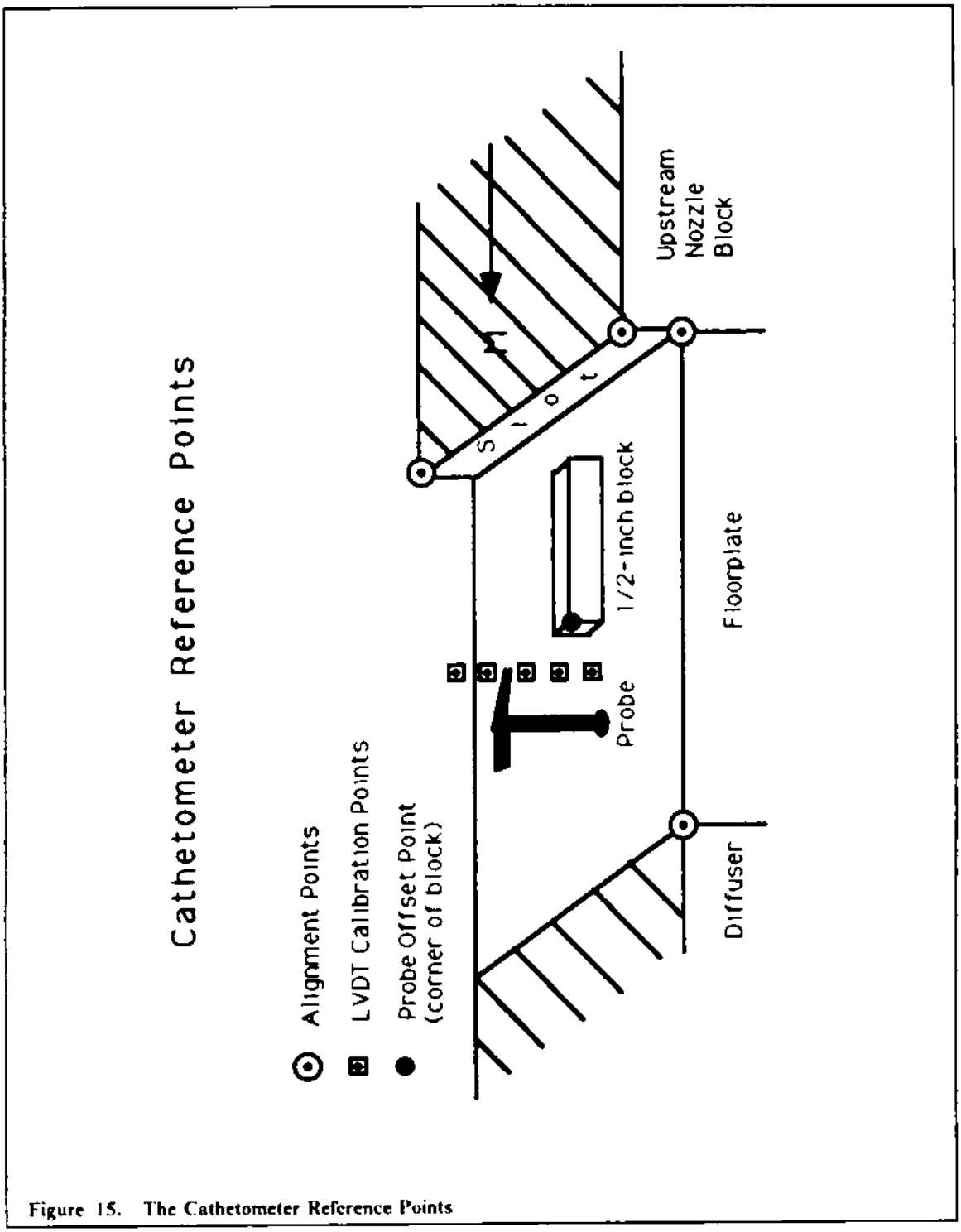

Figure 15. The Cathetometer Reference Points

to dampen out and permit the slot and freestream-flow interaction to develop fully. Moreover, by not raising the probe until 6 sec later, the disruptive starting shock can pass through the test section while the probe is protected behind the slot step. A Schlieren or Shadowgraph picture is taken any time after this 6-sec lapse. The probe traverses to an average height of $y/H = 2.4$ (3.05 cm) in 7.5 sec, a resulting mean velocity of 0.406 cm/sec. Several runs at different speeds confirm that a rate of 0.406 cm/sec captures all mean-flow information and assures that the complete traverse finishes in the limited run time. At $y/H = 2.4$ at all four stations, the probe is above the mixing layer so that helium concentration goes to 0 ($\chi_{He} = 0.00$). This known 0 percent helium region provides a reference which accounts for any small day-to-day drifts in hot-film voltage on every run. Though usually these shifts are small or negligible, this reference, nevertheless, aids in later concentration reduction.

The IBM-PC samples data for 8 sec and only on the upward traverse. When the probe reaches the top, the helium is turned off, the probe traverses down in 1 sec to save time, and the tunnel shuts down 1 sec after the probe reaches the bottom. Again, the probe is protected behind the slot step from strong transient forces arising from the shutdown. The total run time, from the instant the valve opens to the moment it closes, is 16 sec. Because of the blowdown nature of the wind tunnel, the tunnel cannot run for any longer at a 6.5-atm freestream pressure level.

The computer writes the scanned data from RAM to floppy disks where the files are renamed appropriately. A compiled BASIC plotter graphs the data, thus

giving on-the-spot examination of the data to check for incongruities before continuing. If all is well, the system is reconfigured for another run. Ostensibly, four runs (four probes) per measurement station (16 runs total) can completely document the flowfield quantitatively, and four runs each for Schlieren and Shadowgraph pictures (8 runs total) are enough to photograph the entire flow. Of course, extra runs are required to experiment with certain aspects of the test configuration and to correct problems.

5.3 Data Reduction

The data reduction process is divided into two parts: the concentration reduction, completely independent of the other mean-flow measurements (except T_{t2}), is processed first, and then the resulting concentration, Pitot pressure, cone-static pressure, and thermocouple profiles are combined to retrieve Mach number, density, velocity, and mass flux distributions. The concentration calibration curves convert the hot-film voltages to mole fraction of helium in the mixture. The more routine mean-flow reductions employ standard flow equations to retrieve the final quantities.

5.3.1 The Concentration Reduction

In the gas concentration reduction, the hot-film voltage, PI, and T_{t2} are processed into a single concentration profile. After applying calibration constants to the raw pressure and temperature data files, a BASIC program combines these files and the LVDT file into one large file for input into the reduction program. But first, since T_{t2} comes from the thermocouple probe and thus a separate run from the concentration probe, a FORTRAN code matches the LVDT signal of T_{t2} point-by-point to the LVDT signal of the concentration probe, thereby shifting the T_{t2} profile. T_{t2} values corresponding to the LVDT values that overlap the LVDT values of the concentration probe are interpolated to give the new shifted numbers, and for points that do not overlay, the T_{t2} signal is assumed constant in this region. This region usually coincides with the near wall region so that the adiabatic wall temperature can be used as a reference value; however, to calculate this number, the edge velocity needs to be known, so that either a value is assumed or a retroactive procedure is required. As previously stated, though, a moderate temperature difference does not alter the concentration significantly, so that in all likelihood an adiabatic-wall temperature correction will have little significance. With the input data file and a calibration file containing all the calibration constants and system parameters, a FORTRAN reduction code (Program 2 in **App. F**) takes PI and T_{t2} and uses Eqn. [4.2] to calculate lower and upper voltage bounds at calibrated concentration levels (for example, at the start, $\chi_{He} = 0.00$ and 0.25). If the experimental voltage does not

fall within this range of χ_{He}, the program steps the concentration bounds (for example, to $\chi_{He} = 0.25$ and 0.50) and compares the new calculated voltages to the voltage data point. Once the code finds an appropriate range, it interpolates between the limiting values by relative voltage positions to retrieve the experimental χ_{He}. Then Eqn. [5.3] reduces the mole fraction data to mass fraction α_{He}, which provides an alternate way to present the concentration results. Values which describe core decay and penetration of the mixing layer into the freestream are tabulated in these data files.

5.3.2 The Mean-Flow Reduction

A FORTRAN program (Program 3 in **App. F**) combines the concentration profile with the Pitot, cone-static, and temperature measurements to retrieve the remaining mean-flow values. The program employs shock and isentropic relations to find Mach number, density, velocity, and static quantities in the flowfield. The concentration distribution gives γ and the gas constant R for input into the standard flow equations.

First, the ratio of cone-static pressure to Pitot pressure P_c/P_{t2} determines the overall flow dynamics at any measured point and, consequently, the necessary routine to reduce the data. This ratio is compared to a table of critical P_c/P_{t2} values obtained from two equations which relate the pressure-probe data to certain important aspects of the flowfield. One is the Rayleigh Pitot Formula, expressed as

$$\frac{P_1}{P_{t2}} = \frac{\left(\frac{2\gamma}{\gamma+1} M_1^2 - \frac{\gamma-1}{\gamma+1}\right)^{\frac{1}{\gamma-1}}}{\left(\frac{\gamma+1}{2} M_1^2\right)^{\frac{\gamma}{\gamma-1}}} = f1(M_1, \gamma) \qquad [5.4]$$

and the second is the cone-flow equation

$$\frac{P_c}{P_1} = 1 + \frac{\gamma M_1^2}{2} \frac{(P_c - P_1)}{q_1} \qquad [5.5]$$

Since $\frac{P_c - P_1}{q_1} = f(M_1, \gamma)$ for a specified cone half-angle, multiplying the two equations results in

$$\frac{P_c}{P_{t2}} = f2(M_1, \gamma) \qquad [5.6]$$

P_c $P_{t2}|_{crit}$ defines the region where the Mach number is low enough (about $M_1 = 1.1$) that the shock emanating from the cone tip on the cone-static probe becomes detached. In this instance, the cone-flow equation no longer applies. Therefore, P_c/P_{t2} from the data must be less than this critical pressure ratio to apply Equations [5.4] and [5.5]. If not, the mean-flow quantities then are found alternatively. This condition represents the cases dealing with subsonic flow and near-sonic supersonic flow which may occur in a boundary layer or in the wake behind the splitter plate.

If P_c/P_{t2} is below $P_c/P_{t2}|_{crit}$ then the program interpolates for the corresponding M_1 using a table of values generated from Eqns. [5.4] and [5.5] and

the known γ. Table 1 gives these values as well as the critical P_c/P_{t2} values. With M_1, the Rayleigh Pitot Formula determines P_1 from $P_1 = P_{t2} f1(M_1, \gamma)$.

If P_c/P_{t2} is greater than the critical value, then the above method does not work. In this case, the code interpolates for P_1 according to the upper and lower values of P_1 found previously which bound this region. At this point, the program produces a complete P_1 profile. Next, the program tests if the flow in this region is subsonic or still supersonic by comparing the P_1/P_{t2} to the sonic values obtained from the Rayleigh Pitot Formula. This $P_1/P_{t2}|_{crit}$ value varies from 0.4867 for all helium to 0.5283 for all air. If P_1/P_{t2} is less than the critical value, then the flow remains supersonic, but the shock detaches from the cone tip. In this case, the program iterates for M_1 from Eqn. [5.4] using the shooting method. If P_1/P_{t2} is greater than the critical value, then the flow becomes subsonic and $P_{t2} = P_{t1}$. M_1 comes from the isentropic relation

$$M_1 = \left\{ \frac{2}{\gamma - 1} \left[\left(\frac{P_1}{P_{t2}} \right)^{-\frac{\gamma-1}{\gamma}} - 1 \right] \right\}^{\frac{1}{2}} \qquad [5.7]$$

With M_1 and P_1 completely detailed, the program now retrieves the other mean-flow quantities. First, to obtain static temperature, the code uses

$$T_1 = \frac{T_{t1}}{1 + \frac{\gamma - 1}{2} M_1^2} \qquad [5.8]$$

but since $T_{t2} = T_{t1}$ across a shock, then

Table 1. Table of Pc/Pt2 Reference Values

GAMMA	M1 PCP1 PCPT2	M1 PCP1 PCPT2	M1 PCP1 PCPT2	M1 PCP1 PCPT2	M1 PCP1 PCPT2	M1 PCP1 PCPT2	M1 PCP1 PCPT2	M1 PCP1 PCPT2	M1 PCP1 PCPT2
1.38									
	1.12	1.40	1.70	2.00	2.30	2.60	2.90	3.20	3.50
	1.148	1.176	1.228	1.288	1.356	1.432	1.514	1.603	1.700
	.529	.389	.293	.231	.188	.158	.135	.119	.106
1.40									
	1.12	1.40	1.70	2.00	2.30	2.60	2.90	3.20	3.50
	1.150	1.179	1.231	1.292	1.362	1.438	1.522	1.612	1.710
	.526	.387	.291	.229	.187	.157	.135	.118	.105
1.44									
	1.12	1.40	1.70	2.00	2.30	2.60	2.90	3.20	3.50
	1.154	1.184	1.238	1.301	1.372	1.451	1.537	1.631	1.731
	.521	.382	.288	.226	.185	.155	.133	.117	.104
1.48									
	1.12	1.40	1.70	2.00	2.30	2.60	2.90	3.20	3.50
	1.159	1.189	1.244	1.310	1.383	1.464	1.553	1.649	1.753
	.516	.377	.284	.224	.182	.153	.132	.116	.104
1.52									
	1.13	1.40	1.70	2.00	2.30	2.60	2.90	3.20	3.50
	1.163	1.194	1.251	1.318	1.394	1.477	1.568	1.667	1.774
	.504	.373	.281	.221	.181	.152	.131	.115	.103
1.56									
	1.13	1.40	1.70	2.00	2.30	2.60	2.90	3.20	3.50
	1.168	1.200	1.258	1.327	1.404	1.490	1.584	1.686	1.796
	.499	.369	.278	.219	.179	.150	.130	.114	.102
1.60									
	1.13	1.40	1.70	2.00	2.30	2.60	2.90	3.20	3.50
	1.172	1.205	1.265	1.336	1.415	1.503	1.600	1.704	1.817
	.495	.365	.275	.216	.177	.149	.129	.113	.102
1.64									
	1.13	1.40	1.70	2.00	2.30	2.60	2.90	3.20	3.50
	1.177	1.210	1.272	1.344	1.426	1.516	1.615	1.723	1.839
	.490	.361	.272	.214	.175	.148	.128	.113	.101
1.67									
	1.13	1.40	1.70	2.00	2.30	2.60	2.90	3.20	3.50
	1.180	1.214	1.277	1.351	1.434	1.526	1.627	1.737	1.855
	.487	.358	.270	.213	.174	.147	.127	.112	.100

$$T_1 = \frac{T_{t2}}{1 + \frac{\gamma - 1}{2} M_1^2} \qquad [5.9]$$

The speed of sound a_1 is

$$a_1 = \sqrt{\gamma R T_1} \qquad [5.10]$$

which gives the velocity from

$$U_1 = M_1 a_1 \qquad [5.11]$$

The program solves the equation of state for an ideal gas mixture to obtain density ρ_1, i. e.,

$$\rho_1 = \frac{P_1}{R T_1} \qquad [5.12]$$

and then as a consistency check reduces P_{t1} from

$$P_{t1} = P_1 \left(1 + \frac{\gamma - 1}{2} M_1^2\right)^{\frac{\gamma}{\gamma - 1}} \qquad [5.13]$$

With these mean-flow quantities reduced, the program then creates dimensional output files.

5.3.3 Entrainment

Entrainment represents the amount of mainstream air transported into the mixing region by turbulence. This entrained air mixes freely with the helium as the shear layer spreads outward downstream. Furthermore, entrainment can be quantified by calculating the mass flow rate of the air flowing into the injectant region. First, the mass flow rate at Station 4 is computed by numerically integrating the St. 4 ρU profile over the total mixing zone. The limits of the integral are $y = 0$ at the floor to $y = \Delta$ (Δ is the top of the mixing zone at a station), i. e.,

$$\dot{m} = z\int_0^{\Delta} \rho U dy \qquad [5.14]$$

where z is a length in the slotwise direction (22.9 cm in the calculations). This length is constant across the shear layer and from station to station. The Δ value comes from the penetration data. Penetration P is defined as the y-location along a profile that first sees $\chi_{He} < 0.02$ (0.02 χ_{He} is the accuracy limit of the concentration measurement). Next, Eqn. [5.14] is modified so that the helium-jet mass flow (m_e or m_{He} at St. 1) can be deduced from the ρU profile at St. 1. This procedure gives the following:

$$\dot{m}_{He} = z\int_0^{\Delta} \alpha_{He}\rho U dy \qquad [5.15]$$

where Δ at St. 1 is simply the slot height. The following equation then computes the entrained-air mass flow:

$$\dot{m}_{ENT} = \dot{m}_{s4} - \dot{m}_e \qquad [5.16]$$

Therefore, m_{ENT} is the air entrained into the helium core by St. 4.

5.3.4 The Nondimensionalization Scheme

A FORTRAN program (Program 4 in **App. F**) processes the dimensional output from the mean-flow reduction code and produces the same data in non-dimensional form. Free-stream air ($\gamma = 1.4$) acts as a reference from which normalizing values are obtained. First, the slot height $H = 1.21$cm (0.475 in) normalizes all traverse positions so that distances are referred to in terms of the number of slot heights. Next, instead of using nominal freestream values of $M_\infty = 3$, $P_{t\infty} = 6.5$ atm, $P_{t2\infty} = 2.11$ atm, and $P_\infty = 0.177$ atm , the program employs averaged freestream values characteristic of each individual x-location. This procedure accounts for any slight variations in freestream values due to the presence of waves in the flow, which may alter values from one station to the next. Table 2 tabulates these non-dimensionalization numbers. Then, the computer code obtains a T_∞ profile from the $T_{t\infty}$ profile which the data-acqusition computer samples concurrently with the T_{t2} data. Finally, from the above freestream values, the program calculates a_∞, U_∞ , and ρ_∞ using Eqns. [5.10], [5.11], and [5.12], respectively.

Table 2. Nondimensionalization Parameters

Table 2: Nondimensionalization Parameters			
Station Number	$T_{t_2}(°K)$	$P_{t_{2\infty}}$(psia)	M_∞
1	287	31.75	2.97
2	287	28.99	3.19
3	287	32.43	3.09
4	287	34.05	2.93

In summary, the following is an outline of the non-dimensionalization scheme:

- $\frac{P_{t_2}(t)}{P_{t_\infty}(t)}$, $P_{t_\infty}(t)$ taken with Pitot run
- $\frac{P_c(t)}{P_{t_\infty}(t)}$, $P_{t_\infty}(t)$ taken with cone-static run
- $\frac{T_{t_2}(t)}{T_{t_\infty}(t)}$
- $\frac{a_1(t)}{a_\infty(t)}$
- $\frac{P_1(t)}{P_\infty}$
- $\frac{P_{t_1}(t)}{P_{t_\infty}(t)}$, $P_{t_\infty}(t)$ from Pitot run
- $\frac{T_1(t)}{T_\infty(t)}$
- $\frac{U_1(t)}{U_\infty(t)}$

- $\frac{\rho_1(t)}{\rho_\infty(t)}$

where t refers to a profile of time-dependent values (*note*: P_∞ is a single value constant over time derived from the averaged M_∞ and P_{t2} at each station). This non-dimensionalization scheme matches that used previously by Smith[23] in air-injection experiments and, therefore, gives a common basis to compare the helium cases here to the earlier results.

Chapter 6

RESULTS

Once processed, the results are tabulated and plotted. These results include flow visualization and data profiles. This chapter highlights important features of the data and emphasizes certain aspects of the helium-injection flowfield.

6.1 Flow Visualization

The photographs detail regions within the flowfield and the interaction at the boundaries between these regions. Spark-Schlieren pictures emphasize features dependent on the first derivative of density $\frac{\partial \rho}{\partial y}$ and, thus, expose density gradients. Figure 16 shows the helium slot-injection into freestream air. The flow moves from left to right, and the slot is located at the lower left corner. The

air-side boundary layer before the injection station can be seen. First, the air-side flow experiences a Prandtl-Meyer expansion around the lip of the splitter plate. The initial wave propagates into the freestream at 21° from the x-direction. The expansion fan is terminated by a lip shock, which straightens the flow with respect to the lower wall. This shock has a slight curvature through the freestream boundary layer and then extends up at 18.5° in the freestream.

An adjustment shock from the overexpanded base flow angles down from the splitter-plate lip to the wall at −31.5° from the x-direction. This shock reflects off the wall, deflects as it passes through the shear layer, and then propagates downstream at 22.0° in the freestream. Eventually, the lip shock and adjustment shock merge at $x/H = 16$. A couple of weaker shocks at about the same angle as the adjustment shock in the picture may be the tail end of a reflected shock originating inside the injector nozzle. The mainstream air passes through these disturbances and some weak waves and continues relatively undisturbed downstream. Of course, as described previously, the freestream characteristics change slightly from station to station due to these disturbances.

The initial separation line (or dividing streamline) between the air stream and the helium flow extends from the lip of the splitter plate. This feature shows up as a sharp white line from the lip that remains clearly defined until Station 2 where it gradually begins to diffuse into the enveloping shear layer. This line likely corresponds to the maximum density gradient. Because P_j is less than P_∞, the separation line deflects downward at −7° initially. The lowest point of the deflection occurs at $x/H = 3$ with $y/H = 0.84$ (1.02 cm). After this minimum, the

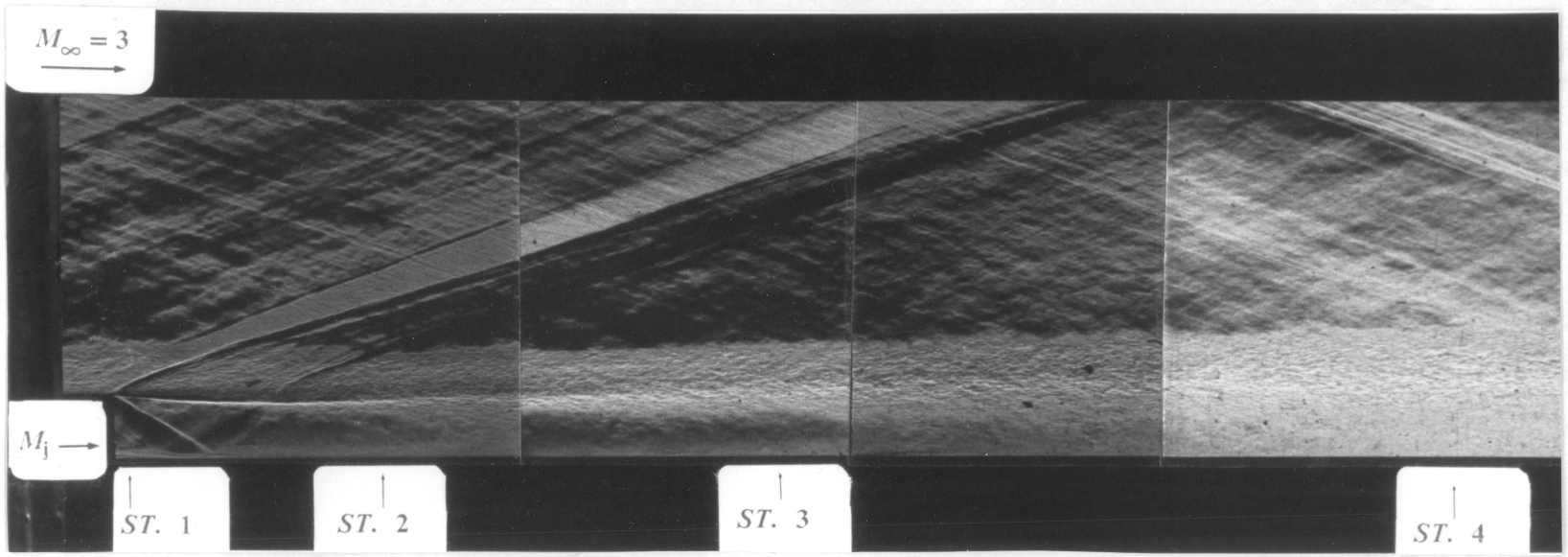

Figure 16. Spark-Schlieren of the Helium/Air Flowfield

separation line moves upward as the pressures on either side equalize and then blends in with the mixing shear layer. As the line diffuses out, it remains fairly level further downstream. The full boundary-layer/shear-layer/wall region, as represented by the light horizontal area near the floor, gradually grows from $y/H = 1.66$ at St. 2 to $y/H = 1.85$ at St. 3 and finally to $y/H = 2.13$ at St. 4. These values cover the region from the wall to the top of the freestream boundary layer.

The potential core of the helium injection appears as the darker region below the lighter shear layer and above the lower wall boundary layer. This core extends to about $x/H = 16$; however, this measurement provides only a rough estimate of the core length, because this dark feature depends on the lighting and arrangement of the optical equipment.

In the Nanoshadowgraph picture in Figure 17, fast-varying gradients are highlighted, so that eddies and fluctuations become clearer as compared to the Schlieren. A Shadowgraph responds to $\frac{\partial^2 \rho}{\partial y^2}$. To begin, Figure 17 shows an extraneous shock upstream of the slot exit. This shock comes from a small step at a seam between two tunnel sections. Fortunately, this shock is weak (as shown in the profile data) and does not appreciably affect the flow dynamics. The boundary layer thickness of the freestream is $\frac{\delta_{air}}{H} = 0.58$ (0.70 cm, 0.275 in), which agrees with the thickness of the boundary layer measured from the reduced velocity profile at St. 1. The helium boundary layer is $\frac{\delta_{He}}{H} = 0.07$ (0.085 cm, 0.033 in).

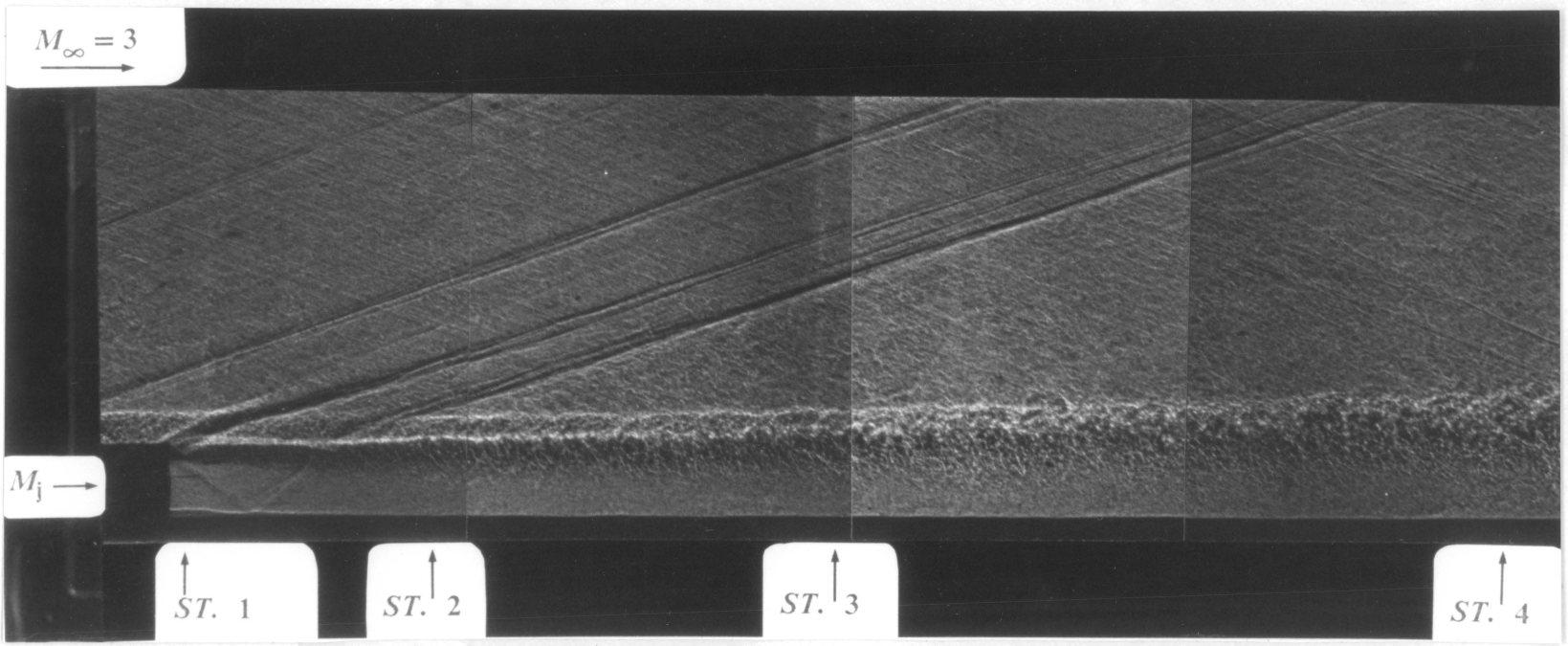

Figure 17. Nanosecond Shadowgraph of the Helium/Air Flowfield

With the shorter-duration Shadowgraph, high-frequency structures become clearer, so that by examining the areas where fine structures can be seen, a value for the turbulence-layer size can be estimated. The turbulence layer is defined as the region in the flow where there is a significantly higher turbulence level than is present in the air freestream or the potential core of helium. At St.2, this region's thickness is about 0.60 slot heights; at St. 3, 0.80 slot heights; and at St. 4, 1.63 slot heights. These visual values match the size and location of the high-turbulence region as given by actual turbulence measurements of the flow with a hot-wire probe. These turbulence results are not part of this report, so they are not presented here. The turbulence data can be found in Reference [38]. As proven subsequently, the turbulence layer is smaller than the total mixing layer.

Initially, the air-side boundary layer and the shear layer are separate zones, but by St. 3 the two regions begin to interact. By St. 4, the shear layer completely engulfs the freestream boundary layer, and an intermingled, fully turbulent region develops. Within the shear layer, large-scale structures can be seen inclined at about 45° and with a size about 1/3 the shear layer thickness. These large-scale structures are mainly restricted to the top half of the shear layer. Moreover, the shear layer on the helium side appears more ragged and not as sharply defined as the air side due specifically to the presence of the large structures on the air side. The helium-side boundary contains finer fluctuations. These small structures encroaching into the potential core of the injectant, nevertheless, are evidence of some turbulence. Furthermore, these small-scale

eddies probably coalesce into larger structures in the far field. Judging by the relative sizes of the structures along the air boundary versus those along the helium boundary, the air side mixes more rapidly. The turbulence in the freestream boundary layer hastens mixing along the air border by promoting and enhancing the turbulent mixing qualities of the shear layer while, by definition, the potential helium core is relatively inviscid in comparison. Thus, mixing into the core must rely heavily on entrainment of air into the injectant and smaller molecular diffusion effects, with no significant turbulence contribution from the core.

6.2 Profile Data

Quantitative results are divided into concentration data and other mean flow data. This procedure permits investigation of the concentration development on an independent basis before the complete mean-flow analysis is examined.

6.2.1 Concentration Results

The concentration probe produces raw data in the form of hot-film voltage, *P1*, and *P2*. Combined with the thermocouple data (T_{t2}), a FORTRAN code (Program 2 in **App. F**) reduces the files into gas composition.

Figure 18 shows the hot-film voltage. For each station, the probe traverses far enough so that the film signal becomes constant, i. e., out of the mixing layer where there is no helium and the pressure and temperature stay fairly constant. Even in this raw form, the data gives some indication of the flow structure. The voltage peaks at the highest helium levels, so that at St. 1, the slot-flow core is well defined. By St. 4, however, the core has decayed noticeably. The minimum on each profile corresponds to the wake region behind the splitter plate where both helium level and total pressure are low.

Figure 19, Figure 20, and Figure 21 show the pressure levels in the concentration probe. *P1* values are always lower than P_{t2} values (Figure 28); this knowledge supports the design premise that the flow shocks down at a higher Mach number than the inlet Mach number. This deduction, in turn, proves that the shock is swallowed, since to achieve a higher Mach number than M_1, the flow must expand supersonically inside the diffuser cap. *P2* mimics all the features of *P1*. Moreover, with *P2*/*P1* always less than 0.487 (worst case at 100 percent helium), the probe exit chokes at all relevant flow conditions.

Figure 22 and Figure 23 display the final concentration profiles deduced from *P1*, voltage, and T_{t2} in terms of molar and mass concentration. Whereas the photographs indicate the turbulence-layer size by the fine flow-structure detail, the concentration profiles show the total mixing layer, which includes the flowfield regions that are mixed from other, lesser effects and not from turbulence. Another important observation is that though minimums occur in the middle of the profiles for hot-film voltage (Figure 18), *P1* (Figure 19), and

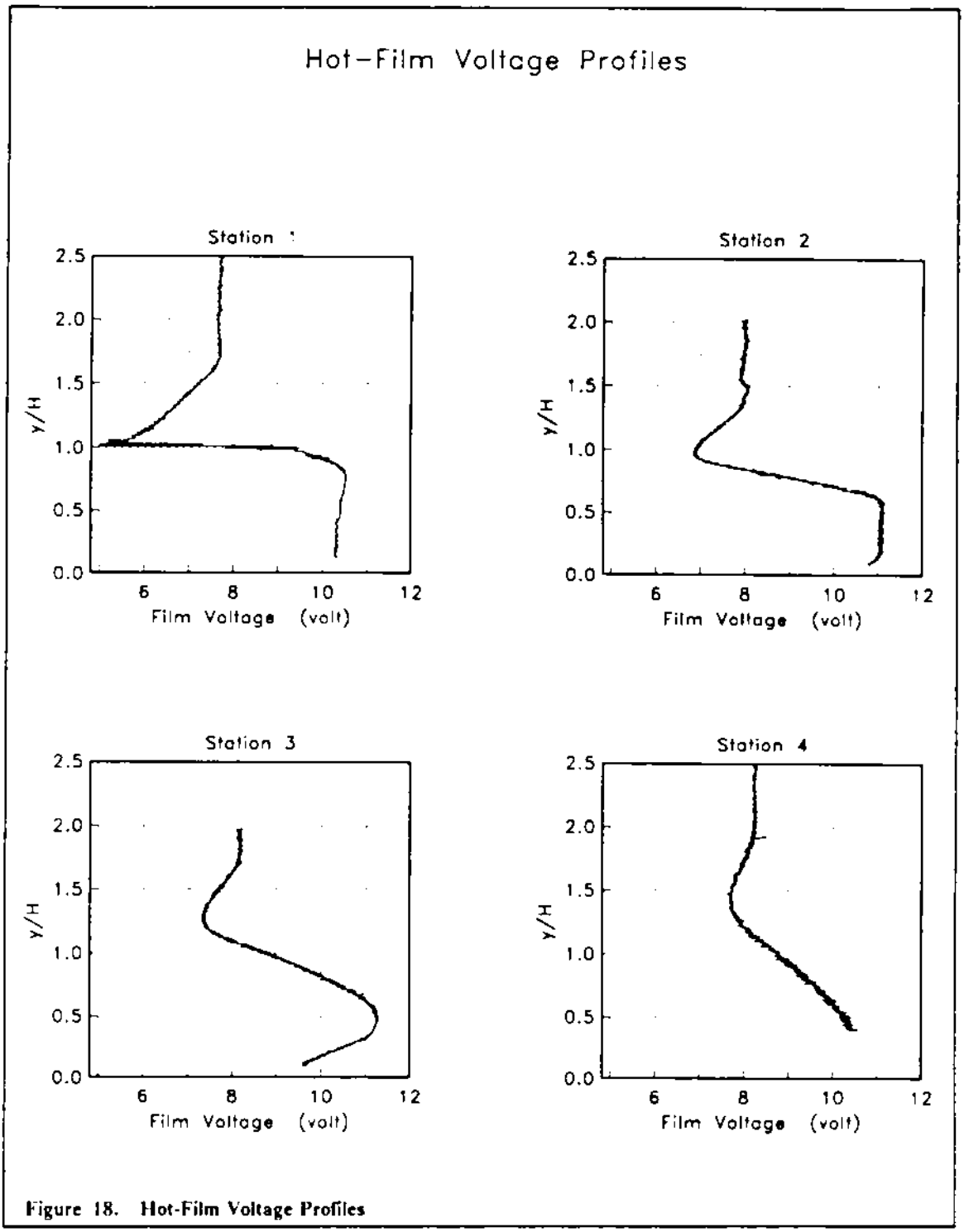

Figure 18. Hot-Film Voltage Profiles

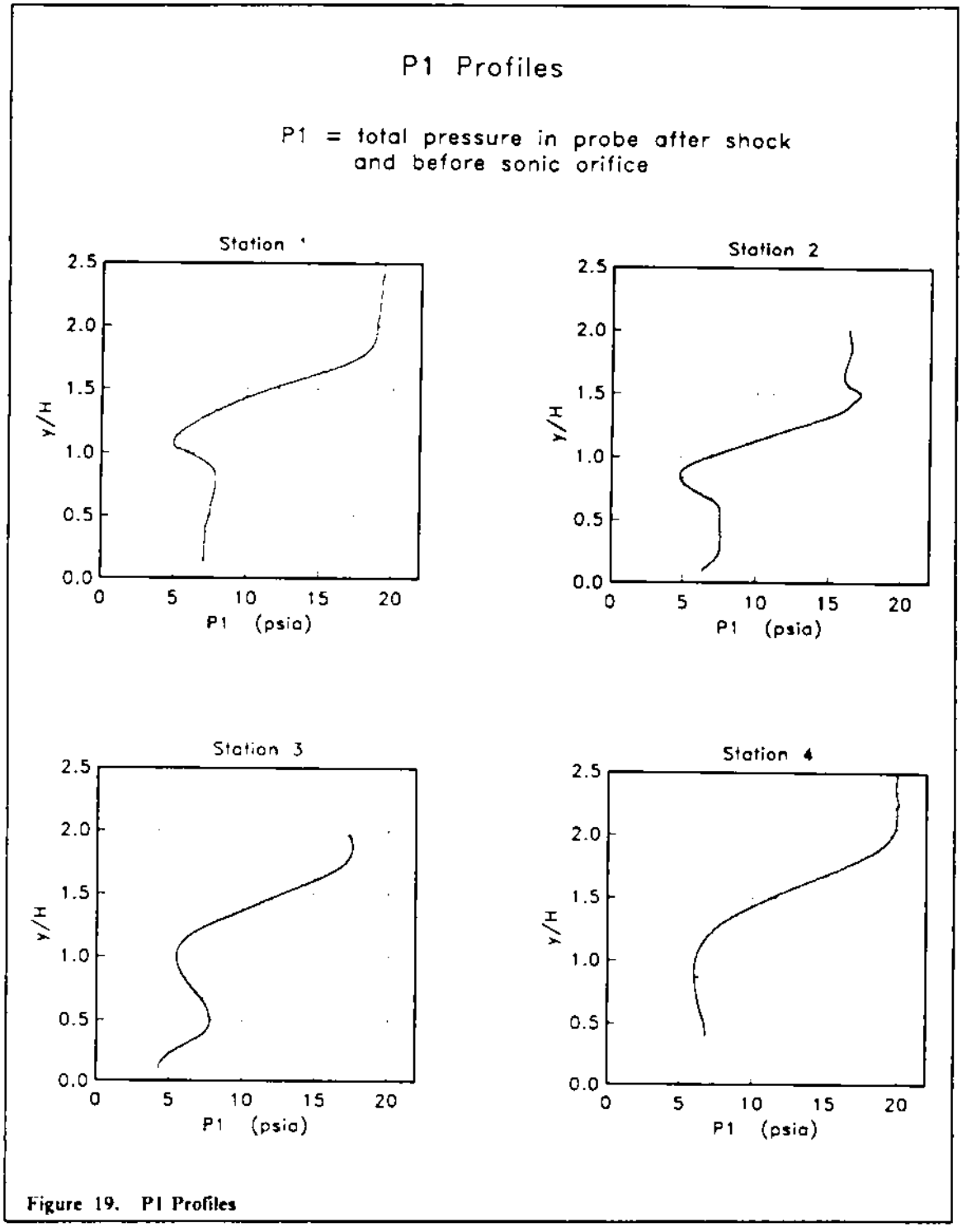

Figure 19. P1 Profiles

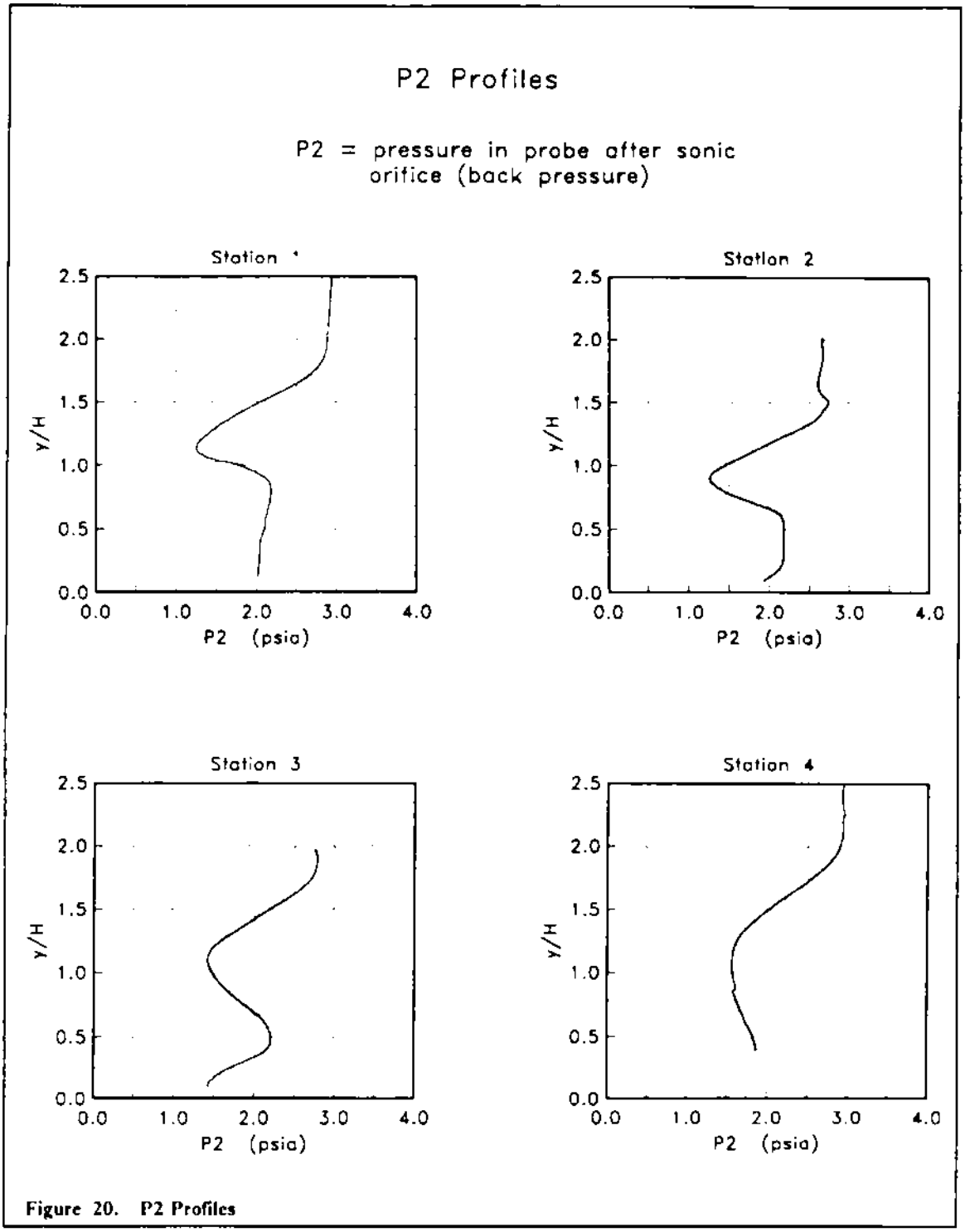

Figure 20. P2 Profiles

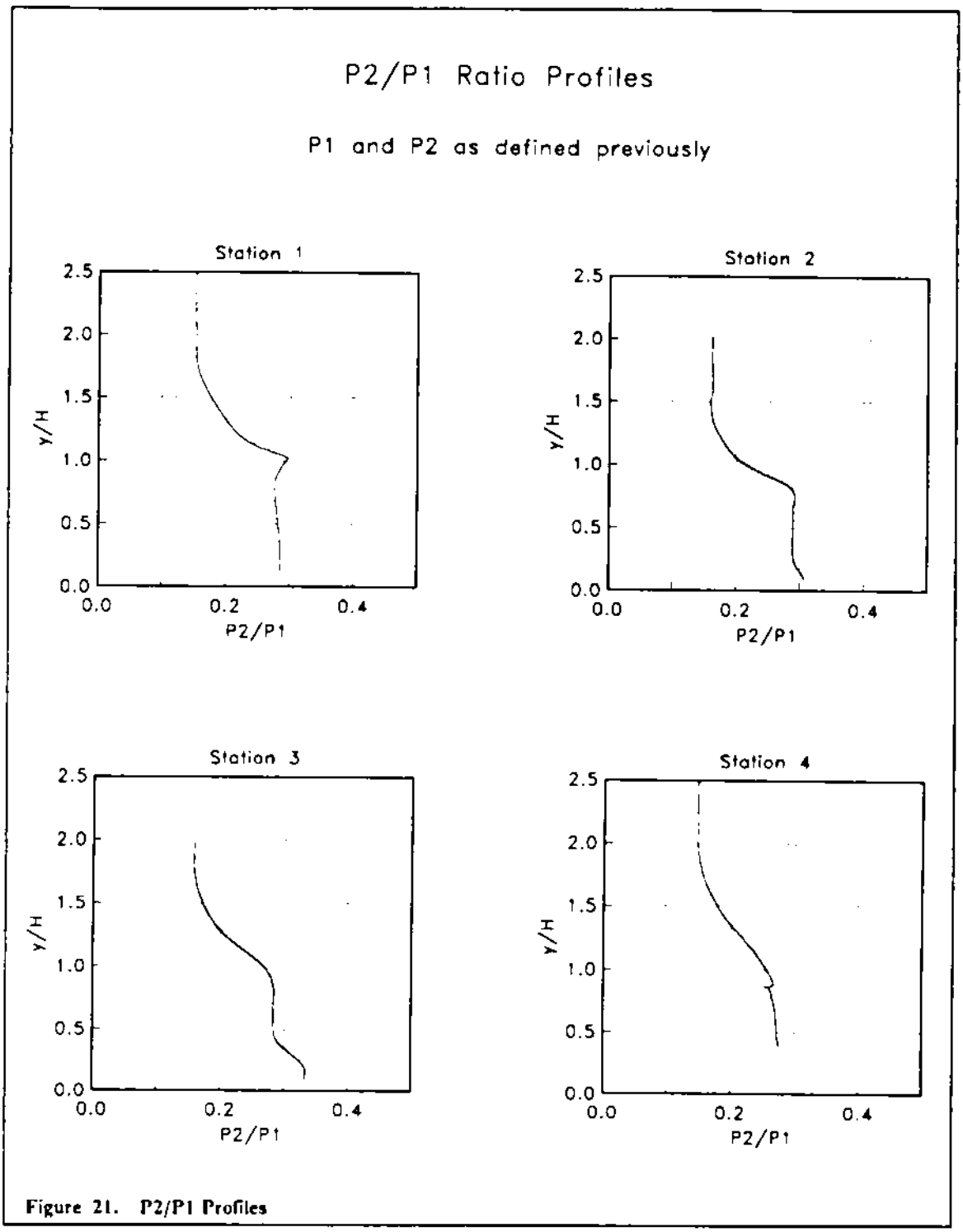

Figure 21. P2/P1 Profiles

T_{t2} (Figure 30), no corresponding minimums occur for the concentration profiles. Instead a smooth transition from maximum helium concentration near the wall to near zero in the freestream is evident and expected. This observation adds confidence to the knowledge that the probe operates properly. Figure 22 shows the decay of the slot flow due to mixing of the two streams. The St. 1 profile essentially shows a step change. The rounded corner near $y/H = 1$ most likely results from a small amount of air mixing with the helium even at St. 1. Above $y/H = 1$, χ_{He} goes to 0.0 as expected. Some fluctuations are present due to some noise in the signal and also the *PI* response not being fast enough to capture the pressure step across the thin splitter-plate lip at this station. The noise level, however, falls within the error bound of ± 2 percent mole fraction helium. At St. 2, χ_{He} is near 1.0 up to $y/H = 0.65$, and then the composition drops off to 0.0 at $y/H = 1.1$. The decrease in the thickness of the 100 percent-helium zone from St. 1 to St. 2 is 15 percent. This drop stems mainly from air entrainment into the helium potential core and, to a lesser degree, from the downward dip of the separation line towards the wall at St. 2, thereby effectively compressing the slot flow down to a thinner region. At St. 2, some perturbations exist on the air side; again the noise level has some effect, but the main cause is the presence of waves and shocks in the freestream at this location. At St. 3, χ_{He} drops below 1.0 throughout the entire profile indicating some degree of mixing in the whole region; however, χ_{He} unexpectedly decreases towards the wall, resulting in the maximum concentration point occurring at $y/H \simeq 0.3$ instead of at the wall. This incongruity is possibly due to the presssure or temperature measurement not

compensating for the output signal correctly in this region. For the same voltage level, the pressure must decrease, the temperature must increase, or both must occur to raise the helium concentration to the proper level, so that the profile at St. 3 does not exhibit the drop shown. Since the reason for this discrepancy is uncertain, though, rather than discarding or correcting the data, dashed lines are placed in Figure 22 and Figure 23 in the region where the data is suspect. At St. 4, χ_{He} again remains below 1.0 in the observed region, but the slot flow is still quite evident even at this station. The mixing layer grows to $y/H = 2.1$ by St. 4.

Figure 24 shows the streamwise decay in α_{He}. At Sts. 1 and 2, $\alpha_{He}|_{max} = 1.0$, signifying that the potential core of the helium wall jet is mostly intact up to St. 2. After St. 2, an almost linear decrease in $\alpha_{He}|_{max}$ is witnessed. By St. 4, the maximum mass fraction of helium has decayed to about 0.65. Figure 25 gives the penetration P of the mixing layer, defined as the point where $\chi_{He} < 0.02$. A χ_{He} of 0.02 is the accuracy of the concentration measurement. Figure 26 depicts the geometry of the mixing zone. For this graph, the mixing zone boundaries are defined as, on the helium side, the highest y-point which sees 100 percent helium and, on the air side, the lowest y-point which corresponds to 0 percent helium. The mixing layer spreads more rapidly than what the flow visualization indicates; of course, measurements from the Shadowgraphs indicate turbulence layer size, not total mixing-layer size. Therefore, from this observation, the mixing layer surrounds and includes this turbulence layer. By St. 3, the mixed region contacts the floor of the model, and by the last measurement station, the size of the mixing

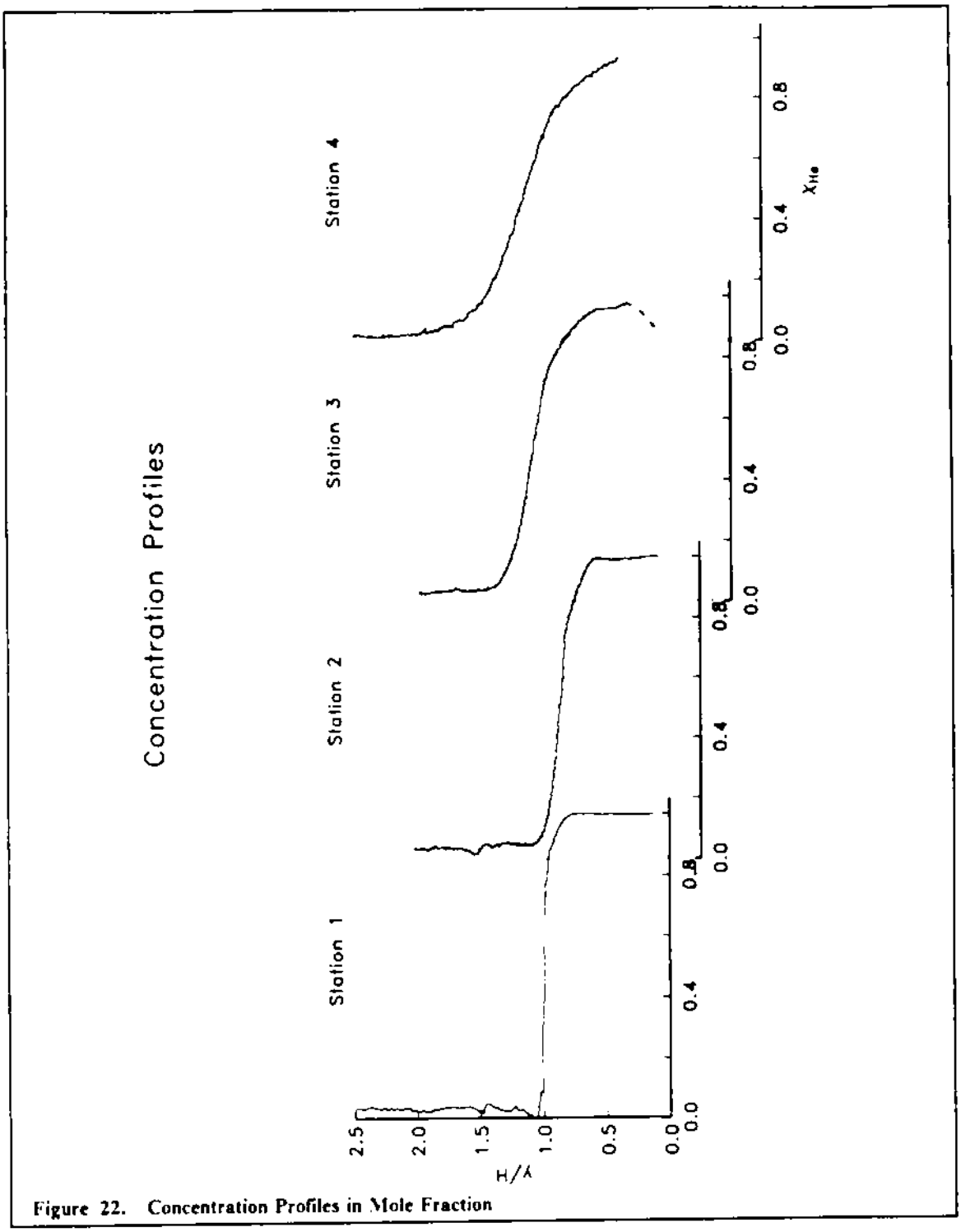

Figure 22. Concentration Profiles in Mole Fraction

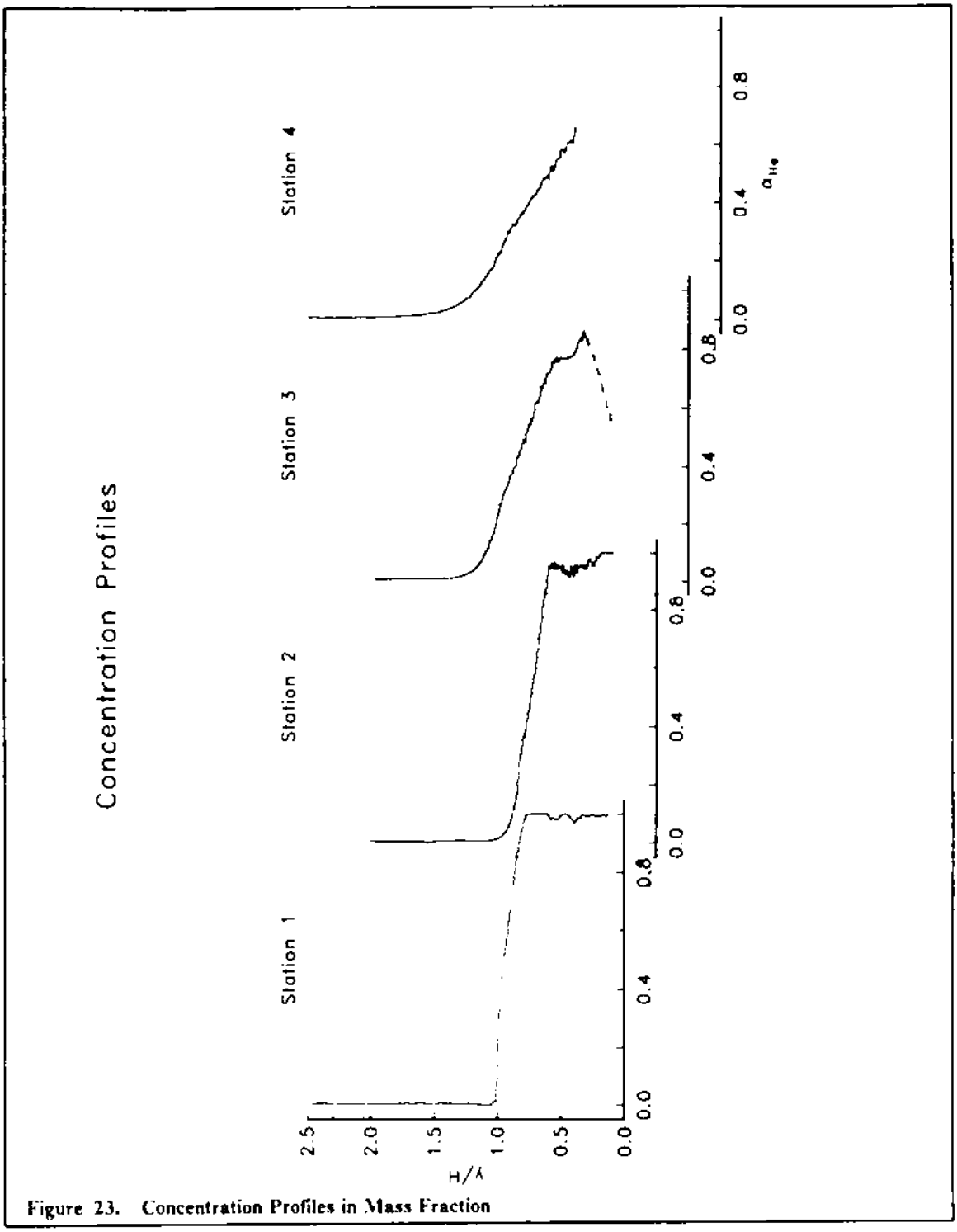

Figure 23. Concentration Profiles in Mass Fraction

zone grows to about two slot heights, larger than the values for the turbulence layer.

If helium is assumed to directly model hydrogen-gas fuel, then a physical thickness can be defined which represents the extent of the mixed flow that lies within the so-called lean and rich flammability limits for combustion. This measurement can be called the reaction thickness[6]. For the H_2/air combination, the fuel-lean boundary is 0.04 mole fraction of H_2, and the fuel-rich limit is $\chi_{H_2} = 0.74$ at ambient temperature and homogeneous conditions. Considering that the actual test case experiences a range of temperatures and a heterogenous environment, these values give only a rough estimate of the flow region capable of sustaining a reaction. Figure 27 shows the reaction layer thickness δ_R at equivalent helium molar concentrations. The reaction thickness remains 40-50 percent smaller than the mixing-layer size at the further downstream stations.

6.2.2 Other Mean-Flow Results

Figure 28, Figure 29, and Figure 30 show the other raw profile data. P_{t2} values are generally well-behaved. On the other hand, the cone-static probe proves very sensitive to impinging waves on the cone tip as witnessed by the double-hump feature in the slot at St. 1. This discrepancy stems from the adjustment shock impacting on the cone tip. Nevertheless, in light of not having a better method, the cone-static measurements are used. T_{t2} profiles show that

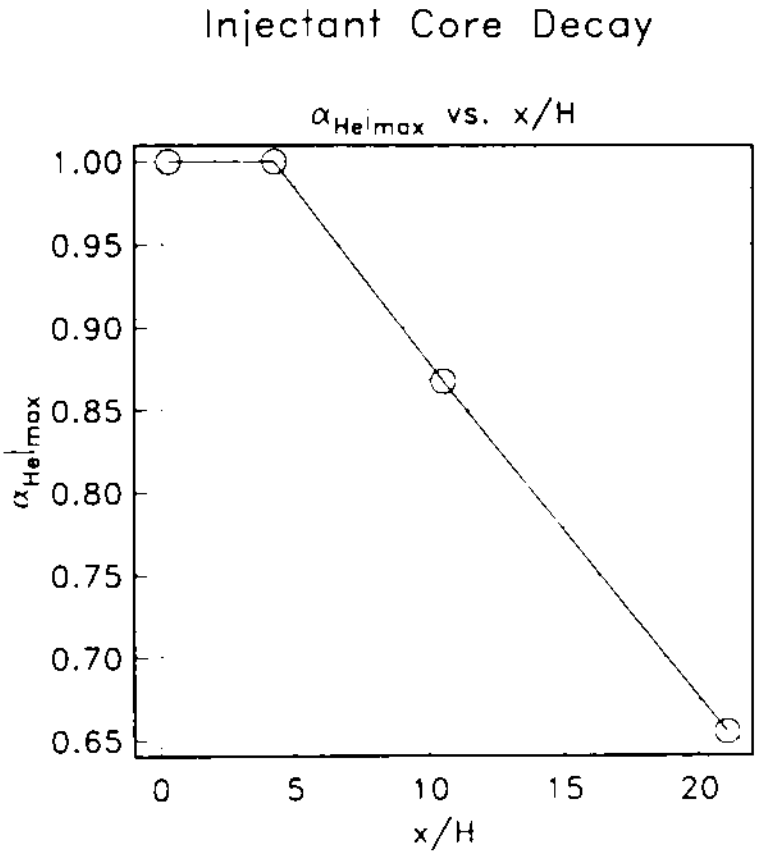

Figure 24. Downstream Injectant Core Decay

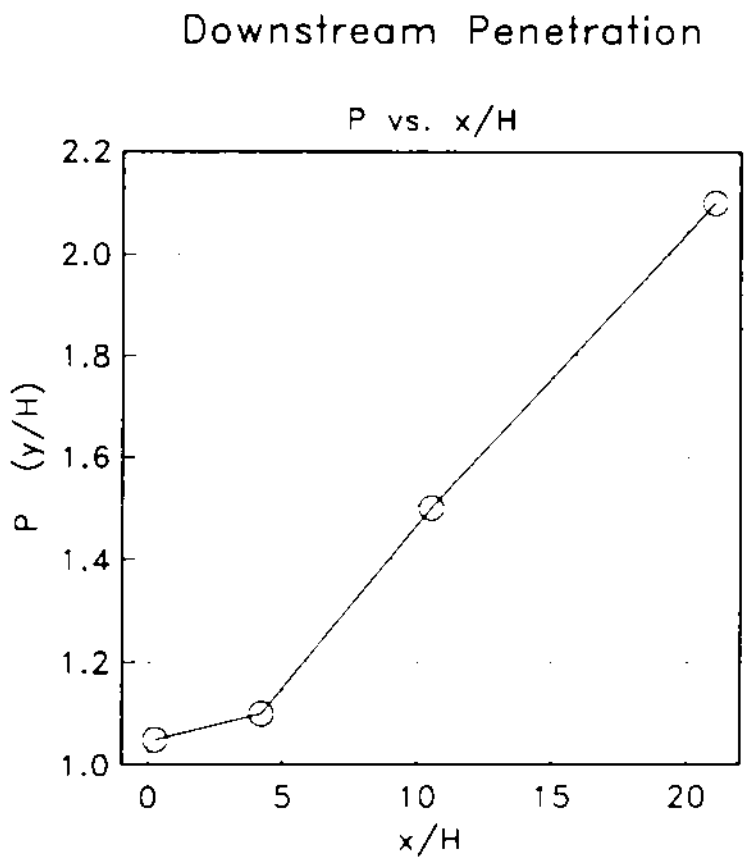

Figure 25. Downstream Penetration

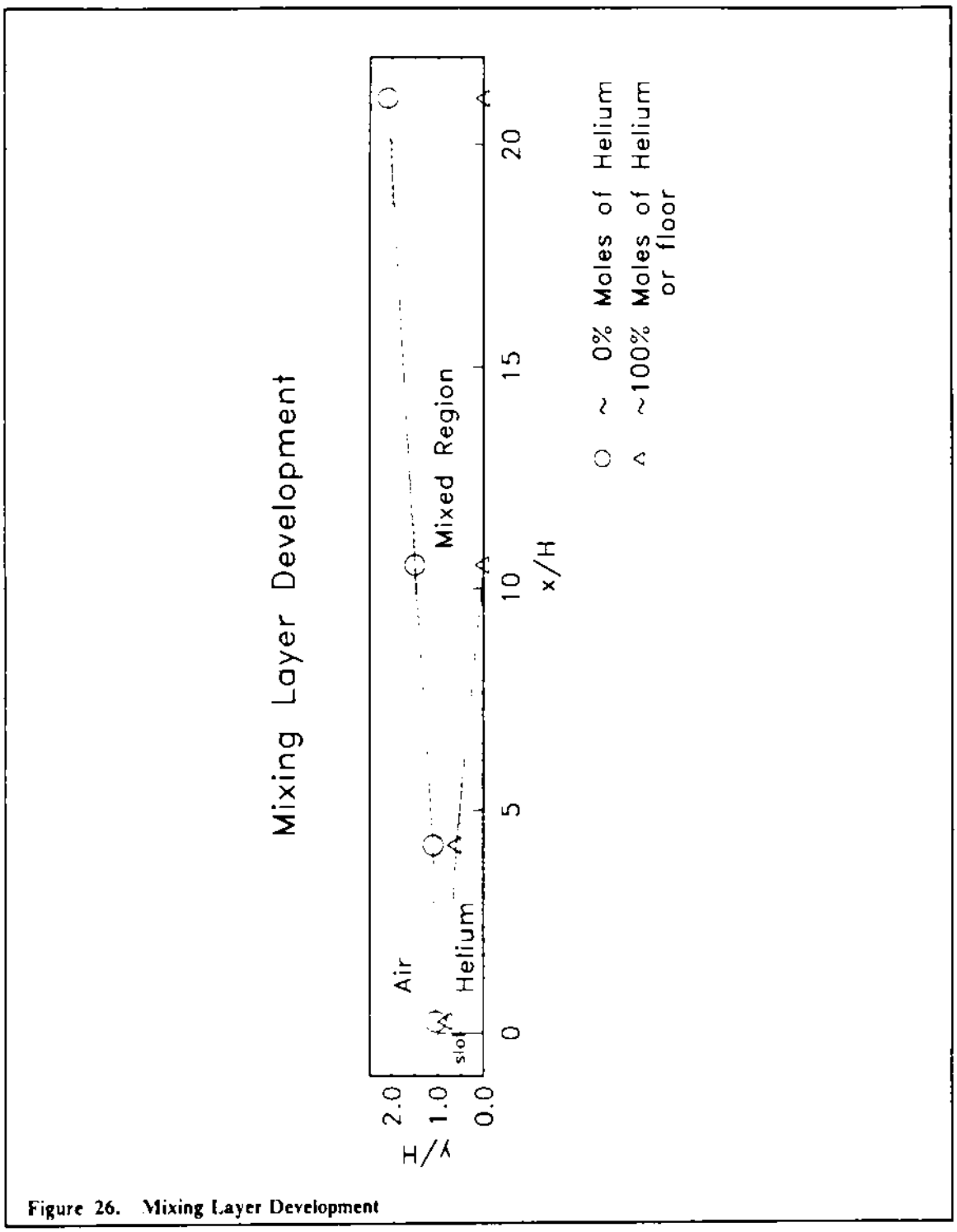

Figure 26. Mixing Layer Development

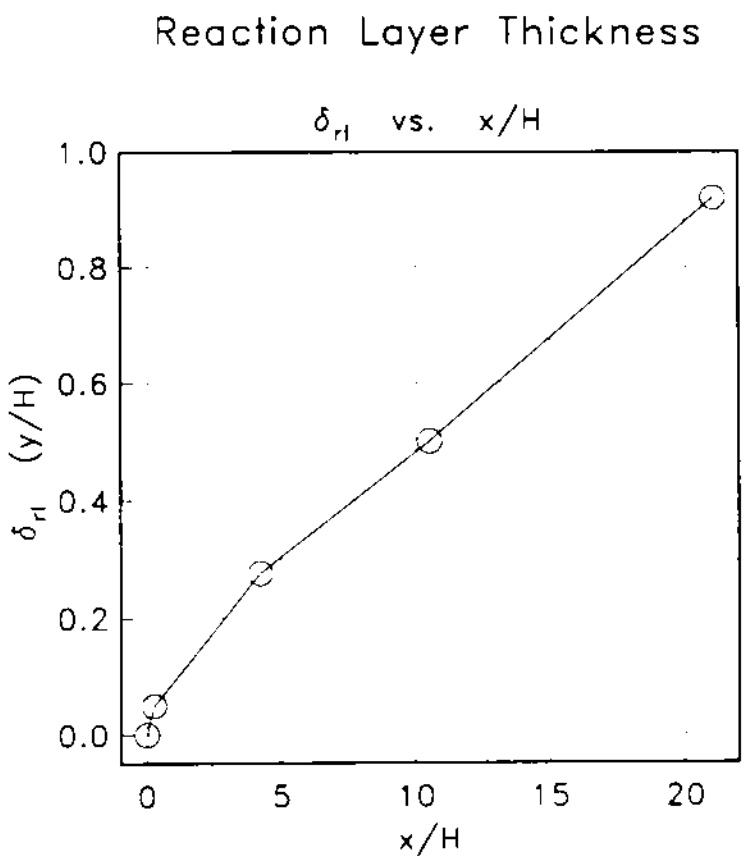

Figure 27. Reaction Layer Thickness

generally the maximum slot temperature is about 5-10 deg Kelvin higher than the freestream.

Figure 31 gives the Mach number profiles. At St. 1, M_j is about the expected value of 1.78. At St. 2, the slot Mach-number distribution is more uniform since there are no waves present to distort the data. The dip from the wake occurs below $y/H = 1$ due to the downward curvature of the separation line. M oscillates around 3.0 above $y/H = 1.4$, due to the complex wave pattern in this region. By St. 4, the slot flow has completely blended in with the wake so that they cannot be separately distinguished. The area from the floor to $M = 3$ extends to $y/H = 1.5$ (St. 1), $y/H = 1.5$ (St. 2), $y/H = 1.7$ (St. 3), and $y/H = 1.9$ (St. 4).

Figure 32 and Figure 33 show the speed of sound and velocity distributions. At the first station, the slot velocity is twice the freestream velocity due to the low molecular weight of helium ($MW = 4.00260$). In fact, the speed of sound in the slot exceeds that of the freestream by 3.4. The maximum ratio of the slot region velocity to freestream velocity decays to 1.8, 1.7, and 1.5 further downstream.

Figure 34 documents the density distribution. Initially, the helium density is about 0.1 of the freestream air density. Shown in Figure 35, the mass flux through the slot is 0.2 that of the freestream. Figure 36 presents the static temperature distribution. The temperature peaks at the near stagnant regions near the wall and in the wake. By St. 4, the peaks diffuse out.

Figure 37 pictures the static pressure profiles. In a boundary-layer type flow, a constant P_t distribution is expected. The profiles exhibit as much as a 40 percent variation in P_t through the region of concern. The larger variations occur

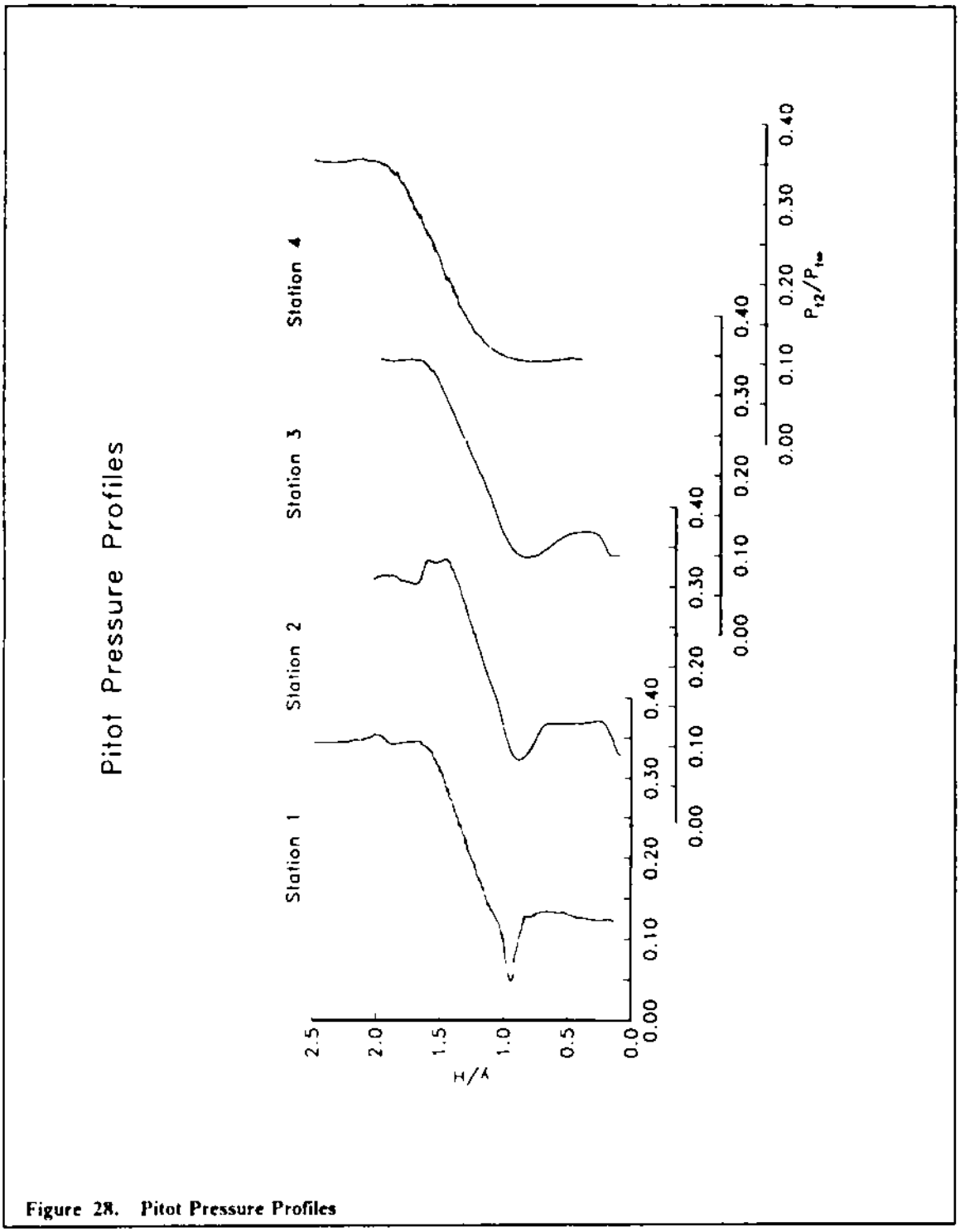

Figure 28. Pitot Pressure Profiles

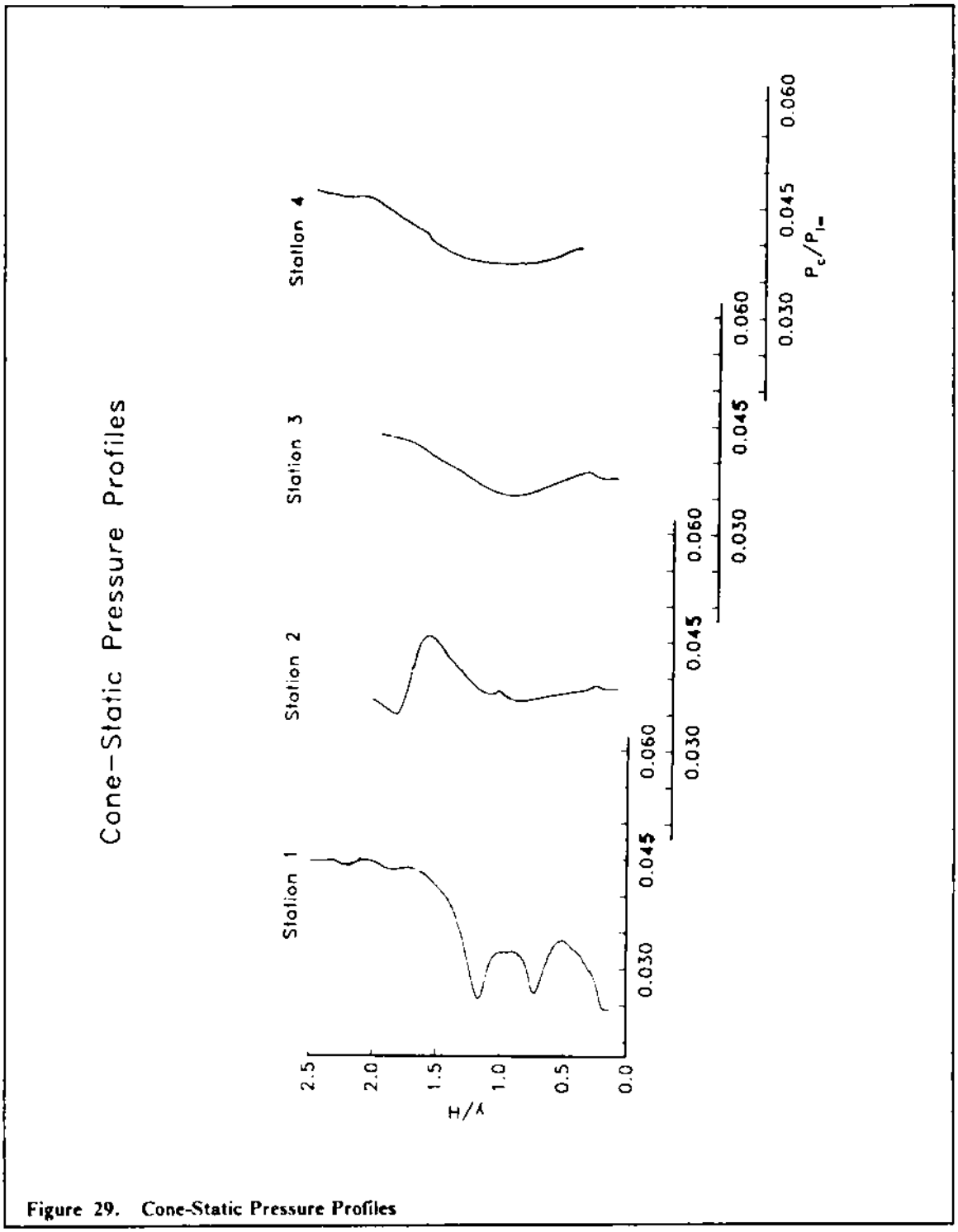

Figure 29. Cone-Static Pressure Profiles

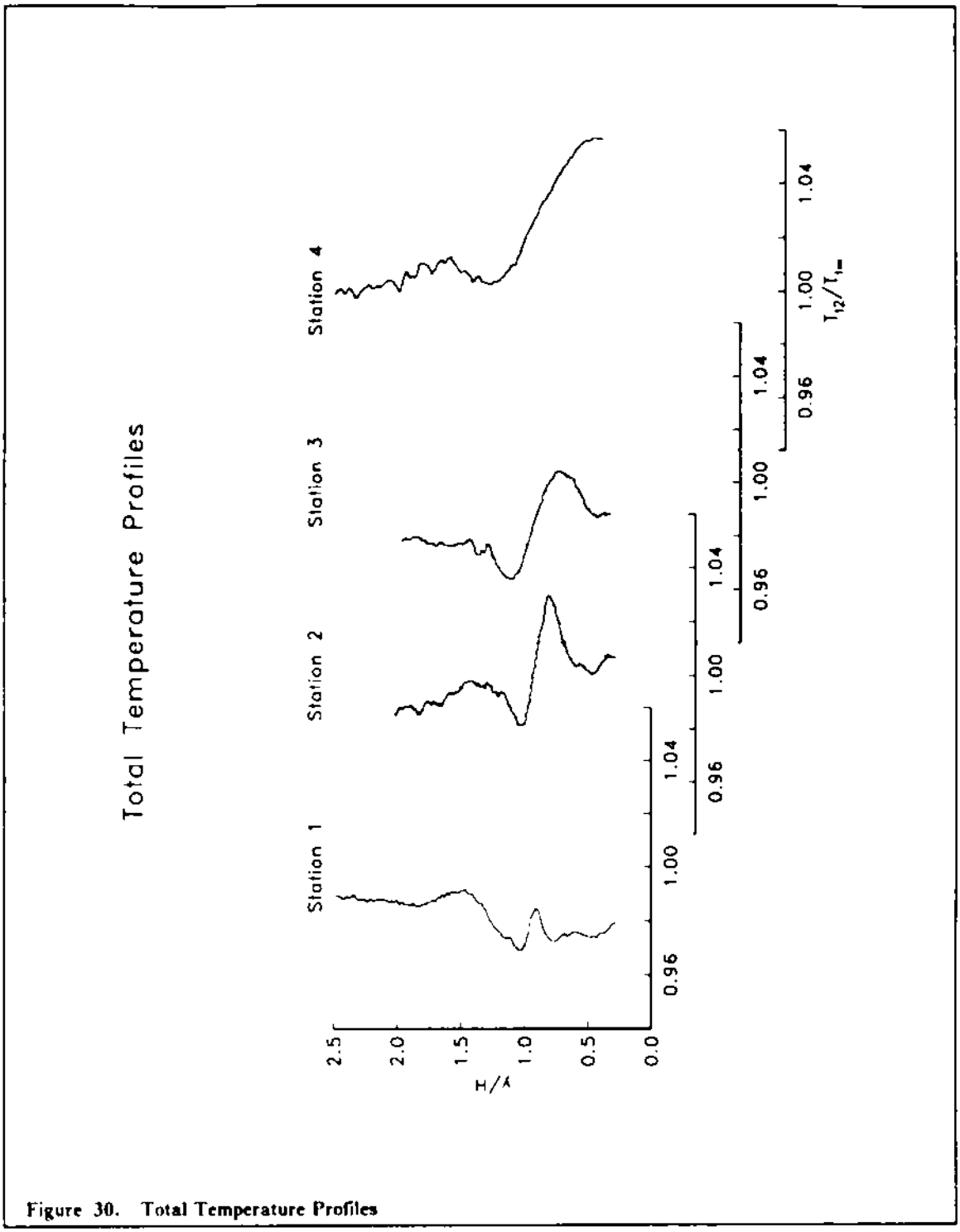

Figure 30. Total Temperature Profiles

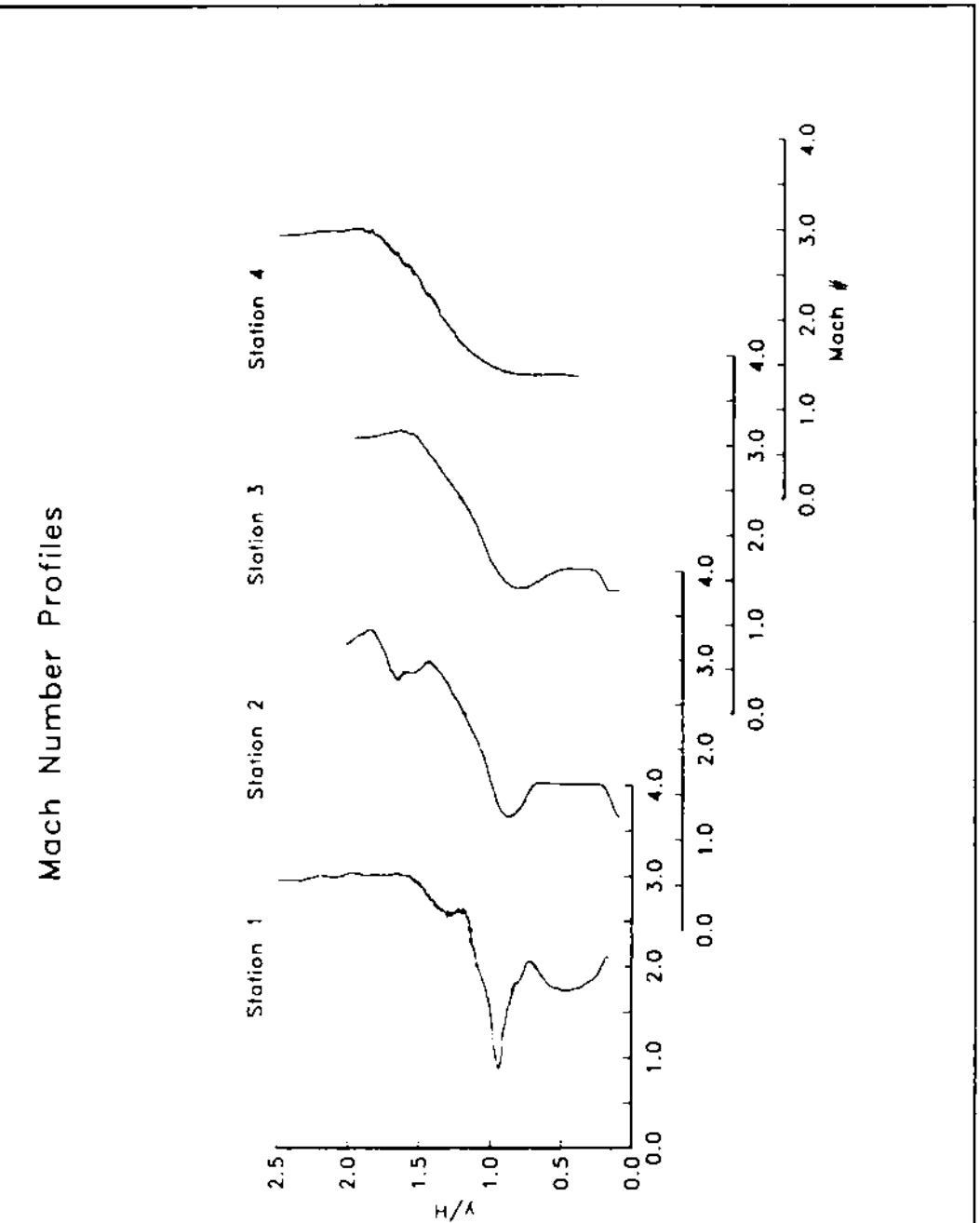

Figure 31. Mach Number Profiles

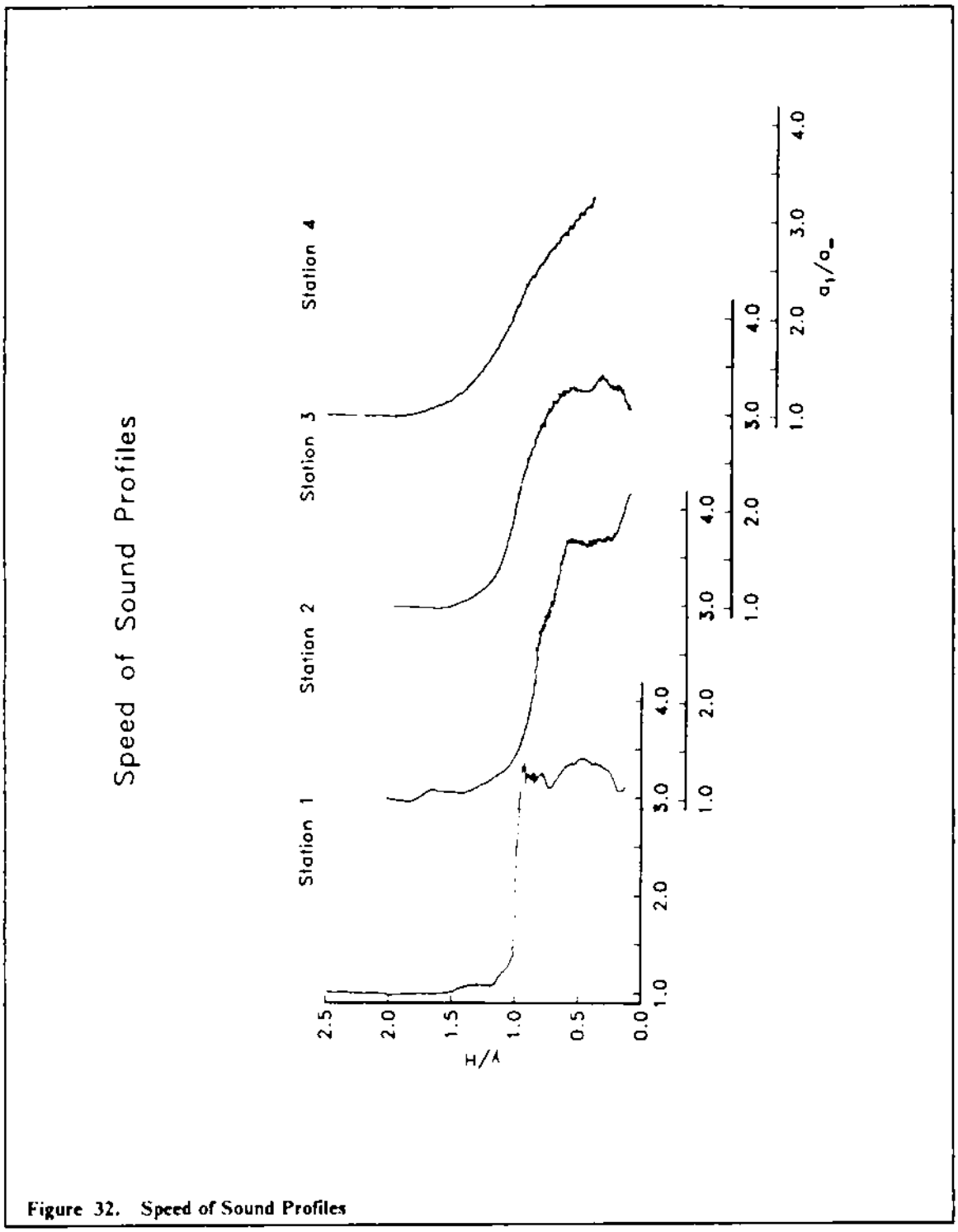

Figure 32. Speed of Sound Profiles

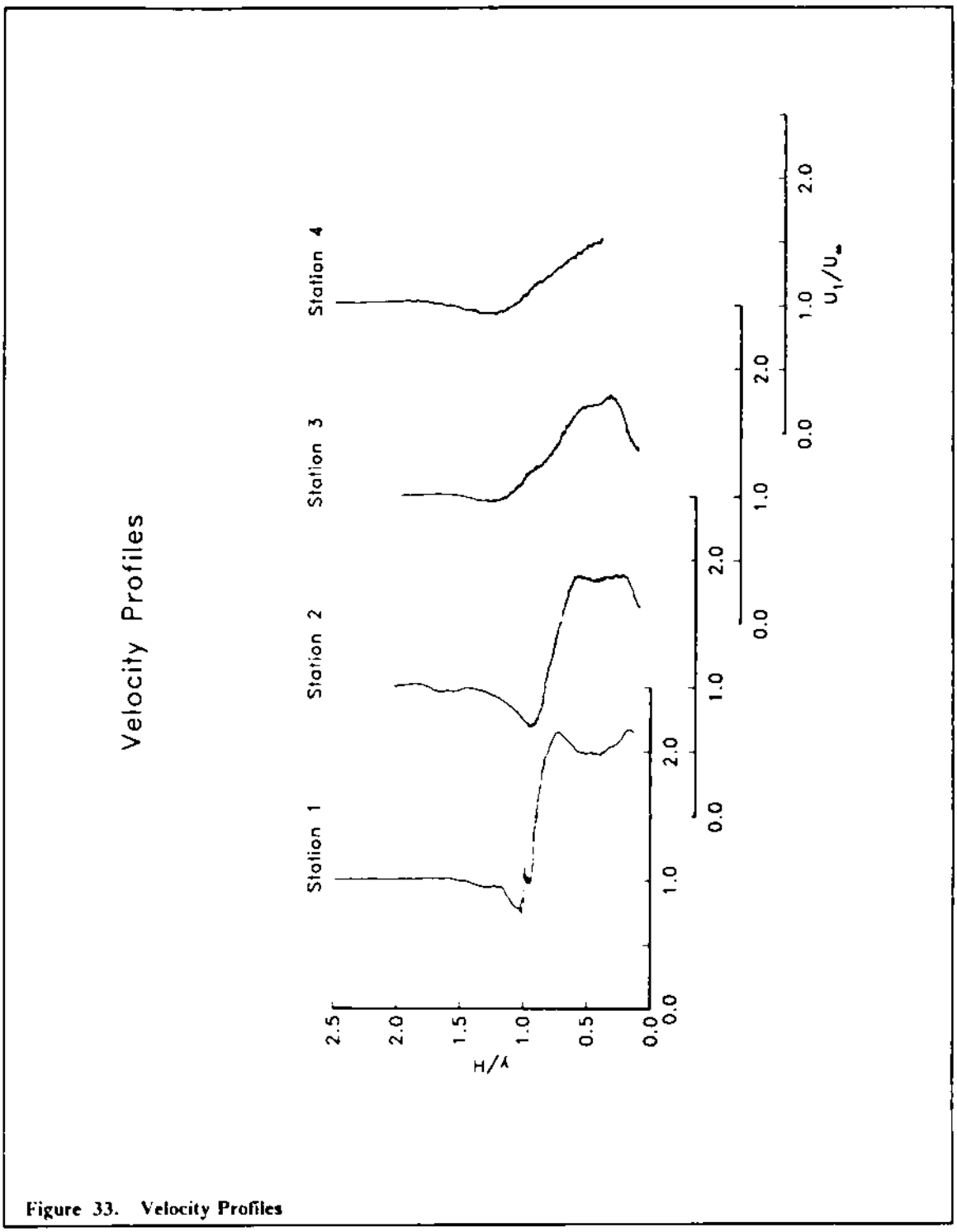

Figure 33. Velocity Profiles

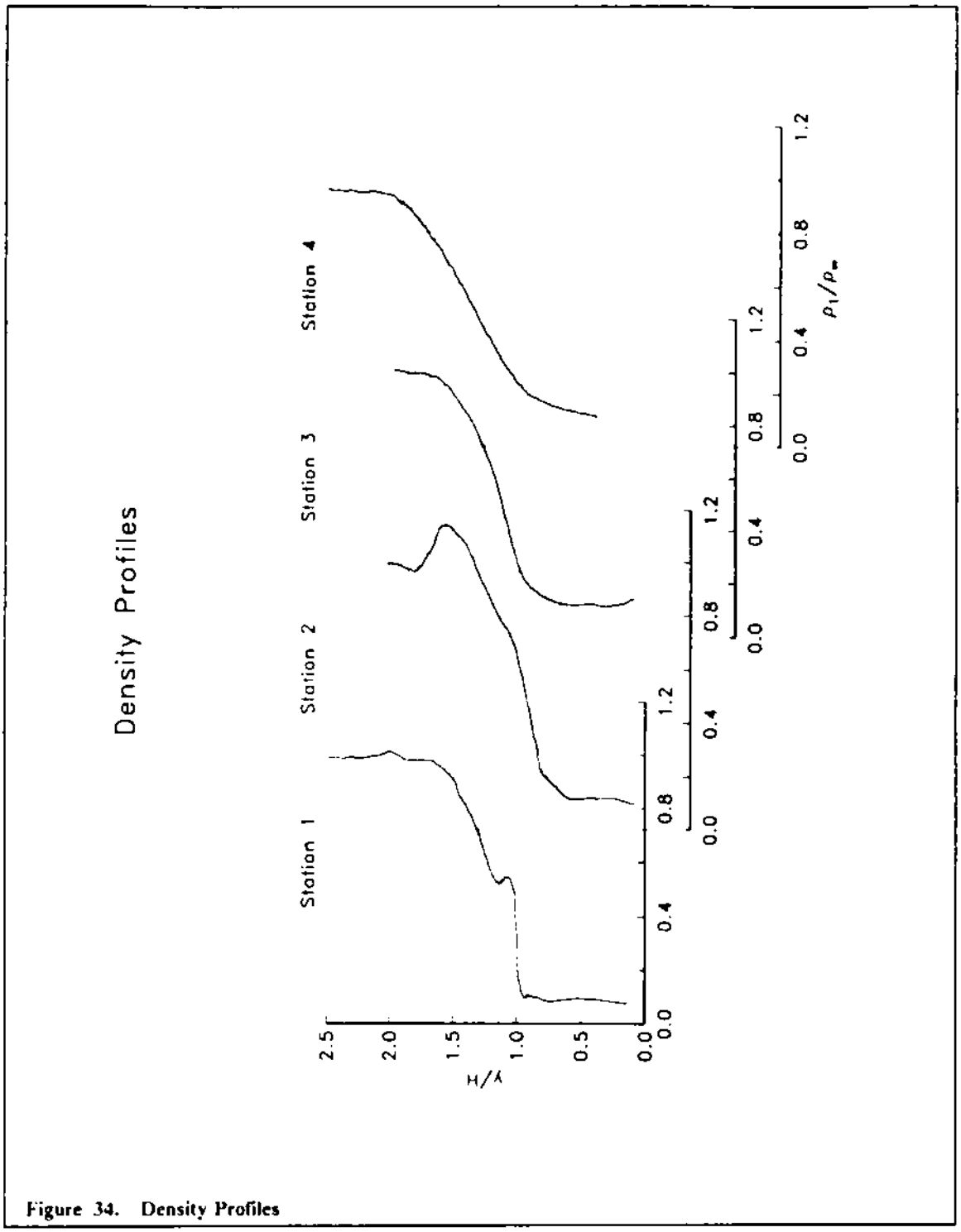

Figure 34. Density Profiles

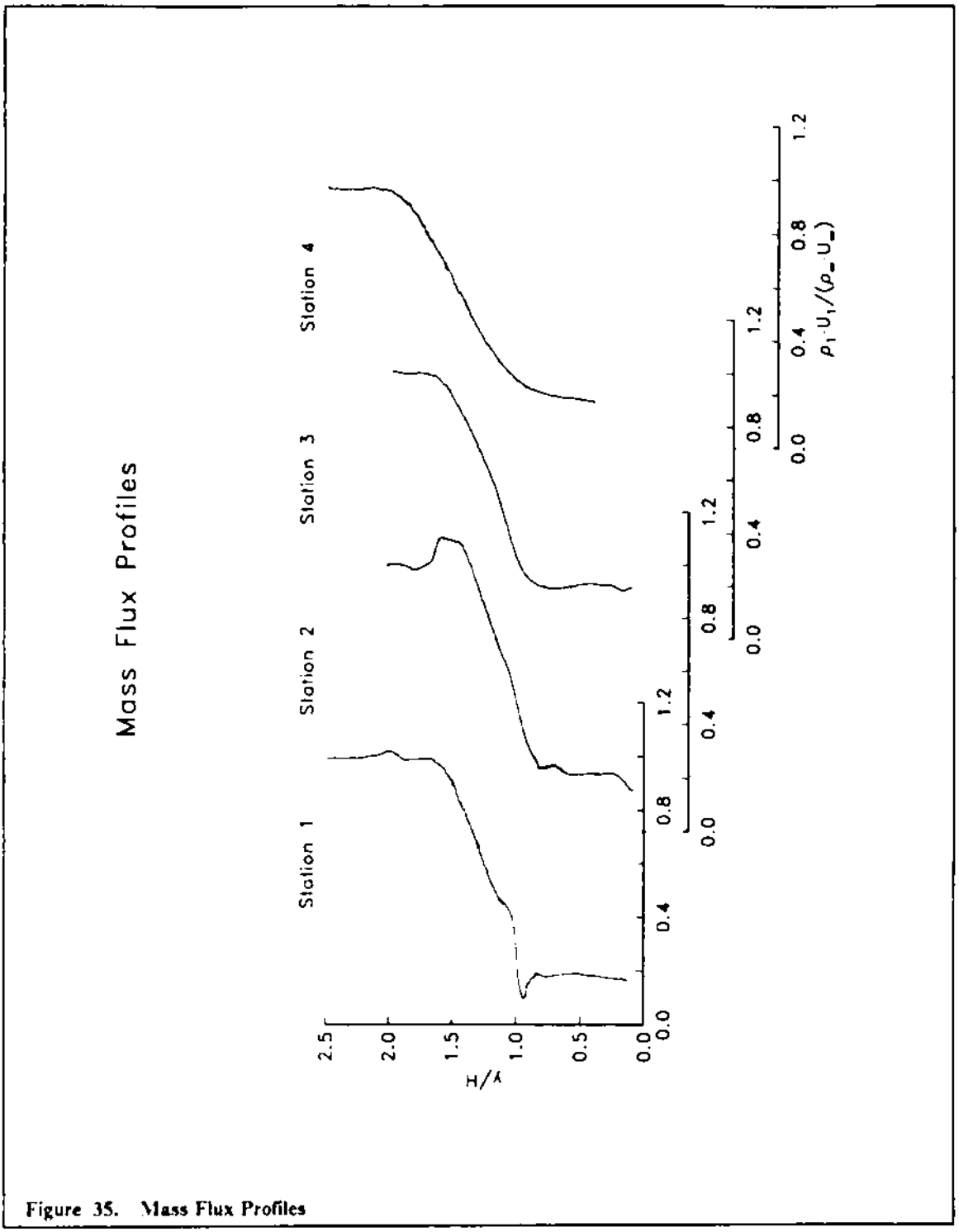

Figure 35. Mass Flux Profiles

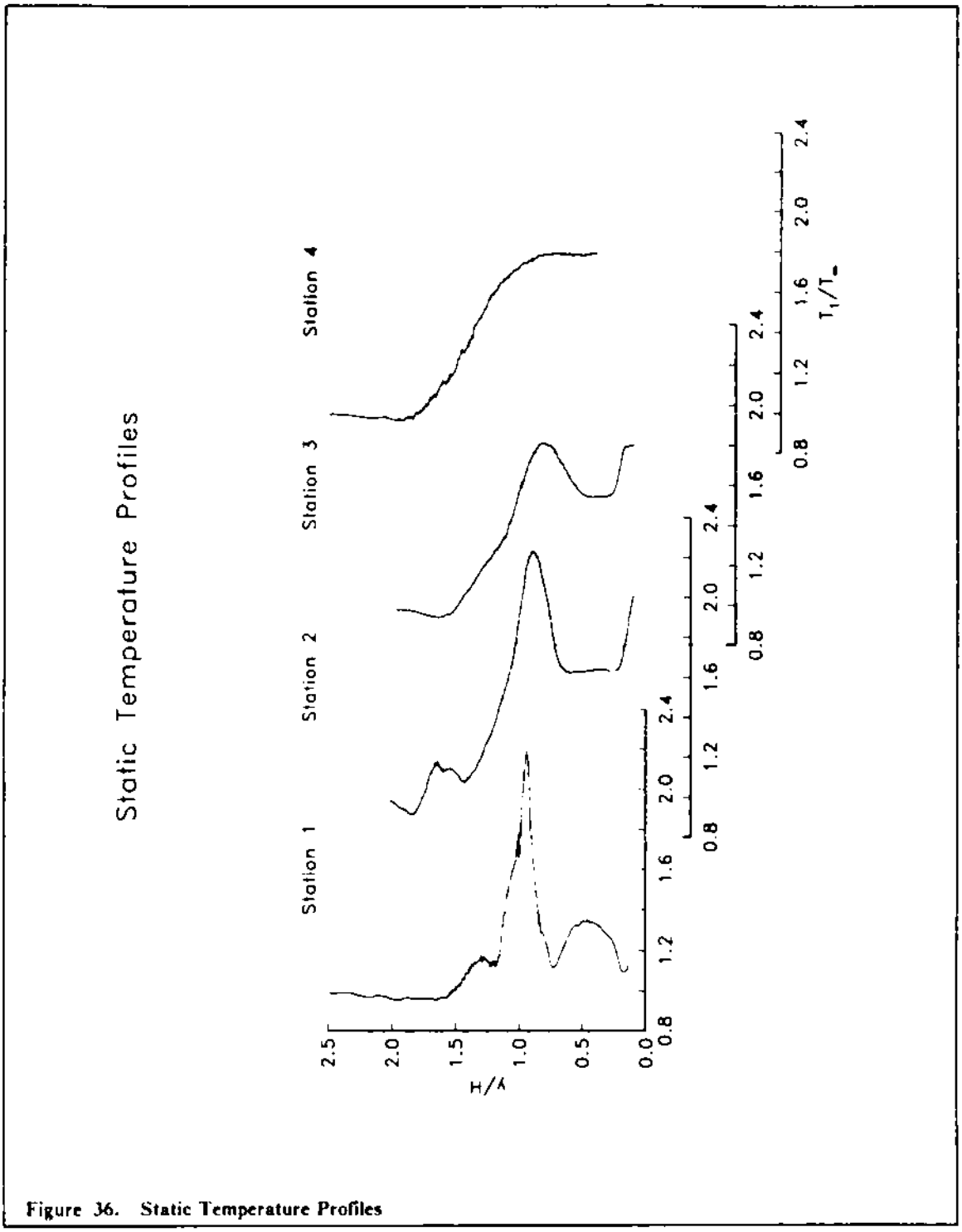

Figure 36. Static Temperature Profiles

at St. 1 in the slot where the probe passes through the adjustment shock and at St. 2 where the probe experiences waves at the upper part of the mixing region. As a consistency check, P_{t1} is found from the static pressure and is plotted in Figure 38. At the second and third stations, P_{t1} overshoots the expected value by 20 percent. A static pressure correction is applied to these profiles in hopes of determining the sensitivity of the results to P_1. A P_1 value in the slot core where the flow remains fairly inviscid is chosen and assumed constant throughout the entire shear layer. This value is chosen at $y/H = 0.42$ (0.51 cm, 0.20 in). This correction applies to only St. 2 and St. 3, since these locations have the largest discrepancies in P_{t1} in the freestream. Figure 39 represents this adjustment; Figures 40-45 give the effect of this P_1 correction on representative profiles. In most cases, the difference is less than 10 percent, not a huge difference but a significant change. $P_{t1}/P_{t\infty}$ at St. 3 goes to 1.0 in the freestream as expected but levels off to 0.8 at St. 2, showing that the adjustment overcompensates there. In short, P_1 is a critical measurement with its inaccuracies chiefly stemming from the cone-static measurement, since the Pitot measurement is quite reliable. Thus, a more dependable method of measuring cone-static pressure may be required.

The helium profiles in **Chapter 7** are the original, unadjusted profiles. If comparisons between the adjusted profiles here and the air-injection cases in **Chapter 7** are desired, then the adjusted profiles for Sts. 2 and 3 can be referred to in this chapter.

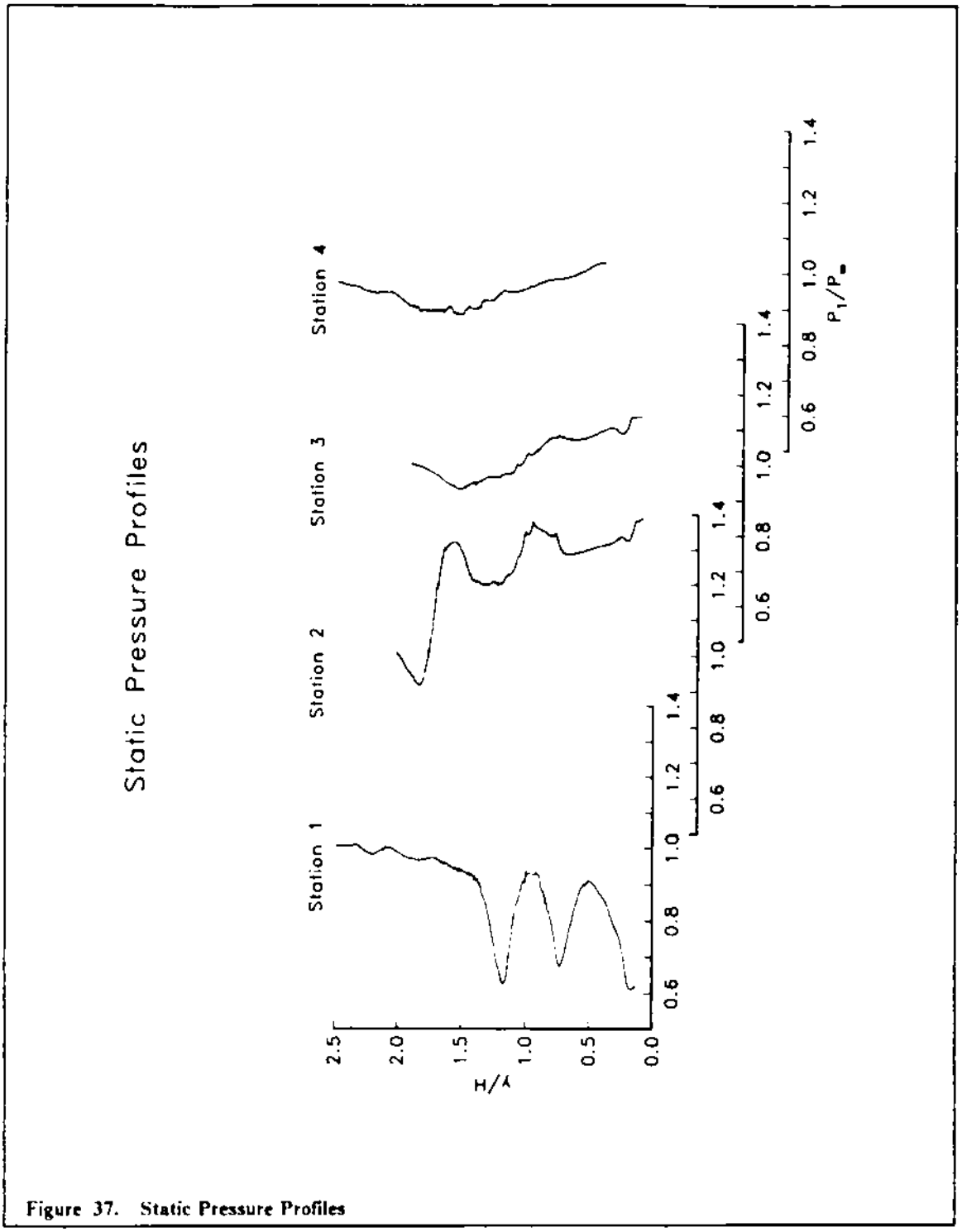

Figure 37. Static Pressure Profiles

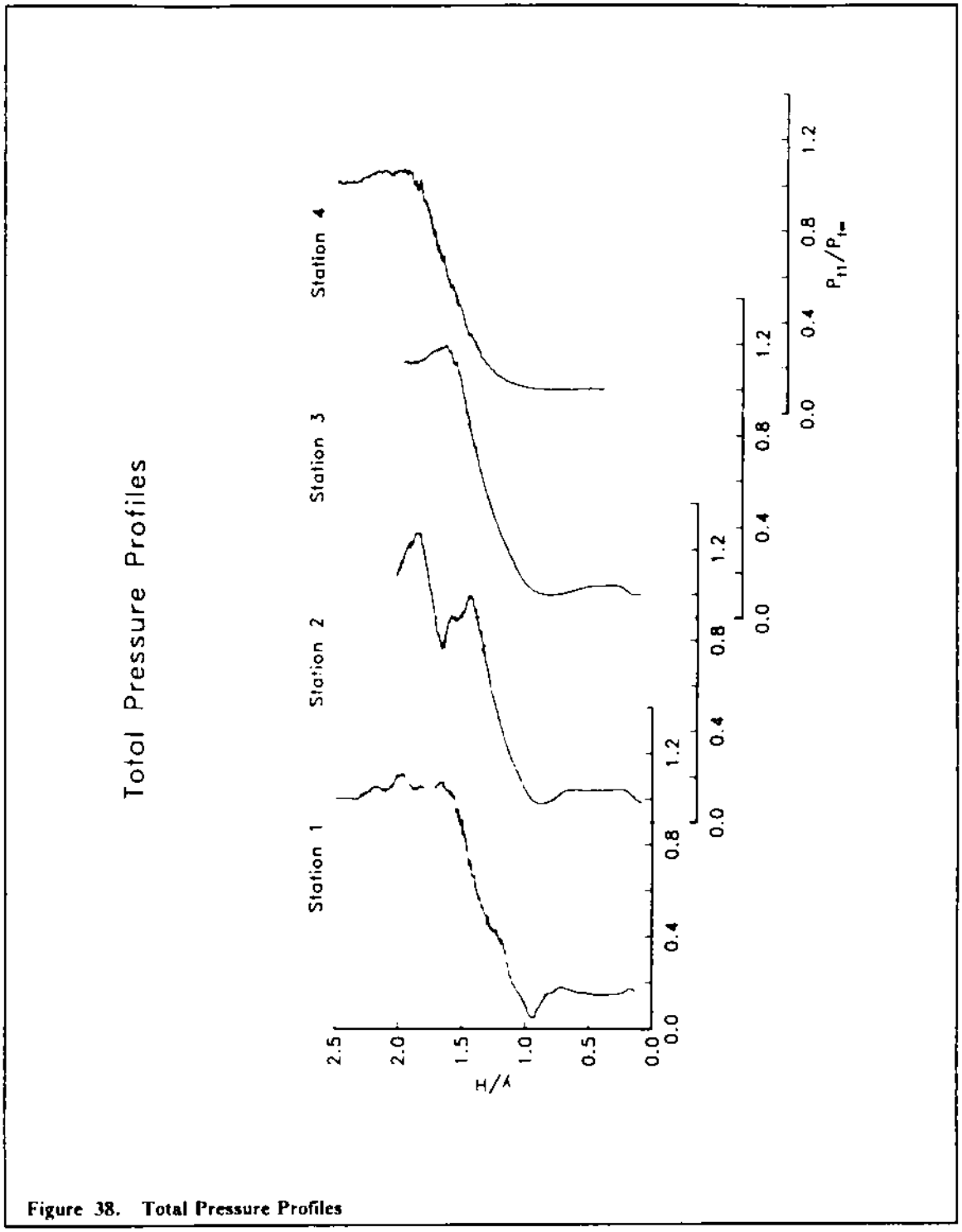

Figure 38. Total Pressure Profiles

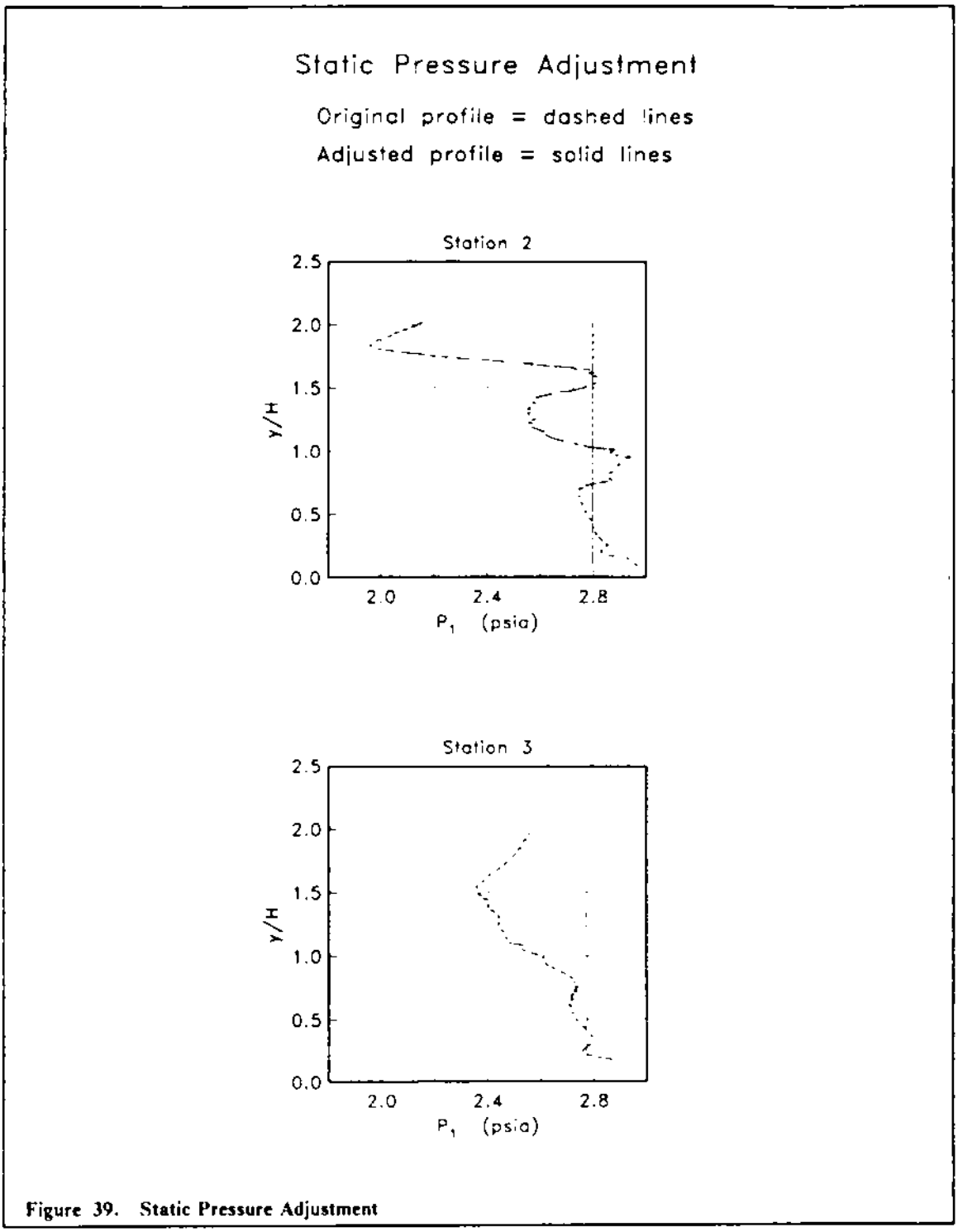

Figure 39. Static Pressure Adjustment

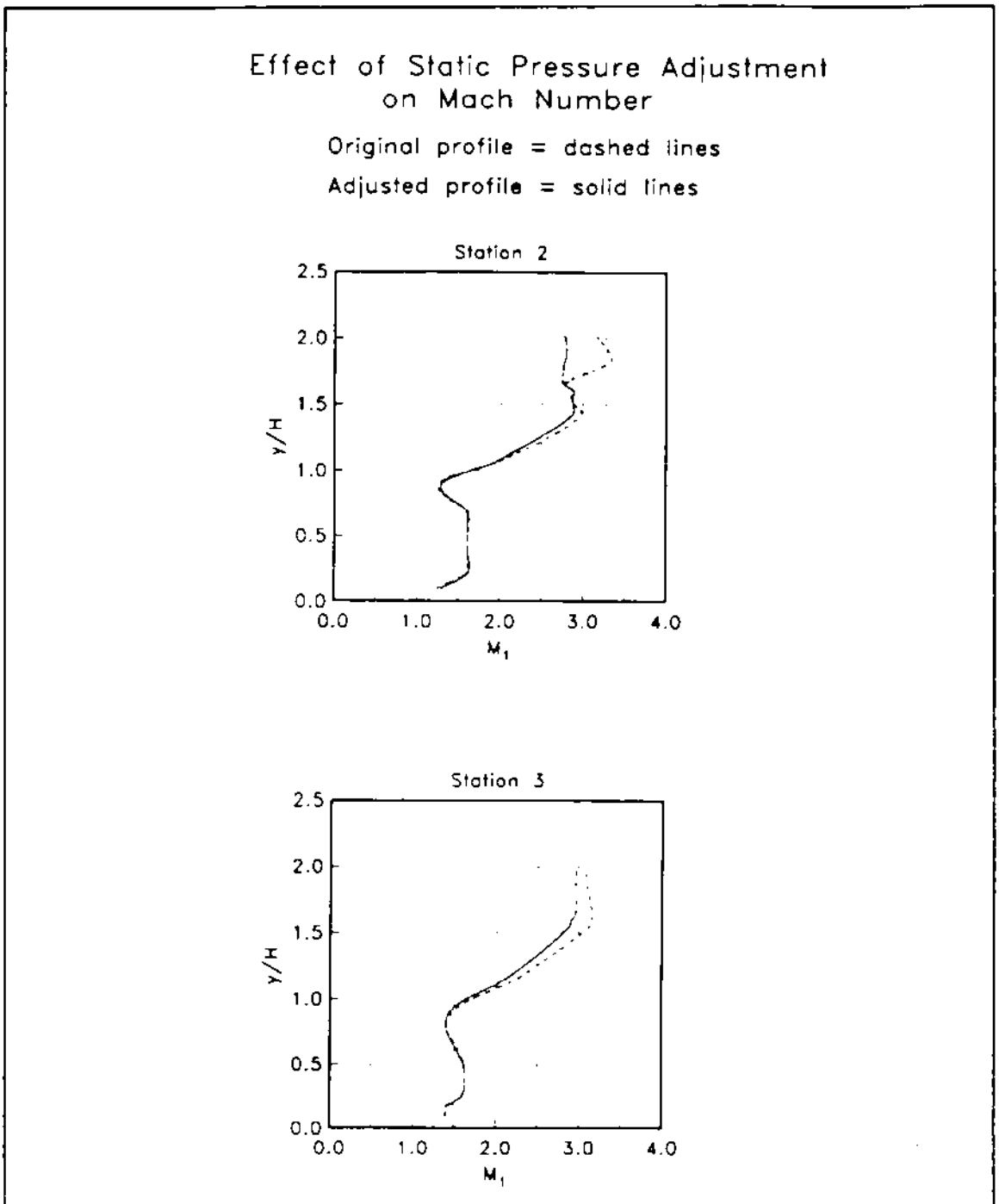

Figure 40. Effect on Mach Number

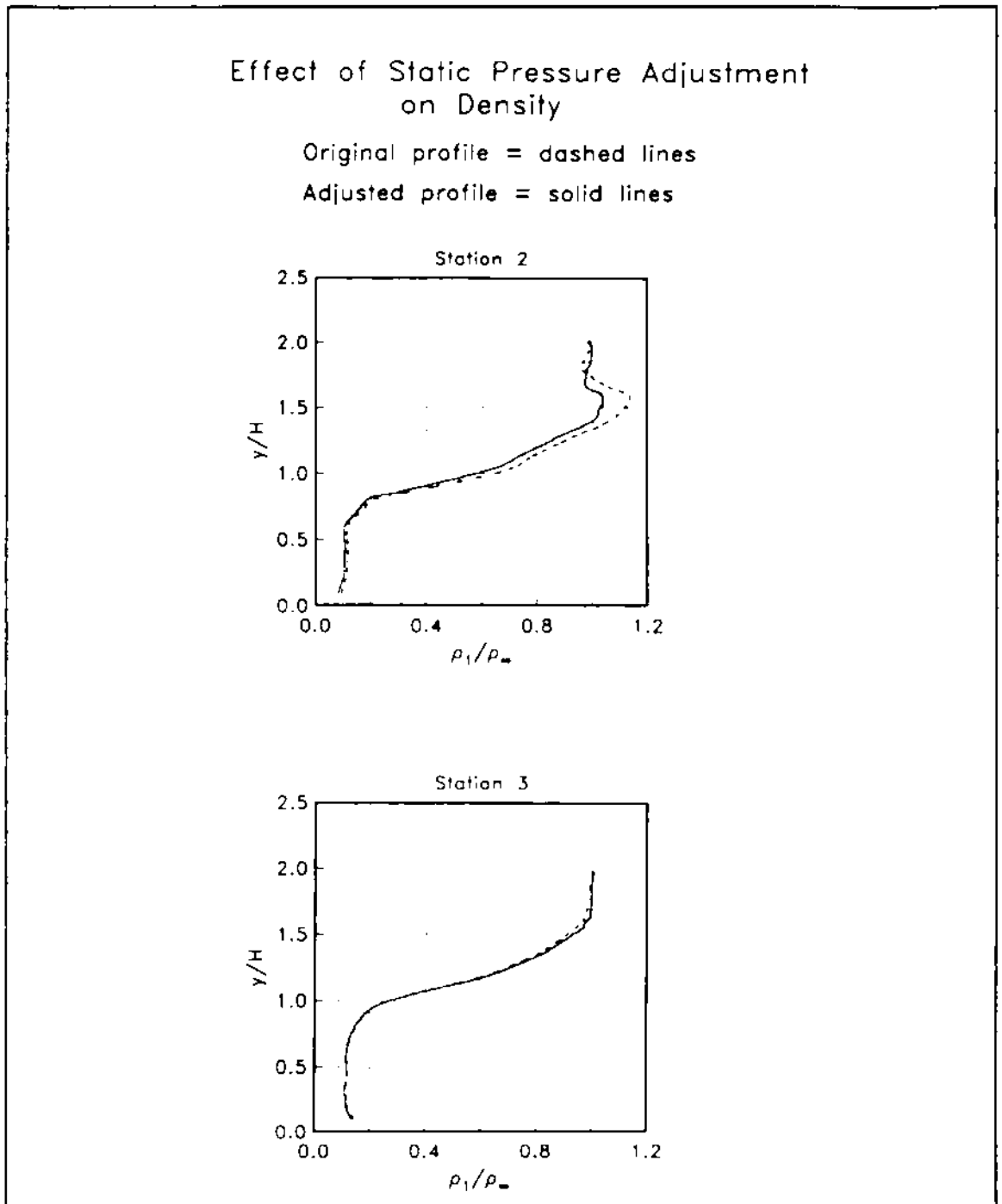

Figure 41. Effect on Density

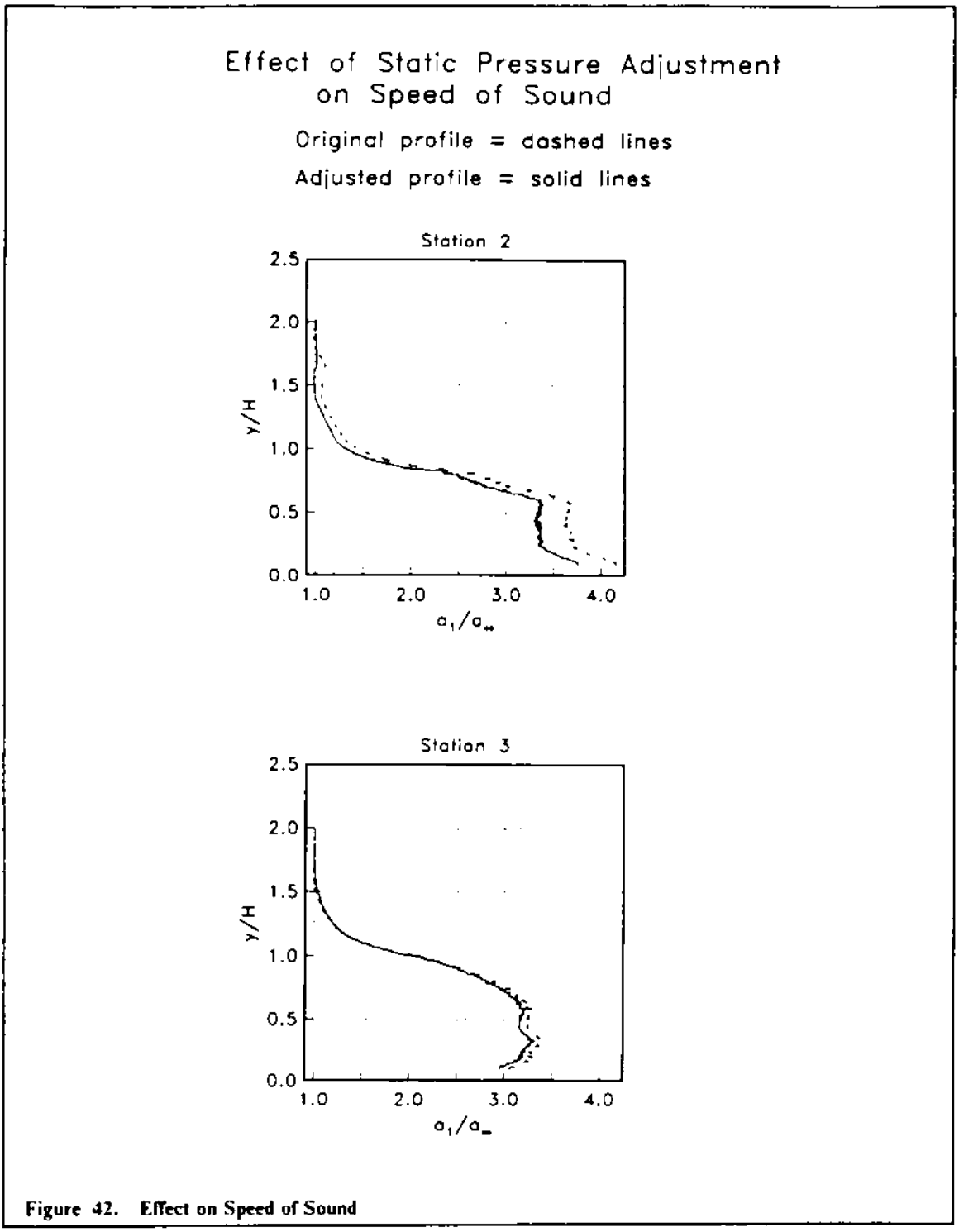

Figure 42. Effect on Speed of Sound

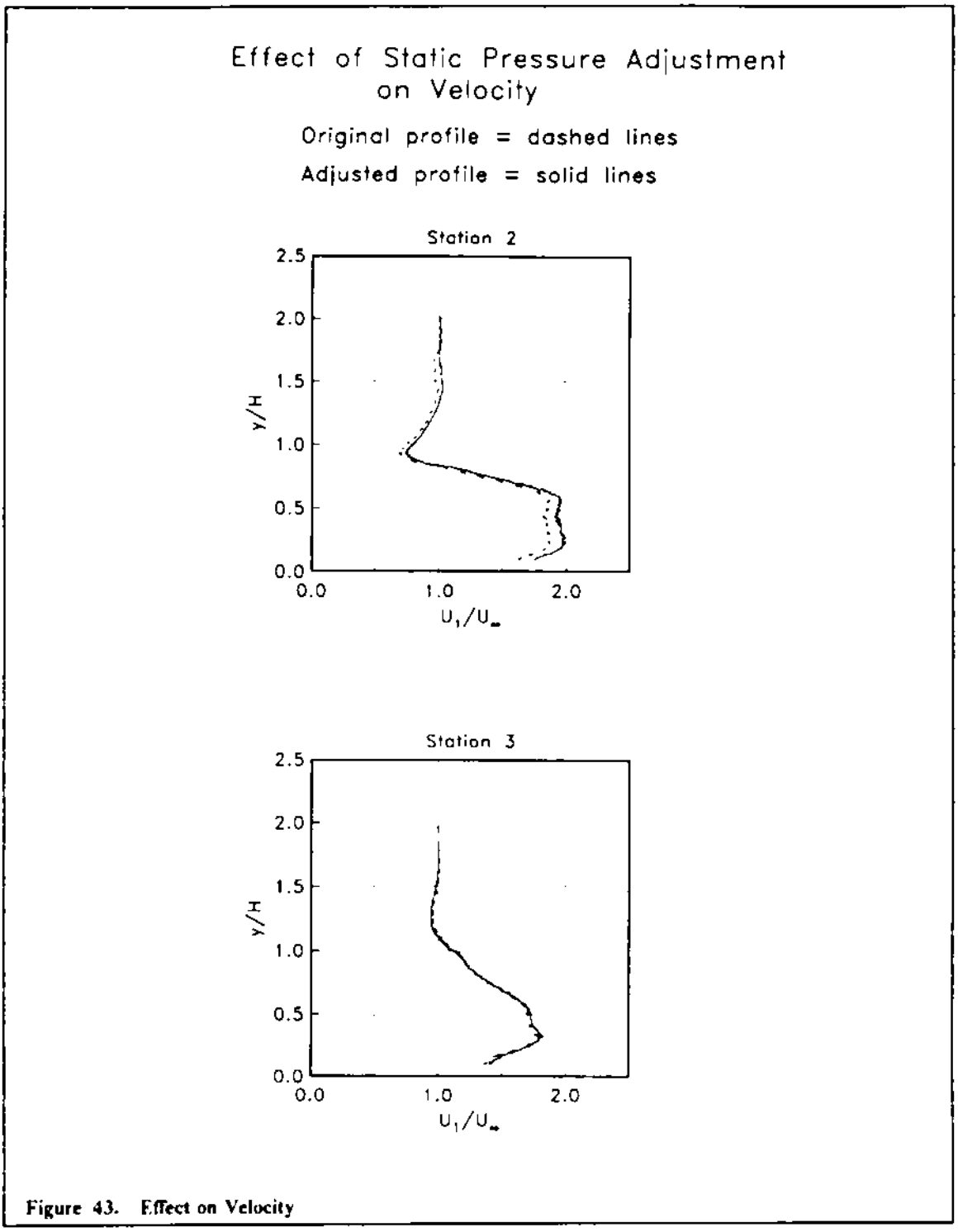

Figure 43. Effect on Velocity

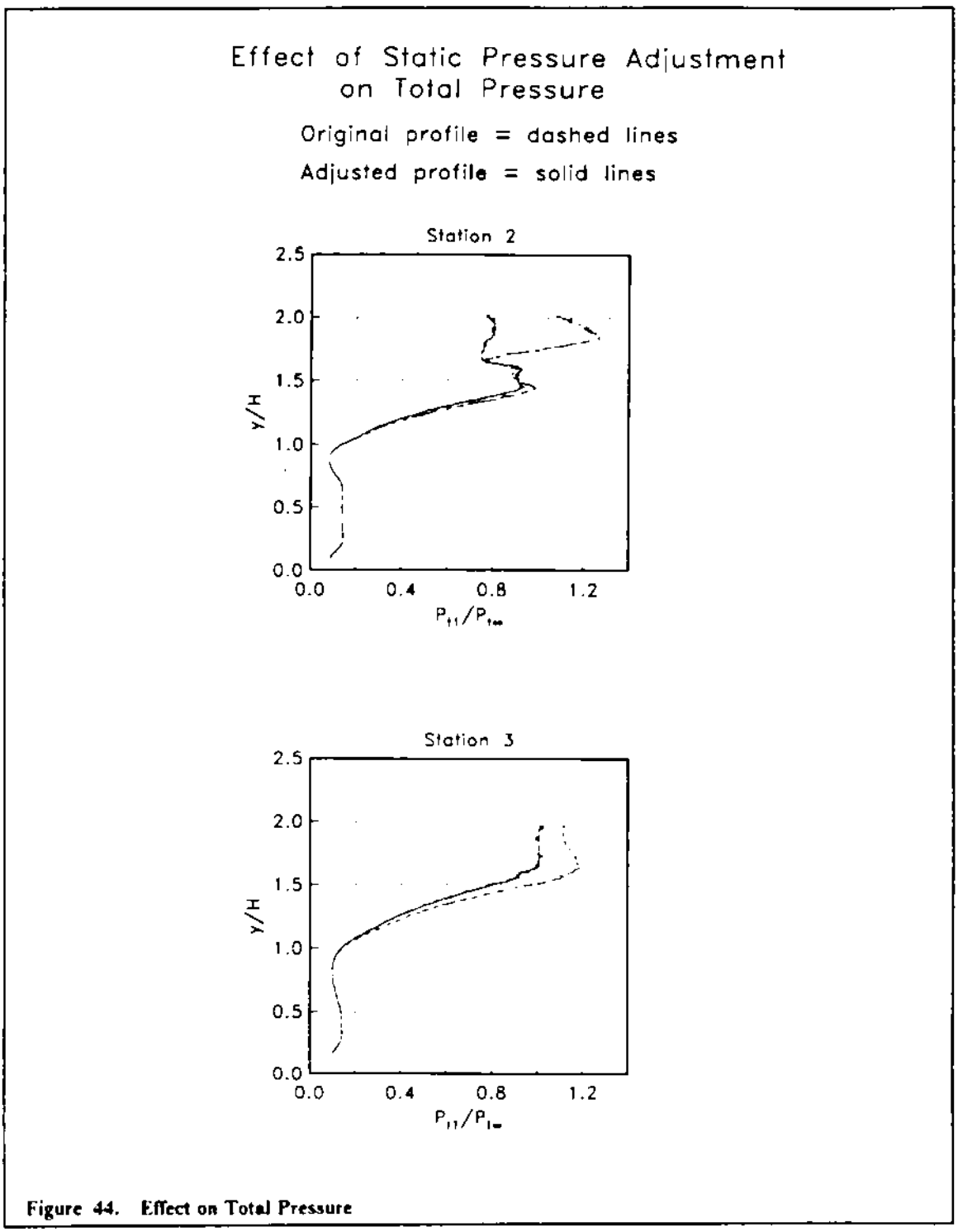

Figure 44. Effect on Total Pressure

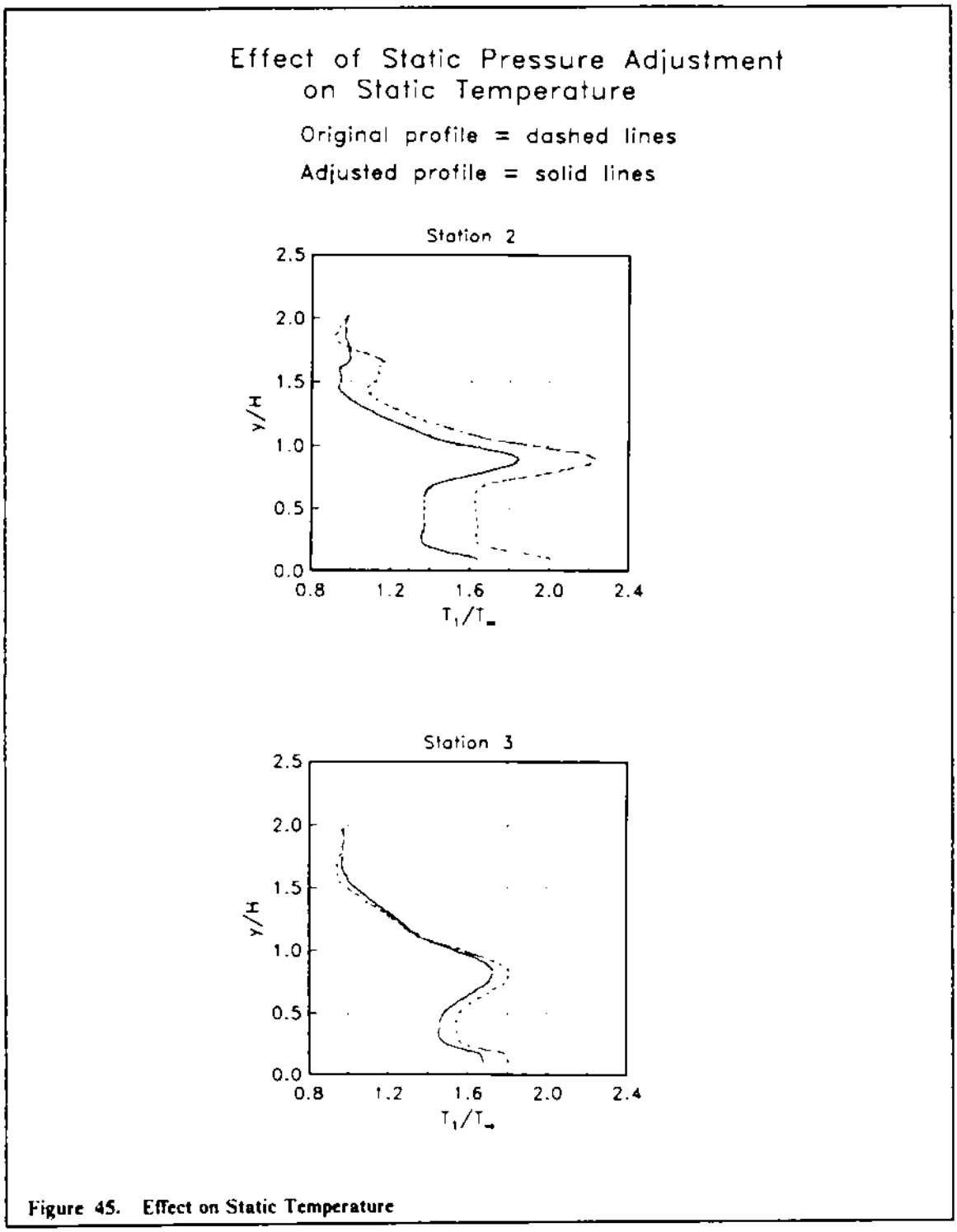

Figure 45. Effect on Static Temperature

Chapter 7

COMPARISON WITH AIR INJECTION AND DISCUSSION

In this chapter, trends in the results mentioned in **Chapter 6** are expounded upon, with particular emphasis placed on how helium injection compares with air injection and what theoretical models say about this flowfield. The air-injection data includes unheated and heated slot flow cases as documented by Smith[23]. In the profiles, helium injection (Case 1) is compared to unheated air (Case 2), since both injectants have about the same ambient temperature. Therefore, differences in mixing come mainly from the effect of having different gases and not from any temperature influences. The heated-air injection (Case 2a) pictures are presented here. As concluded by Smith, no appreciable visual difference occurs between either the unheated-air or the heated-air injection cases.

7.1 Flow Visualization

In the Schlieren photos, the qualitative flow features as described in Figure 1 manifest themselves in both Case 1 and in Case 2a, shown in Figure 16 and Figure 46, respectively. Some differences are apparent. First, the full boundary-layer/shear-layer/wall region, characterized by the lightly shaded area as compared to the darker freestream region, expands to 15-20 percent larger in the helium injection case by St. 4. A more accurate figure is available from the profile data, but this observation already indicates that with the helium injection the shear layer grows faster, signifying better mixing. The potential core characterized by the dark region near the wall seems to extend much further downstream in the air case. Again, this measurement is not reliable since it strongly depends on the lighting of the Schlieren system. Lastly, the sharp white separation line distinctly emanates from the splitter-plate lip in both cases. This feature is more intense in Case 1 as seen by the sharpness and length of the feature downstream; a pronounced white area is visible through St. 4 for helium, albeit it gradually spreads out, while for air the bright white zone disappears by St. 2. Of course, since $\frac{\rho_1}{\rho_\infty}|_{\text{Case 1}} = 0.1$ and $\frac{\rho_1}{\rho_\infty}|_{\text{Case 2}} = 0.5$, there should be a more intense demarkation zone on a Schlieren photo between the air and helium flows in the helium-injection case because of larger density gradients.

The Nanoshadowgraphs in Figure 17 and Figure 47 show evidence of the difference in the separation line as well, thus supporting the fact that such a difference exists and is not just a phenomenon of the optical lighting

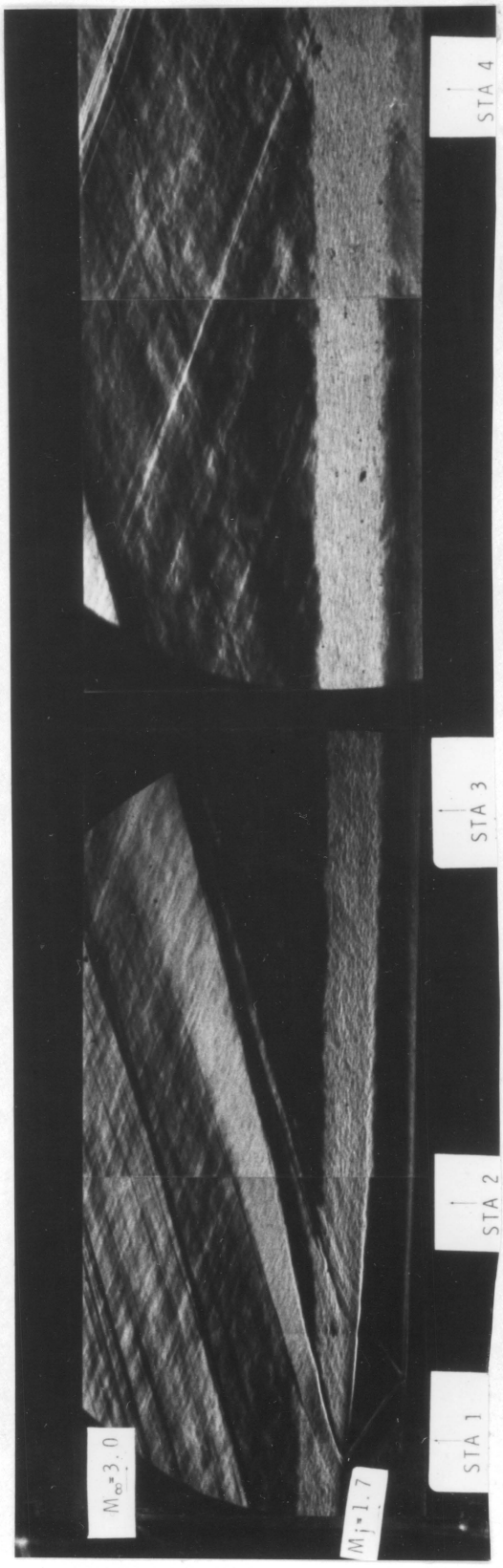

Figure 46. Spark-Schlieren of the Air/Air Flowfield

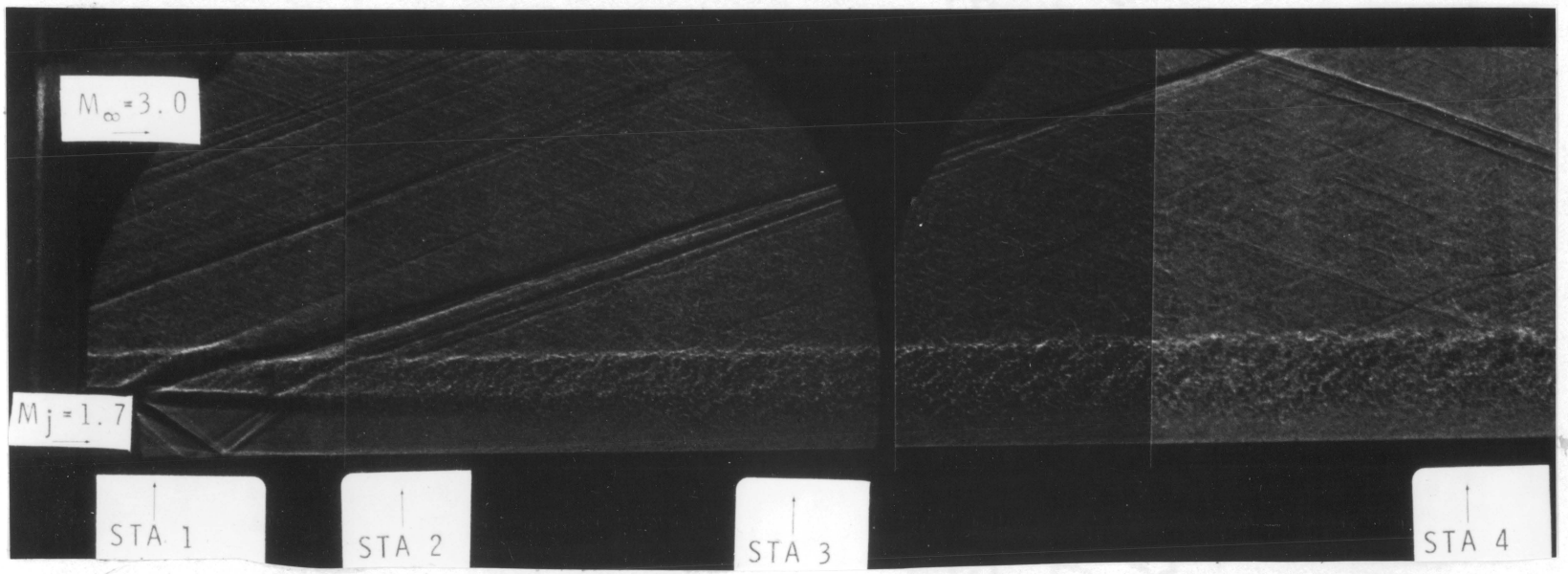

Figure 47. Nanosecond Shadowgraph of the Air/Air Flowfield

arrangement. A final indication that the helium injectant mixes better is that the freestream boundary layer has broken up by $x/H = 16$ while for air the top remnant of the boundary layer is still visible at $x/H = 20$.

7.2 Mean-Flow Data and Modeling

Figure 48, Figure 49, and Figure 50 overlap the raw data files for Case 1 and Case 2. For the most part, the magnitudes and trends are comparable, since test conditions are matched and gas concentration does not effect the Pitot, cone-static, and stagnation-temperature measurements appreciably. The P_{t2} profiles reflect a larger mixing layer; P_{t2} smooths out at about $y/H = 2$ for helium and $y/H = 1.5$ for air at St. 4. The wake region for Case 1 is larger and slightly higher up as shown at St. 2 and St. 3 in Figure 48.

Figure 51 shows the Mach number distribution. Helium enters at 1.78 while the air injection expands to 1.70. The core flow remains more intact for the helium injectant at all downstream stations. At first, this observation seems an incongruity in that, by intuition, the potential core length should shorten for a higher rate of mixing, which the helium injection exhibits. As discussed subsequently, however, these two conditions can coexist. In the density profiles in Figure 52, helium has a density ratio 1/5 of the air injectant as normalized by freestream air. Figure 53 compares the velocity profiles. Interestingly, the helium injection velocity initially is about twice the freestream velocity while the

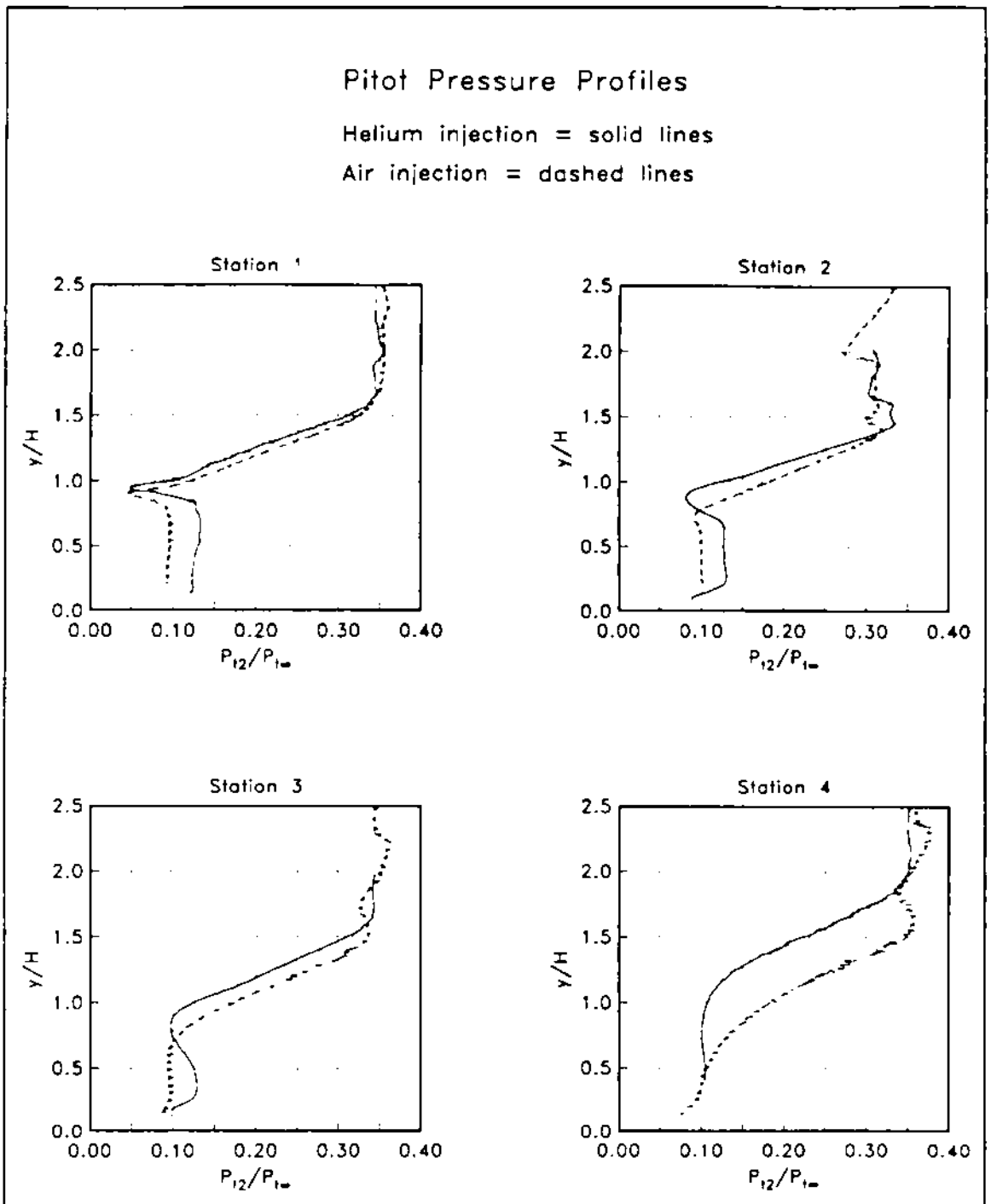

Figure 48. Pitot Pressure Comparison

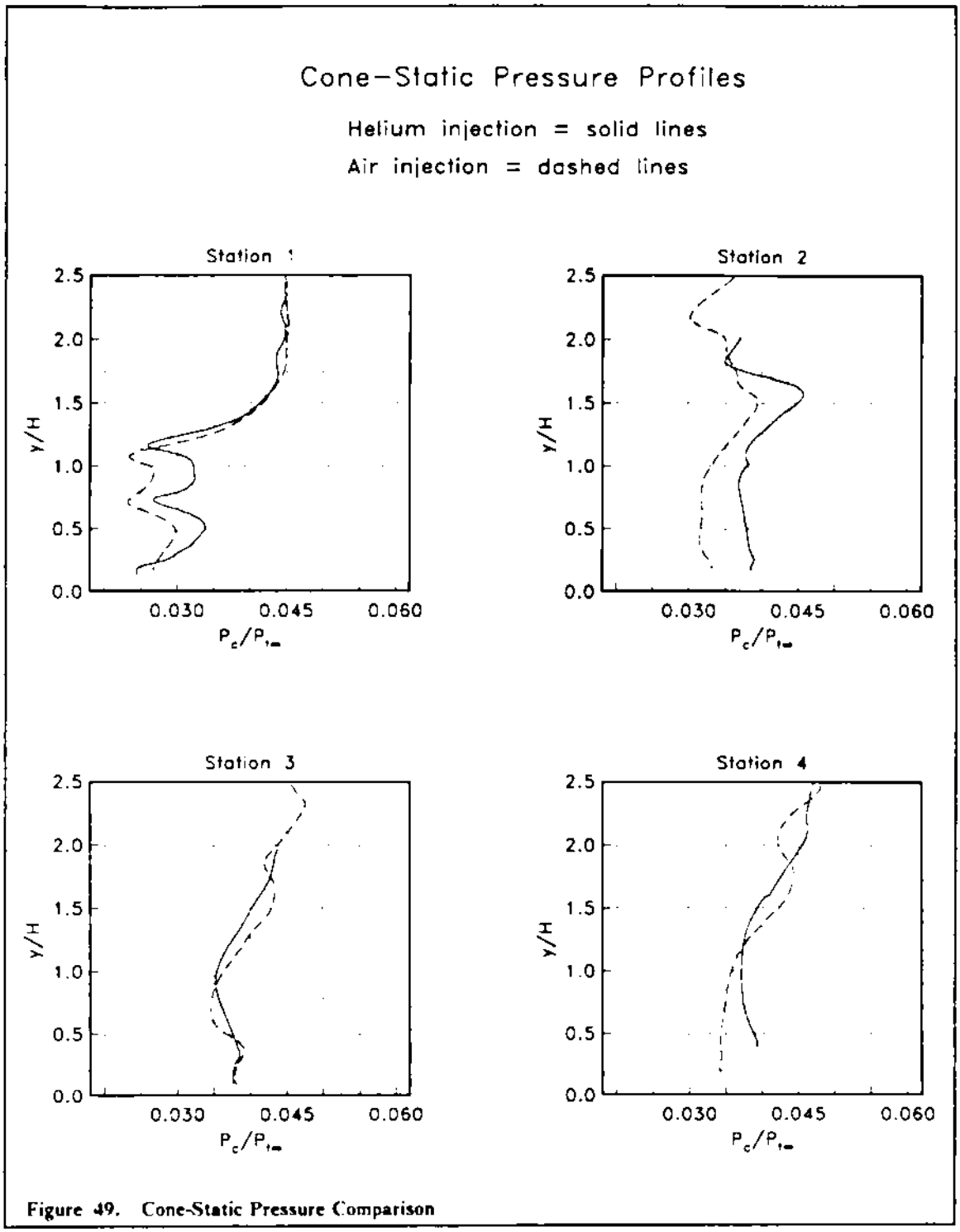

Figure 49. Cone-Static Pressure Comparison

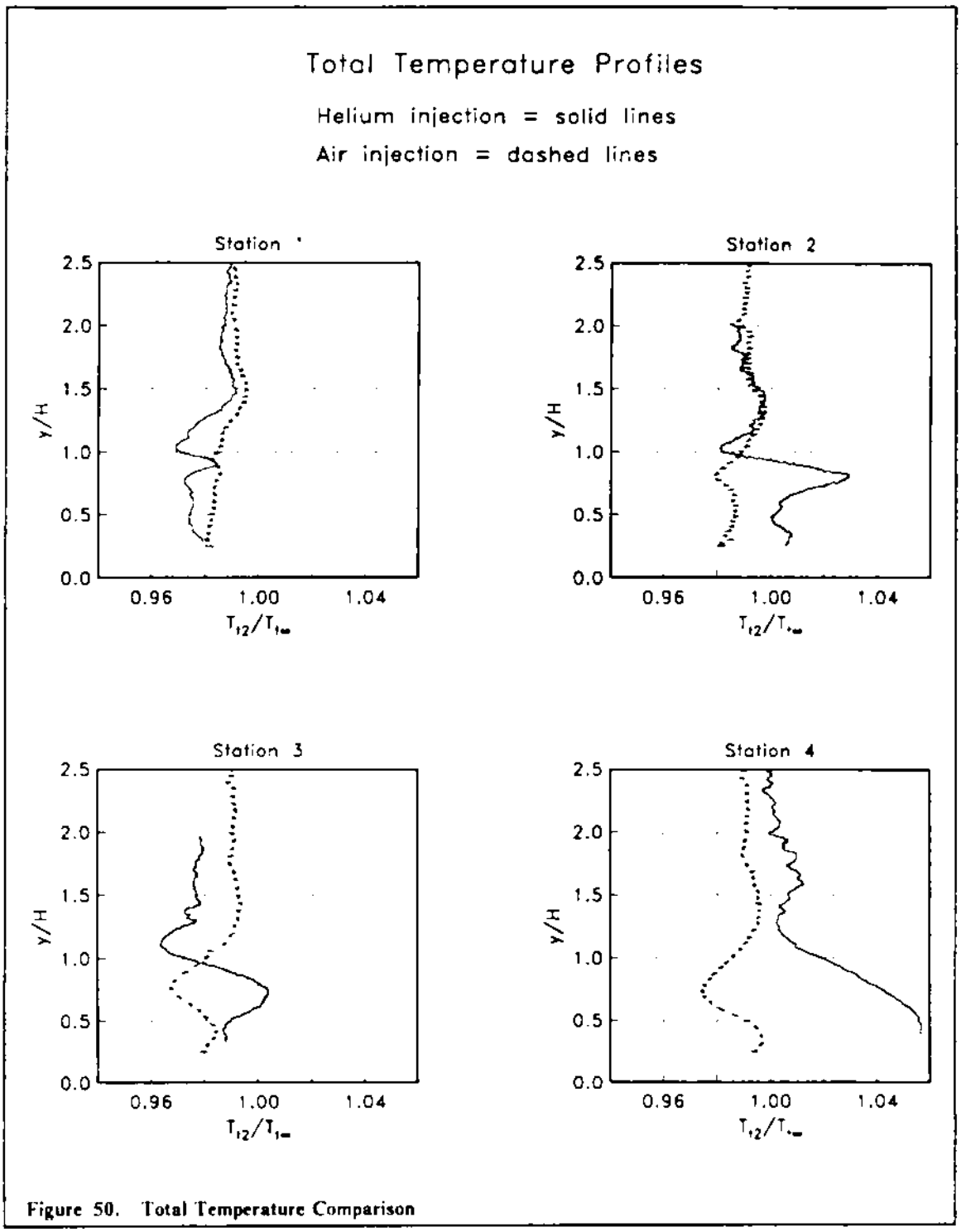

Figure 50. Total Temperature Comparison

air injection has a velocity 0.7 the freestream value. With the velocity gradient $\frac{\partial U}{\partial y}$ greater for Case 1, better mixing is expected due to the higher turbulent shear stresses that a large velocity gradient produces, as modeled by eddy-viscosity and mixing-length formulations[15,39] .

Figure 54 combines the density and velocity effects into a single term ρU, the mass flux. In general, $\frac{\rho U}{\rho_\infty U_\infty}$ values further away from unity promote mixing[17,39], and the comparison between Case 1 and Case 2 supports this trend. The $\frac{\rho_1 U_1}{\rho_\infty U_\infty}|_{\text{Case 1}}$ is 0.2, half the air injection value. The ρU profile also gives a good estimate of the mixing-layer thickness. In the helium-injection case, the concentration profiles directly indicate the mixing-zone size at each station. Unfortunately, with the air-injection case, there is no corresponding measurement. By comparing the trends at St. 4 of the ρU and concentration profiles for helium injection, however, ρU can be seen to reach a constant value at about the same point as the concentration goes to a constant value of $\chi_{He} = 0.0$. Therefore, by this observation, ρU is found to be a good indicator of the mixing-layer height in this slot-injection configuration. For the air-injection case then, if ρU is assumed to indicate mixing-layer size, the nondimensional mixing-layer thickness at St. 4 is about 1.6 from the ρU profile. Thus, the helium case, with a normalized mixing-layer thickness $\frac{\Delta_{s4}}{H}$ of 2.1, shows 25 percent more growth in the mixing layer by St. 4.

Figure 55 depicts the static-pressure comparison. There is a slight shift downward at St. 1 for the air case due to some small variations in flow patterns and also to some error in the LVDT (see **App. A**) between the two cases. These

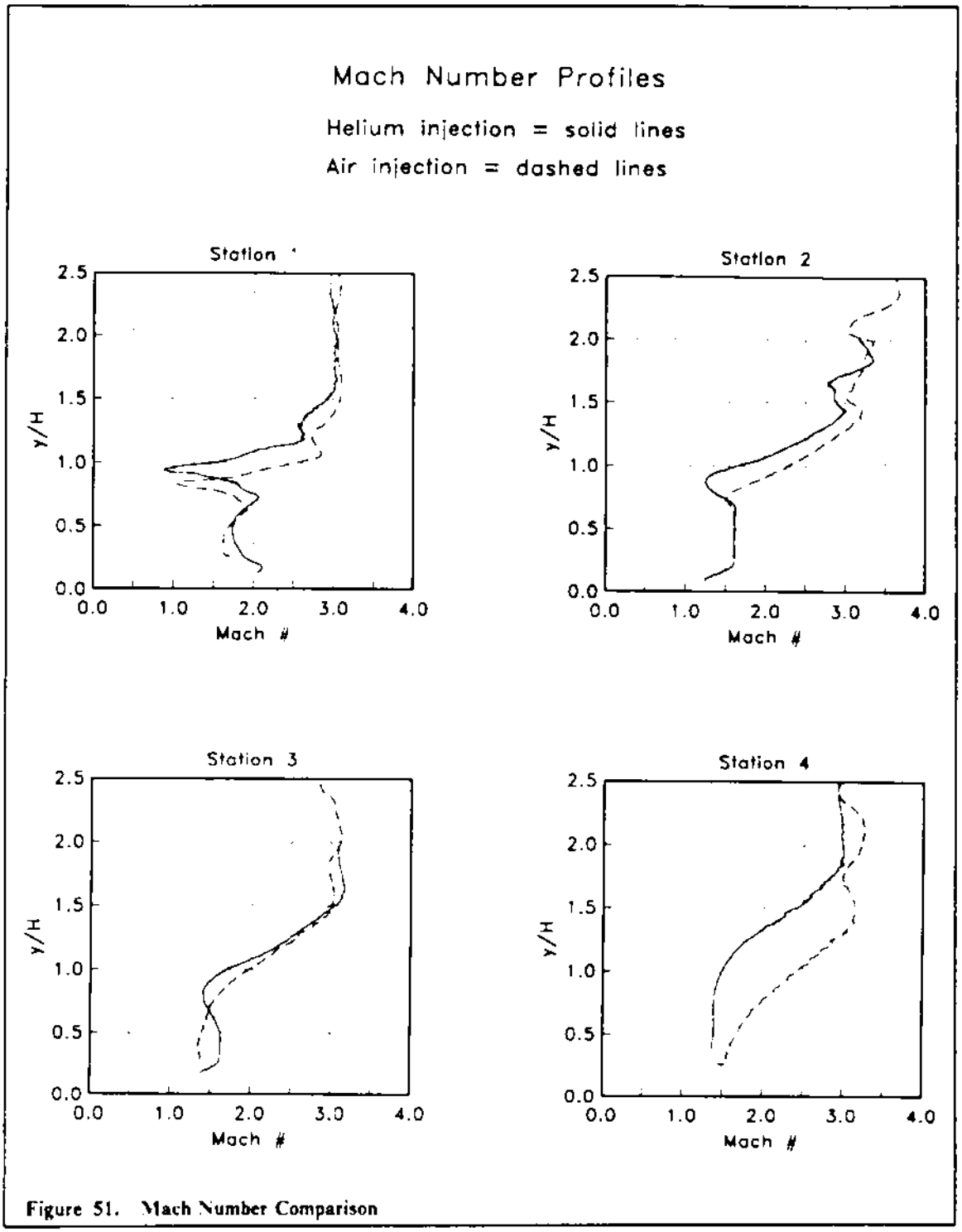

Figure 51. Mach Number Comparison

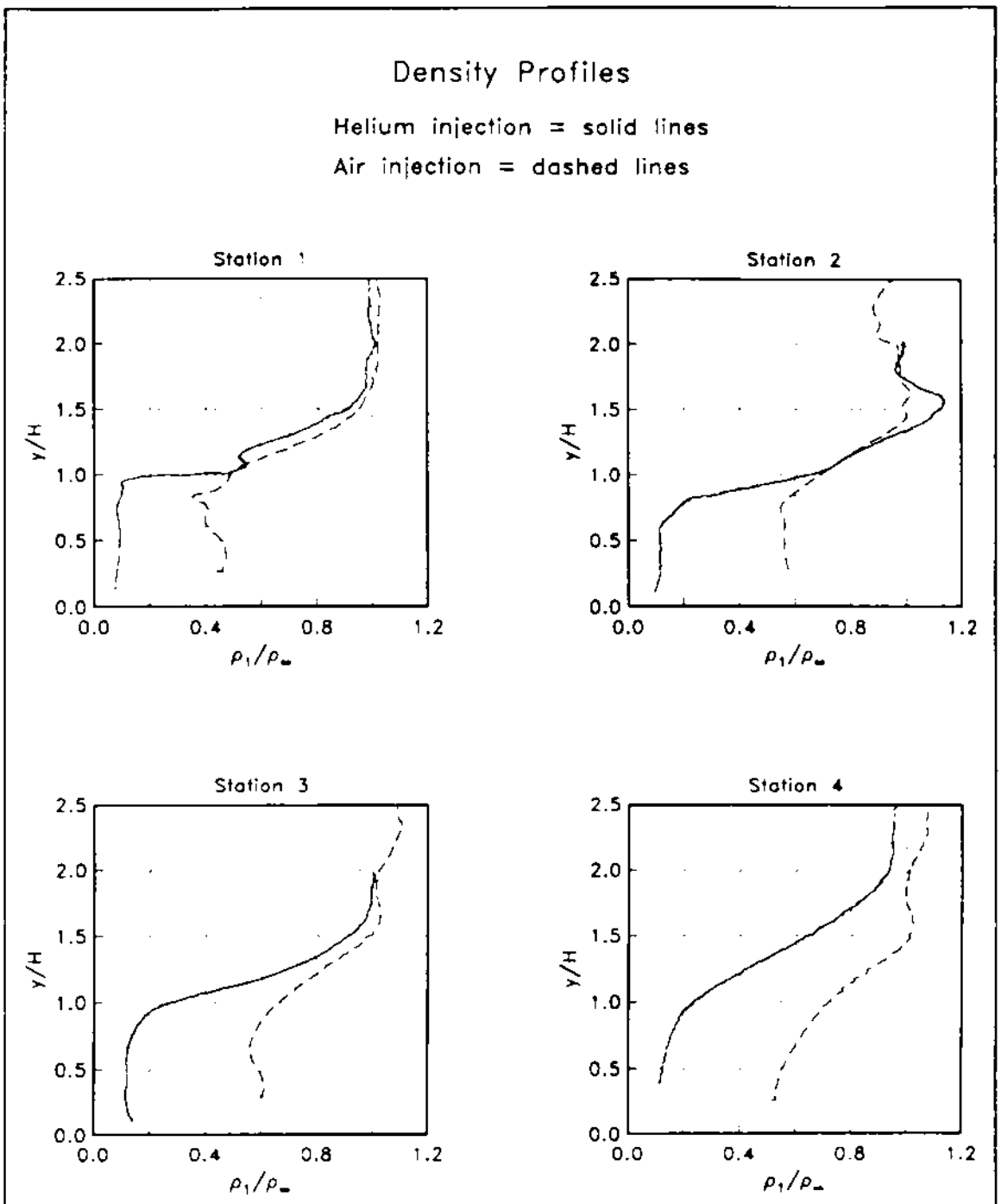

Figure 52. Density Comparison

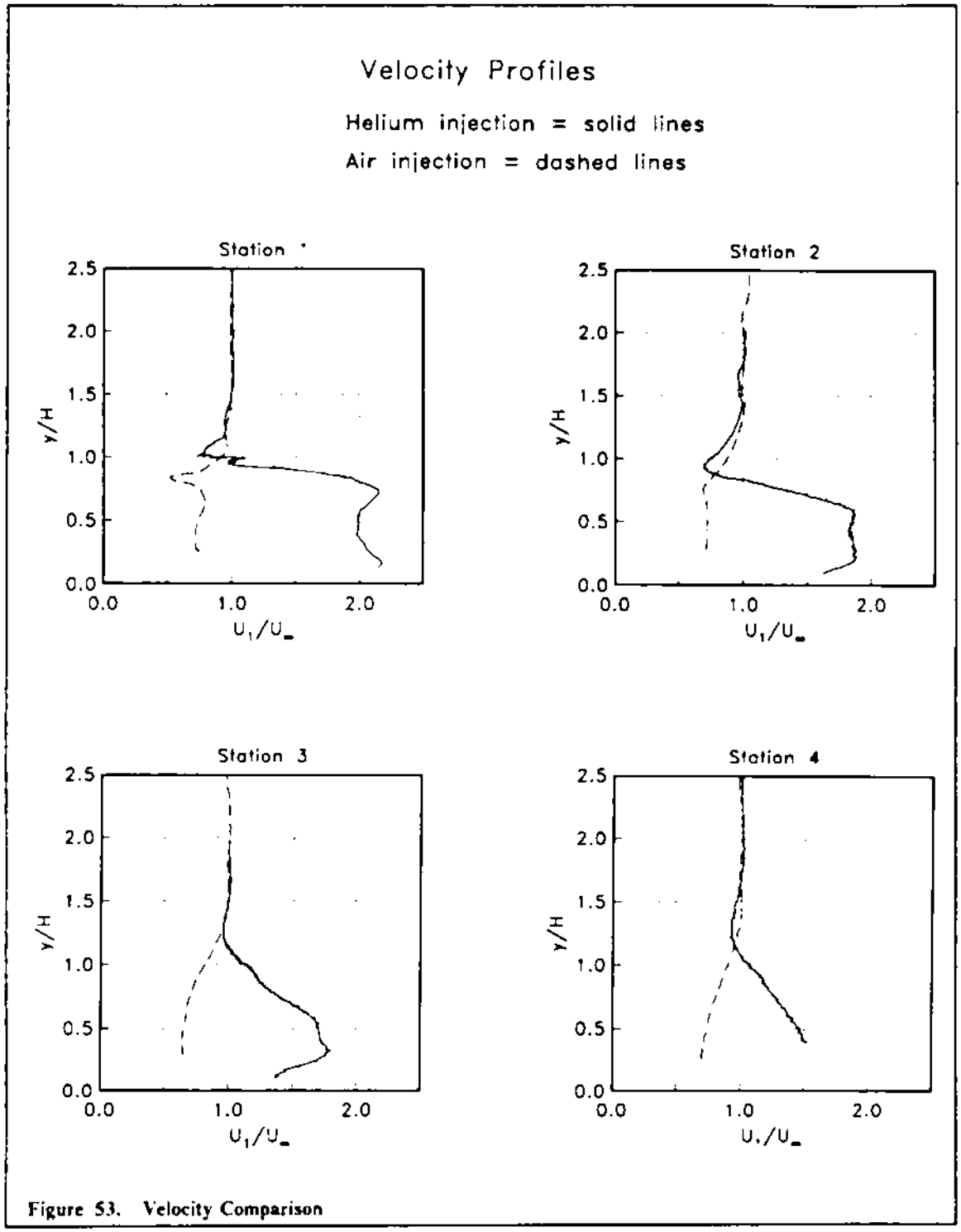

Figure 53. Velocity Comparison

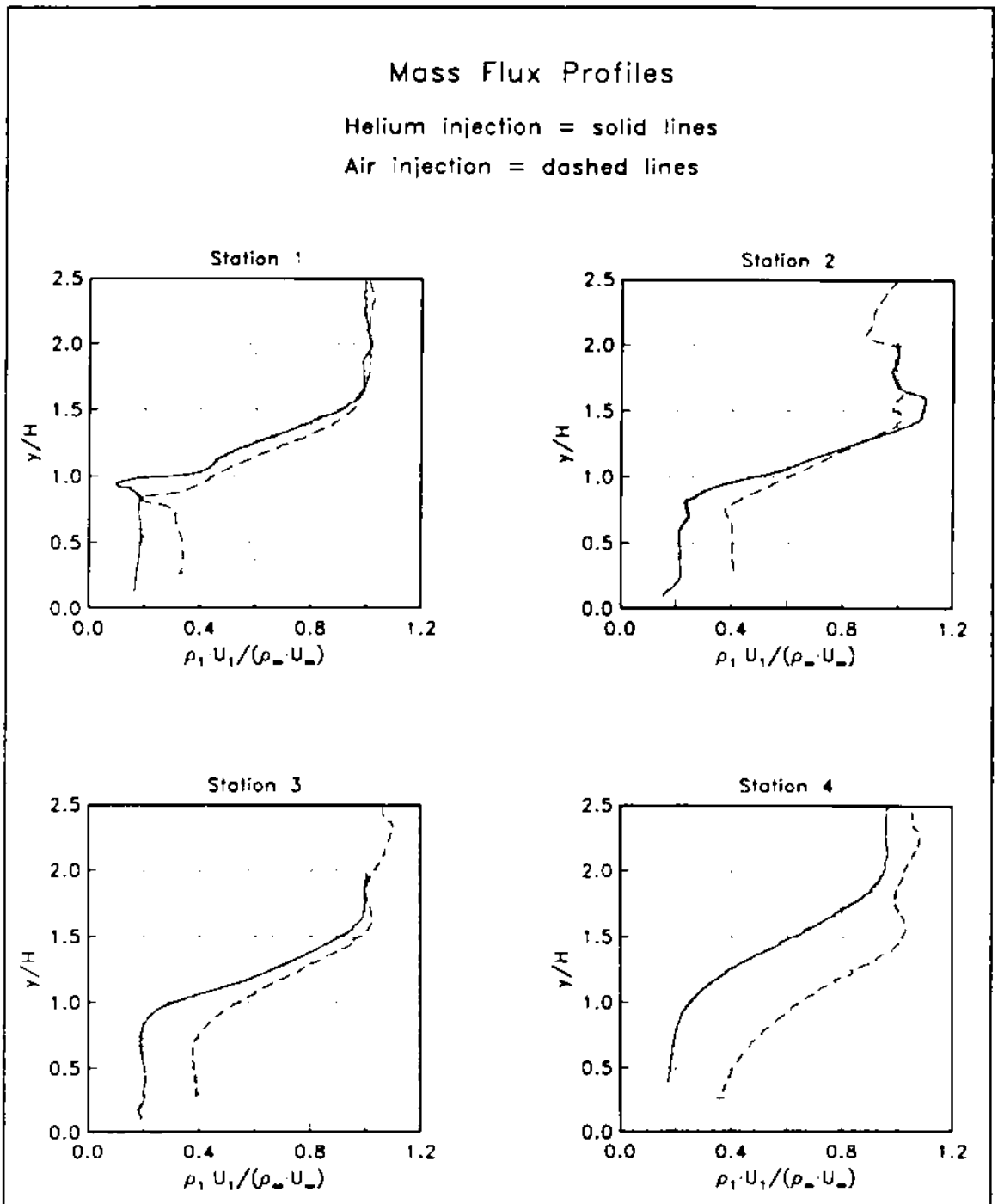

Figure 54. Mass Flux Comparison

reasons probably also contribute to the aforementioned higher location of the wake region in the helium case. At St. 2, $P_t|_{Case\ 1}$ is shifted to the right indicating higher P_t values through the slot and shear layer regions as compared to the freestream. The maximum variation is 40 percent. In a boundary-layer type region, P_t constant across the region is expected, but the experimental values vary significantly. Of course, there are waves in the viscous region here. Considering also the small scale of the fluctuations and the limited accuracy of the cone-static pressure measurement, though, the observed variations are not unreasonable.

In short, the profiles of helium injection versus those of air injection show that the helium case definitely mixes better, with the mixing layer at St. 4 about 25 percent larger in Case 1.

An independent correlation that may shed more light on mixing comparisons is the convective Mach number introduced by Papamoschou and Roshko[40] and used by others[41,42]. Their argument states that, for compressibility effects in supersonic shear flows, the Mach numbers relative to a coordinate frame moving with the large-scale structures within the shear layer strongly influence mixing properties, not the "laboratory" Mach number relative to a fixed coordinate system. Moreover, an important trend is that as the convective Mach number M_{conv} increases toward unity, mixing becomes poorer. Thus, with this model and its related formulas, M_{conv}, as calculated with the current initial conditions, is about 0.7 (for both the air and helium-side M_{conv}) in the helium case and 0.3 for air injection. Accordingly, the air case should mix better than the helium case, based solely on compressibility effects. Helium injection, however, mixes better

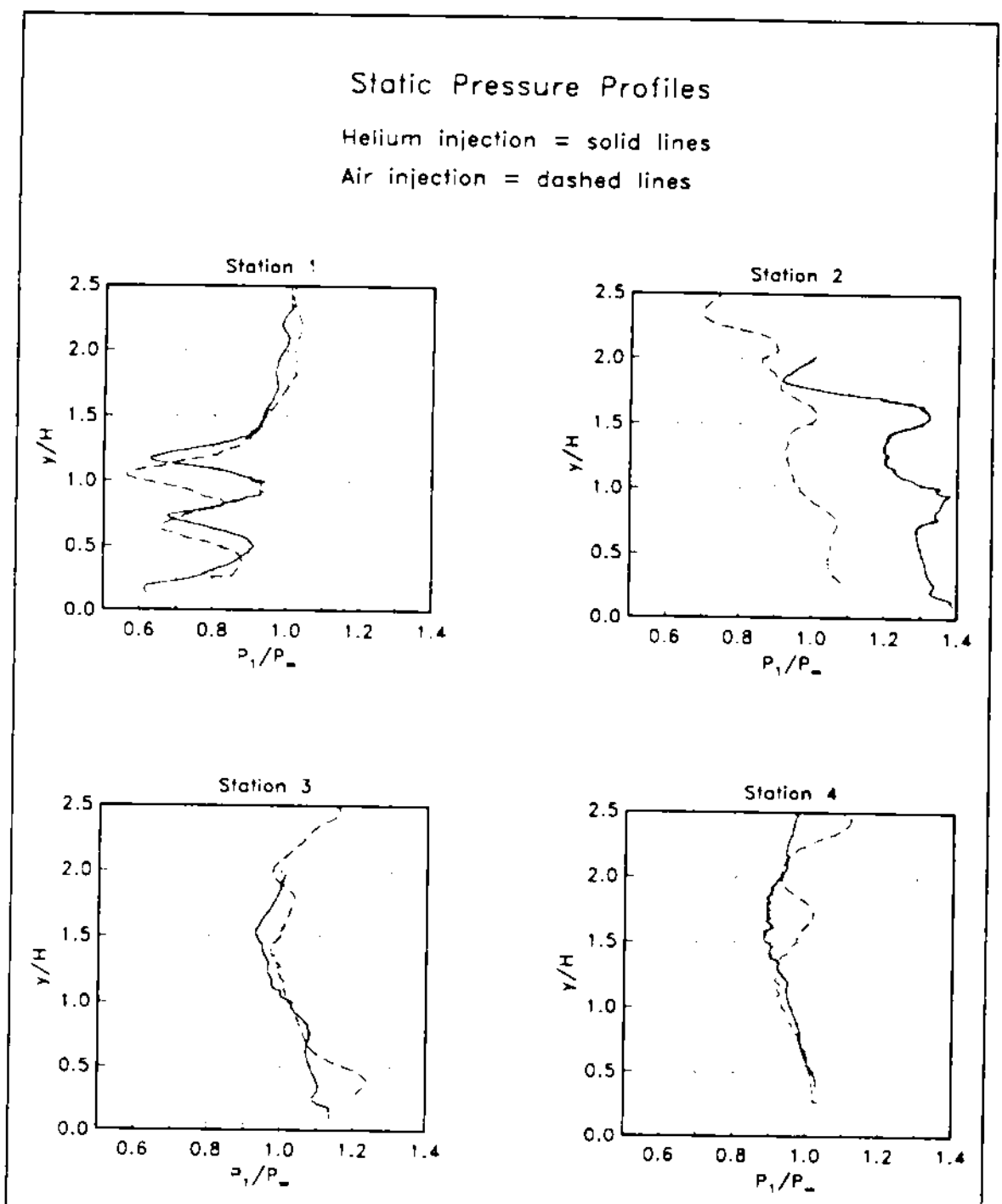

Figure 55. Static Pressure Comparison

in the test cases. Thus, there seems to be a stronger influence in the region of concern than the convective Mach-number compressibility factor. The influence of velocity gradients may prove greater in this region, since they are quite large in the helium case and have direct importance in turbulence models. In addition, the mass-flux ratio is smaller for the helium case, and as has been previously stated, lower ρU values increase mixing. This contribution may be greater than what the M_{conv} model accounts for. Moreover, the convective Mach number model concentrates on free shear layers, whereas in this study the shear layer is wall-bounded on one side. Thus, a wall region interacts with the shear layer. The merging of viscous zones and possible resulting self-induced pressure gradients[43] may have an adverse effect on the applicability of this model. Also, another inherent assumption of the model is that a step change in flow quantities occurs across the lip of the splitter plate. In the actual test case, however, a sizeable freestream boundary layer δ initially "rides" on top of the forming shear layer. Previous experimentation with this theory suggests that in this type of flowfield, the region where the complete M_{conv} similarity solutions apply does not occur until about $x = 25\delta$ downstream[44]. Thus, the furthest downstream stations of this study are located in the part of the flow where M_{conv}-applicability just begins to have a larger influence. In the near-field flow which this report documents, gradients and ρU effects play a more important role.

Another basis for comparison of the two test cases is the entrainment rate of freestream air into the injectant layer. Numerically integrating Eqn. [5.15] for Case 1 and Eqn. [5.14] for Case 2 to the slot height at St. 1 results in values for

the slot mass flow rates for the two cases: $m_e|_{\text{Case 1}} = 0.17$ kg/sec while $m_e|_{\text{Case 2}} = 0.34$ kg/sec, a 50 percent difference. As a reference, the isentropic mass flow rate for a one-dimensional, choked channel is calculated from the following equation[45]:

$$\dot{m} = \frac{P_t A_*}{\sqrt{T_t}} \sqrt{\frac{\gamma}{R}} \left(\frac{2}{\gamma + 1} \right)^{\frac{\gamma+1}{2(\gamma-1)}} \qquad [7.1]$$

With nominal slot conditions, the theoretical $\dot{m}$, then, is 0.175 kg/sec for Case 1 and 0.354 kg/sec for Case 2. The experimental values are quite close to the theoretical predictions, and the discharge coefficient (the ratio of the actual mass flow rate to the isentropic value) is about 0.96 for both cases. This result is especially comforting in Case 1, because the proper operation of the concentration probe is further confirmed. At St. 4, Eqn. [5.14] is integrated to the respective mixing-layer heights for both cases: $\frac{\Delta_{s4}}{H} = 2.1$ for Case 1 and $\frac{\Delta_{s4}}{H} = 1.6$ for Case 2. This integration gives $m_{s4}|_{\text{Case 1}} = 1.03$ kg/sec and $m_{s4}|_{\text{Case 2}} = 1.02$ kg/sec. Thus, by St. 4, $m_{s4}|_{\text{Case 1}}$ is essentially the same as $m_{s4}|_{\text{Case 2}}$, even though the slot helium flow is considerably less than the slot air flow. This increased growth in Case 1 comes from the higher entrainment rate in the helium-injection case. With Eqn. [5.16], entrainment in Case 1 for the entire shear layer up to St. 4 is 0.86 kg/sec, while for Case 2, $m_{ENT} = 0.68$ kg/sec. Therefore, 30 percent more freestream air mixes with helium, which accounts for the higher mass flow rate by St. 4.

Two applicable theoretical formulations for the entrainment rate is one proposed by Crocco and Lees[46], where the mass entrained into a boundary layer-like flow is given by

$$\frac{d\dot{m}}{dx} = n\rho_\infty U_\infty \qquad [7.2]$$

and another proposed by Schetz and Billig[47] for base flows, where the mass entrained is

$$\frac{d\dot{m}}{dx} = n\rho_\infty U_\infty \left| 1 - \frac{\rho_j U_j}{\rho_\infty U_\infty} \right| \qquad [7.3]$$

for $0.01 < n < 0.03$ in both equations. The Crocco and Lees model has been shown to give rough but adequate estimates of the mass entrainment rate[4]. From the profile data in **App. D** and the experimental entrainment rates stated previously, n values of Eqn. [7.2] that match the data are found near the usual range in both test cases. The difference in n between the two cases is about 25 percent. A more representative model, the Schetz and Billig formulation accounts for mass-flux differences between the slot flow and the mainstream. This model also gives n values near the expected range, but in this instance, the constant in Eqn. [7.3] does not vary by more than 5 percent between the two cases. Since n does not change significantly, this model better represents the general slot injection flow where the slot mass flux is different from the mainstream ρU.

As an overall consistency check for the helium case, m_{He} at St. 4 is deduced from m_{s4} and compared to m_e to see if the values are equal, i. e., if the helium slot mass flow is conserved. The $m_{He}|_{s4}$ is found by applying Eqn. [5.15] to the ρU and concentration profiles at St. 4. This procedure, then, gives $m_{He}|_{s4} = 0.14$ kg/sec, a 20 percent difference from $m_e = 0.17$ kg/sec. This difference seems large at first,

but by performing an error analysis similar to the one in **App. A**, the uncertainty of the m calculation is determined as 20 percent. Thus, the disparity between $m_{He}|_{s4}$ and m_e falls in the error range. Of course, to a lesser extent, the difference may also be attributed to a not perfectly 2-D slot flowfield, which will produce slightly different profiles across the z-direction. Nevertheless, m_e and $m_{He}|_{s4}$ are reasonably close to each other and to the theoretical, isentropic value to say that the data is consistent.

Interestingly, for the experimental values, if the Case 1 upper limit of integration for Eqn. [5.14], $\frac{\Delta_{s4}}{H}|_{Case\ 1}$, is taken as the same as in Case 2 ($\frac{\Delta_{s4}}{H}|_{Case\ 2} = 1.6$), then $m_{s4}|_{Case\ 1} = 0.53$ kg/sec, about a 50 percent reduction from 1.03 kg/sec, which is the result of integrating to the actual mixing-layer height at St. 4 in Case 1 ($\frac{\Delta_{s4}}{H}|_{Case\ 1} = 2.1$). This fact indicates that most of the entrainment of air occurs along the top 1/3 of the mixing layer and codifies the observation that though the Case 1 shear layer grows faster, the helium core seems more pronounced at St. 4 than the core in Case 2. In other words, although there is air mixed into the entire region up to the wall, a significant core can still exist if most of the interaction is confined to the upper portion of the shear layer. This phenomenon is more pronounced in the helium-injection case. This feature further suggests that the majority of the mixing occurs along the two-gas interface within the large-scale eddies of the shear layer and that lower-level, almost secondary, mixing occurs within the wall region. In short, there seems to be two regions of mixing: an "active" area at the interface between the two constituents in the shear layer and a relatively "passive" zone below the shear layer. The

active zone corresponds to the turbulence layer, the dimensions of which are obtained from the Shadowgraph photos.

In support of this observation, the convective Mach number model, if assumed applicable to a limited extent by St. 4, provides some concurring data. Papamoschou and Roshko[40] mention a normalized spreading rate $\frac{\delta'}{\delta'_{in}}$ of the shear layer, which is a function of M_{conv} and where "in" represents an incompressible case at the same velocity and density ratios as the corresponding compressible case. The following formulation is given for the incompressible case:

$$\frac{\delta_{vis}}{x} = 0.17\,\frac{\Delta U}{U_{conv}} = 0.17\,\frac{(1-r)(1+\sqrt{s})}{1+r\sqrt{s}} \qquad [7.4]$$

where ΔU is the difference in velocity between the "fast" stream and the "slow" stream and δ_{vis} is the visual shear-layer thickness. With nominal values of $r = 0.487$ and $s = 12$ for the helium-injection case, $\delta'_{in} = 0.145$ from Eqn [7.4]. The experimental Case 1 δ' comes from measuring two sources: the turbulence layer thickness in the Shadowgraph photo and the mixing-layer distribution in Figure 26. From the visual record, δ increases to 0.60 slot heights at St. 2, 0.80 slot heights at St. 3, and 1.63 at the last station; with $\delta' \simeq \frac{\Delta\delta}{\Delta x}$, this gives $\delta' = 0.076$. From the mixing-zone data, δ is 0.25, 0.50, 1.50, and 2.1 at Sts. 1, 2, 3, and 4, respectively, which results in an average value of $\delta' = 0.142$. From Figure 10 in Reference [38], at $M_{conv} = 0.7$, $\frac{\delta'}{\delta'_{in}} = 0.5$. For the turbulence layer points, $\frac{\delta'}{\delta'_{in}}\Big|_{exp} = 0.52$, and for the mixing-layer points, $\frac{\delta'}{\delta'_{in}}\Big|_{exp} = 0.98$. The visual points agree well with the reported values whereas, with the mixing layer points, the ratio shows significantly better mixing than what is expected. Thus,

the mixing layer is not the same size as the turbulence layer, with the visual turbulence-layer data from the Shadowgraph assumed as fairly accurate, since it matches what is expected. In fact, these results also suggest the turbulence layer size corresponds to the free shear layer development as predicted by the M_{conv}-model. If taken alone, this information can provide no definite conclusions, since the visual measurement can be regarded as too subjective; however, with this observation combined with the previous m_{ENT} evidence and the observation that the mixing-layer size from the concentration distribution is larger than what the Shadowgraph indicates for the turbulent region, the mixing layer is concluded to be noticeably larger than the turbulence layer, most of which lies within the mixing layer. This independent correlation also suggests the aforementioned presence of the two distinct zones of mixing: primary mixing in the turbulence layer and some secondary mixing outside the turbulence layer but within the mixing layer. Lower-energy diffusion effects and density differences drive the mixing in this passive zone in the injectant core, where the mixture composition, though not all helium, remains nearly so.

Figure 56 summarizes the characteristic layers in the helium slot-injection flowfield. The plot includes the reaction layer.

To determine how well the data from this study fits in with other tests, Figure 57 from Thomas et al.[5] plots data from various experiments involving slot injection into a supersonic airstream. This plot includes the present study as well as investigations by Yates[17], Burrows and Kurkov[48], and Cary and Hefner[11] and shows α_{max}-decay at several downstream locations. Yates injected hydrogen at

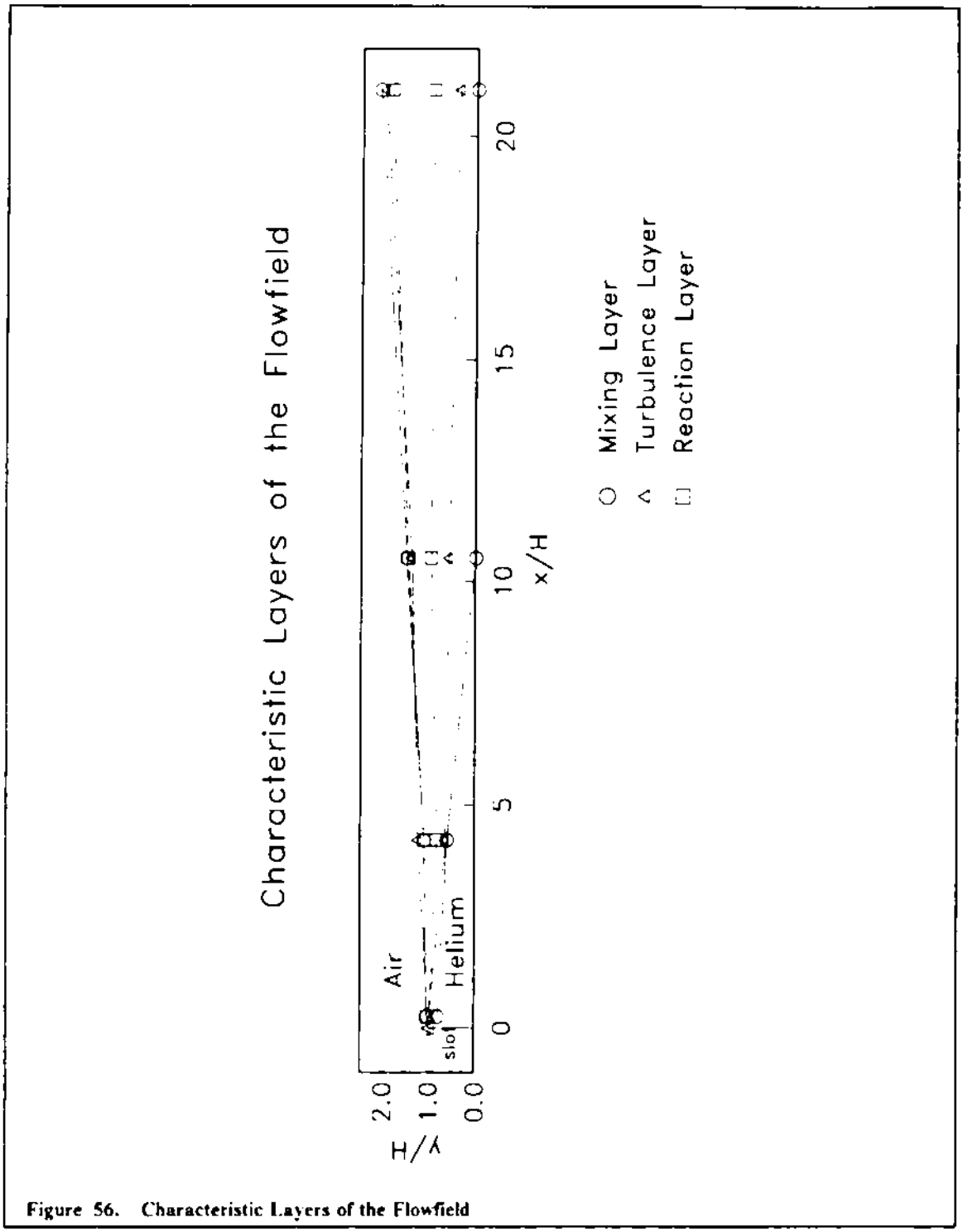

Figure 56. Characteristic Layers of the Flowfield

$M_j = 1.2$ into a freestream at $M_\infty = 2.1$ and captured gas-composition information using a sampling probe. The data of Yates compares reasonably well with the present study, performed at roughly similar conditions. Investigating sonic hydrogen injection into a Mach 2.5 freestream, Burrows and Kurkov provide one concentration point at $x/H = 89$. Also, the experiments of Cary and Hefner indirectly give concentration levels at several locations beyond $x/H = 21$; the α_{max} is deduced from their data on wall effectiveness of sonic slot-injection film cooling with air ($M_\infty = 6$). These last two data sets provide an indication of possible far-field mixing and α_{max}-decay for the present helium slot-injection case.

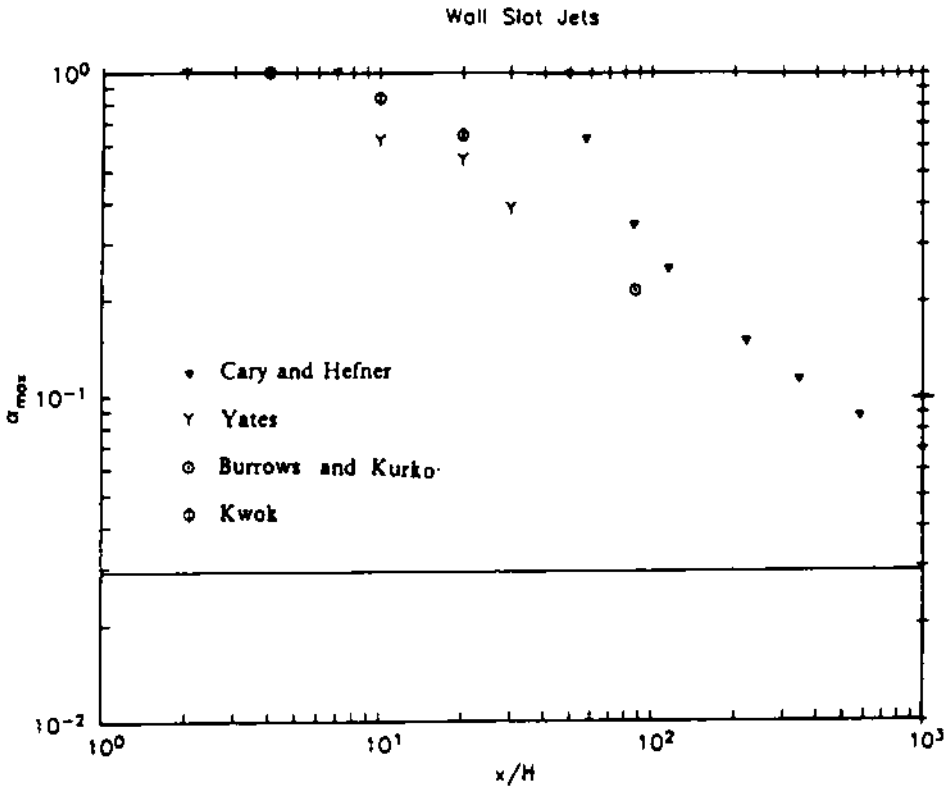

Downstream Decay of the Maximum Concentration for Wall Slot Jets.

Figure 57. Downstream Decay of the Maximum Concentration: from Reference [5], Figure 3.

Chapter 8

CONCLUDING REMARKS

8.1 Conclusions

In summary, this investigation accomplishes several purposes. First, the study tests the concentration probe for its application towards mean flow measurements in supersonic shear layers. From the resulting concentration profiles, data accurate to within 0.02 mole fraction of helium is obtainable; however, the probe data analysis exhibits an inherent increased sensitivity to errors near 100 percent helium levels (see **App. A**), which necessitates more accurate measurements there. Nevertheless, this probe configuration is recommended for further use in any binary-gas flowfield. Secondly, this study compares the helium slot injection to air slot injection in supersonic flow, which helps to provide more information on flow dynamics within the shear layer and

the effect of different gases in similar test configurations. The mixing layer in the helium-injection case grows faster, so that by St. 4, the mixing layer is 25 percent larger than that in the air-injection case. Also, 30 percent more freestream air is entrained into the shear layer. Interestingly, even though by St. 3 some degree of mixing occurs throughout the shear-layer/wall region, most of the mixing is confined to an active zone at the top third of the mixing layer, where gradients are largest and transport mechanisms are most energetic. This observation indicates that most of the mixing occurs in the turbulence layer while a smaller degree of mixing is present outside the turbulence layer but within the mixing layer. Lastly, the main thrust of this investigation is to further document the slot-injection flowfield at supersonic conditions and contribute good information to the growing database of injection schemes. Of course, slot injection does not offer the best mixing qualities, but it has other advantages and is a good baseline case. This study has generated a consistent and representative set of data which, hopefully, can serve as a reference for future comparisons with experiments, computational models, and theoretical analyses.

8.2 Future Work

This investigation represents a step toward detailing the flowfields of different injection schemes and providing more information on high-speed mixing dynamics. More work is necessary. This study looks at slot injection conditions

at one pressure ratio $\frac{P_j}{P_\infty}$. Varying the pressure ratio across a range of underexpanded and overexpanded cases should provide some interesting differences. Heating the helium wall jet to change the mass-flux ratio should give more data about mass-flux effects, which are acknowledged as an important influence. Also, running the same tests with different freestream values and/or slightly different combustor model dimensions may offer further insight. A combustor-model arrangement which permits further downstream measurements would give a more thorough documentation of the injectant decay and mixing.

A natural area for future work is experimentation with different injection schemes, mostly 3-D configurations such as an array of jets. Another worthwhile venture may be to return to previously investigated injection schemes, such as the combination slot and normal injections of King et al.[4], where air is used for simplicity, and substitute helium, which exhibits different qualities than air. Hopefully, by doing this, injection of an actual fuel such as hydrogen can be better modeled, since helium should behave more like hydrogen because they are both light gases compared to air.

Finally, developing a concentration probe to capture turbulent quantities may provide valuable insight to turbulent mixing, and also, a natural progression to understanding the mixing problem is actual combustion tests with these injection schemes. These combustion tests would give a more detailed and real-case scenario of the flow dynamics and combustion-reaction attributes of the injection schemes.

APPENDICES

Appendix A

Error Analysis

Naturally, measurements are kept as accurate as possible, but, nonetheless, some errors occur. As mentioned in **Section 4.1**, the errors in PI, T_{t2}, and dc voltage of the sensor limit the accuracy of the concentration values to $\pm$ 1-2 percent mole fraction of helium.

In general, with the Pitot, cone-static, and thermocouple probes, the errors mainly stem from transducer restrictions and curve-fit deviations. The Pitot measurement has an accuracy better than $\pm$ 0.034 atm ($\pm$ 0.5 psia, 1 percent); the cone-static transducer reads to $\pm$ 0.0068 atm ($\pm$ 0.1 psia, 1 percent). With the thermocouple, additional discrepancies enter into the computation. These include a possible lack of sufficient venting which causes superfluous gas retention in the probe tip, unavoidable heat transfer to the end supports of the wire, and time lag in the response of the thermocouple wire to fast temperature changes. This lag is on the order of 0.1 sec [24]. From Reference [23], the total temperature error is

estimated as ± 2 percent in a small temperature-gradient field. In all cases, the calibration curve-fit error remains less than ± 0.2 percent, so that the curve-fit does not introduce any significant inaccuracies.

Unfortunately, the measurement procedure cannot account for waves and shocks impacting on the probe tip, which is especially true for the cone-static probe. Also, the spatial resolution of a measurement is limited by practical considerations of the probe inlet size. Good spatial resolution is important in delineating points along a traverse, since with too large a probe inlet, local information of flow quantities is reduced.

For the LVDT, errors in cathetometer reading, calibration curve fits, and probe time response affect the accuracy of the displacement measurement. The cathetometer resolves to 0.001 cm (0.0004 in), less than 0.5 percent error, while the curve-fit introduces a 1 percent deviation. The slowest time response of any probe is 0.1 sec, so given a traverse velocity of 0.406 cm/sec, the maximum offset due to time lag is 0.0406 cm. Over a 3.05-cm traverse distance, this lag gives less than a 1.5-percent maximum error.

Accounting for these factors, a numerical analysis determines the accuracy of the reduced mean-flow profiles: M, U, ρ, ρU, a, P, and T. In this procedure, the measurement variations which give the largest combined errors are used to calculate a worst-case upper limit on the error band. The ρ, U, and a depend more strongly on the concentration level, especially concentrations near 100 percent helium, than do the other variables so that concentration variation causes larger errors in these three variables. This dependence arises from the gas

constant R directly entering into the formulas that compute ρ and a (Eqns. [5.12] and [5.10], respectively). Furthermore, the effects of R are more pronounced for χ_{He} near 1.0. For example, at 100 percent helium, $R = 2078 \frac{J}{kg°K}$; at 98 percent helium level, R drops to $1847 \frac{J}{kg°K}$, an 11 percent change which is introduced into the density and velocity calculations. Thus, with this R-dependence in mind, a program computes errors for the mean-flow variables at two reference cases, 100 percent helium and 0 percent helium. The results follow:

	All Helium	All Air
• M	0.54 %	0.71 %
• ρ	10.0 %	1.7 %
• U	6.7 %	1.5 %
• ρU	2.7 %	0.52 %
• a	6.5 %	2.4 %
• P	2.9 %	2.3 %
• T	1.5 %	2.7 %

As expected, ρ, U, and a have much larger errors for the 100 percent helium case. Thus, in terms of these variables, an accurate measurement of

concentration on the all-helium end is essential. Apparently, when ρ and U are combined, the errors partially cancel so that ρU varies by only 2.7 percent in the 100 percent helium reference. For the other flow variables and for those cases away from 100 percent helium, the errors are acceptably reasonable.

Appendix B

Static-Pressure Ratio Derivation

This section outlines how the desired injection pressure is calculated. First, with isentropic-flow relations, the freestream conditions are defined as

$$\gamma = 1.4$$

$$M_\infty = 3 \rightarrow \frac{P}{P_t} = 0.0272$$

$$P_{t_\infty} = 95 \text{ psia} \rightarrow P_\infty = 2.586 \text{ psia}$$

In previous air slot-injection tests involving the same model configuration, the injection conditions were

$$\gamma = 1.4$$

$$\frac{A_e}{A^*} = 1.34$$

$$P_{t_j} = 10.7 \text{ psia}$$

which gives

$$M_j = 1.7 \rightarrow \frac{P}{P_t} = 0.2026$$

$$P_j = 2.168 \text{ psia} \rightarrow \frac{P_j}{P_\infty} = 0.838$$

In the helium slot-injection, $\frac{P_j}{P_\infty}$ remains the same as that in the air injection case. In this way, the flow dynamics will be similar so that comparisons from a common basis can be made. Therefore, if $\frac{P_j}{P_\infty} = 0.838$ ($P_j = 2.168$ psia) and the area ratio stays the same, then, with $\gamma = 1.67$, the results are

$$M_j = 1.78 \rightarrow \frac{P}{P_t} = 0.1650$$

and finally

$$P_{t_j} = 13.1 \text{ psia}$$

Thus, the plenum chamber of the injector block must see 13.1 psia for proper expansion of the helium injectant to the desired ratio.

Appendix C

Other Effects on Concentration-Probe Response

In addition to the response of the pressure measurements (0.1 sec), the "flush-out" time of the concentration probe affects the frequency response of the probe as well. The internal throat governs the mass flow rate in the probe, and for any instant in time, the assumption is that the hot film sees the same mass flow as the sonic orifice. So, this time constant is then the period a fluid particle takes to travel from the sensor plane to the choked exit. Based on the dimensions of the probe and typical velocitites inside the probe, the flush-out time is about 0.5 msec. Thus, even with this factor accounted for, the pressure response remains the limiting value.

Next, an analysis is performed to see how much error is introduced in the concentration result if the stagnation temperature is assumed constant across the shear layer. In general, T_{t2} profiles vary by about 12 deg Kelvin maximum. In the analysis, a constant-temperature line of reasonable value is passed through

the shear layer. With a maximum 12 deg Kelvin variation, this change causes an error in concentration of less than 2 percent mole fraction of helium. Thus, with reasonable fluctuations in T_{t2} at typical test conditions, the concentration probe is relatively insensitive to stagnation temperature changes. The following figure summarizes these results at St. 2. In addition to the insensitivity of the probe to moderate temperature changes, the probe has an acceptable response to flow angularity. With the probe pitched at 15°, concentration changes by less than 2.5 percent in molar composition[36].

More details are available in References [36] and [37].

Temperature Effect on Concentration

Station 2

Temperature profile = solid lines

Temperature constant = Δ

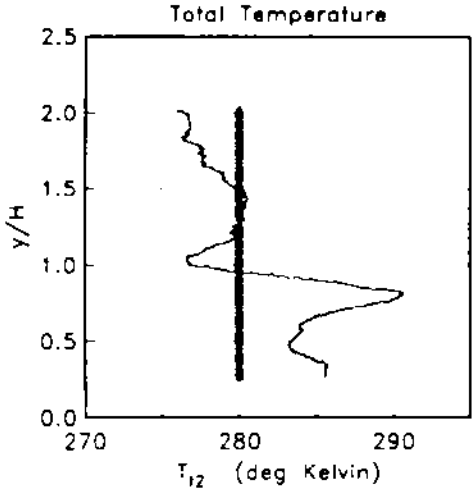

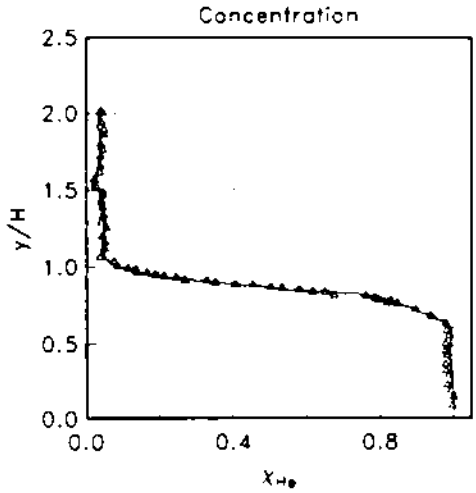

Appendix D

Dimensional Helium Profiles

The following plots correspond to the nondimensional figures discussed in the text. Only helium injection data is included. Units (English and SI) are specified on each graph.

Concentration Profiles

Helium injection only

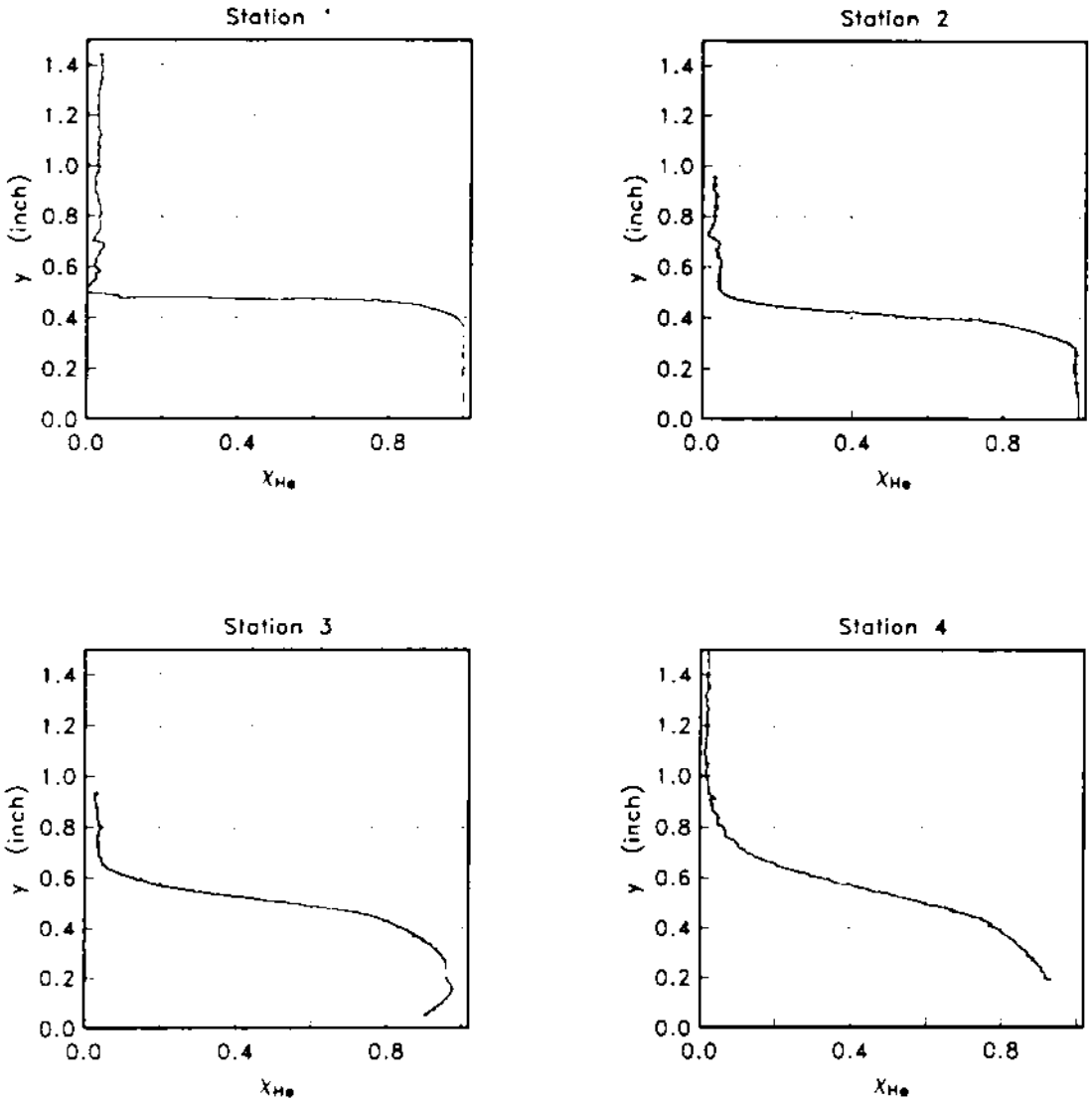

Pitot Pressure Profiles

Helium injection only

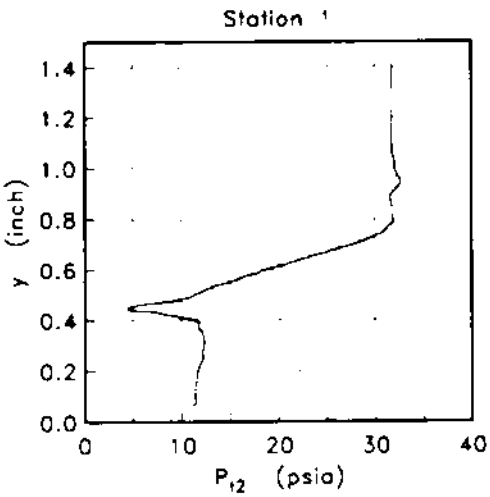

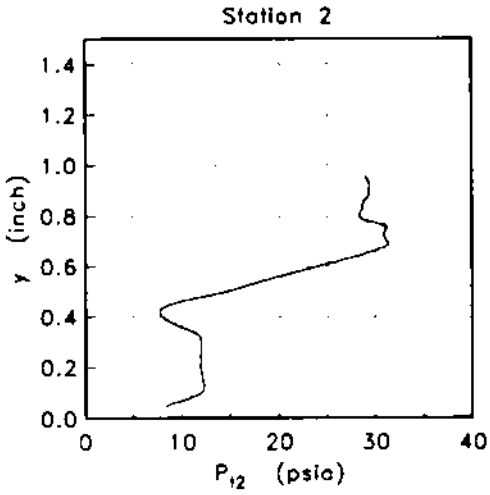

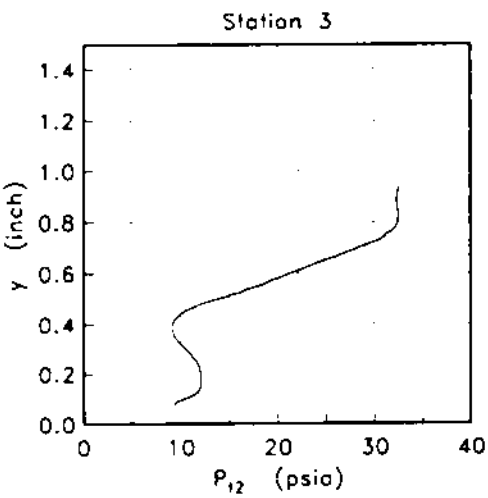

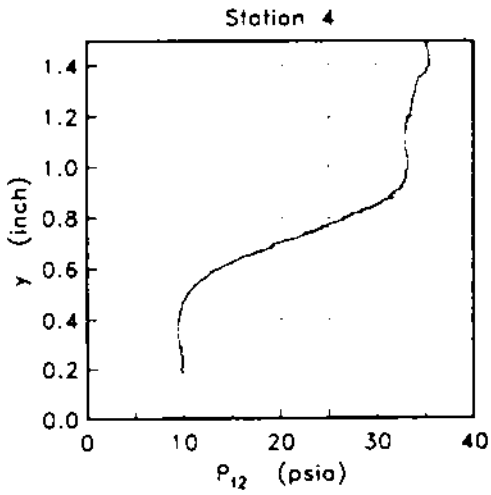

Cone–Static Pressure Profiles

Helium injection only

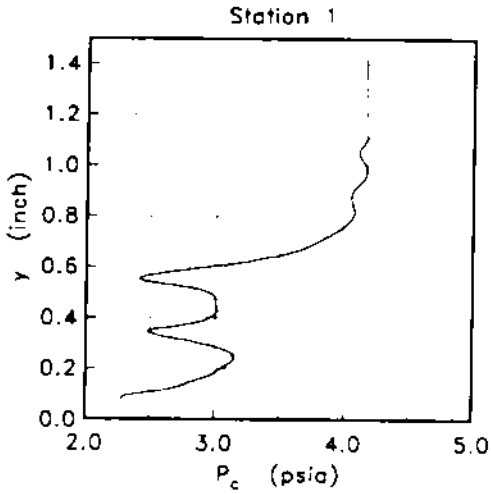

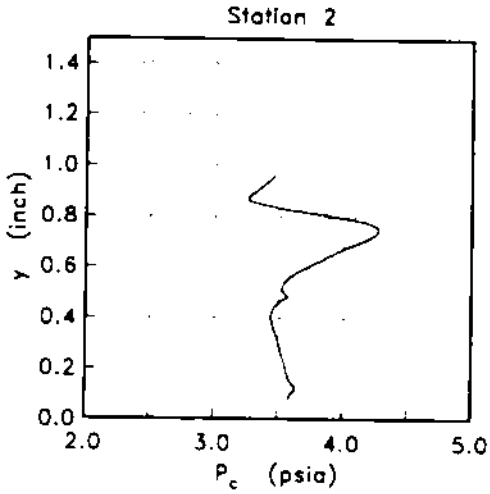

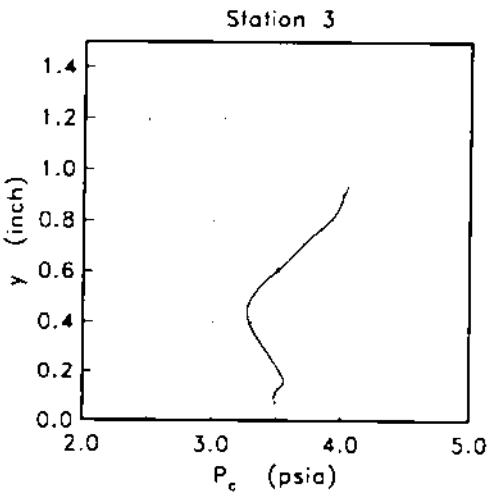

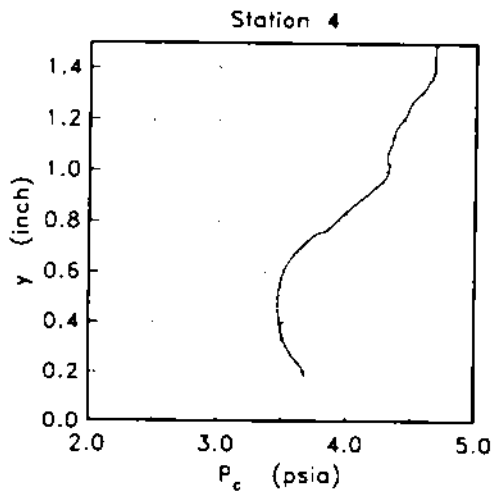

Total Temperature Profiles

Helium injection only

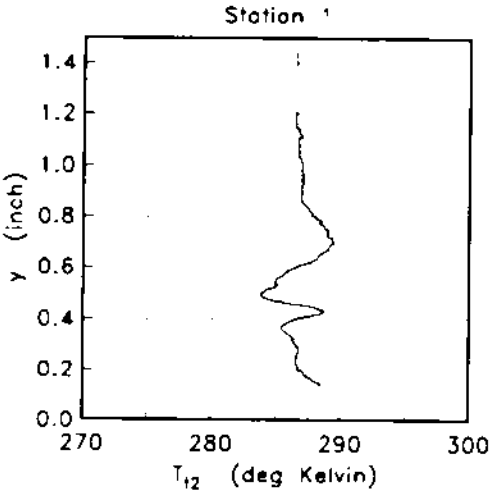

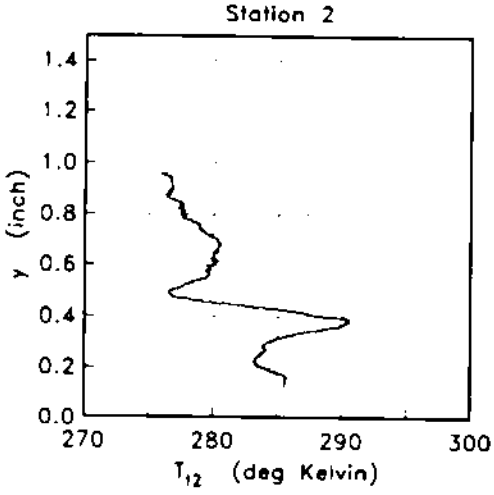

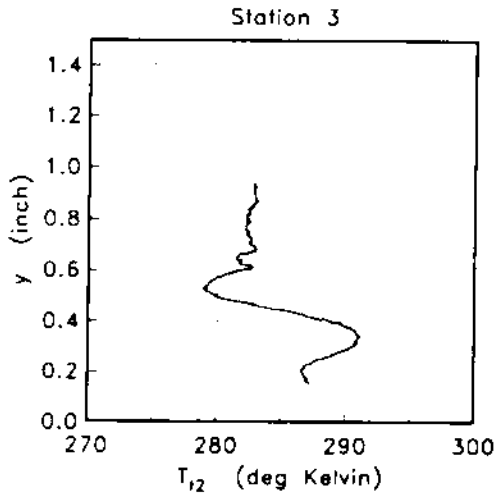

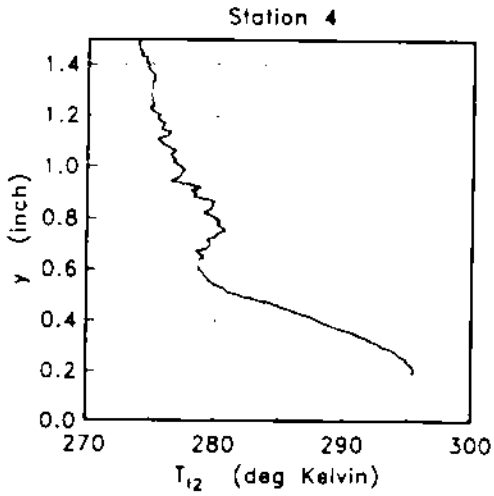

Gamma (γ) Profiles

Helium injection only

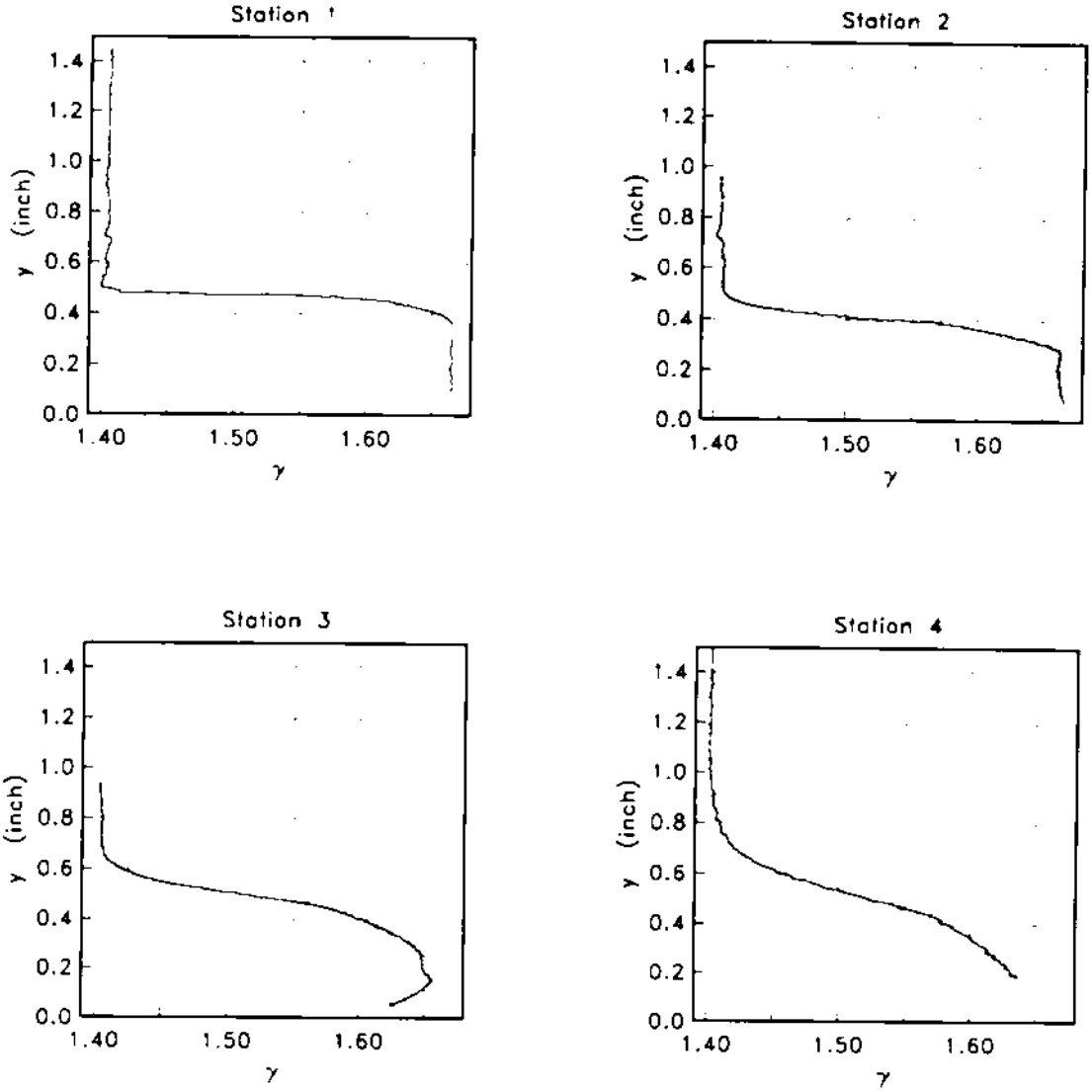

Gas Constant Profiles

Helium injection only

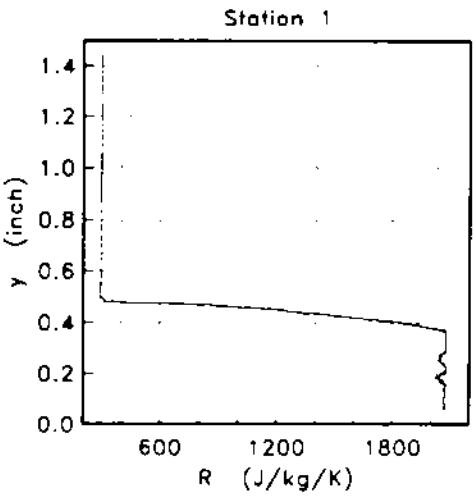

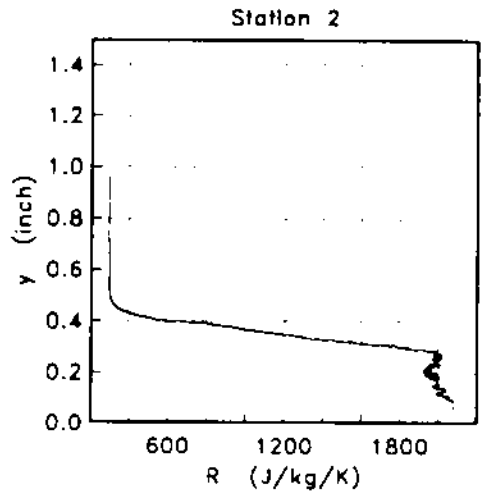

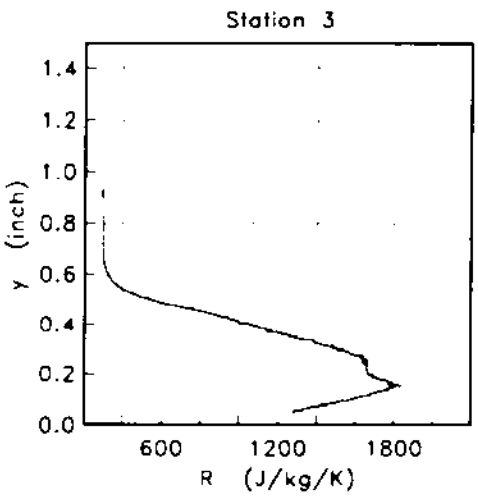

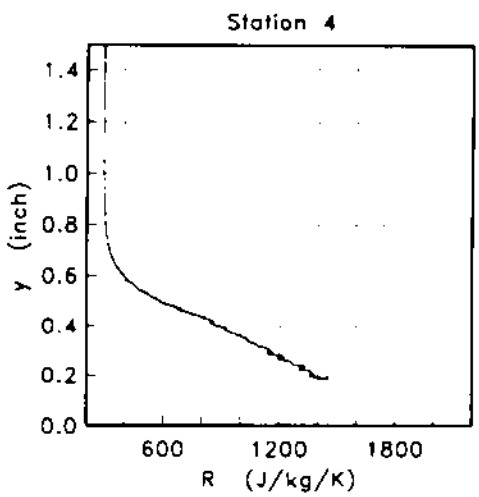

Mach Number Profiles

Helium injection only

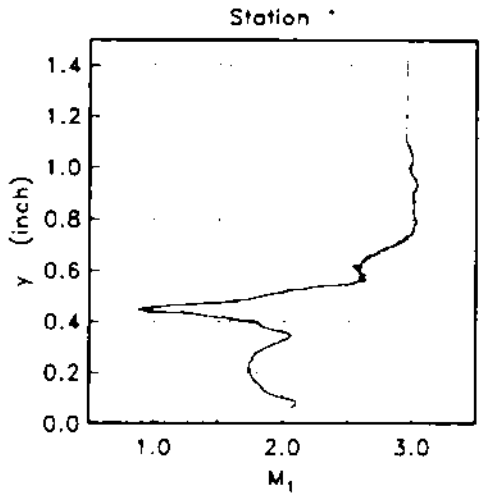

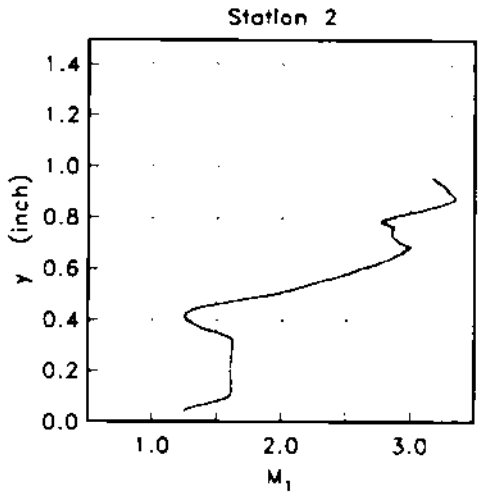

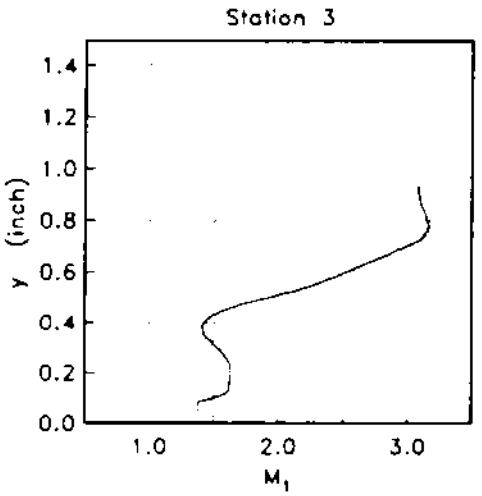

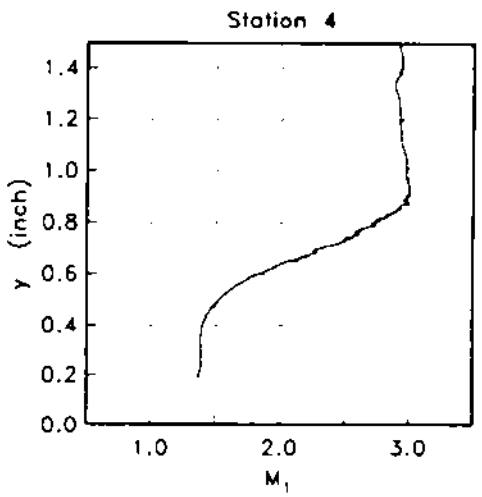

Speed of Sound Profiles

Helium injection only

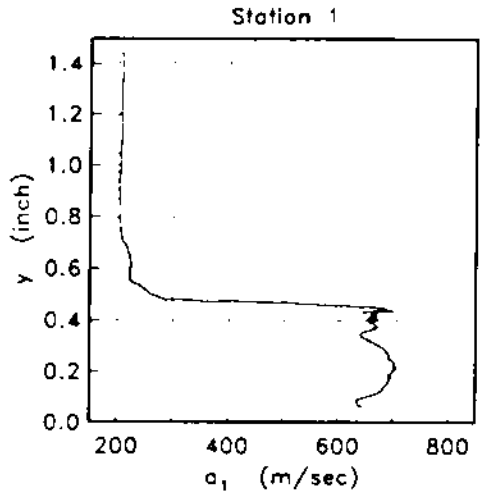

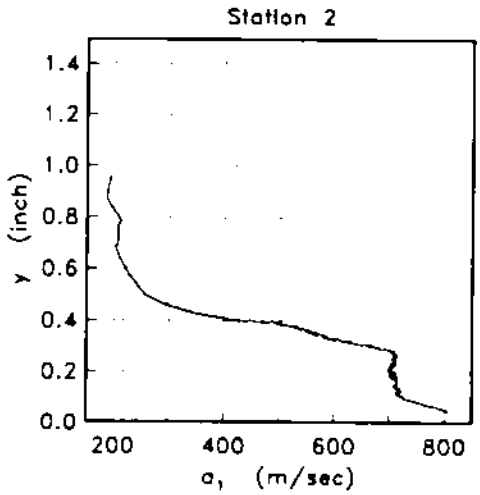

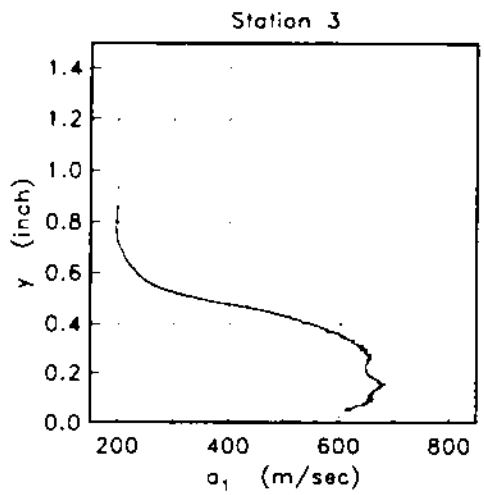

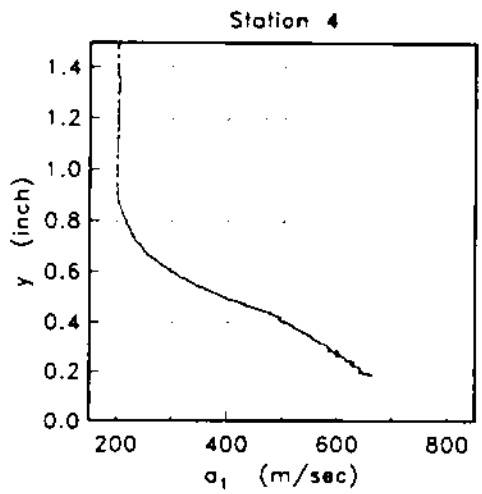

Velocity Profiles

Helium injection only

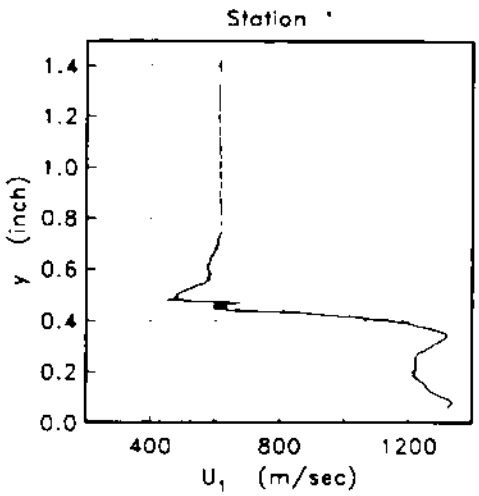

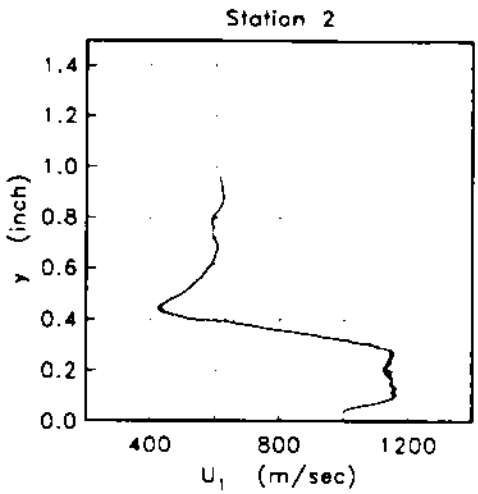

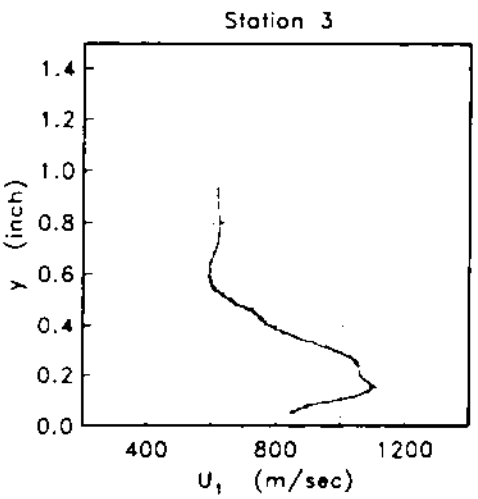

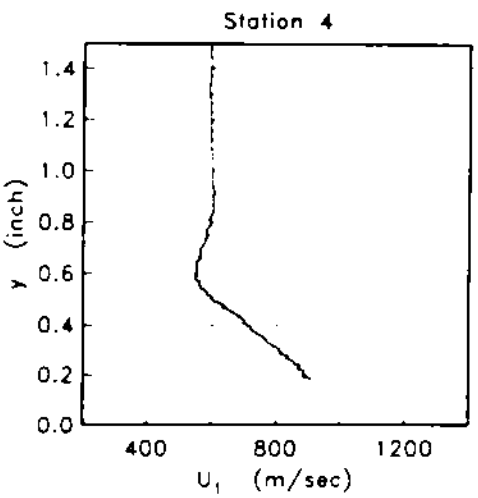

Density Profiles

Helium injection only

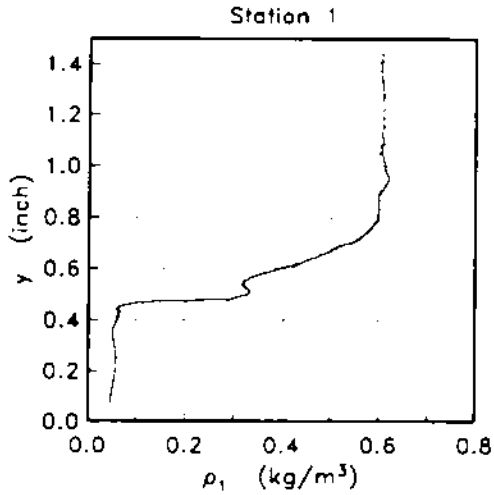

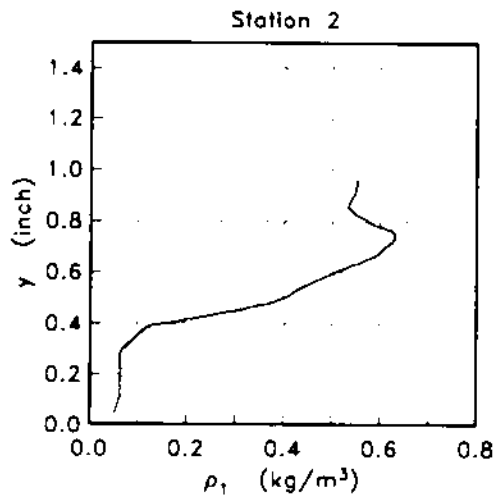

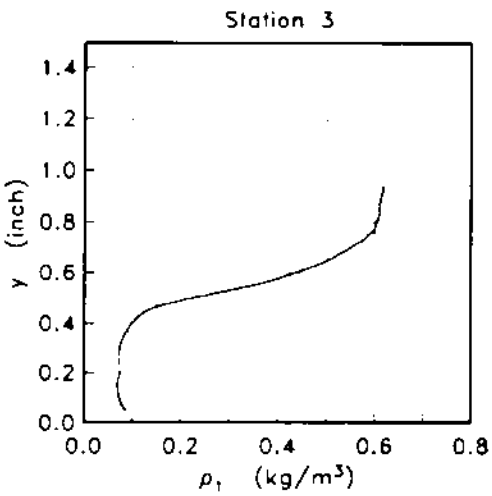

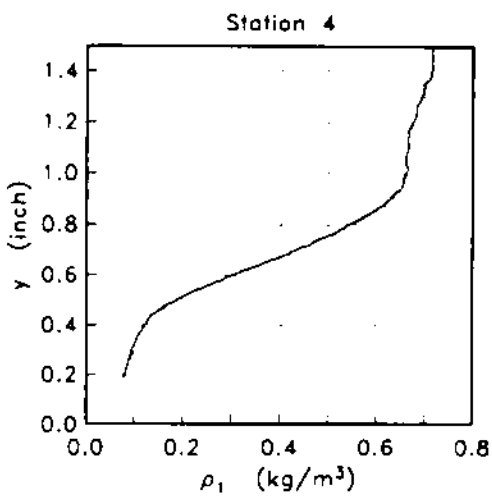

Mass Flux Profiles

Helium injection only

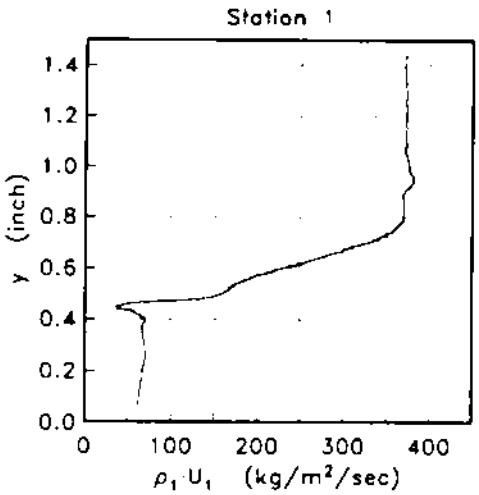

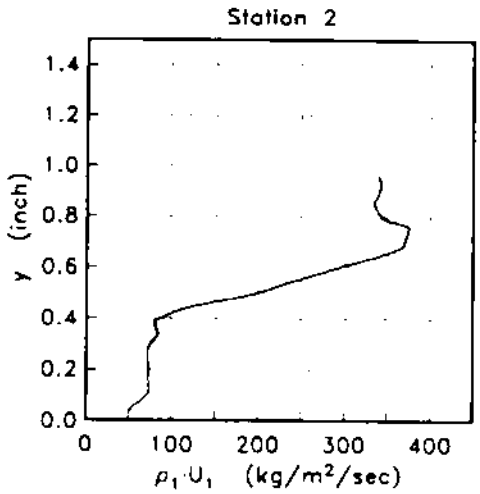

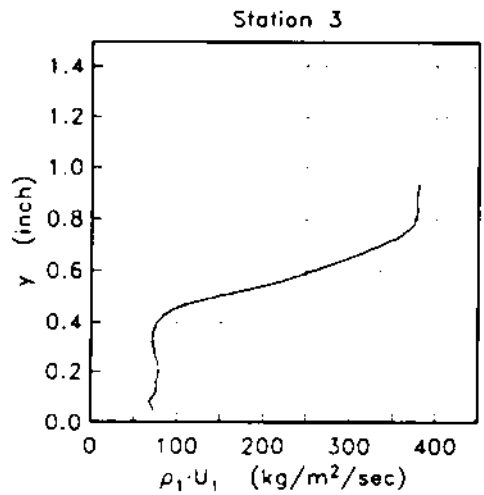

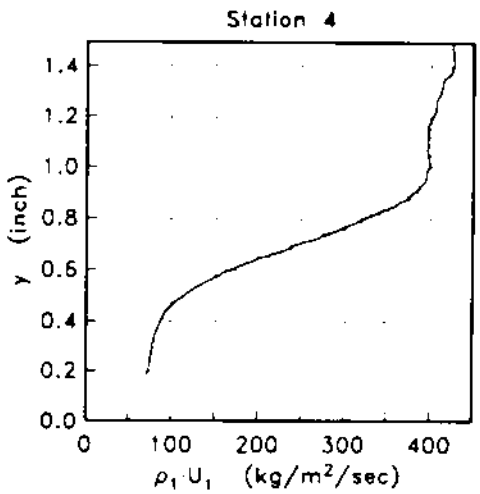

Static Pressure Profiles

Helium injection only

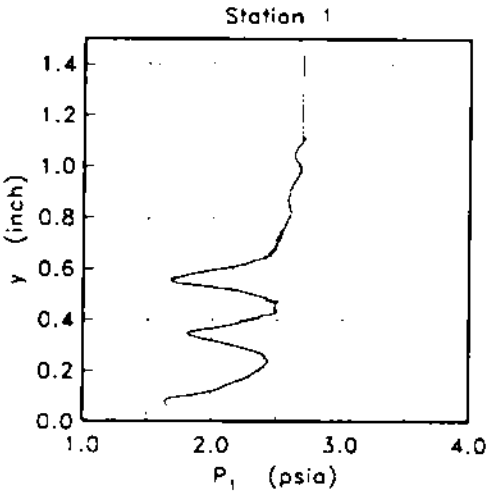

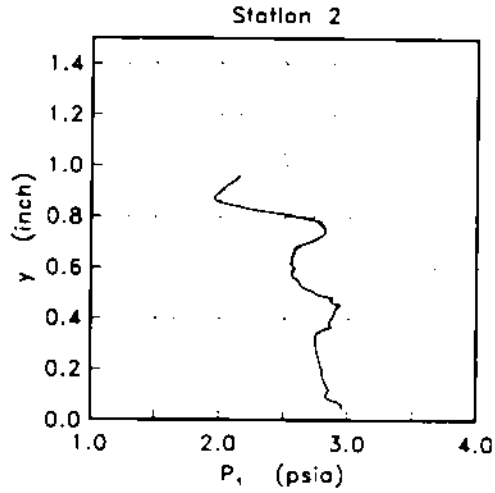

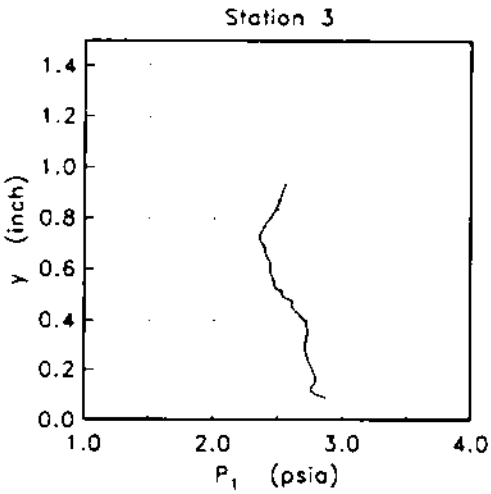

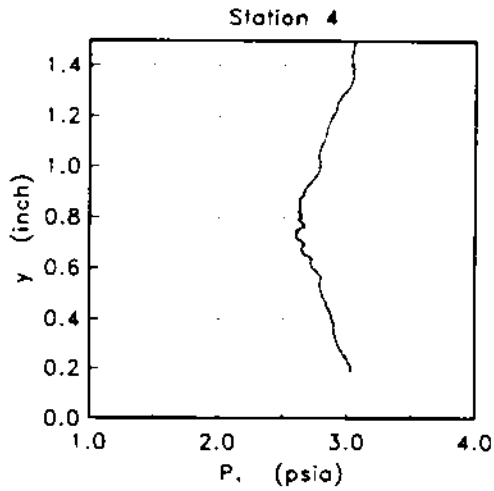

Static Temperature Profiles

Helium injection only

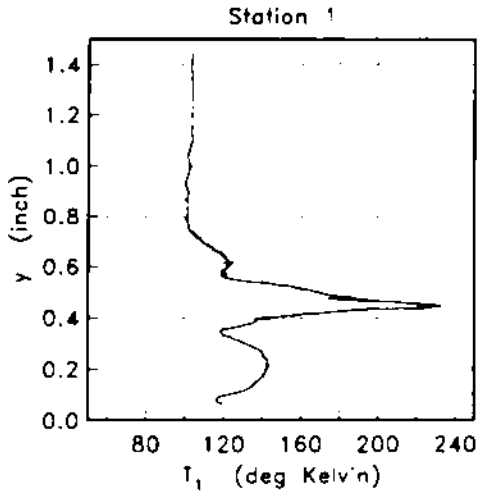

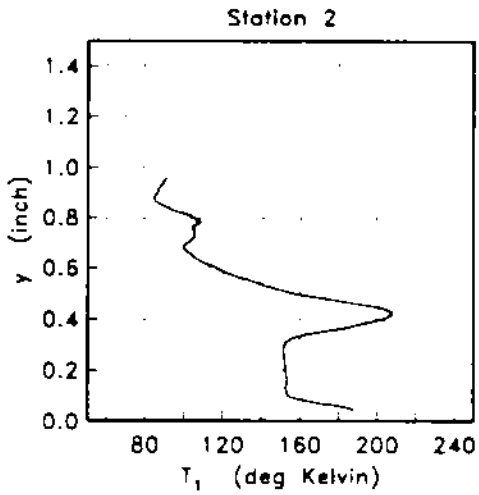

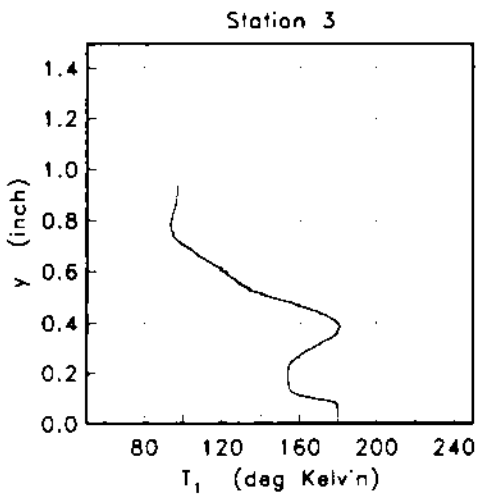

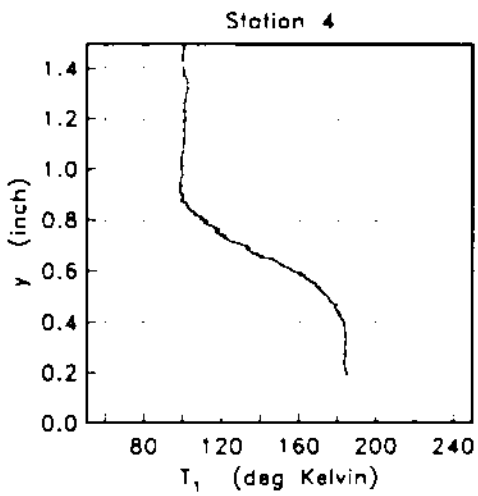

Total Pressure Profiles

Helium injection only

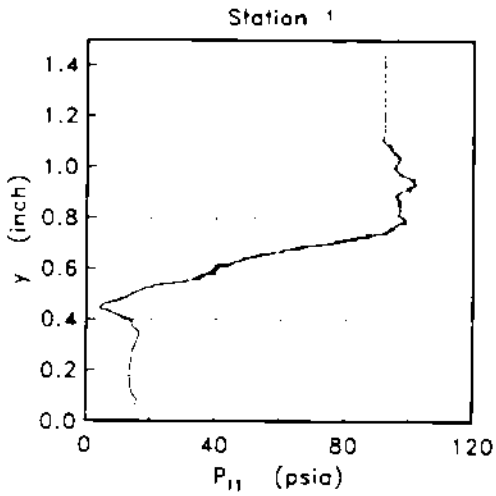

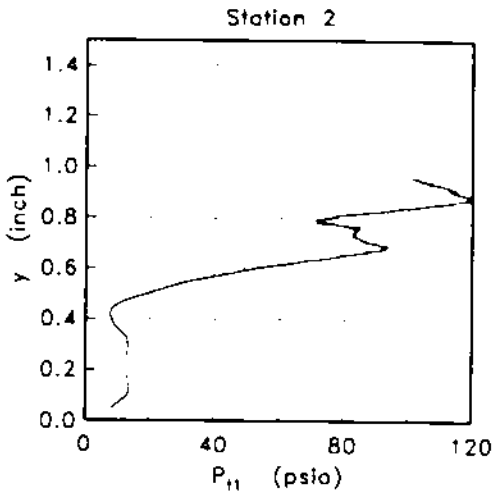

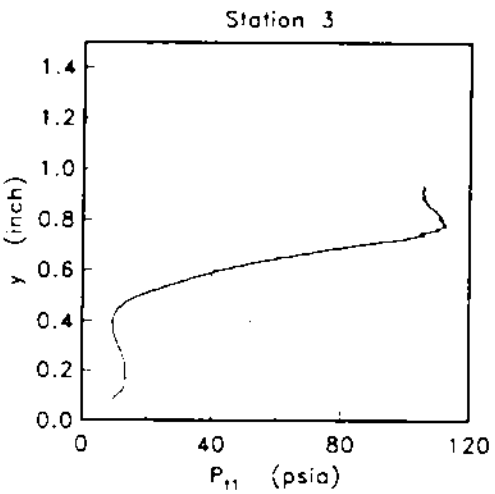

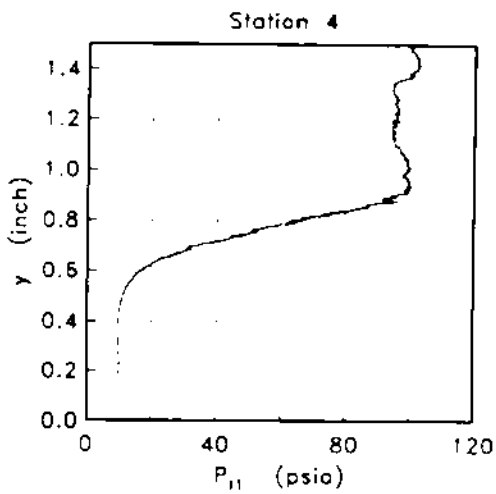

Appendix E

Tables of Data

This section tabulates 150 of the 1200 total points which comprise a single profile of one variable at one station. The tables consist of representative points taken at equal intervals along a complete traverse. Provided is a listing of both nondimensional and dimensional (English and SI units) data of the helium injection flowfield at all four stations.

E.1 Nondimensional Data

The E1 Tables give data that is nondimensionalized, except for concentration. The data columns are defined as follows:

- $y/H \rightarrow H = 0.475$ inch

- Xhe → mole fraction of helium
- Mach number
- Density → $\frac{\rho}{\rho_\infty}$
- Velocity → $\frac{U}{U_\infty}$
- Static Press. → $\frac{P}{P_\infty}$

Table E1.1: Station 1 Profile Data

y/H	Xhe	Mach #	Density	Velocity	Static Press.
0.1319	0.9995	2.0573	0.0764	2.1504	0.6204
0.1478	0.9989	2.0928	0.0775	2.1617	0.6148
0.1637	0.9998	2.1059	0.0774	2.1732	0.6128
[illegible]	[illegible]	[illegible]	[illegible]	[illegible]	[illegible]
0.2133	0.9992	2.0151	0.0794	2.1297	0.6591
0.2292	0.9993	1.9554	0.0811	2.1031	0.6975
0.2570	0.9998	1.8876	0.0830	2.0727	0.7439
0.2888	0.9992	1.8456	0.0851	2.0479	0.7785
0.3067	0.9991	1.8325	0.0855	2.0404	0.7882
0.3285	0.9998	1.8077	0.0867	2.0297	0.8119
0.3424	0.9980	1.7929	0.0884	2.0101	0.8257
0.3702	0.9988	1.7686	0.0895	1.9997	0.8510
0.3901	0.9950	1.7601	0.0923	1.9725	0.8626
0.4159	0.9978	1.7481	0.0915	1.9820	0.8748
0.4358	0.9988	1.7371	0.0916	1.9807	0.8855
0.4556	1.0000	1.7291	0.0919	1.9839	0.8986
0.4834	0.9998	1.7400	0.0933	1.9887	0.9058
0.5132	0.9987	1.7573	0.0950	1.9921	0.9073
0.5370	0.9974	1.7740	0.0955	1.9936	0.8968
0.5589	0.9980	1.7711	0.0946	1.9962	0.8933
0.5748	0.9975	1.7855	0.0941	2.0014	0.8794
0.6006	0.9999	1.8274	0.0914	2.0394	0.8463
0.6165	0.9999	1.8485	0.0913	2.0501	0.8348
0.6443	1.0000	1.9081	0.0894	2.0800	0.7890
0.6642	1.0000	1.9544	0.0881	2.1018	0.7575
0.6820	1.0000	1.9845	0.0863	2.1165	0.7292
0.7098	1.0000	2.0514	0.0845	2.1457	0.6871
0.7396	0.9999	2.0529	0.0838	2.1441	0.6795
0.7674	0.9997	1.9410	0.0868	2.0915	0.7317
0.7873	0.9977	1.8747	0.0872	2.0463	0.7727
0.8051	0.9921	1.8339	0.0926	1.9929	0.8053
0.8369	0.9843	1.7983	0.0973	1.9325	0.8386
0.8468	0.9761	1.7848	0.1016	1.9841	0.8469
0.8766	0.9580	1.5406	0.1011	1.6676	0.8900
0.8945	0.9391	1.3814	0.1046	1.4975	0.9282
0.9124	0.9137	1.3110	0.1115	1.3712	0.9269
0.9442	0.8897	0.8767	0.0987	0.9727	0.9283
0.9660	0.8473	0.9850	0.1198	0.9874	0.9293
0.9918	0.7669	1.3651	0.1800	1.1074	0.9305
1.0156	0.2069	1.6605	0.4433	0.8076	0.9044
1.0335	0.0880	1.7694	0.5030	0.7934	0.8854
1.0573	0.0000	1.8445	0.5404	0.7835	0.8627
1.0712	0.0000	1.9129	0.5447	0.8010	0.8450
1.0971	0.0051	2.0464	0.5395	0.8344	0.7931
1.1189	0.0115	2.1869	0.5262	0.8670	0.7307
1.1368	0.0159	2.3727	0.5273	0.9037	0.6756
1.1586	0.0238	2.5541	0.5306	0.9372	0.6304
1.1844	0.0257	2.6358	0.5471	0.9512	0.6285
1.2043	0.0238	2.5945	0.5669	0.9446	0.6631
1.2261	0.0359	2.6192	0.5915	0.9532	0.6904
1.2440	0.0337	2.5899	0.6195	0.9483	0.7321
1.2679	0.0238	2.5627	0.6510	0.9414	0.7751
1.2798	0.0203	2.5651	0.6728	0.9410	0.7991
1.3056	0.0256	2.6093	0.7165	0.9511	0.8398
1.3314	0.0245	2.6194	0.7420	0.9531	0.8667
1.3433	0.0280	2.6160	0.7512	0.9543	0.8816
1.3632	0.0321	2.6638	0.7766	0.9632	0.8951
1.3850	0.0350	2.6586	0.7898	0.9642	0.9154
1.4108	0.0385	2.7425	0.8217	0.9783	0.9210
1.4347	0.0448	2.8052	0.8424	0.9897	0.9229
1.4466	0.0485	2.7721	0.8369	0.9865	0.9325
1.4664	0.0418	2.8339	0.8627	0.9933	0.9332
1.4764	0.0170	2.8667	0.8909	0.9882	0.9349
1.5101	0.0201	2.9385	0.9184	0.9984	0.9358
1.5260	0.0237	2.9671	0.9277	1.0027	0.9350
1.5439	0.0297	2.9558	0.9300	1.0037	0.9456
1.5598	0.0334	3.0077	0.9437	1.0115	0.9406
1.5816	0.0375	3.0082	0.9498	1.0128	0.9485
1.6074	0.0372	3.0213	0.9590	1.0130	0.9563
1.6273	0.0371	3.0290	0.9629	1.0132	0.9603
1.6452	0.0367	3.0164	0.9697	1.0133	0.9630
1.6611	0.0329	3.0295	0.9783	1.0128	0.9637
1.6750	0.0338	3.0237	0.9790	1.0126	0.9676
1.7087	0.0382	3.0079	0.9773	1.0116	0.9737
1.7206	0.0375	3.0107	0.9789	1.0118	0.9740

1.7425	0.0360	3.0114	0.9792	1.0110	0.9725
1.7643	0.0357	3.0099	0.9791	1.0106	0.9726
1.7922	0.0361	3.0111	0.9786	1.0106	0.9714
1.8040	0.0323	3.0086	0.9779	1.0089	0.9693
1.8239	0.0325	3.0169	0.9797	1.0096	0.9671
1.8398	0.0288	3.0110	0.9805	1.0076	0.9683
1.8616	0.0302	3.0099	0.9795	1.0079	0.9683
1.8755	0.0278	3.0038	0.9801	1.0068	0.9710
1.9053	0.0222	3.0135	0.9897	1.0055	0.9724
1.9172	0.0219	3.0197	0.9917	1.0063	0.9721
1.9411	0.0239	3.0218	0.9971	1.0073	0.9777
1.9589	0.0261	3.0360	1.0030	1.0101	0.9795
1.9709	0.0229	3.0388	1.0088	1.0091	0.9816
1.9967	0.0218	3.0274	1.0105	1.0077	0.9882
2.0225	0.0246	3.0190	1.0100	1.0077	0.9928
2.0463	0.0258	2.9918	1.0040	1.0051	0.9936
2.0642	0.0336	2.9888	0.9988	1.0073	0.9999
2.0781	0.0316	2.9851	0.9989	1.0065	1.0011
2.1059	0.0347	2.9880	0.9961	1.0082	0.9994
2.1218	0.0307	2.9859	0.9958	1.0065	0.9976
2.1456	0.0295	2.9968	0.9947	1.0073	0.9910
2.1655	0.0324	2.9982	0.9909	1.0085	0.9892
2.1853	0.0303	3.0063	0.9901	1.0085	0.9825
2.2072	0.0323	2.9976	0.9868	1.0084	0.9845
2.2310	0.0298	2.9934	0.9884	1.0067	0.9858
2.2548	0.0319	2.9834	0.9876	1.0065	0.9908
2.2767	0.0353	2.9669	0.9854	1.0061	0.9985
2.2886	0.0287	2.9736	0.9946	1.0042	1.0002
2.3184	0.0321	2.9515	0.9917	1.0028	1.0092
2.3323	0.0338	2.9526	0.9895	1.0040	1.0083
2.3502	0.0354	2.9488	0.9884	1.0045	1.0107
2.3720	0.0372	2.9546	0.9866	1.0056	1.0068
2.3879	0.0359	2.9547	0.9873	1.0052	1.0068
2.4078	0.0324	2.9551	0.9903	1.0036	1.0069
2.4375	0.0312	2.9552	0.9910	1.0032	1.0069
2.4653	0.0330	2.9550	0.9890	1.0043	1.0069
2.4812	0.0330	2.9550	0.9888	1.0044	1.0069
2.5031	0.0310	2.9552	0.9902	1.0037	1.0069
2.5269	0.0320	2.9551	0.9894	1.0040	1.0069
2.5408	0.0319	2.9551	0.9895	1.0040	1.0069
2.5666	0.0317	2.9551	0.9896	1.0039	1.0069
2.5746	0.0305	2.9552	0.9905	1.0035	1.0069
2.5964	0.0296	2.9553	0.9911	1.0032	1.0069
2.6163	0.0314	2.9552	0.9899	1.0038	1.0069
2.6401	0.0329	2.9550	0.9888	1.0044	1.0069
2.6639	0.0330	2.9550	0.9888	1.0044	1.0069
2.6878	0.0304	2.9553	0.9906	1.0034	1.0069
2.7076	0.0321	2.9551	0.9894	1.0041	1.0069
2.7334	0.0320	2.9551	0.9894	1.0040	1.0069
2.7434	0.0345	2.9549	0.9878	1.0049	1.0068
2.7652	0.0365	2.9547	0.9864	1.0057	1.0068
2.7851	0.0371	2.9546	0.9859	1.0059	1.0068
2.7990	0.0375	2.9546	0.9857	1.0060	1.0068
2.8208	0.0398	2.9544	0.9841	1.0069	1.0067
2.8446	0.0407	2.9543	0.9835	1.0072	1.0067
2.8526	0.0395	2.9544	0.9843	1.0067	1.0067
2.8764	0.0392	2.9544	0.9845	1.0067	1.0067
2.8943	0.0415	2.9542	0.9830	1.0075	1.0067
2.9142	0.0433	2.9540	0.9817	1.0082	1.0066
2.9300	0.0430	2.9541	0.9820	1.0080	1.0066
2.9san	0.0421	2.9544	0.9844	1.0066	1.0067
2.9717	0.0403	2.9543	0.9838	1.0071	1.0067
2.9837	0.0403	2.9543	0.9838	1.0071	1.0067
2.9995	0.0390	2.9544	0.9847	1.0066	1.0067
3.0254	0.0370	2.9546	0.9860	1.0058	1.0068
3.0353	0.0394	2.9544	0.9844	1.0067	1.0067
3.0353	0.0385	2.9545	0.9850	1.0064	1.0067
3.0333	0.0365	2.9547	0.9864	1.0057	1.0068
3.0254	0.0364	2.9547	0.9864	1.0056	1.0068
3.0273	0.0387	2.9545	0.9849	1.0064	1.0067
3.0333	0.0356	2.9548	0.9870	1.0053	1.0068
3.0333	0.0355	2.9548	0.9871	1.0053	1.0068
3.0293	0.0398	2.9544	0.9841	1.0069	1.0067
3.0273	0.0407	2.9543	0.9835	1.0072	1.0067
3.0313	0.0396	2.9544	0.9843	1.0068	1.0067

Table E1.2: Station 2 Profile Data

y/H	Xhe	Mach #	Density	Velocity	Static Press
0.1134	1.0000	1.2735	0.0965	1.6495	1.3842
0.1173	1.0000	1.2908	0.0973	1.6639	1.3821
0.1272	1.0000	1.3301	0.0993	1.6960	1.3800
0.1523	1.0000	1.4322	0.1045	1.7744	1.3714
0.1678	1.0000	1.4720	0.1055	1.8033	1.3538
0.1756	1.0000	1.4980	0.1064	1.8213	1.3451
0.1892	1.0000	1.5566	0.1087	1.8614	1.3294
0.2028	0.9978	1.5879	0.1117	1.8691	1.3244
0.2125	0.9972	1.6012	0.1130	1.8743	1.3253
0.2378	0.9957	1.6155	0.1155	1.8744	1.3310
0.2514	0.9935	1.6132	0.1172	1.8610	1.3358
0.2534	0.9946	1.6132	0.1165	1.8669	1.3363
0.2728	0.9967	1.6185	0.1150	1.8826	1.3323
0.2923	0.9952	1.6183	0.1154	1.8747	1.3261
0.3040	0.9940	1.6156	0.1159	1.8663	1.3243
0.3215	0.9918	1.6132	0.1170	1.8522	1.3219
0.3331	0.9939	1.6128	0.1151	1.8645	1.3178
0.3351	0.9933	1.6135	0.1155	1.8615	1.3175
0.3604	0.9935	1.6106	0.1151	1.8606	1.3160
0.3817	0.9905	1.6091	0.1170	1.8415	1.3138
0.3856	0.9934	1.6092	0.1151	1.8575	1.3138
0.3992	0.9877	1.6122	0.1190	1.8271	1.3117
0.4109	0.9916	1.6096	0.1162	1.8458	1.3102
0.4187	0.9914	1.6108	0.1166	1.8438	1.3100
0.4459	0.9879	1.6107	0.1188	1.8246	1.3077
0.4634	0.9909	1.6090	0.1166	1.8390	1.3064
0.4634	0.9885	1.6093	0.1182	1.8267	1.3065
0.4751	0.9927	1.6122	0.1154	1.8513	1.3042
0.4945	0.9902	1.6142	0.1170	1.8390	1.3027
0.5101	0.9922	1.6141	0.1154	1.8506	1.3002
0.5257	0.9928	1.6178	0.1150	1.8567	1.2976
0.5393	0.9925	1.6172	0.1150	1.8551	1.2969
0.5432	0.9930	1.6174	0.1146	1.8588	1.2975
0.5587	0.9949	1.6185	0.1132	1.8703	1.2944
0.5859	0.9924	1.6224	0.1148	1.8585	1.2911
0.5937	0.9927	1.6239	0.1147	1.8610	1.2905
0.6073	0.9877	1.6241	0.1180	1.8339	1.2906
0.6171	0.9792	1.6286	0.1235	1.7942	1.2895
0.6248	0.9772	1.6291	0.1245	1.7862	1.2882
0.6443	0.9691	1.6272	0.1294	1.7476	1.2876
0.6657	0.9542	1.6300	0.1388	1.6862	1.2858
0.6696	0.9442	1.6283	0.1448	1.6474	1.2859
0.6774	0.9342	1.6193	0.1503	1.6076	1.2884
0.6929	0.9209	1.6143	0.1576	1.5612	1.2869
0.7124	0.9045	1.5795	0.1645	1.4941	1.2900
0.7260	0.8953	1.5351	0.1666	1.4462	1.2988
0.7435	0.8790	1.4940	0.1729	1.3838	1.3076
0.7435	0.8611	1.4960	0.1830	1.3443	1.3080
0.7571	0.8446	1.4344	0.1885	1.2782	1.3306
0.7804	0.8271	1.3716	0.1931	1.2097	1.3403
0.7921	0.8079	1.3604	0.2015	1.1711	1.3381
0.8018	0.7852	1.3374	0.2106	1.1232	1.3377
0.8232	0.7574	1.2952	0.2205	1.0606	1.3393
0.8252	0.7054	1.2977	0.2479	0.9380	1.3420
0.8427	0.5859	1.2757	0.3068	0.8743	1.3492
0.8660	0.5301	1.2532	0.3325	0.8221	1.3533
0.8738	0.4974	1.2565	0.3490	0.8023	1.3528
0.8796	0.4190	1.2624	0.3890	0.7593	1.3552
0.8971	0.3648	1.2645	0.4167	0.7322	1.3566
0.9068	0.3059	1.2772	0.4492	0.7100	1.3594
0.9243	0.2614	1.3076	0.4793	0.7021	1.3618
0.9457	0.2109	1.3729	0.5219	0.7064	1.3711
0.9438	0.1801	1.3710	0.5396	0.6926	1.3721
0.9535	0.1464	1.4052	0.5688	0.6914	1.3777
0.9749	0.1268	1.5235	0.5953	0.7233	1.3862
0.9924	0.1044	1.5890	0.6240	0.7346	1.3813
1.0021	0.0891	1.6330	0.6477	0.7415	1.3855
1.0196	0.0738	1.7409	0.6857	0.7667	1.3827
1.0216	0.0691	1.7466	0.6881	0.7666	1.3887
1.0391	0.0590	1.9278	0.7123	0.7841	1.3876
1.0644	0.0534	1.9851	0.7387	0.8208	1.2793
1.0721	0.0524	1.9973	0.7410	0.8245	1.2781
1.0799	0.0466	2.0360	0.7484	0.8314	1.2638
1.0955	0.0442	2.0931	0.7584	0.8433	1.2473
1.1033	0.0443	2.1264	0.7624	0.8489	1.2425

1.1208	0.0479	2.1788	0.7739	0.8636	1.2311
1.1441	0.0416	2.2499	0.7977	0.8758	1.2251
1.1499	0.0461	2.2687	0.8015	0.8819	1.2267
1.1558	0.0480	2.2814	0.8032	0.8855	1.2254
1.1791	0.0463	2.3824	0.8288	0.9036	1.2076
1.1927	0.0475	2.4252	0.8404	0.9114	1.2020
1.2025	0.0508	2.4395	0.8457	0.9146	1.2033
1.2258	0.0471	2.5352	0.8801	0.9291	1.1971
1.2277	0.0513	2.5381	0.8775	0.9316	1.1967
1.2375	0.0505	2.5495	0.8857	0.9330	1.2008
1.2627	0.0466	2.6059	0.9173	0.9405	1.2103
1.2705	0.0538	2.6223	0.9155	0.9465	1.2070
1.2841	0.0519	2.6621	0.9291	0.9518	1.2022
1.3016	0.0505	2.7382	0.9551	0.9626	1.1950
1.3075	0.0514	2.7478	0.9625	0.9633	1.1975
1.3250	0.0526	2.7841	0.9764	0.9691	1.1973
1.3503	0.0467	2.8519	1.0130	0.9758	1.2012
1.3561	0.0455	2.8652	1.0186	0.9769	1.1993
1.3639	0.0469	2.8775	1.0253	0.9797	1.2037
1.3833	0.0434	2.9132	1.0455	0.9825	1.2048
1.3989	0.0393	2.9477	1.0638	0.9857	1.2058
1.4105	0.0379	2.9398	1.0682	0.9844	1.2143
1.4339	0.0463	2.9760	1.0835	0.9920	1.2194
1.4397	0.0461	2.9704	1.0891	0.9911	1.2282
1.4456	0.0498	2.9754	1.0890	0.9929	1.2279
1.4747	0.0459	2.9451	1.0991	0.9879	1.2526
1.4864	0.0425	2.9043	1.1068	0.9813	1.2804
1.4981	0.0347	2.8962	1.1142	0.9765	1.2848
1.5175	0.0250	2.8774	1.1245	0.9709	1.2999
1.5195	0.0161	2.8770	1.1332	0.9668	1.3006
1.5370	0.0180	2.8627	1.1361	0.9656	1.3136
1.5661	0.0195	2.8621	1.1409	0.9656	1.3194
1.5720	0.0222	2.8543	1.1363	0.9659	1.3217
1.5817	0.0274	2.8628	1.1357	0.9686	1.3198
1.6031	0.0313	2.8555	1.1234	0.9694	1.3135
1.6128	0.0285	2.8708	1.1283	0.9696	1.3063
1.6284	0.0337	2.8243	1.1010	0.9651	1.3039
1.6517	0.0337	2.7849	1.0723	0.9589	1.2896
1.6575	0.0379	2.7925	1.0616	0.9612	1.2753
1.6634	0.0339	2.7767	1.0595	0.9576	1.2783
1.6906	0.0374	2.8571	1.0346	0.9696	1.2082
1.7062	0.0327	2.8838	1.0294	0.9716	1.1854
1.7139	0.0345	2.9257	1.0207	0.9777	1.1560
1.7392	0.0364	3.0572	0.9983	0.9934	1.0687
1.7392	0.0411	3.0568	0.9945	0.9954	1.0686
1.7509	0.0386	3.0993	0.9868	0.9994	1.0402
1.7801	0.0325	3.2064	0.9781	1.0080	0.9807
1.7917	0.0399	3.2364	0.9661	1.0137	0.9608
1.8015	0.0391	3.2760	0.9655	1.0162	0.9418
1.8170	0.0379	3.3086	0.9628	1.0181	0.9243
1.8267	0.0365	3.3355	0.9673	1.0204	0.9180
1.8423	0.0362	3.3414	0.9719	1.0203	0.9189
1.8676	0.0410	3.3371	0.9722	1.0231	0.9260
1.8792	0.0395	3.3262	0.9750	1.0212	0.9316
1.8831	0.0361	3.3181	0.9778	1.0199	0.9368
1.9045	0.0358	3.2979	0.9847	1.0161	0.9484
1.9220	0.0295	3.2940	0.9881	1.0148	0.9518
1.9337	0.0332	3.2768	0.9888	1.0148	0.9621
1.9531	0.0373	3.2549	0.9884	1.0139	0.9724
1.9609	0.0361	3.2457	0.9902	1.0122	0.9765
[illegible]	[illegible]	[illegible]	[illegible]	[illegible]	[illegible]
1.9901	0.0350	3.1946	0.9903	1.0070	0.9979
2.0076	0.0355	3.1859	0.9924	1.0054	1.0024
2.0154	0.0358	3.1778	0.9927	1.0044	1.0056
2.0154	0.0363	3.1778	0.9922	1.0046	1.0056
2.0076	0.0394	3.1855	0.9903	1.0065	1.0022
2.0134	0.0371	3.1786	0.9917	1.0051	1.0054
2.0173	0.0311	3.1684	0.9949	1.0016	1.0088
2.0173	0.0352	3.1681	0.9924	1.0029	1.0086
2.0134	0.0323	3.1790	0.9963	1.0027	1.0056
2.0095	0.0354	3.1850	0.9929	1.0049	1.0025
2.0134	0.0318	3.1790	0.9955	1.0031	1.0056
2.0193	0.0373	3.1667	0.9904	1.0038	1.0090
2.0154	0.0380	3.1776	0.9911	1.0052	1.0055
2.0154	0.0370	3.1777	0.9922	1.0046	1.0055

Table E1.3: Station 3 Profile Data

y/H	Xhe	Mach #	Density	Velocity	Static Press.
0.1192	0.9045	1.3805	0.1388	1.3750	1.1351
0.1272	0.9004	1.3808	0.1410	1.3642	1.1354
0.1372	0.9158	1.3796	0.1329	1.4058	1.1345
0.1492	0.9250	1.3788	0.1281	1.4325	1.1342
0.1672	0.9266	1.3787	0.1272	1.4374	1.1339
0.1832	0.9364	1.3944	0.1234	1.4790	1.1354
0.1972	0.9409	1.4489	0.1228	1.5293	1.1179
0.2171	0.9487	1.5129	0.1210	1.5971	1.0991
0.2191	0.9533	1.5136	0.1185	1.6151	1.0990
0.2351	0.9569	1.5585	0.1187	1.6564	1.0908
0.2531	0.9617	1.5957	0.1182	1.6983	1.0882
0.2731	0.9645	1.6136	0.1182	1.7206	1.0918
0.2811	0.9675	1.6148	0.1167	1.7349	1.0927
0.2831	0.9725	1.6157	0.1139	1.7579	1.0931
0.3071	0.9737	1.6197	0.1143	1.7658	1.1005
0.3271	0.9767	1.6211	0.1129	1.7815	1.1032
0.3371	0.9716	1.6229	0.1160	1.7584	1.1043
0.3491	0.9739	1.6230	0.1146	1.7688	1.1028
0.3670	0.9711	1.6241	0.1162	1.7564	1.1018
0.3710	0.9678	1.6244	0.1181	1.7419	1.1020
0.3890	0.9646	1.6281	0.1197	1.7299	1.0975
0.4110	0.9624	1.6292	0.1209	1.7199	1.0943
0.4250	0.9609	1.6291	0.1217	1.7134	1.0943
0.4290	0.9603	1.6342	0.1221	1.7134	1.0909
0.4390	0.9598	1.6299	0.1217	1.7098	1.0892
0.4630	0.9600	1.6297	0.1211	1.7108	1.0850
0.4770	0.9591	1.6269	0.1213	1.7055	1.0838
0.4870	0.9590	1.6236	0.1208	1.7040	1.0818
0.4990	0.9596	1.6231	0.1200	1.7071	1.0797
0.5149	0.9579	1.6097	0.1200	1.6926	1.0797
0.5209	0.9572	1.6103	0.1202	1.6905	1.0776
0.5389	0.9606	1.6015	0.1170	1.7017	1.0739
0.5629	0.9574	1.5812	0.1171	1.6780	1.0725
0.5709	0.9556	1.5799	0.1178	1.6710	1.0725
0.5729	0.9529	1.5793	0.1189	1.6608	1.0708
0.5909	0.9482	1.5672	0.1205	1.6358	1.0704
0.6209	0.9477	1.5335	0.1183	1.6154	1.0710
0.6269	0.9412	1.5258	0.1210	1.5879	1.0705
0.6329	0.9415	1.5192	0.1204	1.5854	1.0712
0.6649	0.9357	1.4838	0.1214	1.5439	1.0747
0.6649	0.9294	1.4846	0.1246	1.5235	1.0748
0.6808	0.9243	1.4829	0.1265	1.5065	1.0714
0.6908	0.9203	1.4706	0.1281	1.4862	1.0743
0.7128	0.9182	1.4405	0.1276	1.4622	1.0799
0.7128	0.9090	1.4417	0.1322	1.4361	1.0800
0.7248	0.9009	1.4387	0.1357	1.4116	1.0780
0.7468	0.8937	1.4188	0.1382	1.3805	1.0816
0.7628	0.8926	1.4186	0.1382	1.3776	1.0770
0.7708	0.8856	1.4178	0.1417	1.3589	1.0779
0.7748	0.8710	1.4214	0.1489	1.3252	1.0755
0.7928	0.8724	1.4106	0.1477	1.3219	1.0778
0.8128	0.8628	1.4073	0.1520	1.2977	1.0760
0.8247	0.8568	1.4099	0.1549	1.2857	1.0742
0.8327	0.8488	1.4157	0.1588	1.2718	1.0705
0.8507	0.8405	1.4257	0.1630	1.2598	1.0654
0.8587	0.8250	1.4320	0.1709	1.2320	1.0621
0.8727	0.8229	1.4484	0.1729	1.2360	1.0579
0.8927	0.8098	1.4732	0.1805	1.2242	1.0504
0.9087	0.8044	1.4910	0.1840	1.2228	1.0443
0.9107	0.7905	1.4969	0.1915	1.2015	1.0440
0.9187	0.7799	1.5269	0.1987	1.1981	1.0373
0.9427	0.7689	1.5579	0.2066	1.1944	1.0322
0.9587	0.7527	1.6027	0.2193	1.1882	1.0280
0.9667	0.7312	1.6178	0.2319	1.1638	1.0283
0.9786	0.7123	1.6503	0.2459	1.1511	1.0286
0.9926	0.6873	1.6860	0.2641	1.1333	1.0314
1.0026	0.6546	1.7177	0.2847	1.1072	1.0296
1.0186	0.6207	1.7730	0.3068	1.0905	1.0257
1.0406	0.5863	1.8593	0.3345	1.0947	1.0020
1.0486	0.5587	1.9422	0.3553	1.0724	0.9949
1.0526	0.5355	1.9087	0.3683	1.0545	0.9990
1.0686	0.4866	1.9779	0.4064	1.0360	0.9990
1.0926	0.4628	2.0489	0.4300	1.0368	0.9904
1.0986	0.4359	2.0873	0.4493	1.0275	0.9835
1.1066	0.3963	2.1201	0.4751	1.0099	0.9800

1.1186	0.3610	2.1544	0.4995	0.9968	0.9771
1.1385	0.3282	2.2101	0.5282	0.9904	0.9742
1.1485	0.2994	2.2520	0.5527	0.9840	0.9730
1.1645	0.2701	2.2850	0.5774	0.9759	0.9751
1.1825	0.2442	2.3339	0.6016	0.9731	0.9717
1.1865	0.2167	2.3423	0.6170	0.9623	0.9713
1.1985	0.1936	2.3652	0.6340	0.9567	0.9703
1.2185	0.1773	2.4211	0.6548	0.9598	0.9647
1.2385	0.1653	2.4673	0.6730	0.9631	0.9627
1.2445	0.1439	2.4768	0.6863	0.9566	0.9639
1.2485	0.1330	2.4879	0.6943	0.9544	0.9632
1.2725	0.1178	2.5453	0.7183	0.9587	0.9626
1.2904	0.1048	2.5783	0.7364	0.9596	0.9652
1.2964	0.0971	2.5942	0.7456	0.9593	0.9654
1.3124	0.0822	2.6247	0.7654	0.9570	0.9653
1.3264	0.0754	2.6591	0.7779	0.9590	0.9606
1.3324	0.0665	2.6727	0.7868	0.9579	0.9606
1.3504	0.0564	2.7095	0.8038	0.9590	0.9582
1.3724	0.0556	2.7594	0.8181	0.9653	0.9528
1.3824	0.0477	2.8001	0.8333	0.9679	0.9485
1.3864	0.0482	2.8064	0.8356	0.9692	0.9494
1.3964	0.0476	2.8351	0.8424	0.9741	0.9474
1.4244	0.0434	2.8773	0.8604	0.9787	0.9488
1.4363	0.0473	2.9015	0.8651	0.9837	0.9474
1.4443	0.0374	2.9117	0.8758	0.9811	0.9483
1.4583	0.0396	2.9613	0.8853	0.9877	0.9392
1.4743	0.0399	2.9842	0.8945	0.9902	0.9390
1.4863	0.0381	3.0206	0.9039	0.9937	0.9329
1.5043	0.0377	3.0480	0.9140	0.9968	0.9323
1.5283	0.0369	3.1003	0.9327	1.0023	0.9299
1.5323	0.0338	3.1006	0.9354	1.0012	0.9307
1.5383	0.0382	3.1029	0.9353	1.0027	0.9315
1.5543	0.0365	3.1345	0.9479	1.0056	0.9306
1.5803	0.0385	3.1251	0.9527	1.0052	0.9399
1.5882	0.0336	3.1368	0.9609	1.0047	0.9406
1.5962	0.0347	3.1446	0.9647	1.0058	0.9416
1.6122	0.0388	3.1519	0.9687	1.0082	0.9452
1.6302	0.0351	3.1621	0.9781	1.0080	0.9482
1.6462	0.0375	3.1630	0.9908	1.0092	0.9524
1.6562	0.0417	3.1563	0.9786	1.0102	0.9556
1.6822	0.0410	3.1464	0.9821	1.0091	0.9630
1.6822	0.0478	3.1458	0.9787	1.0109	0.9628
1.6962	0.0388	3.1451	0.9879	1.0074	0.9667
1.7182	0.0388	3.1403	0.9898	1.0070	0.9706
1.7361	0.0402	3.1335	0.9895	1.0071	0.9746
1.7461	0.0347	3.1317	0.9935	1.0050	0.9762
1.7501	0.0339	3.1253	0.9939	1.0038	0.9783
1.7721	0.0343	3.1198	0.9949	1.0037	0.9825
1.7921	0.0355	3.1090	0.9921	1.0035	0.9860
1.8041	0.0327	3.1042	0.9953	1.0017	0.9890
1.8161	0.0319	3.1031	0.9953	1.0017	0.9897
1.8381	0.0369	3.0963	0.9916	1.0032	0.9930
1.8401	0.0326	3.0952	0.9948	1.0014	0.9937
1.8581	0.0339	3.0882	0.9931	1.0012	0.9960
1.8821	0.0306	3.0816	0.9977	1.0005	0.9967
1.8901	0.0311	3.0864	0.9972	0.9998	0.9988
1.8980	0.0262	3.0846	1.0023	0.9974	1.0009
1.9080	0.0281	3.0824	1.0009	0.9979	1.0016
1.9300	0.0303	3.0837	1.0018	0.9990	1.0035
1.9440	0.0298	3.0813	1.0040	0.9986	1.0066
1.9580	1.0246	3.0814	1.0073	1.0071	1.0076
1.9660	0.0309	3.0836	1.0058	0.9985	1.0086
1.9600	0.0312	3.0797	1.0045	0.9986	1.0080
1.9620	0.0326	3.0797	1.0037	0.9991	1.0081
1.9720	0.0304	3.0803	1.0071	0.9983	1.0098
1.9700	0.0347	3.0798	1.0036	0.9999	1.0093
1.9660	0.0295	3.0807	1.0065	0.9981	1.0087
1.9620	0.0334	3.0796	1.0030	0.9995	1.0081
1.9640	0.0339	3.0801	1.0030	0.9997	1.0082
1.9700	0.0335	3.0799	1.0044	0.9995	1.0093
1.9660	0.0293	3.0807	1.0066	0.9981	1.0087
1.9660	0.0353	3.0802	1.0025	1.0002	1.0085
1.9600	0.0311	3.0797	1.0044	0.9986	1.0080
1.9620	0.0361	3.0794	1.0012	1.0004	1.0080
1.9660	0.0336	3.0803	1.0037	0.9996	1.0085

Table E1.4: Station 4 Profile Data

y/R	Xhe	Mach #	Density	Velocity	Static Press.
0.3990	0.9268	1.3727	0.1151	1.5122	1.0274
0.4092	0.9162	1.3757	0.1204	1.4806	1.0284
0.4255	0.9177	1.3773	0.1199	1.4865	1.0290
[illegible]	[illegible]	[illegible]	[illegible]	[illegible]	[illegible]
0.4725	0.9103	1.3882	0.1230	1.4715	1.0207
0.4888	0.9064	1.3951	0.1251	1.4644	1.0187
0.4949	0.9136	1.3897	0.1229	1.4728	1.0189
0.5174	0.8984	1.3991	0.1283	1.4440	1.0122
0.5419	0.8972	1.3912	0.1279	1.4353	1.0081
0.5603	0.8877	1.3916	0.1316	1.4099	1.0032
0.5725	0.8841	1.3956	0.1334	1.4026	1.0014
0.5827	0.8833	1.3976	0.1341	1.4014	1.0023
0.6052	0.8726	1.3913	0.1381	1.3704	0.9981
0.6338	0.8697	1.3910	0.1387	1.3620	0.9972
0.6501	0.8679	1.3864	0.1391	1.3547	0.9909
0.6665	0.8572	1.3962	0.1447	1.3354	0.9898
0.6808	0.8530	1.3879	0.1458	1.3205	0.9877
0.6971	0.8435	1.3914	0.1500	1.3018	0.9850
0.7155	0.8411	1.3886	0.1509	1.2944	0.9839
0.7420	0.8359	1.3926	0.1535	1.2856	0.9829
0.7604	0.8257	1.3971	0.1583	1.2676	0.9814
0.7767	0.8188	1.3940	0.1614	1.2520	0.9822
0.7870	0.8075	1.3942	0.1668	1.2305	0.9824
0.8053	0.7994	1.3931	0.1704	1.2152	0.9819
0.8298	0.7927	1.4029	0.1740	1.2085	0.9795
0.8523	0.7841	1.4050	0.1779	1.1950	0.9780
0.8625	0.7660	1.4138	0.1865	1.1712	0.9766
0.8809	0.7700	1.4165	0.1851	1.1777	0.9752
0.9034	0.7573	1.4338	0.1916	1.1661	0.9686
0.9299	0.7511	1.4384	0.1945	1.1593	0.9668
0.9462	0.7206	1.4516	0.2089	1.1238	0.9642
0.9565	0.7051	1.4582	0.2163	1.1069	0.9625
0.9707	0.6768	1.4654	0.2294	1.0766	0.9619
0.9973	0.6741	1.4799	0.2317	1.0793	0.9578
1.0177	0.6528	1.5051	0.2432	1.0666	0.9533
1.0320	0.6202	1.5163	0.2589	1.0377	0.9522
1.0463	0.5941	1.5253	0.2713	1.0165	0.9508
1.0647	0.5790	1.5480	0.2809	1.0116	0.9491
1.0810	0.5580	1.5543	0.2913	0.9955	0.9489
1.1035	0.5288	1.5856	0.3077	0.9847	0.9469
1.1219	0.5101	1.6050	0.3185	0.9773	0.9454
1.1484	0.4765	1.6378	0.3386	0.9646	0.9457
1.1627	0.4501	1.6500	0.3530	0.9507	0.9473
1.1688	0.4273	1.6617	0.3651	0.9396	0.9472
1.1974	0.4101	1.7168	0.3828	0.9468	0.9474
1.2219	0.3668	1.7455	0.4052	0.9302	0.9424
1.2423	0.3519	1.7917	0.4161	0.9361	0.9322
1.2526	0.3301	1.8003	0.4277	0.9265	0.9328
1.2648	0.3060	1.8517	0.4459	0.9283	0.9259
1.2934	0.2899	1.8982	0.4609	0.9330	0.9222
1.3220	0.2620	1.9565	0.4854	0.9349	0.9213
1.3302	0.2419	1.9822	0.5009	0.9316	0.9225
1.3465	0.2213	2.0290	0.5179	0.9341	0.9176
1.3628	0.2041	2.0425	0.5278	0.9301	0.9171
1.3914	0.1951	2.1611	0.5512	0.9528	0.8990
1.4078	0.1749	2.2192	0.5739	0.9556	0.8951
1.4241	0.1605	2.2393	0.5860	0.9540	0.8963
1.4425	0.1455	2.2637	0.6007	0.9532	0.8993
1.4690	0.1310	2.2933	0.6192	0.9536	0.9056
1.4813	0.1229	2.3448	0.6313	0.9601	0.8962
1.5037	0.1137	2.4277	0.6524	0.9716	0.8857
1.5262	0.1015	2.4868	0.6724	0.9772	0.8815
1.5425	0.1006	2.5057	0.6778	0.9810	0.8820
1.5589	0.0957	2.5063	0.6839	0.9796	0.8875
1.5752	0.0855	2.5710	0.7063	0.9872	0.9858
1.6058	0.0723	2.5969	0.7342	0.9860	0.9018
1.6303	0.0695	2.6271	0.7462	0.9889	0.9012
1.6406	0.0696	2.6688	0.7554	0.9954	0.8955
1.6589	0.0669	2.7339	0.7716	1.0043	0.8878
[illegible]	[illegible]	[illegible]	[illegible]	[illegible]	[illegible]
1.7059	0.0533	2.7759	0.7989	1.0037	0.8919
1.7263	0.0519	2.8303	0.8166	1.0100	0.8882
1.7386	0.0487	2.8403	0.8235	1.0099	0.8894
1.7570	0.0525	2.8480	0.8252	1.0134	0.8922
1.7835	0.0485	2.8952	0.8452	1.0184	0.8936

1.8060	0.0410	2.9240	0.8588	1.0134	0.8926
1.8203	0.0330	2.9262	0.8667	1.0166	0.8953
1.8427	0.0377	3.0003	0.8854	1.0267	0.8870
1.8591	0.0316	2.9777	0.8923	1.0201	0.8964
1.8815	0.0303	2.9887	0.8998	1.0211	0.8992
1.9019	0.0280	2.9785	0.9052	1.0187	0.9068
1.9203	0.0450	3.0035	0.9029	1.0288	0.9055
1.9469	0.0310	2.9914	0.9150	1.0221	0.9145
1.9591	0.0253	2.9980	0.9237	1.0195	0.9152
1.9734	0.0255	3.0063	0.9328	1.0187	0.9175
2.0020	0.0239	2.9925	0.9385	1.0168	0.9284
2.0326	0.0232	2.9849	0.9415	1.0163	0.9352
2.0510	0.0220	2.9842	0.9432	1.0165	0.9379
2.0571	0.0243	2.9697	0.9407	1.0155	0.9425
2.0755	0.0197	2.9741	0.9452	1.0146	0.9439
2.1000	0.0211	2.9802	0.9480	1.0153	0.9431
2.1389	0.0179	2.9779	0.9525	1.0133	0.9456
2.1472	0.0178	2.9760	0.9527	1.0127	0.9460
2.1613	0.0206	2.9764	0.9499	1.0142	0.9454
2.1776	0.0194	2.9837	0.9504	1.0142	0.9414
2.1980	0.0208	2.9810	0.9478	1.0143	0.9407
2.2287	0.0187	2.9730	0.9471	1.0131	0.9430
2.2430	0.0174	2.9722	0.9481	1.0124	0.9433
2.2634	0.0181	2.9649	0.9484	1.0113	0.9461
2.2756	0.0147	2.9605	0.9518	1.0091	0.9485
2.3001	0.0141	2.9541	0.9547	1.0074	0.9525
2.3247	0.0137	2.9432	0.9562	1.0053	0.9569
2.3492	0.0178	2.9395	0.9542	1.0065	0.9592
2.3696	0.0154	2.9412	0.9542	1.0069	0.9592
2.3818	0.0178	2.9384	0.9530	1.0079	0.9615
2.3982	0.0179	2.9340	0.9546	1.0067	0.9636
2.4268	0.0177	2.9353	0.9565	1.0064	0.9642
2.4513	0.0221	2.9308	0.9529	1.0083	0.9667
2.4676	0.0229	2.9262	0.9546	1.0081	0.9708
2.4737	0.0218	2.9306	0.9575	1.0075	0.9699
2.4962	0.0191	2.9299	0.9620	1.0065	0.9732
2.5309	0.0202	2.9320	0.9672	1.0071	0.9781
2.5472	0.0199	2.9331	0.9715	1.0067	0.9810
2.5615	0.0193	2.9291	0.9746	1.0049	0.9836
2.5820	0.0205	2.9227	0.9763	1.0043	0.9861
2.6024	0.0197	2.9266	0.9775	1.0053	0.9887
2.6289	0.0209	2.9273	0.9777	1.0059	0.9895
2.6473	0.0219	2.9225	0.9783	1.0054	0.9924
2.6739	0.0256	2.9189	0.9785	1.0065	0.9966
2.6943	0.0204	2.9225	0.9867	1.0049	1.0001
2.7208	0.0176	2.9145	0.9925	1.0029	1.0027
2.7229	0.0197	2.9113	0.9907	1.0034	1.0088
2.7535	0.0200	2.8993	0.9931	1.0022	1.0173
2.7780	0.0152	2.8929	0.9994	1.0000	1.0242
2.7903	0.0195	2.8927	0.9980	1.0015	1.0256
2.8148	0.0218	2.8924	0.9987	1.0025	1.0283
2.8311	0.0218	2.8913	0.9993	1.0025	1.0297
2.8556	0.0264	2.9012	1.0038	1.0054	1.0326
2.8801	0.0246	2.9135	1.0100	1.0065	1.0328
2.8903	0.0205	2.9235	1.0170	1.0059	1.0321
2.9067	0.0209	2.9361	1.0246	1.0075	1.0280
2.9271	0.0245	2.9263	1.0184	1.0078	1.0349
2.9618	0.0235	2.9424	1.0202	1.0097	1.0295
2.9802	0.0227	2.9421	1.0211	1.0093	1.0298
2.9924	0.0220	2.9453	1.0205	1.0098	1.0281
3.0108	0.0241	2.9416	1.0183	1.0091	1.0286
3.0353	0.0266	2.9426	1.0200	1.0102	1.0297
3.0619	0.0248	2.9339	1.0193	1.0086	1.0321
3.0700	0.0214	2.9366	1.0228	1.0072	1.0314
3.1047	0.0247	2.9256	1.0184	1.0070	1.0336
3.1068	0.0230	2.9259	1.0206	1.0059	1.0338
3.1252	0.0224	2.9230	1.0212	1.0054	1.0355
3.1517	0.0225	2.9193	1.0199	1.0055	1.0369
3.1599	0.0236	2.9053	1.0216	1.0042	1.0459
3.1599	0.0225	2.9054	1.0223	1.0038	1.0459
3.1558	0.0256	2.9169	1.0182	1.0063	1.0381
3.1517	0.0218	2.9194	1.0203	1.0053	1.0369
3.1599	0.0228	2.9054	1.0223	1.0039	1.0459
3.1599	0.0256	2.9051	1.0202	1.0049	1.0459
3.1619	0.0264	2.9037	1.0198	1.0050	1.0466

E.2 Dimensional Data

The E2 Tables contain dimensional data with the columns having the following units:

- y → inch
- Xhe → mole fraction of helium
- Mach number
- Density → kg/m^3
- Velocity → m/sec
- Static Press. → psia

Table E2.1: Station 1 Profile Data

y	Xhe	Mach #	Density	Velocity	Static Press.
0.0627	0.9995	2.0573	0.0462	1322.41	1.6611
0.0702	0.9989	2.0928	0.0468	1329.37	1.6460
[illegible]	0.9998	2.1059	0.0468	1336.44	1.6407
[illegible]	[illegible]	[illegible]	[illegible]	[illegible]	[illegible]
0.1013	0.9992	2.0151	0.0480	1309.73	1.7648
0.1089	0.9993	1.9554	0.0490	1293.34	1.8675
0.1221	0.9998	1.9876	0.0502	1274.66	1.9917
0.1372	0.9992	1.8456	0.0514	1259.38	2.0844
0.1457	0.9991	1.8325	0.0517	1254.80	2.1103
0.1560	0.9998	1.8077	0.0524	1248.32	2.1739
0.1627	0.9980	1.7929	0.0534	1236.21	2.2108
0.1759	0.9988	1.7686	0.0541	1229.80	2.2785
0.1853	0.9950	1.7601	0.0558	1212.67	2.3094
0.1976	0.9978	1.7481	0.0553	1218.39	2.3421
0.2070	0.9988	1.7371	0.0554	1217.64	2.3707
0.2164	1.0000	1.7291	0.0556	1219.27	2.4060
0.2296	0.9998	1.7400	0.0565	1222.14	2.4253
0.2438	0.9987	1.7573	0.0575	1224.09	2.4292
0.2551	0.9974	1.7740	0.0578	1224.88	2.4011
0.2655	0.9980	1.7711	0.0573	1226.29	2.3916
0.2730	0.9975	1.7855	0.0570	1229.39	2.3545
0.2853	0.9999	1.8274	0.0554	1252.70	2.2659
0.2928	0.9999	1.8485	0.0553	1259.05	2.2351
0.3060	1.0000	1.9081	0.0541	1277.35	2.1125
0.3155	1.0000	1.9544	0.0534	1290.80	2.0282
0.3240	1.0000	1.9845	0.0523	1299.40	1.9524
0.3372	1.0000	2.0514	0.0512	1317.33	1.8395
0.3513	0.9999	2.0529	0.0508	1316.35	1.8192
0.3645	0.9997	1.9410	0.0514	1283.94	1.9590
0.3740	0.9977	1.8747	0.0529	1256.17	2.0689
0.3824	0.9921	1.8339	0.0555	1223.39	2.1562
0.3975	0.9843	1.7983	0.0590	1186.26	2.2452
0.4022	0.9761	1.7848	0.0616	1156.46	2.2676
0.4164	0.9580	1.5406	0.0613	1023.38	2.3828
0.4249	0.9391	1.3814	0.0635	918.89	2.4851
0.4334	0.9137	1.3110	0.0677	841.31	2.4817
0.4485	0.8897	0.8767	0.0599	596.71	2.4856
0.4588	0.8473	0.9850	0.0728	605.69	2.4882
0.4711	0.7669	1.3651	0.1093	679.28	2.4914
0.4824	0.2069	1.6605	0.2693	495.29	2.4214
0.4909	0.0880	1.7694	0.3056	486.49	2.3707
0.5022	0.0000	1.8445	0.3284	480.38	2.3099
0.5088	0.0000	1.9129	0.3311	491.07	2.2624
0.5211	0.0051	2.0464	0.3279	511.57	2.1235
0.5315	0.0115	2.1869	0.3199	531.47	1.9565
0.5400	0.0159	2.3727	0.3207	553.95	1.8088
0.5503	0.0238	2.5541	0.3227	574.46	1.6878
0.5626	0.0257	2.6358	0.3328	582.94	1.6828
0.5720	0.0238	2.5945	0.3449	578.90	1.7754
0.5824	0.0359	2.6192	0.3599	584.12	1.8484
0.5909	0.0337	2.5899	0.3770	581.09	1.9601
0.6022	0.0238	2.5627	0.3962	576.81	2.0754
0.6079	0.0203	2.5651	0.4094	576.57	2.1397
0.6202	0.0256	2.6093	0.4362	582.68	2.2484
0.6324	0.0245	2.6194	0.4518	583.85	2.3205
0.6381	0.0280	2.6160	0.4574	584.56	2.3605
0.6475	0.0321	2.6638	0.4730	590.00	2.3967
0.6579	0.0350	2.6586	0.4811	590.49	2.4509
0.6701	0.0385	2.7425	0.5007	599.05	2.4660
0.6815	0.0448	2.8052	0.5133	606.03	2.4711
0.6871	0.0485	2.7721	0.5099	604.11	2.4967
0.6966	0.0418	2.8339	0.5259	608.10	2.4985
0.7013	0.0170	2.8667	0.5431	605.00	2.5030
0.7173	0.0201	2.9385	0.5599	611.19	2.5055
[illegible]	0.0237	2.9671	0.5657	613.82	2.5033
0.7333	0.0297	2.9558	0.5673	614.32	2.5318
[illegible]	0.0334	3.0077	0.5757	619.01	2.5184
0.7513	0.0375	3.0082	0.5794	619.87	2.5396
[illegible]	0.0372	3.0110	0.5852	619.87	2.5605
[illegible]	[illegible]	[illegible]	[illegible]	[illegible]	[illegible]
0.7815	0.0367	3.0164	0.5913	619.91	2.5784
0.7890	0.0329	3.0295	0.5972	619.62	2.5802
0.7956	0.0338	3.0237	0.5979	619.34	2.5906
0.8116	0.0382	3.0079	0.5967	618.81	2.6079
0.8173	0.0375	3.0107	0.5979	618.87	2.6080

0.8277	0.0360	3.0114	0.5982	618.34	2.6038
0.9381	0.0357	3.0099	0.5981	618.05	2.6040
0.8465	0.0361	3.0111	0.5980	618.00	2.6039
0.8569	0.0323	3.0086	0.5978	616.83	2.5953
0.8664	0.0325	3.0169	0.5988	617.27	2.5892
0.8739	0.0288	3.0110	0.5994	616.00	2.5924
0.8843	0.0302	3.0099	0.5987	616.20	2.5927
0.8909	0.0278	3.0038	0.5994	615.37	2.5999
0.9050	0.0222	3.0135	0.6052	614.63	2.6036
0.9107	0.0219	3.0197	0.6065	615.10	2.6027
0.9220	0.0239	3.0218	0.6098	615.72	2.6176
0.9305	0.0261	3.0360	0.6136	617.35	2.6224
0.9362	0.0229	3.0388	0.6171	616.69	2.6281
0.9484	0.0218	3.0274	0.6184	615.74	2.6457
0.9607	0.0246	3.0190	0.6182	615.68	2.6582
0.9720	0.0258	2.9918	0.6147	614.03	2.6764
0.9805	0.0336	2.9888	0.6113	615.47	2.6771
0.9871	0.0316	2.9851	0.6117	614.83	2.6804
1.0003	0.0347	2.9880	0.6101	615.79	2.6758
1.0078	0.0307	2.9859	0.6100	614.70	2.6711
1.0192	0.0295	2.9968	0.6096	615.10	2.6533
1.0286	0.0324	2.9982	0.6072	615.80	2.6459
1.0380	0.0303	3.0063	0.6069	615.77	2.6304
1.0484	0.0323	2.9976	0.6050	615.63	2.6359
1.0597	0.0298	2.9934	0.6058	614.66	2.6394
1.0710	0.0319	2.9834	0.6055	614.45	2.6529
1.0814	0.0353	2.9669	0.6043	614.12	2.6734
1.0871	0.0287	2.9736	0.6100	612.91	2.6780
1.1012	0.0321	2.9515	0.6083	612.06	2.7022
1.1078	0.0338	2.9526	0.6072	612.68	2.6998
1.1163	0.0354	2.9488	0.6066	612.93	2.7062
1.1267	0.0372	2.9546	0.6055	613.56	2.6956
1.1342	0.0359	2.9547	0.6061	613.27	2.6956
1.1437	0.0324	2.9551	0.6079	612.31	2.6958
1.1578	0.0312	2.9552	0.6085	611.98	2.6959
1.1710	0.0330	2.9550	0.6078	612.37	2.6958
1.1786	0.0330	2.9550	0.6079	612.33	2.6958
1.1890	0.0310	2.9552	0.6087	611.88	2.6959
1.2003	0.0320	2.9551	0.6083	612.12	2.6959
1.2069	0.0319	2.9551	0.6083	612.09	2.6959
1.2191	0.0317	2.9551	0.6084	612.05	2.6959
1.2229	0.0305	2.9552	0.6089	611.79	2.6959
1.2333	0.0296	2.9553	0.6093	611.59	2.6960
1.2427	0.0314	2.9552	0.6085	611.97	2.6959
1.2540	0.0329	2.9550	0.6079	612.32	2.6958
1.2654	0.0330	2.9550	0.6079	612.32	2.6958
1.2767	0.0304	2.9553	0.6090	611.75	2.6960
1.2861	0.0321	2.9551	0.6083	612.12	2.6959
1.2984	0.0320	2.9551	0.6083	612.11	2.6959
1.3031	0.0345	2.9549	0.6072	612.66	2.6957
1.3135	0.0365	2.9547	0.6064	613.10	2.6956
1.3229	0.0371	2.9546	0.6061	613.25	2.6956
1.3295	0.0375	2.9546	0.6060	613.32	2.6955
1.3399	0.0398	2.9544	0.6050	613.85	2.6954
1.3512	0.0407	2.9543	0.6046	614.04	2.6954
1.3540	0.0395	2.9544	0.6051	613.77	2.6954
1.3663	0.0392	2.9544	0.6052	613.71	2.6954
1.3748	0.0415	2.9542	0.6043	614.21	2.6953
1.3842	0.0433	2.9540	0.6035	614.63	2.6952
1.3918	0.0430	2.9541	0.6037	614.55	2.6952
1.4050	0.0391	2.9544	0.6053	613.69	2.6954
1.4116	0.0403	2.9543	0.6048	613.96	2.6954
1.4172	0.0403	2.9543	0.6048	613.96	2.6954
1.4248	0.0390	2.9544	0.6053	613.66	2.6955
1.4370	0.0370	2.9546	0.6062	613.22	2.6956
1.4418	0.0394	2.9544	0.6052	613.76	2.6954
1.4418	0.0385	2.9545	0.6056	613.54	2.6955
1.4408	0.0365	2.9547	0.6064	613.11	2.6956
1.4370	0.0364	2.9547	0.6064	613.08	2.6956
1.4380	0.0387	2.9545	0.6055	613.58	2.6955
1.4408	0.0356	2.9548	0.6068	612.90	2.6957
1.4408	0.0355	2.9548	0.6068	612.88	2.6957
1.4389	0.0398	2.9544	0.6050	613.84	2.6954
1.4380	0.0407	2.9543	0.6046	614.05	2.6954
1.4399	0.0396	2.9544	0.6051	613.79	2.6954

Table E2.2: Station 2 Profile Data

y	Xhe	Mach #	Density	Velocity	Static Press.
0.0539	1.0000	1.2735	0.0529	1020.22	2.9563
0.0557	1.0000	1.2908	0.0533	1029.15	2.9518
0.0603	1.0000	1.3301	0.0544	1048.99	2.9473
[illegible]	[illegible]	1.4322	0.0573	1097.52	2.9293
0.0797	1.0000	1.4720	0.0578	1115.35	2.8915
0.0834	1.0000	1.4980	0.0583	1126.53	2.8728
0.0899	1.0000	1.5566	0.0596	1151.30	2.8393
0.0963	0.9978	1.5879	0.0613	1156.06	2.8285
0.1010	0.9972	1.6012	0.0620	1159.31	2.8305
0.1130	0.9957	1.6155	0.0634	1159.35	2.8444
0.1194	0.9935	1.6132	0.0642	1151.06	2.8530
0.1204	0.9946	1.6132	0.0639	1154.69	2.8540
0.1296	0.9967	1.6185	0.0631	1164.26	2.8453
0.1308	0.9952	1.6183	0.0633	1159.17	2.8321
0.1444	0.9940	1.6156	0.0636	1153.86	2.8284
0.1527	0.9918	1.6132	0.0642	1145.07	2.8233
0.1582	0.9939	1.6128	0.0632	1152.50	2.8145
0.1592	0.9933	1.6135	0.0635	1150.50	2.8139
0.1712	0.9935	1.6106	0.0632	1149.76	2.8105
0.1813	0.9905	1.6091	0.0643	1137.96	2.8058
0.1832	0.9934	1.6092	0.0633	1147.63	2.8060
0.1896	0.9877	1.6122	0.0654	1128.78	2.8015
0.1952	0.9916	1.6096	0.0639	1140.27	2.7982
0.1989	0.9914	1.6108	0.0641	1139.16	2.7979
0.2118	0.9879	1.6107	0.0653	1127.09	2.7930
0.2201	0.9909	1.6090	0.0641	1135.87	2.7901
0.2201	0.9885	1.6093	0.0650	1128.31	2.7904
0.2257	0.9927	1.6122	0.0635	1143.41	2.7854
0.2349	0.9902	1.6142	0.0644	1135.67	2.7823
0.2423	0.9922	1.6141	0.0635	1142.69	2.7768
0.2497	0.9928	1.6178	0.0633	1146.49	2.7713
0.2562	0.9925	1.6172	0.0633	1145.26	2.7698
0.2580	0.9930	1.6174	0.0631	1147.60	2.7711
0.2654	0.9949	1.6185	0.0623	1154.75	2.7646
0.2783	0.9924	1.6224	0.0632	1147.70	2.7574
0.2820	0.9927	1.6239	0.0631	1149.13	2.7562
0.2885	0.9877	1.6241	0.0649	1132.35	2.7565
0.2931	0.9792	1.6286	0.0680	1107.74	2.7541
0.2968	0.9772	1.6291	0.0686	1102.62	2.7513
0.3060	0.9691	1.6272	0.0713	1078.81	2.7499
0.3162	0.9542	1.6300	0.0764	1040.87	2.7462
0.3180	0.9442	1.6283	0.0797	1016.82	2.7464
0.3217	0.9342	1.6193	0.0828	992.11	2.7517
0.3291	0.9209	1.6143	0.0868	963.48	2.7485
0.3374	0.9045	1.5795	0.0906	922.12	2.7551
0.3448	0.8953	1.5351	0.0918	892.58	2.7739
0.3532	0.8790	1.4940	0.0952	854.02	2.7926
0.3532	0.8611	1.4960	0.1008	829.68	2.7935
0.3596	0.8446	1.4344	0.1039	788.73	2.8417
0.3707	0.8271	1.3716	0.1064	746.43	2.8626
0.3762	0.8079	1.3604	0.1111	722.47	2.8579
0.3809	0.7852	1.3374	0.1161	692.81	2.8571
0.3910	0.7574	1.2952	0.1216	654.14	2.8605
0.3920	0.7054	1.2977	0.1367	615.48	2.8661
0.4003	0.5859	1.2757	0.1692	539.13	2.8816
0.4114	0.5301	1.2532	0.1834	507.07	2.8903
0.4150	0.4974	1.2565	0.1924	494.88	2.8893
0.4178	0.4190	1.2624	0.2144	468.40	2.8943
0.4261	0.3648	1.2645	0.2297	451.67	2.8973
0.4307	0.3059	1.2772	0.2477	437.92	2.9034
0.4391	0.2614	1.3076	0.2643	433.07	2.9084
0.4492	0.2109	1.3729	0.2880	435.57	2.9283
0.4483	0.1801	1.3710	0.2978	427.00	2.9304
0.4529	0.1464	1.4052	0.3139	426.24	2.9424
[illegible]	0.1268	1.4235	0.3296	445.91	2.8748
0.4714	0.1044	1.5890	0.3444	452.87	2.8647
0.4760	0.0891	1.6330	0.3574	457.14	2.8737
0.4843	0.0738	1.7409	0.3785	472.62	2.8675
0.4953	0.0691	1.7466	0.3799	472.47	2.8592
[illegible]	0.0580	1.8275	0.3878	483.25	2.7927
0.5056	0.0534	1.9851	0.4080	505.88	2.7300
0.5093	0.0524	1.9973	0.4094	508.03	2.7298
0.5130	0.0466	2.0360	0.4135	512.28	2.6992
0.5204	0.0442	2.0931	0.4191	519.56	2.6638
0.5241	0.0443	2.1164	0.4214	522.92	2.6536

0.5324	0.0479	2.1788	0.4278	531.97	2.6293
0.5435	0.0416	2.2499	0.4409	539.54	2.6164
0.5462	0.0461	2.2687	0.4431	543.22	2.6200
0.5490	0.0480	2.2814	0.4442	545.37	2.6170
0.5601	0.0463	2.3824	0.4583	556.54	2.5792
0.5665	0.0475	2.4252	0.4646	561.40	2.5671
0.5712	0.0508	2.4395	0.4673	563.48	2.5698
0.5822	0.0471	2.5352	0.4865	572.33	2.5567
0.5832	0.0513	2.5381	0.4852	573.79	2.5559
0.5878	0.0505	2.5495	0.4899	574.60	2.5646
0.5998	0.0466	2.6059	0.5074	579.18	2.5848
0.6035	0.0538	2.6223	0.5066	582.77	2.5778
0.6100	0.0519	2.6621	0.5143	585.92	2.5676
0.6183	0.0505	2.7382	0.5288	592.52	2.5521
0.6210	0.0514	2.7478	0.5327	593.05	2.5575
0.6294	0.0526	2.7841	0.5405	596.57	2.5570
0.6414	0.0467	2.8519	0.5607	600.73	2.5655
0.6441	0.0455	2.8652	0.5636	601.47	2.5614
0.6478	0.0469	2.8775	0.5676	603.06	2.5709
0.6571	0.0434	2.9132	0.5786	604.87	2.5731
0.6645	0.0393	2.9477	0.5890	606.71	2.5752
0.6700	0.0379	2.9398	0.5915	605.86	2.5933
0.6811	0.0463	2.9760	0.5999	610.62	2.6043
0.6839	0.0461	2.9704	0.6029	610.09	2.6231
0.6866	0.0498	2.9754	0.6030	611.14	2.6224
0.7005	0.0459	2.9451	0.6087	608.02	2.6753
0.7060	0.0425	2.9043	0.6128	604.03	2.7345
0.7116	0.0347	2.8962	0.6169	601.11	2.7439
0.7208	0.0250	2.8774	0.6225	597.64	2.7763
0.7217	0.0161	2.8770	0.6275	595.06	2.7778
0.7301	0.0180	2.8627	0.6293	594.21	2.8055
0.7439	0.0195	2.8621	0.6321	594.18	2.8180
0.7467	0.0222	2.8543	0.6297	594.28	2.8229
0.7513	0.0274	2.8628	0.6294	595.95	2.8188
0.7615	0.0313	2.8555	0.6226	596.39	2.8054
0.7661	0.0285	2.8708	0.6254	596.50	2.7900
0.7735	0.0337	2.8243	0.6102	593.71	2.7848
0.7846	0.0337	2.7849	0.5943	589.95	2.7542
0.7873	0.0379	2.7925	0.5884	591.35	2.7237
0.7901	0.0339	2.7767	0.5874	589.07	2.7302
0.8030	0.0374	2.8571	0.5737	596.35	2.5803
0.8104	0.0327	2.8838	0.5711	597.42	2.5317
0.8141	0.0345	2.9257	0.5663	601.14	2.4690
0.8261	0.0364	3.0572	0.5540	610.71	2.2825
0.8261	0.0411	3.0568	0.5520	611.91	2.2822
0.8317	0.0386	3.0993	0.5478	614.35	2.2215
0.8455	0.0325	3.2064	0.5431	619.57	2.0944
0.8511	0.0399	3.2364	0.5362	623.19	2.0519
0.8557	0.0391	3.2760	0.5357	624.83	2.0114
0.8631	0.0379	3.3086	0.5342	626.02	1.9740
0.8677	0.0365	3.3355	0.5369	627.30	1.9606
0.8751	0.0362	3.3414	0.5394	627.26	1.9626
0.8871	0.0410	3.3371	0.5400	628.70	1.9778
0.8926	0.0395	3.3262	0.5417	627.49	1.9896
0.8945	0.0361	3.3181	0.5435	626.53	2.0007
0.9046	0.0308	3.2979	0.5473	624.21	2.0255
0.9130	0.0295	3.2940	0.5490	623.57	2.0328
0.9185	0.0332	3.2768	0.5497	623.42	2.0548
0.9277	0.0373	3.2549	0.5492	622.96	2.0768
0.9314	0.0361	3.2457	0.5493	622.08	2.0856
0.9342	0.0337	3.2284	0.5502	620.55	2.0994
0.9453	0.0350	3.1946	0.5503	618.69	2.1312
0.9536	0.0355	3.1853	0.5513	617.85	2.1408
0.9573	0.0358	3.1778	0.5512	617.32	2.1476
0.9573	0.0363	3.1778	0.5510	617.42	2.1476
0.9536	0.0394	3.1855	0.5499	618.66	2.1405
0.9564	0.0371	3.1786	0.5508	617.71	2.1472
0.9582	0.0311	3.1684	0.5524	615.61	2.1545
0.9582	0.0352	3.1681	0.5511	616.41	2.1542
0.9564	0.0323	3.1790	0.5533	616.25	2.1476
0.9545	0.0354	3.1850	0.5514	617.63	2.1411
0.9564	0.0318	3.1790	0.5528	616.53	2.1477
0.9592	0.0373	3.1667	0.5500	616.95	2.1549
0.9573	0.0380	3.1776	0.5504	617.77	2.1475
0.9573	0.0370	3.1777	0.5509	617.47	2.1475

Table E2.3: Station 3 Profile Data

Y	Xhe	Mach #	Density	Velocity	Static Press.
0.0566	0.9045	1.3805	0.0847	851.91	2.8761
0.0604	0.9004	1.3808	0.0860	845.26	2.8767
0.0652	0.9158	1.3796	0.0811	871.02	2.8745
[illegible]	0.9252	1.3788	0.0781	887.57	2.8731
0.0794	0.9266	1.3787	0.0776	890.58	2.8729
0.0870	0.9364	1.3944	0.0753	916.37	2.8767
0.0937	0.9409	1.4489	0.0749	947.53	2.8324
0.1031	0.9487	1.5129	0.0738	989.56	2.7849
0.1041	0.9533	1.5136	0.0723	1000.72	2.7846
0.1117	0.9569	1.5585	0.0724	1026.29	2.7638
0.1202	0.9617	1.5957	0.0721	1052.24	2.7573
0.1297	0.9645	1.6136	0.0721	1066.07	2.7664
0.1335	0.9675	1.6148	0.0711	1074.94	2.7686
0.1345	0.9725	1.6157	0.0695	1089.15	2.7696
0.1459	0.9737	1.6197	0.0697	1094.07	2.7885
0.1554	0.9767	1.6211	0.0688	1103.67	2.7953
0.1601	0.9716	1.6229	0.0708	1089.04	2.7980
0.1658	0.9739	1.6230	0.0700	1095.30	2.7942
0.1743	0.9711	1.6241	0.0709	1087.77	2.7916
0.1762	0.9678	1.6244	0.0722	1078.35	2.7921
0.1848	0.9646	1.6281	0.0731	1070.93	2.7809
0.1952	0.9624	1.6292	0.0738	1064.84	2.7727
0.2019	0.9609	1.6291	0.0743	1060.93	2.7727
0.2038	0.9603	1.6342	0.0745	1060.96	2.7640
0.2085	0.9598	1.6299	0.0744	1058.42	2.7597
0.2199	0.9600	1.6297	0.0740	1059.20	2.7490
0.2266	0.9591	1.6269	0.0741	1055.93	2.7460
0.2313	0.9590	1.6236	0.0738	1054.77	2.7411
0.2370	0.9596	1.6231	0.0733	1056.88	2.7355
0.2446	0.9579	1.6097	0.0733	1047.94	2.7356
0.2474	0.9571	1.6103	0.0734	1046.60	2.7303
0.2560	0.9606	1.6015	0.0715	1053.36	2.7210
0.2674	0.9574	1.5812	0.0715	1038.50	2.7174
0.2712	0.9556	1.5799	0.0720	1034.11	2.7174
0.2721	0.9529	1.5793	0.0727	1027.49	2.7131
0.2807	0.9482	1.5672	0.0736	1012.39	2.7122
0.2949	0.9477	1.5335	0.0724	999.55	2.7136
0.2978	0.9412	1.5258	0.0740	982.31	2.7124
0.3006	0.9415	1.5192	0.0736	981.13	2.7142
0.3158	0.9357	1.4838	0.0742	955.44	2.7229
0.3158	0.9294	1.4846	0.0761	942.85	2.7231
0.3234	0.9243	1.4829	0.0774	932.33	2.7146
0.3281	0.9203	1.4706	0.0783	919.62	2.7220
0.3386	0.9182	1.4405	0.0781	904.52	2.7363
0.3386	0.9090	1.4417	0.0808	888.57	2.7364
0.3443	0.9009	1.4387	0.0830	873.31	2.7314
0.3547	0.8937	1.4188	0.0846	853.86	2.7406
0.3623	0.8926	1.4186	0.0846	852.03	2.7289
0.3661	0.8856	1.4178	0.0867	840.78	2.7311
0.3680	0.8710	1.4214	0.0910	820.10	2.7252
0.3766	0.8724	1.4106	0.0903	817.92	2.7310
0.3861	0.8628	1.4073	0.0930	802.96	2.7264
0.3918	0.8568	1.4099	0.0947	795.57	2.7217
0.3956	0.8488	1.4157	0.0971	786.88	2.7124
0.4041	0.8405	1.4257	0.0997	779.38	2.6994
0.4079	0.8250	1.4320	0.1045	762.15	2.6911
0.4145	0.8229	1.4484	0.1058	764.48	2.6805
0.4240	0.8098	1.4732	0.1105	757.24	2.6614
0.4316	0.8044	1.4910	0.1126	756.58	2.6460
0.4326	0.7905	1.4969	0.1171	743.30	2.6452
0.4364	0.7799	1.5269	0.1215	741.19	2.6282
0.4478	0.7689	1.5579	0.1264	738.76	2.6152
0.4554	0.7527	1.6027	0.1342	734.79	2.6047
0.4592	0.7312	1.6178	0.1420	719.50	2.6054
0.4649	0.7123	1.6503	0.1505	711.85	2.6063
0.4715	0.6873	1.6860	0.1617	700.84	2.6133
0.4762	0.6546	1.7177	0.1743	684.55	2.6063
0.4838	0.6207	1.7730	0.1879	674.17	2.5736
0.4943	0.5863	1.8599	0.2048	670.62	2.5389
[illegible]	[illegible]	[illegible]	[illegible]	[illegible]	[illegible]
0.4997	0.5555	1.9087	0.2255	652.07	2.5312
0.5076	0.4866	1.9779	0.2489	640.53	2.5311
0.5190	0.4628	2.0489	0.2633	641.03	2.5093
0.5218	0.4359	2.0873	0.2750	635.38	2.4920
0.5256	0.3963	2.1201	0.2910	624.34	2.4830

0.5313	0.3610	2.1544	0.3059	616.32	2.4758
0.5408	0.3282	2.2101	0.3234	612.47	2.4683
0.5456	0.2994	2.2520	0.3384	608.48	2.4653
0.5531	0.2701	2.2850	0.3536	603.36	2.4706
0.5617	0.2442	2.3339	0.3685	601.60	2.4621
0.5636	0.2167	2.3423	0.3780	594.91	2.4611
0.5693	0.1936	2.3652	0.3883	591.41	2.4584
0.5788	0.1773	2.4211	0.4010	593.40	2.4444
0.5883	0.1653	2.4673	0.4121	595.46	2.4392
0.5911	0.1439	2.4768	0.4205	591.33	2.4422
0.5930	0.1330	2.4879	0.4253	589.97	2.4406
0.6044	0.1178	2.5453	0.4399	592.74	2.4390
0.6130	0.1048	2.5783	0.4510	593.29	2.4455
0.6158	0.0971	2.5942	0.4569	592.91	2.4461
0.6234	0.0822	2.6247	0.4690	591.47	2.4458
0.6300	0.0754	2.6591	0.4767	592.69	2.4339
0.6329	0.0665	2.6727	0.4823	591.99	2.4340
0.6414	0.0564	2.7095	0.4926	592.70	2.4280
0.6519	0.0556	2.7594	0.5012	596.69	2.4142
0.6566	0.0477	2.8001	0.5104	598.36	2.4032
0.6585	0.0482	2.8064	0.5120	599.39	2.4055
0.6633	0.0476	2.8351	0.5163	602.03	2.4005
0.6766	0.0434	2.8773	0.5274	604.80	2.4040
0.6823	0.0473	2.9015	0.5304	607.87	2.4003
0.6861	0.0374	2.9117	0.5368	606.29	2.4028
0.6927	0.0396	2.9613	0.5427	610.43	2.3797
0.7003	0.0399	2.9842	0.5483	611.92	2.3793
0.7060	0.0381	3.0206	0.5541	614.05	2.3637
0.7145	0.0377	3.0480	0.5602	616.04	2.3622
0.7259	0.0369	3.1003	0.5717	619.42	2.3561
0.7278	0.0338	3.1006	0.5734	618.75	2.3580
0.7307	0.0382	3.1029	0.5734	619.63	2.3601
0.7383	0.0365	3.1345	0.5812	621.37	2.3579
0.7506	0.0385	3.1251	0.5841	621.11	2.3816
0.7544	0.0336	3.1368	0.5890	620.91	2.3833
0.7582	0.0347	3.1446	0.5916	621.42	2.3857
0.7658	0.0388	3.1519	0.5941	622.87	2.3948
0.7744	0.0351	3.1621	0.5999	622.71	2.4025
0.7819	0.0375	3.1630	0.6018	623.41	2.4132
0.7867	0.0417	3.1563	0.6007	623.87	2.4213
0.7990	0.0410	3.1464	0.6025	623.30	2.4400
0.7990	0.0478	3.1458	0.6001	624.62	2.4394
0.8057	0.0388	3.1451	0.6057	622.54	2.4493
0.8161	0.0388	3.1403	0.6070	622.18	2.4592
0.8247	0.0402	3.1335	0.6068	622.25	2.4694
0.8285	0.0347	3.1317	0.6094	620.90	2.4735
0.8313	0.0339	3.1253	0.6096	620.14	2.4787
0.8418	0.0343	3.1198	0.6102	620.08	2.4895
0.8513	0.0355	3.1090	0.6085	619.95	2.4983
0.8569	0.0327	3.1042	0.6104	618.88	2.5058
0.8626	0.0319	3.1031	0.6104	618.84	2.5077
0.8731	0.0369	3.0963	0.6084	619.71	2.5159
0.8740	0.0326	3.0952	0.6105	618.48	2.5177
0.8826	0.0339	3.0882	0.6095	618.34	2.5236
0.8940	0.0306	3.0926	0.6125	617.83	2.5253
0.8978	0.0311	3.0864	0.6121	617.46	2.5307
0.9016	0.0262	3.0846	0.6149	616.16	2.5361
0.9063	0.0281	3.0824	0.6139	616.52	2.5378
0.9168	0.0303	3.0837	0.6148	616.99	2.5427
0.9234	0.0298	3.0813	0.6158	616.90	2.5505
0.9301	0.0265	3.0814	0.6171	616.14	2.5536
0.9338	0.0309	3.0806	0.6168	616.95	2.5556
0.9310	0.0312	3.0797	0.6160	616.97	2.5539
0.9320	0.0326	3.0797	0.6155	617.30	2.5543
0.9367	0.0304	3.0803	0.6176	616.81	2.5585
0.9357	0.0347	3.0798	0.6155	617.78	2.5573
0.9338	0.0295	3.0807	0.6174	616.64	2.5557
0.9320	0.0334	3.0796	0.6152	617.46	2.5543
0.9329	0.0339	3.0801	0.6152	617.63	2.5546
0.9357	0.0335	3.0799	0.6160	617.50	2.5574
0.9338	0.0293	3.0807	0.6174	616.61	2.5557
0.9338	0.0353	3.0802	0.6148	617.95	2.5552
0.9310	0.0311	3.0797	0.6160	616.95	2.5539
0.9320	0.0361	3.0794	0.6141	618.04	2.5541
0.9338	0.0336	3.0803	0.6156	617.53	2.5553

Table E2.4: Station 4 Profile Data

y	Xhe	Mach #	Density	Velocity	Static Press.
0.1895	0.9268	1.3727	0.0793	901.18	3.0339
0.1944	0.9162	1.3757	0.0830	882.48	3.0369
0.2001	0.9177	1.3773	0.0826	885.96	3.0387
[illegible]	0.9171	1.3823	0.0826	886.38	3.0265
0.2244	0.9103	1.3882	0.0848	876.79	3.0143
0.2322	0.9064	1.3951	0.0862	872.62	3.0084
0.2351	0.9106	1.3897	0.0847	877.48	3.0089
0.2458	0.8984	1.3991	0.0885	860.10	2.9892
0.2574	0.8972	1.3912	0.0882	854.87	2.9771
0.2661	0.8877	1.3916	0.0909	839.48	2.9625
0.2720	0.8841	1.3956	0.0921	835.27	2.9574
0.2768	0.8833	1.3976	0.0926	834.53	2.9599
0.2875	0.8726	1.3913	0.0953	816.07	2.9476
0.3011	0.8697	1.3910	0.0957	810.95	2.9271
0.3088	0.8679	1.3864	0.0961	806.51	2.9262
0.3166	0.8572	1.3962	0.0999	795.05	2.9231
0.3234	0.8530	1.3879	0.1007	786.06	2.9169
0.3311	0.8435	1.3914	0.1036	774.91	2.9088
0.3399	0.8411	1.3886	0.1042	770.50	2.9057
0.3525	0.8359	1.3926	0.1060	765.26	2.9027
0.3612	0.8257	1.3971	0.1094	754.37	2.8983
0.3690	0.8188	1.3940	0.1116	744.92	2.9005
0.3738	0.8075	1.3942	0.1153	732.26	2.9011
0.3825	0.7994	1.3931	0.1178	723.01	2.8997
0.3942	0.7927	1.4029	0.1203	718.98	2.8927
0.4048	0.7841	1.4050	0.1230	710.98	2.8881
0.4097	0.7660	1.4138	0.1290	696.74	2.8839
0.4184	0.7700	1.4165	0.1280	700.57	2.8798
0.4291	0.7570	1.4338	0.1325	693.69	2.8603
0.4417	0.7511	1.4384	0.1345	689.54	2.8551
0.4495	0.7206	1.4516	0.1445	668.41	2.8474
0.4543	0.7051	1.4582	0.1496	658.27	2.8423
0.4611	0.6768	1.4654	0.1587	640.25	2.8406
0.4737	0.6741	1.4799	0.1603	641.85	2.8284
0.4834	0.6528	1.5051	0.1685	634.06	2.8151
0.4902	0.6202	1.5163	0.1792	617.03	2.8121
0.4970	0.5941	1.5253	0.1879	604.34	2.8077
0.5057	0.5790	1.5480	0.1946	601.35	2.8029
0.5135	0.5580	1.5543	0.2017	591.84	2.8023
0.5242	0.5288	1.5856	0.2132	585.19	2.7963
0.5329	0.5101	1.6050	0.2207	580.77	2.7920
0.5455	0.4765	1.6378	0.2347	573.18	2.7929
0.5523	0.4501	1.6500	0.2447	564.90	2.7976
0.5552	0.4273	1.6617	0.2530	558.41	2.7972
0.5688	0.4101	1.7168	0.2652	562.84	2.7977
0.5804	0.3668	1.7455	0.2806	552.94	2.7830
0.5901	0.3519	1.7917	0.2884	556.25	2.7529
0.5950	0.3301	1.8003	0.2964	550.57	2.7547
0.6008	0.3060	1.8517	0.3090	551.63	2.7343
0.6144	0.2899	1.8982	0.3194	554.45	2.7233
0.6279	0.2620	1.9565	0.3366	555.35	2.7208
0.6318	0.2419	1.9822	0.3473	553.47	2.7241
0.6396	0.2213	2.0290	0.3593	554.76	2.7099
0.6473	0.2041	2.0425	0.3664	552.26	2.7083
0.6609	0.1951	2.1611	0.3827	565.72	2.6548
0.6687	0.1749	2.2192	0.3984	567.42	2.6434
0.6764	0.1605	2.2393	0.4067	566.50	2.6468
0.6852	0.1455	2.2637	0.4168	566.17	2.6558
0.6978	0.1310	2.2933	0.4298	566.21	2.6742
0.7036	0.1229	2.3448	0.4381	570.15	2.6467
0.7143	0.1137	2.4277	0.4530	576.82	2.6157
0.7249	0.1015	2.4868	0.4666	580.30	2.6031
0.7327	0.1006	2.5057	0.4706	582.39	2.6047
0.7405	0.0957	2.5063	0.4751	581.41	2.6209
[illegible]	0.0855	2.5710	0.4909	585.84	2.6160
0.7628	0.0723	2.5969	0.5103	585.09	2.6632
0.7744	0.0695	2.6271	0.5184	586.96	2.6612
0.7793	0.0696	2.6688	0.5250	590.65	2.6445
0.7890	0.0669	2.7339	0.5364	595.91	2.6216
[illegible]	0.0649	[illegible]	0.5361	593.13	2.6423
0.8103	0.0533	2.7759	0.5550	595.75	2.6340
0.8200	0.0519	2.8303	0.5674	599.44	2.6229
0.8258	0.0487	2.8403	0.5722	599.37	2.6266
0.8346	0.0525	2.8480	0.5736	601.29	2.6348
0.8472	0.0485	2.8952	0.5878	604.16	2.6388

0.9578	0.0410	2.9240	0.5973	604.72	2.6360
0.9646	0.0330	2.9262	0.6029	602.99	2.6440
0.9753	0.0377	3.0003	0.6160	608.97	2.6194
0.9831	0.0316	2.9777	0.6208	604.96	2.6471
0.9937	0.0303	2.9887	0.6259	605.64	2.6556
0.9934	0.0280	2.9785	0.6299	604.10	2.6779
1.0122	0.0450	3.0035	0.6285	610.00	2.6739
1.0248	0.0310	2.9914	0.6368	606.11	2.7006
0.9306	0.0253	2.9980	0.6430	604.53	2.7027
0.9374	0.0255	3.0063	0.6496	603.86	2.7094
0.9510	0.0239	2.9925	0.6535	602.78	2.7416
0.9655	0.0232	2.9849	0.6558	602.41	2.7618
0.9742	0.0220	2.9842	0.6576	602.24	2.7698
0.9771	0.0243	2.9697	0.6557	601.73	2.7832
0.9859	0.0197	2.9741	0.6587	601.25	2.7846
0.9975	0.0211	2.9802	0.6605	601.72	2.7850
1.0159	0.0179	2.9779	0.6639	600.44	2.7924
1.0198	0.0178	2.9760	0.6641	600.07	2.7936
1.0266	0.0206	2.9764	0.6624	600.85	2.7920
1.0344	0.0194	2.9837	0.6627	600.83	2.7799
1.0441	0.0208	2.9810	0.6610	600.87	2.7779
1.0586	0.0187	2.9730	0.6608	600.01	2.7847
1.0654	0.0174	2.9722	0.6612	599.71	2.7855
1.0751	0.0181	2.9649	0.6617	598.95	2.7940
1.0809	0.0147	2.9605	0.6643	597.54	2.8011
1.0926	0.0141	2.9541	0.6662	596.61	2.8128
1.1042	0.0137	2.9432	0.6669	595.48	2.8259
1.1159	0.0178	2.9395	0.6654	596.27	2.8326
1.1256	0.0154	2.9412	0.6652	596.61	2.8325
1.1314	0.0178	2.9384	0.6648	597.02	2.8395
1.1391	0.0179	2.9340	0.6662	596.13	2.8457
1.1527	0.0177	2.9353	0.6675	596.02	2.8474
1.1644	0.0221	2.9308	0.6657	596.80	2.8548
1.1721	0.0229	2.9262	0.6667	596.75	2.8670
1.1750	0.0218	2.9306	0.6687	596.41	2.8641
1.1857	0.0191	2.9299	0.6723	595.59	2.8741
1.2022	0.0202	2.9320	0.6758	596.04	2.8886
1.2099	0.0199	2.9331	0.6783	595.99	2.8970
1.2167	0.0193	2.9291	0.6803	595.06	2.9045
1.2264	0.0205	2.9227	0.6815	594.67	2.9180
1.2361	0.0197	2.9266	0.6827	595.07	2.9197
1.2487	0.0209	2.9273	0.6829	595.39	2.9221
1.2575	0.0219	2.9225	0.6833	595.15	2.9306
1.2701	0.0256	2.9189	0.6834	595.75	2.9431
1.2798	0.0204	2.9225	0.6894	594.76	2.9534
1.2924	0.0176	2.9145	0.6934	593.56	2.9758
1.2934	0.0197	2.9113	0.6923	593.79	2.9790
1.3079	0.0200	2.8993	0.6943	592.99	3.0042
1.3195	0.0152	2.8929	0.6990	591.54	3.0247
1.3254	0.0195	2.8927	0.6982	592.36	3.0286
1.3370	0.0218	2.8924	0.6985	593.05	3.0367
1.3448	0.0218	2.8913	0.6991	592.95	3.0407
1.3564	0.0264	2.9012	0.7022	594.66	3.0494
1.3680	0.0246	2.9135	0.7060	595.24	3.0501
1.3729	0.0205	2.9235	0.7119	594.79	3.0478
1.3807	0.0208	2.9361	0.7133	595.59	3.0359
1.3904	0.0245	2.9263	0.7134	595.69	3.0563
1.4068	0.0235	2.9424	0.7151	596.66	3.0404
1.4156	0.0227	2.9421	0.7160	596.26	3.0412
1.4214	0.0220	2.9453	0.7158	596.49	3.0361
1.4311	0.0261	2.9419	0.7141	596.71	3.0376
1.4418	0.0266	2.9426	0.7153	596.78	3.0408
1.4544	0.0248	2.9339	0.7150	595.74	3.0478
1.4583	0.0214	2.9366	0.7174	594.98	3.0458
1.4747	0.0247	2.9256	0.7140	594.94	3.0525
1.4757	0.0230	2.9259	0.7153	594.45	3.0529
1.4844	0.0224	2.9230	0.7156	594.18	3.0578
1.4971	0.0225	2.9193	0.7151	594.04	3.0620
1.5009	0.0236	2.9053	0.7164	593.27	3.0886
1.5009	0.0225	2.9054	0.7169	593.03	3.0887
1.4990	0.0256	2.9169	0.7139	594.53	3.0657
1.4971	0.0218	2.9194	0.7154	593.90	3.0620
1.5009	0.0228	2.9054	0.7168	593.09	3.0887
1.5009	0.0256	2.9051	0.7154	593.69	3.0885
1.5019	0.0264	2.9037	0.7151	593.75	3.0907

Appendix F

Computer Programs

The following programs are the major codes used to acquire and reduce the data from the wind-tunnel experiments. Program WINDF.FOR controls the wind tunnel operations and data acquisition. Program AHREDUCE.FOR reduces the raw concentration-probe data to actual concentration profiles in χ_{He}. Programs MEAN.FOR and NDMEAN.FOR reduce the raw data from the Pitot, cone-static, and thermocouple probes in conjunction with the concentration profiles to final, pertinent mean flow data in dimensional and nondimensional forms.

Program 1: WINDF.FOR

```
C*********************************************************************
C*********************************************************************
C****                  WINDF.FOR  Tunnel Program                  ****
C****                                                             ****
C****       -- program to operate wind tunnel and take data       ****
C****       -- link with dasifor.lib, numer.lib, forfram.lib, and ****
C****          math.lib and assycomm.obj                          ****
C*********************************************************************
C*********************************************************************

      INTEGER*2 IHOUR0,IHOUR1,IMIN0,IMIN1,ISEC0,ISEC1,IHUND0,
     $          DACN,RTNFLG,DATCUT,DATARRAY(28000),BASEADDR,
     $          STARTC,MODE,ENDCH,NOS,IPAR,DMALEV,CNT1,CNT2,
     $          INTLEV,IHUND1,DAT0(9),DACN0
      REAL MAXPSI,SECS,VOLT,TIME0,TIME1,TIMDIF
      character*14 fname(6), RUN*3
      character*42     pgm(2),pgm1,pgm2,pgm3,pgm4
      character*2      exe1,exe2,exe3,exe4,exe5,exe6,exe7,exe8,exe9,exe10
C       data     pgm1     / 'V400 D200 Z1 R1                          ' /
C       data     pgm2     / 'V400 D200 Z0 R1                          ' /
        data     pgm3     / 'V100 D200 Z1 R1 Z0 R1                    ' /
        data     pgm4     / 'V10 D200 Z1 R1 Z0 R1                     ' /
        data     exe1     / 'Y1' /
        data     exe2     / 'Y2' /
        data     exe3     / 'Y3' /
        data     exe4     / 'Y4' /
        data     exe5     / 'Y5' /
        data     exe6     / 'Y6' /
        data     exe7     / 'Y7' /
        data     exe8     / 'Y8' /
        data     exe9     / 'Y9' /
        data     exe10    / 'xx' /
      DATA DAT0 /4095,3391,2882,2403,2006,1553,988,475,0/

        call cinit


      write(*,*)'INSURE STEPPER POWER IS ON AND STEPPER RESET'
C
C**   Input initial program parameters  **
C
      write(*,*)' input traverse up command'
      read(*,'(A)')pgm(1)
      write(*,*)' input traverse down command'
      read(*,'(A)')pgm(2)


      WRITE(*,*)'INPUT PRESSURE'
      READ(*,*)MAXPSI
      WRITE(*,*)'input calibration constant (around 1.60)'
      read(*,*)fudge
      write(*,*)' input hot-film offset'
      read(*,*)hfoffset
      offset = 0.0

        call outpgm (pgm(1))

C
C**   Set time delays and Metrabyte parameters  **
C
      TDEL = 2.0
      TRUP = 6.0
      TDATA = 6.0
      SHUTD = 16.0
      TVAL = 0.00000
```

```
      DACN = 1
      DACN0 = 0
      BASEADDR = 768
      DMALEV = 3
      INTLEV = 2
      CALL LOCATE(15,2)
      MODE = 18
      RTNFLG = 0
C
C**  Initialize Metrabyte  **
C
      CALL ADINIT(BASEADDR,DMALEV,INTLEV,RTNFLG)
      IF (RTNFLG.NE.0) GOTO 200
C
      CALL DIGOUT(0)
   10 CALL CLRSCN(7,0)
      CALL LOCATE(5,5)
C
C**  Show default time parameters and change if necessary  **
C
      WRITE(*,*)'DEFAULT TIME PARAMETERS ARE AS FOLLOWS:'
      WRITE(*,*)'  '
      WRITE(*,*)TDEL,' SECONDS DELAY BEFORE TUNNEL VALVE'
      WRITE(*,*)TVAL,' VALVE OPENS AT T=0'
      WRITE(*,*)TRUP,' SECONDS TRAVERSE UP'
      WRITE(*,*)TDATA,' SECONDS UNTIL DATA STARTS'
      WRITE(*,*)SHUTD,' SECONDS DIGITAL OUTPUTS OFF'
      CALL LOCATE(15,5)
      WRITE(*,*)'WANT TO CHANGE PARAMETERS? ENTER (1) IF YES'
      READ(*,'(F2.0)')CHA
      IF(CHA.NE.1.) GO TO 20
C
      CALL CLRSCN(7,0)
      CALL LOCATE(5,5)
      WRITE(*,*)'TIME IS SET AT ZERO WHEN WIND TUNNEL VALVE OPEN'
      WRITE(*,*)'  '
      WRITE(*,*)'ENTER TIME FOR TRAVERSE UP'
      READ(*,*)TRUP
      WRITE(*,*)'ENTER TIME TO START TAKING DATA'
      READ(*,*)TDATA
      WRITE(*,*)'ENTER TIME FOR TUNNEL SHUTDOWN'
      READ(*,*)SHUTD
      WRITE(*,*)'ENTER TIME DELAY BEFORE TIMER IS ENABLED'
      READ(*,*)TDEL
      WRITE(*,*)'  '
      WRITE(*,*)'TIMES OK AS ENTERED?  ENTER (2) TO CORRECT.'
      READ(*,'(F2.0)')CORR
      IF(CORR.EQ.2.)GOTO 10
C
C** Set up A/D sampling parameters  **
C
   20 CALL CLRSCN (7,0)
      CALL LOCATE (4,0)
      WRITE(*,'(A\)')' ENTER THE START CHANNEL  = '
      READ(*,'(I2)')STARTC
      WRITE(*,'(A\)')' ENTER THE END CHANNEL    = '
      READ(*,'(I2)')ENDCH
      WRITE(*,*)
      WRITE(*,*)' # OF DATA POINTS PER CHANNEL'
      READ(*,'(I5)')NOS
C
C**  Set sample rate  **
C
  250 CALL CLRSCN(7,0)
      CALL LOCATE (0,0)
```

```
        WRITE(*,*)' SET SAMPLE RATE.....'
        WRITE(*,*)'  '
        WRITE(*,*)'  '
        WRITE(*,*)'    RATE IS ESTABLISHED BY DIVIDING THE CLOCK RATE'
        WRITE(*,*)'    (1 MHZ) BY THE PRODUCT OF THE TWO COUNTS.     '
        WRITE(*,*)'    AS AN EXAMPLE:'
        WRITE(*,*)'  '
        WRITE(*,*)'    HIGH COUNT = 10, LOW COUNT = 10 '
        WRITE(*,*)'    SAMPLE RATE = (1000000/(10*10)) = 10000 '
        WRITE(*,*)'           SAMPLES PER SECOND PER CHANNEL'
        WRITE(*,*)'  '
        WRITE(*,'(A\)')' ENTER THE LOW COUNT   =  '
        READ(*,'(I6)')CNT1
        WRITE(*,'(A\)')' ENTER THE HIGH COUNT  =  '
        READ(*,'(I6)')CNT2
      DELTA = 1000000./FLOAT(CNT1*CNT2)
      SECS = NOS/DELTA
      ISECS = INT(SECS*100.)
      WRITE(*,*)
      WRITE(*,*)' THE COUNT SELECTION AS ENTERED WILL PROVIDE...'
      WRITE(*,*)'  '
      WRITE(*,*)'    ',DELTA,' SAMPLES PER SECOND PER CHANNEL'
      WRITE(*,*)'FOR '
      WRITE(*,*)'    ',SECS,' SECONDS'
      WRITE(*,*)' '
      WRITE(*,*)' IF PARAMETERS OK, PRESS RETURN.  IF NO, ENTER 1'
      READ(*,'(I2)')IPAR
      IF(IPAR.EQ.1)GOTO 250
  666 CALL CNTMO1 (2,CNT1)
      CALL CNTMO2 (2,CNT2)
C
C  **  Countdown to start  **
C
      WRITE(*,*)'ENTER (1) WHEN READY TO BEGIN COUNTDOWN'
      READ(*,'(F1.0)')BEGIN
      IF(BEGIN.NE.1.)GOTO 10
      CALL GTIME(IHOUR0,IMIN0,ISEC0,IHUND0)
      TIME0 = IHOUR0*3600.+IMIN0*60.+ISEC0+IHUND0/100.
   51 CALL GTIME(IHOUR1,IMIN1,ISEC1,IHUND1)
      TIME1 = IHOUR1*3600.+IMIN1*60.+ISEC1+IHUND1/100.
      TIMDIF = TIME1 - TIME0
      IF(TIMDIF.LT.TDEL)GOTO 51
      CALL CLRSCN(7,0)
      CALL LOCATE(10,10)
      IHOUR0=0
      IMIN0=0
      ISEC0=0
      IHUND0=0
      IHOUR1=0
      IMIN1=0
      ISEC1=0
      IHUND1=0
      TIME0=0
      TIME1=0
C
      WRITE(*,*)'  *******   TIMER ENABLED   ********'
C
      CALL GTIME(IHOUR0,IMIN0,ISEC0,IHUND0)
      TIME0 = IHOUR0*3600.+IMIN0*60.+ISEC0+IHUND0/100.
C
C  **  Set tunnel pressure  **
C
      VOLT = MAXPSI / (10. * fudge)
      DATOUT = INT(VOLT/2.96E-3)
      CALL DAOUT(DACN,DATOUT,RTNFLG)
C
```

```
C  **  Switch valve on  **

      WRITE(*,*)'VALVE ON'
      CALL DIGOUT(1)

C     CALL GTIME(IHOUR1,IMIN1,ISEC1,IHUND1)
      TIME1 = IHOUR1*3600.+IMIN1*60.+ISEC1+IHUND1/100.
      TIMDIF = TIME1 - TIME0
      IF(TIMDIF.LT.TRUP)GOTO 39

C  **  Traverse up  **

      WRITE(*,*)'TRAVERSE UP'
      WRITE(*,*)

        call outexe (exe1)
        call outexe (exe10)

      CALL DIGOUT(11)
  159 CALL GTIME(IHOUR1,IMIN1,ISEC1,IHUND1)
      TIME1 = IHOUR1*3600.+IMIN1*60.+ISEC1+IHUND1/100.
      TIMDIF = TIME1 - TIME0
      IF(TIMDIF.LT.TDATA)GOTO 159

C  **  Perform A/D conversions (take data)  **

      NCONV = NOS * (ENDCH - STARTC + 1)
      CALL ADCONV(MODE,STARTC,ENDCH,NOS,DATARRAY(1),RTNFLG)
      IF(RTNFLG.NE.0) GO TO 200

C       call outpgm (pgm(2))
      WRITE(*,*)

C  **  Traverse down  **

      WRITE(*,*)'TRAVERSE DOWN'
        call outexe (exe1)
        call outexe (exe10)
      CALL DIGOUT(5)
   29 CALL GTIME(IHOUR1,IMIN1,ISEC1,IHUND1)
      TIME1 = IHOUR1*3600.+IMIN1*60.+ISEC1+IHUND1/100.
      TIMDIF = TIME1 - TIME0

C  **  Switch everything off  **

      IF(TIMDIF.LT.SHUTD)GOTO 29
      CALL DIGOUT(0)
      WRITE(*,*)'ALL DIGITAL OUTPUTS OFF'
      WRITE(*,*)

C  **  Write to files  **
      --  6 channels of data
      --  form of write:
                  1st line -- channel  #
                  2nd line -- sample rate
                  3rd line -- voltage offset
                  4th line -- number of points
          5th and up lines -- digital data in one column

      NSTEPS = 1
      write(*,*)'WRITING TO FILES . . .'
      nch = endch - startc + 1
      fname(1) = 'b:ch0.run'
      fname(2) = 'b:ch1.run'
      fname(3) = 'b:ch2.run'
      fname(4) = 'b:ch3.run'
```

```
      fname(5) = 'b:ch4.run'
      fname(6) = 'b:ch5.run'
      do 23 j =1, nch
        open(j,file=fname(j),status='new', form ='FORMATTED')
        in2 = j
        write(j,'(I3)')j-1
        write(j,*)delta
        if(j.eq.1)then
           write(j,*)hfoffset
        else
           write(j,*)offset
        end if
        write(j,'(i5)') nos
        do 13 i = 1,nos*nsteps
             write(j,'(i5)') datarray(in2)
             in2 = in2 + nch
   13   continue
        close (j)
   23 continue
      GO TO 188
C
C  **  Display any errors in Metrabyte setup  **
C
  200 CALL CLRSCN(7,0)
      CALL DIGOUT(0)
      CALL LOCATE(2,2)
      WRITE(*,*)'** THERE HAS BEEN AN ERROR NUMBER ',RTNFLG
      WRITE(*,*)
      WRITE(*,'(A\)')' HIT <ENTER> TO RETURN TO MAIN MENU '
      READ(*,'(I2)')IERR
  188 CONTINUE
         END
C
C
C  ***********************************************************************
C  ****              Traverse Subroutines                              ****
C  ***********************************************************************
C
C  -- outpgm
C
        subroutine      outpgm (pgm)
        character*42    pgm
          do 100 i = 1,42
            call cout (pgm(i:i))
  100     continue
          call cout (13)
          return
        end
C
C  -- outexe
C
        subroutine      outexe (exe)
        character*2     exe
          do 100 i = 1,2
            call cout (exe(i:i))
  100     continue
          call cout (13)
          return
        end
```

Program 2: AHREDUCE.FOR

```
C     ****************************************************************
C     ****************************************************************
C     ****              AHREDUCE.FOR  Reduction Program              ****
C     ****                                                           ****
C     ****    -- this program reduces the hot-film voltage,          ****
C     ****       total pressure, and total temperature into          ****
C     ****       helium concentration knowing the calibration        ****
C     ****       constants found from a previous program             ****
C     ****    -- viscosity and thermal conductivity are functions    ****
C     ****       of temperature and 1 atm pressure; most values      ****
C     ****       are interpolated                                    ****
C     ****                                                           ****
C     ****    by Joel C. Rosson     Begun:  February  1985           ****
C     ****       Fei T. Kwok     Modified:  September  1989          ****
C     ****************************************************************
C     ****************************************************************
C
C
      DIMENSION TT(2000),PT(2000),AP1(2000),XHE(2000),YLVDT(2000)
      DIMENSION VISA(16,2),CONA(16,2),VISHE(16,2),CONHE(16,2)
      DIMENSION CC1(10) , XN1(10)
C
C  **  Voltage vs. total temperature and pressure data  **
C      -- TT(K), PT(PSIA), XHE(MOLE FRACTION of HELIUM)
C      -- CALIB.IN is a calibration file with calibration info.
C         RUN.IN is the file that contains all run info. as
C           lvdt(units)   voltage(v)   pressure(psia)   temperature(K)
C         RUN.OUT is the output file with
C            lvdt(units)       concentration(Xhe)
C      -- LIMIT is an output check file
C
      OPEN(5,FILE='CALIB.IN',STATUS='OLD',FORM='FORMATTED')
      OPEN(6,FILE='RUN.IN',STATUS='OLD',FORM='FORMATTED')
      OPEN(7,FILE='RUN.OUT',STATUS='NEW',FORM='FORMATTED')
      OPEN(8,FILE='LIMIT',STATUS='NEW',FORM='FORMATTED')
C
C  **  Input parameters  **
C      -- NR      =  1
C      -- L       =  number of data values from experimental run
C      -- TRT     =  reference temperature; ambient temperature at
C                    time of wire-tuning (K)
C      -- RCAB    =  cable resistance (ohms)
C      -- RRT     =  film resistance (ohms)
C      -- RSET1   =  anemometer operating resistance setting
C      -- D       =  static temp./stagn. temp.
C      -- TOL     =  tolerance limit on iteration
C      -- NCONST  =  number of calibr. concentration levels or
C                    number of calibr. constant sets
C      -- DELX    =  increment in Xhe between calibration levels
C
      READ(5,*) NR,L,TRT,RCAB,RRT,RSET1,D,TOL,NCONST,DELX
      WRITE(*,*)NR,L,TRT,RCAB,RRT,RSET1,D,TOL,-TOL,NCONST,DELX
      WRITE(*,*)
C
C  *** Input constans from  XHE = 0.0  TO  XHE = 1.0  ***
C
      DO 252 I = 1 , NCONST
        READ(5,*) CC1(I) , XN1(I)
        WRITE(*,*) CC1(I) , XN1(I)
  252 CONTINUE
      WRITE(*,*)' LOADING DATA VALUES . . .'
C
C  **  Input data values from run  **
C
      DO 10 I=1,L
      READ(6,*) YLVDT(I),AP1(I),PT(I),TT(I)
```

```
C     CONTINUE
C
C  ** VISCOSITY FOR AIR IN KG/M*S OR N*S/M**2  **
C
      DATA VISA/140.,150.,160.,180.,200.,220.,240.,260.,280.,
     1       290.,300.,310.,320.,330.,340.,350.,
     1    .96112E-5,1.0283E-5,1.08842E-5,1.20866E-5,1.3289E-5,
     1    1.43694E-5,1.54498E-5,1.64844E-5,1.74732E-5,1.79676E-5,
     1    1.8462E-5,1.89196E-5,1.93772E-5,1.9834E-5,2.02924E-5,
     1     2.075E-5/
C
C  **  THERMAL CONDUCTIVITY FOR AIR IN W/M*K  **
C
      DATA CONA/140.,150.,160.,180.,200.,220.,240.,260.,290.,
     1       290.,300.,310.,320.,330.,340.,350.,
     1    .0128372,.013735,.014606,.016348,.01809,.019762,
     1    .021434,.023064,.024652,.025446,.02624,.026998,
     1     .027756,.028514,.029272,.03003/
C
C  **  VISCOSITY FOR HELIUM IN KG/M*S  **
C
      DATA VISHE/140.,150.,160.,180.,200.,220.,240.,260.,280.,
     1      290.,300.,310.,320.,330.,340.,350.,
     1      1.22E-5,1.288E-5,1.344E-5,1.455E-5,1.566E-5,
     1      1.657E-5,1.749E-5,1.839E-5,1.927E-5,1.971E-5,2.015E-5,
     1     2.059E-5,2.103E-5,2.147E-5,2.191E-5,2.235E-5/
C
C  **  THERMAL CONDUCTIVITY FOR HELIUM IN W/M*K  **
C
      DATA CONHE/140.,150.,160.,180.,200.,220.,240.,260.,280.,
     1      290.,300.,310.,320.,330.,340.,350.,
     2      9.07E-2,9.5E-2,9.92E-2,1.072E-1,1.151E-1,
     3     1.228E-1,1.304E-1,1.374E-1,1.447E-1,1.484E-1,1.52E-1,
     4      1.555E-1,1.591E-1,1.626E-1,1.662E-1,1.697E-1/
C
C*********************************************************
C**             System Parameters                       **
C
C  RS     = series resistance (ohms)
C
       RS= 50.0
C
C  RCAB   = cable resistance (ohms)
C  RSET1  = anemometer resistance setting (ohms)
C  RWIRE1= hot-wire resistance at operating temp.
C        = RRT(1+Y(TWIRE-TRT)
C
       RWIRE1=RSET1-RCAB
C
C  RRT    = hot-wire resistance at TRT (ohms)
C  TRT    = standard room temp. (K)
C  Y      = thermal coefficient of resistivity for hot-film (1/K)
C
       Y=0.0024
C
C  TWIRE1 = operating temperature
C
       TWIRE1=TRT+(RWIRE1/RRT-1.0)/Y
C
C  XL = wire length (inches converted to meters)
C  XD = wire diameter (inch to meter)
C  B  = ratio of throat area to wire-plane area
C  D  = ratio of static to total temp. at wire-plane
C  A  = ratio of specific heats
C  R  = gas constant (J/kg/K)
```

```
      XL=0.040*0.0254
      XD=0.002*0.0254
      B=0.214515
      PI=3.141593
      A = 0.0
      R = 0.0
C
C  ***********************************************************
C  **                  Reduction                            **
C
C  **  Input shift voltage to correct for drift  **
C      -- ideally,  SH = 0.0
C
       WRITE(*,*)' INPUT SHIFT VALUE IN VOLTS (EXP-CALC)'
       READ(*,*) SH
       WRITE(8,*) SH
       WRITE(*,*) SH
C
      V = 0.0
      C = 0.0
      G = 0.0
      NCOUNT = 0
      NC0 = 0
      NC1 = 0
C
C  **  Loop to interpolate for Xhe according to bounds  **
C  **          calculated from calibration              **
C
      DO 1000 I=1,L
       T=D*TT(I)
       PT(I)=PT(I)*6894.757
C
C  --  Loop to get proper temperature range  --
C
       DO 50 J=1,15
          IF((T.GE.VISA(J,1)).AND.(T.LE.VISA(J+1,1))) GO TO 55
   50  CONTINUE
   55  CONTINUE
C
C  --  Loop to compute upper and lower concentration bound  --
C  --    and then to interpolate to get Xhe                 --
C
       XLOW = 0.0
       XUP = DELX
       DO 253 ILIMS = 1 , NCONST-1
C
C  >>  Calculate lower bound  <<
C
        CALL MIXTURE(VISA,CONA,VISHE,CONHE,A,R,J,XLOW,T,V,C,G)
        VLOW =((RS+RWIRE1+RCAB)**2/RWIRE1*PI*XL*C*CC1(ILIMS)*(TWIRE1-
     1     T)*(XD/V*B*G*PT(I)*(A/(R*TT(I)))**0.5)**XN1(ILIMS))**0.5
     2       + SH
C
C  >>  Calculate upper bound  <<
C
        CALL MIXTURE(VISA,CONA,VISHE,CONHE,A,R,J,XUP,T,V,C,G)
       VUP=((RS+RWIRE1+RCAB)**2/RWIRE1*PI*XL*C*CC1(ILIMS+1)*(TWIRE1-
     1   T)*(XD/V*B*G*PT(I)*(A/(R*TT(I)))**0.5)**XN1(ILIMS+1))**0.5
     2       + SH
C
C  >>  Accounts for values that fall below Xhe=0. and exceed  <<
C  >>          Xhe=1.0 due to experimental error              <<
C
        IF(ILIMS.EQ.1.AND.AP1(I).LT.VLOW)THEN
           XHE(I) = 0.0
           NC0 = NC0 + 1
```

```
            WRITE(8,*) I,XHE(I),AP1(I)-VLOW
            GO TO 1600
          ELSE IF(ILIMS.EQ.NCONST-1.AND.AP1(I).GT.VUP)THEN
            XHE(I) = 1.0
            NC1 = NC1 + 1
            WRITE(8,*) I,XHE(I),AP1(I)-VUP
            GO TO 1600
          END IF
C
C     >>  Interpolate to get Xhe  <<
C
          IF(AP1(I).EQ.VLOW)THEN
             XHE(I) = XLOW
              GO TO 1600
          ELSE IF(AP1(I).EQ.VUP)THEN
             XHE(I) = XUP
             GO TO 1600
          ELSE IF(AP1(I).GT.VLOW.AND.AP1(I).LT.VUP) THEN
             XM = (XUP - XLOW) / (VUP - VLOW)
             XHE(I) = XM * (AP1(I) - VLOW) + XLOW
             GO TO 1600
          END IF
          XLOW = XUP
          XUP = XLOW + DELX
  253 CONTINUE
C
 1600  WRITE(7,*) YLVDT(I),XHE(I)
       NCOUNT = NCOUNT + 1
      WRITE(*,*)I
 1000 CONTINUE
C
C     **  Gives a record of what is done to data points  **
C
      WRITE(*,*)' Number of pts used = ',NCOUNT,' out of ',L
      WRITE(*,*)
      WRITE(*,*)' Number of pts. forced to 1.0 = ',NC1
      WRITE(*,*)
      WRITE(*,*)' Number of pts. forced to 0.0 = ',NC0
C
      CLOSE(5)
      CLOSE(6)
      CLOSE(7)
      CLOSE(8)
       STOP
       END
C
C*********************************************************************
C****                    Subroutine  MIXTURE                      ****
C*********************************************************************
C          --  determines mixture properties
C
      SUBROUTINE MIXTURE(VISA,CONA,VISHE,CONHE,A,R,J,TT,T,V,C,G)
      DIMENSION VIS(16,2),CON(16,2),VISA(16,2),CONA(16,2),
     1          VISHE(16,2),CONHE(16,2)
      REAL MHE,MA,M,MUA,MUHE,KHE,KA
C
C** HELIUM PROPERTIES **
C
      XHE = TT
      MHE = 4.00260
      RHE = 8317./MHE
      CPHE = 5200.
C
C** AIR PROPERTIES **
C
```

```
      XA = 1. - XHE
      MA = 29.
      RA = 8317./MA
      CPA = 1005.7
C
C     ** MIXTURE PROPERTIES **
C
      M = XHE * MHE + XA * MA
      CP = ( XHE * CPHE * MHE + XA * CPA * MA ) / M
      R = 8317./M
      CV = CP - R
      A = CP / CV
C
C     **  Calculate the bounds on the mixture viscosity and  **
C     **              thermal conductivity                   **
C
      IXHE = NINT(100. * XHE)
      DO 10 I = J , J+1
         VIS(I,1) = VISHE(I,1)
         CON(I,1) = CONHE(I,1)
      IF(IXHE.EQ.100)THEN
         VIS(I,2) = VISHE(I,2)
         CON(I,2) = CONHE(I,2)
      ELSE IF(IXHE.EQ.0)THEN
         VIS(I,2) = VISA(I,2)
         CON(I,2) = CONA(I,2)
      ELSE
         MUA = VISA(I,2)/(1+XHE/XA*(1+SQRT(VISA(I,2)/VISHE(I,2))
     1         *(MHE/MA)**.25)**2/(2.82843*SQRT(1+MA/MHE)))
         MUHE = VISHE(I,2)/(1+XA/XHE*(1+SQRT(VISHE(I,2)/
     1          VISA(I,2))*(MA/MHE)**.25)**2/(2.82843*
     2          SQRT(1+MHE/MA)))
         VIS(I,2) = MUA + MUHE
         KA = CONA(I,2)/(1+XHE/XA*(1+SQRT(CONA(I,2)/CONHE(I,2))
     1        *(MHE/MA)**.25)**2/(2.82843*SQRT(1+MA/MHE)))
         KHE = CONHE(I,2)/(1+XA/XHE*(1+SQRT(CONHE(I,2)/CONA(I,2)
     1         )*(MA/MHE)**.25)**2/(2.82843*SQRT(1+MHE/MA)))
         CON(I,2) = KA + KHE
      END IF
   10 CONTINUE
C
      G=(2.0/(A+1.0))**((A+1.0)/(2.0*(A-1.0)))
C
C     **  Calculate the mixture viscosity and thermal conductivity  **
C
      VIS1=VIS(J,2)
      VIS2=VIS(J+1,2)
      CON1=CON(J,2)
      CON2=CON(J+1,2)
      TEMP1=VIS(J,1)
      TEMP2=VIS(J+1,1)
      V=VIS1+(VIS2-VIS1)*(T-TEMP1)/(TEMP2-TEMP1)
      C=CON1+(CON2-CON1)*(T-TEMP1)/(TEMP2-TEMP1)
C
      RETURN
      END
```

Program 3: MEAN.FOR

```
C*********************************************************************
C*********************************************************************
C****                MEAN.F  Reduction Program                    ****
C****                                                             ****
C****       -- Program to reduce mean-flow variables from         ****
C****          given concentration, Pitot, cone-static, and       ****
C****          total temperature profiles                         ****
C****       -- m1.dat is a reference file containing Pc/Pt2       ****
C****          values versus Mach numbers and gammas, as          ****
C****          defined by the Rayleigh Pitot Formula and          ****
C****          the Cone Flow Equation                             ****
C****                                                             ****
C****       by  Fei T. Kwok              September  1989           ****
C*********************************************************************
C*********************************************************************


      REAL  G(20) , M1(20,20) , PCPT2C(20,20) , PT2(2000) , PC(2000) ,
     1      TT2(2000) , XHE(2000) , LVDT(2000) , M(2000) , P1(2000) ,
     2      GS(2000) , RS(2000) , T1(2000) , A1(2000) , RHO1(2000) ,
     3      U1(2000) , PT1(2000)
      INTEGER  NP1(200) , CH
      CHARACTER*3  RN

C**   INPUT  FILES   **
      -- default filenames are as listed below
      -- conc.*, pt2.*, pc.*, and tt2.* are data files from runs;
         m1.dat is a reference file and remains the same for each case
      -- conc.* stored as lvdt vs. signal (mole fraction of helium)
      -- pt2.*, pc.*, and tt2.* stored as:
         1st line . . . channel #, sample rate, volt. offset, # pts.
         2nd - up . . . signal in single column
                     ** pressures in psia
                     ** temperature in deg Kelvin

      WRITE(*,*)' ENTER THE FILETYPE :'
      READ(*,'(A3)') RN
      OPEN(1,FILE='m1.dat',STATUS='OLD',FORM='FORMATTED')
      OPEN(2,FILE='conc.'//RN,STATUS='OLD',FORM='FORMATTED')
      OPEN(3,FILE='pt2.'//RN,STATUS='OLD',FORM='FORMATTED')
      OPEN(4,FILE='pc.'//RN,STATUS='OLD',FORM='FORMATTED')
      OPEN(5,FILE='tt2.'//RN,STATUS='OLD',FORM='FORMATTED')

C**   OUTPUT  FILES   ***
      -- written as signal vs. lvdt

      OPEN(18,FILE='m1.'//RN,STATUS='NEW',FORM='FORMATTED')
      OPEN(7,FILE='p1.'//RN,STATUS='NEW',FORM='FORMATTED')
      OPEN(8,FILE='u1.'//RN,STATUS='NEW',FORM='FORMATTED')
      OPEN(9,FILE='rho1.'//RN,STATUS='NEW',FORM='FORMATTED')
      OPEN(11,FILE='t1.'//RN,STATUS='NEW',FORM='FORMATTED')
      OPEN(12,FILE='a1.'//RN,STATUS='NEW',FORM='FORMATTED')
      OPEN(13,FILE='rlu1.'//RN,STATUS='NEW',FORM='FORMATTED')
      OPEN(14,FILE='conz.'//RN,STATUS='NEW',FORM='FORMATTED')
      OPEN(15,FILE='g.'//RN,STATUS='NEW',FORM='FORMATTED')
      OPEN(16,FILE='r.'//RN,STATUS='NEW',FORM='FORMATTED')
      OPEN(17,FILE='pt1.'//RN,STATUS='NEW',FORM='FORMATTED')

C**   Read input files   ***

      DO 1 I = 3 , 5
         READ(I,*) CH,SR,OFF,NPTS
    1 CONTINUE

      DO 2 I = 1 , NPTS
         READ(2,*) LVDT(I) , XHE(I)
```

```
      READ(3,*) PT2(I)
      READ(4,*) PC(I)
      READ(5,*) TT2(I)
    2 CONTINUE
C
C**   Read m1.dat reference file   ***
C
      READ(1,*) NG , NP
      DO 3 IG = 1 , NG
         READ(1,*) G(IG)
         DO 3 IP = 1 , NP
            READ(1,*) M1(IG,IP) , PCPT2C(IG,IP)
    3 CONTINUE
C
C**   Loop using gas mixture properties and Pc/Pt2 ratio   **
C**           to determine Mach number and P1               **
C
      NMC = 0
      DO 4 I = 1 , NPTS
C
C--   From concentration, determine gamma and R values   --
C
         CALL MIXTURE( XHE(I) , GAM , RS(I) )
C
         GS(I) = GAM
         PCPT2 = PC(I) / PT2(I)
C
C--   From gamma, Pc/Pt2, and reference values from   --
C--          m1.dat, determine Mach numbers            --
C
         CALL MACH1( GAM,PCPT2,NG,NP,G,M1,PCPT2C,M(I),NMC,I,NP1 )
C
         GAMM1 = GAM - 1.
         GAMP1 = GAM + 1.
C
C--   If Mach number reasonable, find P1 from Ray. Pitot   --
C
         IF( M(I).GT.-0.1) P1(I) = (2.*GAM/GAMP1*M(I)**2 - GAMM1/
     1      GAMP1)**(1./GAMM1) / (GAMP1/2.*M(I)**2)**(GAM/GAMM1) *
     2      PT2(I)
    4 CONTINUE
C
C**   Loop to find any remaining values of P1 not found previously   **
C**     because of M = -1.0 (used to mark values where Cone Flow     **
C**                   Equation does not apply)                       **
C
      IF(NMC.NE.0) THEN
         NI = 1
   10    IFLAG = 0
         DO 5 I = NI , NMC
            IF( NP1(I+1).NE.NP1(I)+1 ) THEN
                IF(IFLAG.EQ.0)THEN
                   N1 = NP1(I)
                   N2 = NP1(I)
                END IF
                GO TO 6
            ELSE
            IF(IFLAG.EQ.0) N1 = NP1(I)
                N2 = NP1(I+1)
                IFLAG = 1
            END IF
    5    CONTINUE
C
C**   Interpolate for remaining P1's   **
C
    6    IF(N1.EQ.1) THEN
```

```
            DO 7 I2 = NI , I
               P1(NP1(I2)) = P1(N2+1)
    7       CONTINUE
         ELSE IF( N2.EQ.NPTS ) THEN
            DO 8 I2 = I , NI , -1
               P1(NP1(I2)) = P1(N1-1)
    8       CONTINUE
         ELSE
            DO 9 I2 = NI , I
               CALL INTERP( LVDT(N2+1),LVDT(N1-1),LVDT(NP1(I2)),
     1                      P1(N2+1),P1(N1-1),P1(NP1(I2)) )
    9       CONTINUE
         END IF
C
         NI = I + 1
         IF( I.LT.NMC ) GO TO 10
      END IF
C
C  **   Loop to find remaining M's with interpolated P1's from above   **
C
      DO 11 I = 1 , NMC
         N = NP1(I)
C
C  --   With gamma, Pt2, and new P1, get M   --
C
         CALL MACH2( GS(N) , P1(N) , PT2(N) , M(N) )
   11 CONTINUE
C
C  **   Loop to determine other variables from standard   **
C  **     isentropic flow eqns. and ideal gas eqn.        **
C
      DO 12 I = 1 , NPTS
         T1(I) = TT2(I) / (1.+(GS(I)-1.)/2.*M(I)**2)
         A1(I) = SQRT( GS(I)*RS(I)*T1(I) )
         U1(I) = M(I) * A1(I)
         RHO1(I) = P1(I)*6894.757 / (RS(I)*T1(I))
         PT1(I) = P1(I)*(1.+(GS(I)-1.)/2.*M(I)**2)**(GS(I)/
     1             (GS(I)-1.))
   12 CONTINUE
C
C  **   Loop to write data to output files   **
C       -- LVDT . . anything, but used inches
C       -- P1,Pt1 . psia
C       -- U1,A1. . m/sec
C       -- RHO1 . . kg/m^3
C       -- T1 . . . deg Kelvin
C       -- XHE. . . mole fraction of helium
C       -- R  . . . J/(kg*deg Kelvin)
C
      DO 13 I = 1 , NPTS
         YL = LVDT(I)
         WRITE(18,*)  M(I) , YL
         WRITE(7,*)  P1(I) , YL
         WRITE(8,*)  U1(I) , YL
         WRITE(9,*)  RHO1(I) , YL
         WRITE(11,*) T1(I) , YL
         WRITE(12,*) A1(I) , YL
         WRITE(13,*) RHO1(I) * U1(I) , YL
         WRITE(14,*) XHE(I) , YL
         WRITE(15,*) GS(I) , YL
         WRITE(16,*) RS(I) , YL
         WRITE(17,*) PT1(I) , YL
   13 CONTINUE
C
      DO 1000 I = 1 , 18
         CLOSE(I)
```

```
      CONTINUE
      STOP
      END
C
C
C     ******************************************************************
C     ****                    Subroutine MIXTURE                    ****
C     ******************************************************************
C        -- determines gamma and gas constant R
C
      SUBROUTINE MIXTURE(XHE,G,R)
      REAL M , MHE , MA
C
C     **  Molecular weight (kg/kmol) and Cp (J/kg/Kelvin)    **
C     **                 of helium and air                   **
C
      MHE = 4.0026
      CPHE = 5200.
      MA = 29.0
      CPA = 1005.7
C
C     **  Calculate mixture molecular weight from mole fraction helium   **
C     **              and then retrieve R and gamma                     **
C
      XA = 1. - XHE
      M = XHE * MHE + XA * MA
      CP = ( XHE * CPHE * MHE + XA * CPA * MA ) / M
      R = 8317. / M
      CV = CP - R
      G = CP / CV
      RETURN
      END
C
C
C     ******************************************************************
C     ****                    Subroutine MACH1                      ****
C     ******************************************************************
C        -- determines Mach numbers over profile, if applicable
C
      SUBROUTINE MACH1(GAM,PCPT2,NG,NP,G,M1,PCPT2C,M,NMC,I,NP1)
      REAL  G(20) , M1(20,20) , PCPT2C(20,20) , M , PCPT2L(20) ,
     1      ML(20)
      INTEGER  NP1(200)
C
C     **   Loop to find proper interval of gamma as compared   **
C     **              to values in m1.dat                      **
C
      DO 1 IG = 1 , NG-1
         IF(GAM.GE.G(IG).AND.GAM.LE.G(IG+1)) GO TO 2
    1 CONTINUE
    2 GIG = G(IG)
      GIG1 = G(IG+1)
C
C     **   Interpolate for proper interval of Pc/Pt2 references   **
C
      CALL INTERP(GIG,GIG1,GAM,PCPT2C(IG,1),PCPT2C(IG+1,1),PCPT2L(1))
C
C     **   Loop to check experimental Pc/Pt2 against critical Pc/Pt2   **
C     **     from m1.dat to determine if Cone Flow Eqn. applies        **
C
      IF(PCPT2.GT.PCPT2L(1)) THEN
         M = -1.0
         NMC = NMC + 1
         NP1(NMC) = I
         RETURN
      END IF
```

```
C
C  **   Loop to determine Pc/Pt2 and Mach number intervals   **
C
      DO 3 IP = 1 , NP
         CALL INTERP(GIG,GIG1,GAM,PCPT2C(IG,IP),PCPT2C(IG+1,IP),
     1               PCPT2L(IP))
         CALL INTERP(GIG,GIG1,GAM,M1(IG,IP),M1(IG+1,IP),ML(IP))
    3 CONTINUE
C
C  **   Loop to find final Mach number value according to   **
C  **             corresponding Pc/Pt2 ratio                **
C
      DO 4 IP = 1 , NP-1
         IF(PCPT2.LE.PCPT2L(IP).AND.PCPT2.GE.PCPT2L(IP+1)) THEN
             CALL INTERP(PCPT2L(IP),PCPT2L(IP+1),PCPT2,ML(IP),
     1                   ML(IP+1),M)
             RETURN
         END IF
    4 CONTINUE
C
      RETURN
      END
C
C
C  ***********************************************************************
C  ****                    Subroutine MACH2                           ****
C  ***********************************************************************
C        -- determines remaining unknown Mach numbers
C
      SUBROUTINE MACH2( G , P1 , PT2 , M )
      REAL  M , M1 , M2
      GM1 = G - 1.
      GP1 = G + 1.
      P1PT2 = P1 / PT2
      SONIC = ( 2.*G/GP1-GM1/GP1 )**(1/GM1) /
     1        ( GP1/2. )**(G/GM1)
C
C  **   Loop to find if flow is supersonic, sonic, or subsonic   **
C  **     and then determine Mach number accordingly             **
C
      IF(P1PT2.GT.SONIC) THEN
C
C  --   If subsonic, then M from isentropic flow eqn.   --
C
         IF(P1PT2.GT.1.0) P1PT2 = 1.0
         M = SQRT( 2./(G-1.)*(P1PT2**((1.-G)/G)-1.))
         RETURN
      ELSE
C
C  --   If supersonic, then M iterated from Rayl. Pitot   --
C
         M1 = 2.0
C
C  >>   Use shooting method to iterate for M   <<<
C
         DO 1 I = 2 , 4
            DELM = 10. * 0.1**I
    2       M2 = M1 - DELM
            PM1 = (2.*G/GP1*M1*M1 - GM1/GP1)**(1./GM1) /
     1            (GP1/2.*M1*M1)**(G/GM1)
            PM2 = (2.*G/GP1*M2*M2 - GM1/GP1)**(1./GM1) /
     1            (GP1/2.*M2*M2)**(G/GM1)
            DM1 = PM1 - P1PT2
            DM2 = PM2 - P1PT2
            IF(ABS(DM1).LE.1E-3) THEN
               M = M1
```

```
            GO TO 3
         ELSE IF(ABS(DM2).LE.1E-3) THEN
            M = M2
            GO TO 3
         END IF
         IF((DM1*DM2).LT.0.0) GO TO 1
         M1 = M2
         GO TO 2
 1    CONTINUE
      IF(ABS(DM1).LE.ABS(DM2)) THEN
         M = M1
      ELSE
         M = M2
      END IF
   END IF
 3 IF( M.GT.1.12) M = 1.10
   RETURN
   END
C
C
C  ***********************************************************************
C  ****                    Subroutine INTERP                          ****
C  ***********************************************************************
C      -- interpolation routine
C
      SUBROUTINE INTERP(X2,X1,X,Y2,Y1,Y)
      SM = (Y2-Y1) / (X2-X1)
      Y = SM * (X-X1) + Y1
      RETURN
      END
```

Program 4: NDMEAN.FOR

```
c     ******************************************************************
c     ******************************************************************
c     ****              NDMEAN.F  Reduction Program                   ****
c     ****                                                            ****
c     ****       -- nondimensionalizes files from MEAN.F program      ****
c     ****                                                            ****
c     ****       by  Fei T. Kwok                  September  1989      ****
c     ******************************************************************
c     ******************************************************************
c
c
      real  mlinf , ml(2000) , lvdt(2000) , pl(2000) , ul(2000) ,
     1      rhol(2000) , tl(2000) , al(2000) , rlul(2000) , xhe(2000) ,
     2      pt2(2000) , pc(2000) , tt2(2000) , ptlpt2(2000) ,
     3      ptlpc(2000) , ttl(2000) , alinf(2000) , ulinf(2000) ,
     4      rholinf(2000) , rlulinf(2000) , tlinf(2000) , ptl(2000)
      character*3  rn
c
c  **  Enter averaged freestream values for M and Pt2  **
c      -- pt2inf . . . psia
c
      write(*,*)' enter the filetype :'
      read(*,'(a3)') rn
      write(*,*)' enter the averaged free-stream Mach # :'
      read(*,*) mlinf
      write(*,*)' enter the averaged free-stream Pt2 value :'
      read(*,*) pt2inf
c
c  **  Enter nondimensionalizing height, gamma, and gas constant  **
c      -- h . . . inch here (but can use any units)
c      -- gas constant r . . . J/(kg*deg K)
c
      h = 0.475
      g = 1.399
      r = 8317./29.
c
c   **   input files   **
c        -- files 1-9 and 16 are outputs of MEAN.F '
c        -- files 10-15 are raw data files from runs
c
      open(1,file='ml.'//rn,status='old',form='formatted')
      open(2,file='pl.'//rn,status='old',form='formatted')
      open(3,file='ul.'//rn,status='old',form='formatted')
      open(4,file='rhol.'//rn,status='old',form='formatted')
      open(5,file='tl.'//rn,status='old',form='formatted')
      open(7,file='al.'//rn,status='old',form='formatted')
      open(8,file='rlul.'//rn,status='old',form='formatted')
      open(9,file='conz.'//rn,status='old',form='formatted')
      open(10,file='pt2.'//rn,status='old',form='formatted')
      open(11,file='pc.'//rn,status='old',form='formatted')
      open(12,file='tt2.'//rn,status='old',form='formatted')
      open(13,file='ptlpt2.'//rn,status='old',form='formatted')
      open(14,file='ptlpc.'//rn,status='old',form='formatted')
      open(15,file='ttl.'//rn,status='old',form='formatted')
      open(16,file='ptl.'//rn,status='old',form='formatted')
c
c  **  Loop to read initial file parameters from raw files  **
c
      do 1 i = 10 , 15
         read(i,*) ich , sr , off , npts
    1 continue
c
c  **  Loop to read in data of all files  **
c
      do 2 i = 1 , npts
         read(1,*) ml(i) , lvdt(i)
```

```
      read(2,*) pl(i) , yhold
      read(3,*) ul(i) , yhold
      read(4,*) rhol(i) , yhold
      read(5,*) tl(i) , yhold
      read(7,*) al(i) , yhold
      read(8,*) rlul(i) , yhold
      read(9,*) xhe(i) , yhold
      read(10,*) pt2(i)
      read(11,*) pc(i)
      read(12,*) tt2(i)
      read(13,*) ptlpt2(i)
      read(14,*) ptlpc(i)
      read(15,*) ttl(i)
      read(16,*) ptl(i) , yhold
    2 continue
c
      gml = g - 1.
      gpl = g + 1.
c
c  **  Find nondimensionalizing Pl value  **
c      -- plinf . . . psia
c
      plinf = (2.*g/gpl*mlinf*mlinf - gml/gpl)**(1./gml) /
     1        (gpl/2.*mlinf*mlinf)**(g/gml) * pt2inf
c
c  **  Loop to find nondimensionalizing parameters of  **
c  **                other variables                   **
c      -- tlinf . . . deg K
c      -- alinf,ulinf . . . m/sec
c      -- rholinf . . . kg/m^3
c
      do 3 i = 1 , npts
         lvdt(i) = lvdt(i) / h
         tlinf(i) = ttl(i) / (1.+gml/2.*mlinf*mlinf)
         alinf(i) = sqrt( g*r*tlinf(i) )
         ulinf(i) = mlinf * alinf(i)
         rholinf(i) = plinf*6894.757 / (r*tlinf(i))
         rlulinf(i) = rholinf(i) * ulinf(i)
    3 continue
c
      do 4 i = 1 , 16
         close(i)
    4 continue
c
c
c   ***   output files   ***
c
      open(1,file='pt2nd.'//rn,status='new',form='formatted')
      open(2,file='pcnd.'//rn,status='new',form='formatted')
      open(3,file='tt2nd.'//rn,status='new',form='formatted')
      open(4,file='mlnd.'//rn,status='new',form='formatted')
      open(5,file='plnd.'//rn,status='new',form='formatted')
      open(7,file='ulnd.'//rn,status='new',form='formatted')
      open(8,file='rholnd.'//rn,status='new',form='formatted')
      open(9,file='tlnd.'//rn,status='new',form='formatted')
      open(10,file='alnd.'//rn,status='new',form='formated')
      open(11,file='rlulnd.'//rn,status='new',form='formatted')
      open(12,file='conznd.'//rn,status='new',form='formatted')
      open(13,file='ptlnd.'//rn,status='new',form='formatted')
c
c  **  Loop to write nondimensioned data into files  **
c
      do 5 i = 1 , npts
         yl = lvdt(i)
         write(1,*) pt2(i)/ptlpt2(i) , yl
         write(2,*) pc(i)/ptlpc(i) , yl
```

```
            write(3,*) tt2(i)/tt1(i) , yl
            write(4,*) m1(i) , yl
            write(5,*) p1(i)/plinf , yl
            write(7,*) u1(i)/ulinf(i) , yl
            write(8,*) rho1(i)/rholinf(i) , yl
            write(9,*) t1(i)/tlinf(i) , yl
            write(10,*) a1(i)/alinf(i) , yl
            write(11,*) rlu1(i)/rlulinf(i) , yl
            write(12,*) xhe(i) , yl
            write(13,*) pt1(i)/pt1pt2(i) , yl
      5 continue
c
        do 6 i = 1 , 13
           close(i)
      6 continue
c
        stop
        end
```

REFERENCES

1. Waltrup, P. J., "Liquid Fueled Supersonic Combustion Ramjets: A Research Perspective of the Past, Present and Future," AIAA-86-0158, AIAA 24th Aerospace Sciences Meeting, Reno, NV, January 6-9, 1986.

2. Mays, R. B., R. H. Thomas, and J. A. Schetz, "Low Angle Injection Into a Supersonic Flow," AIAA-89-2461, AIAA/ASME/SAE/ASEE 25th Joint Propulsion Conference, Monterey, CA, July 10-12, 1989.

3. Schetz, J. A., R. A. Weinraub, and R. E. Mahaffey, Jr., "Supersonic Transverse Injection into a Supersonic Stream," *AIAA Journal*, Vol. 6, No. 5, 1968, p. 934.

4. King, P. S., R. H. Thomas, J. A. Schetz, and F. S. Billig, "Combined Tangential-Normal Injection Into A Supersonic Flow," AIAA-89-0622, 27th Aerospace Sciences Meeting, Reno, NV, January 9-12, 1989.

5. Thomas, R. H., J. A. Schetz, and F. S. Billig, "Gaseous Injection in High Speed Flow," Ninth International Symposium on Air Breathing Engines, Athens, Greece, September 3-8, 1989.

6. Keady, J., J. A. Schetz, R. Baker, L. Roe, and W. F. Ng, "Mixing Measurements of Hypermixing Nozzle Injection Into a Supersonic Stream," Final Report to Pratt and Whitney Aircraft, 1989.

7. Goldstein, R. J., E. R. G. Eckert, F. K. Tsou, and A. Haji-Sheikh, "Film Cooling with Air and Helium Injection through a Rearward-Facing Slot into a Supersonic Air Flow," *AIAA Journal*, Vol. 4, No. 6, June, 1986, pp. 981-85.

8. Goldstein, R. J., R. B. Rask, and E. R. G. Eckert, "Film Cooling with Helium Injection into an Incompressible Air Flow," *Intl. Journal of Heat Mass Transfer*, Vol. 9, 1966, pp. 1341-50.

9. Stollery, J. L. and A. A. M. El-Ehwany, "Shorter Communication on the Use of a Boundary-Layer Model for Correlating Film Cooling Data," *Intl. Journal of Heat Mass Transfer*, Vol. 10, 1967, pp. 101-5.

10. Burns, W. K. and J. L. Stollery, "The Influence of Foreign Gas Injection and Slot Geometry on Film Cooling Effectiveness," *Intl. Journal of Heat Mass Transfer*, Vol. 12, 1969, pp. 935-50.

11. Cary, Jr., A. M. and J. N. Hefner, "Film Cooling Effectiveness in Hypersonic Turbulent Flow," *AIAA Journal*, Vol. 8, No. 11, 1970, pp. 2090-1.

12. Kenworthy, M. and J. A. Schetz, "Experimental Study of Slot Injection into a Supersonic Stream," *AIAA Journal*, Vol. 11, No. 5, May, 1973, pp. 585-6.

13. Schetz, J. A. and Johannes vanOvereem, "Skin Friction Reduction by Injection Through Combinations of Slots and Porous Sections," *AIAA Journal*, Vol. 13, No. 8, August, 1975, pp. 971-2.

14. Schetz, J. A., F. S. Billig, and S. Favin, "Simplified Analysis of Slot Injection in Hypersonic Flow," AIAA-88-3056, AIAA/ASME/SAE/ASEE 24th Joint Propulsion Conference, Boston, MA, July 11-13, 1988.

15. Situ, M. and J. Schetz, "New Mixing Length Model for Turbulent High-Speed Flows," AIAA-89-1821, AIAA 20th Fluid Dynamics, Plasma Dynamics and Lasers Conference, Buffalo, NY, June 12-14, 1989.

16. Visich, Jr., M. and P. A. Libby, "Experimental Investigation of Mixing of Mach Number 3.95 Stream in Presence of Wall," NASA Technical Note D-247, February, 1960.

17. Yates, C. L., "Two-Dimensional, Supersonic Mixing of Hydrogen and Air Near a Wall," NASA Contractor Report 1793, Washington, D. C., March, 1971.

18. Waltrup, P. J. and J. A. Schetz, "Tangential Slot Injection of Carbon Dioxide and Helium into a Supersonic Air Stream," ASME Paper No. 72-WA/FE-37, July, 1972.

19. Walker, D. A., W. F. Ng, and M. D. Walker, "Hot-Wire Anemometry in Supersonic Shear Layers," AIAA-87-1372, AIAA 19th Fluid Dynamics, Plasma Dynamics and Lasers Conference, Honolulu, HA, June 8-10, 1987.

20. Campbell, R. L., *Experimental Study of Supersonic Slot Injection into a Supersonic Stream*, M. S. Thesis, Virginia Polytechnic Institute and State University, Blacksburg, VA, 1987.

21. Walker, D. A., R. L. Campbell, and J. A. Schetz, "Turbulence Measurements for Slot Injection in Supersonic Flow," AIAA-88-0123, AIAA 26th Aerospace Sciences Meeting, Reno, NV, January 11-14, 1988.

22. Clark, R. L., W. F. Ng, A. L. Rettew, D. A. Walker, and J. A. Schetz, "Turbulence Measurements in High-Speed Shear Flow Using a Dual-Wire Probe," AIAA-88-3055A, July, 1988.

23. Smith, B. R., *Mean Flow Measurements of Heated Supersonic Slot Injection into a High Reynolds Number Supersonic Stream*, M. S. Thesis, Virginia Polytechnic Institute and State University, Blacksburg, VA, February, 1989.

24. Hyde, Jr., C. R., *Turbulence Measurements of Heated Supersonic Slot Injection into a Supersonic Stream*, M. S. Thesis, Virginia Polytechnic Institute and State University, Blacksburg, VA, February, 1989.

25. Ng, W. F. and A. H. Epstein, "High-Frequency Temperature and Pressure Probe for Unsteady Compressible Flows," *Review of Scientific Instruments*, Vol. 54, No. 12, December, 1983, pp. 1678-83.

26. Ng, W. F., "REVIEW--Simultaneous Measurements of Stagnation Temperature and Pressure Using an Aspirating Probe," International Symposium on Pressure and Temperature Measurement, ASME Winter Annual Meeting, Anaheim, CA, December, 1986.

27. Blackshear, P. L. and L. Fingerson, "Rapid-Response Heat Flux Probe for High Temperature Gases," *American Rocket Society Journal*, Vol. 32, No. 1, November, 1962, pp. 1709-15.

28. Way, J. and P. A. Libby, "Hot-Wire Probes for Measuring Velocity and Concentration in Helium-Air Mixtures," *AIAA Journal*, Vol. 8, No. 5, May, 1970, pp. 976-8.

29. Way, J. and P. A. Libby, "Application of Hot-Wire Anemometry and Digital Techniques to Measurements in a Turbulent Helium Jet," *AIAA Journal*, Vol. 9, No. 8, August, 1971, pp. 1567-73.

30. Adler, D., "A Hot-Wire Technique for Continuous Measurement in Unsteady Concentration Fields of Binary Gaseous Mixtures," *J. Phys.*, E. 5, 1972, pp. 163-9.

31. Devillers, J.-F. and G. B. Diep, "Hot-wire Measurements of Gas Mixture Concentrations in a Supersonic Flow," DISA INFO. 14, 1973, pp. 29-36.

32. Brown, G. L. and M. R. Rebollo, "A Small, Fast-Response Probe to Measure Composition of a Binary Gas Mixture," *AIAA Journal*, Vol. 10, No. 5, May, 1972, pp. 649-52.

33. Jones, B. G. and R. J. Wilson, "Gas Concentration Measurements with a Temperature Compensated Aspirating Probe," *Proceedings of the Fifth Biennial Symposium on Turbulence, 1977*, edited by G. K. Patterson and J. L. Zakin, Science Press, Princeton, NJ, 1979, pp. 205-10.

34. Thomas, R. H. and J. A. Schetz, "Distributions Across the Plume of Transverse Liquid and Slurry Jets in Supersonic Airflow," *AIAA Journal*, Vol. 23, No. 12, December, 1985, pp. 1892-901.

35. Ahmed, S. A. and R. M. C. So, "Concentration Distributions in a Model Combustor," *Experiments in Fluids*, 4, 1986, pp. 107-13.

36. Ng, W. F., F. T. Kwok, and T. A. Ninnemann, "A Concentration Probe for the Study of Mixing in Supersonic Shear Flows," AIAA-89-2459, AIAA/ASME/SAE/ASEE 25th Joint Propulsion Conference, Monterey, CA, July 10-12, 1989.

37. Ninnemann, T. A., M. S. Thesis in preparation, Virginia Polytechnic Institute and State University, Blacksburg, VA.

38. Kwok, F. T., P. L. Andrew, W. F. Ng, and J. A. Schetz, "Experimental Investigation of a Supersonic Shear Layer with Slot Injection of Helium," to be submitted to the 28th Aerospace Sciences Meeting, Airbreathing Propulsion Session, Reno, NV, January 8-11, 1990.

39. Schetz, J. A., *Foundations of Boundary Layer Theory for Momentum, Heat, and Mass Transfer*, Prentice-Hall, Inc., Englewood Cliffs, NJ, 1984.

40. Papamoschou, D. and A. Roshko, "Observations of Supersonic Free Shear Layers," AIAA-86-0162, AIAA 24th Aerospace Sciences Meeting, Reno, NV, January 6-9, 1986.

41. Samimy, M. and G. S. Elliott, "Effects of Compressibility on the Structure of Free Shear Layers," AIAA-88-3054A, AIAA/ASME/SAE/ASEE 24th Joint Propulsion Conference, Boston, MA, July 11-13, 1988.

42. Samimy, M., D. E. Erwin, and G. S. Elliott, "Compressibility and Shock Wave Interaction Effects on Free Shear Layers," AIAA-89-2460, AIAA/ASME/SAE/ASEE 25th Joint Propulsion Conference, Monterey, CA, July 10-12, 1989.

43. Ferri, A., "A Critical Review of Heterogeneous Mixing Problems," *Astronautica Acta*, Vol. 13, Nos. 5 and 6, 1968, pp. 453-65.

44. Bushnell, D. M., private communication.

45. Shapiro, A. H., *The Dynamics and Thermodynamics of Compressible Fluid Flow*, Ronald, NY, 1953, pp. 82-4.

46. Crocco, L. and L. Lees, "A Mixing Theory for the Interaction Between Dissipative Flows and Nearly Isentropic Streams," *Journal Aero. Sci.*, Vol. 19, October, 1952, pp. 649-76.

47. Schetz, J. A. and F. S. Billig, "Approximate Analysis of Base Burning in Supersonic Flow," *Progress in Astronautics and Aeronautics: Aerodynamics of Base Combustion*, Vol. 40, 1975.

48. Burrows, M. C. and A. P. Kurkov, "Supersonic Combustion of Hydrogen in a Vitiated Air Stream Using Stepped-Wall Injection," AIAA-71-721, June, 1971.

49. Chinzei, N., G. Masuya, T. Komuro, A. Murakami, and K. Kudou, "Spreading of Two-Stream Supersonic Turbulent Mixing Layers," *Phys. Fluids*, Vol. 29, No. 5, May, 1986, pp. 1345-7.

50. Schetz, J. A., F. S. Billig, and S. Favin, "Modular Analysis of Scramjet Flowfields," *J. Propulsion*, Vol. 5, No. 2, March-April, 1989, pp. 172-80.

51. Ames Research Staff, "Equations, Tables, and Charts for Compressible Flow," NACA Report 1135, 1953.

52. Volluz, R. J., "Handbook of Supersonic Aerodynamics," NAVORD Report 1488, Vol. 6, January, 1961.

53. Ho, "Thermal Conductivity of the Elements," Table 67 of *J. Phys. Chem. Ref. Data*, Vol. 3, Suppl. 1, 1974.

54. Bradshaw, P., *An Introduction to Turbulence and Its Measurement*, First Edition, Pergamon, 1975.

55. Brown, T. L. and H. E. LeMay, Jr., *Chemistry, The Central Science*, 2nd Edition, Prentice-Hall, Inc., Englewood Cliffs, NJ, 1981.

56. Anderson, Jr., J. D., *Modern Compressible Flow with Historical Perspective*, McGraw-Hill Book Company, New York, 1982.

57. Fellinger, R. C. and W. J. Cook, *Introduction to Engineering Thermodynamics*, Wm. C. Brown Publishers, Dubuque, IA, 1985.

58. Holman, J. P., *Heat Transfer*, 6th Edition, McGraw-Hill Book Company, 1986.

59. Pratt and Whitney Aircraft, "Tables of Compressible Flow Functions."

The vita has been removed from the scanned document